WL-TR-92-4002

ADA251730

# MICROWAVE PROCESSING OF POLYMERIC MATERIALS

James E. McGrath, Jack D. Graybeal, Thomas C. Ward, James F. Wolfe, and Garth L. Wilkes
Virginia Polytechnic Institute and State University
Blacksburg, VA 24061-0212

April 1992

Final Report for Period September 1985 to July 1991

**BEST AVAILABLE COPY**
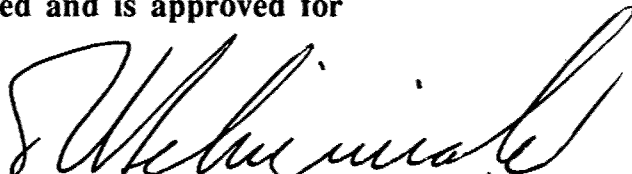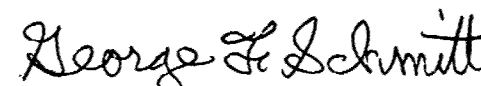
20040 226 152

# NOTICE

When Government drawings, specifications, or other data are used for any purpose other than in connection with a definitely Government-related procurement, the United States Government incurs no responsibility or any obligation whatsoever. The fact that the Government may have formulated or in any way supplied the said drawings, specifications, or other data, is not to be regarded by implication, or otherwise in any manner construed, as licensing the holder, or any other person or corporation; or as conveying any rights or permission to manufacture, use, or sell any patented invention that may in any way be related thereto.

This report is releasable to the National Technical Information Service (NTIS). At NTIS, it will be available to the general public including foreign nations.

This technical report has been reviewed and is approved for publication.

CHARLES Y-C LEE, Project Engineer
Polymer Branch
Nonmetallic Materials Division

T. E. HELMINIAK, Chief
Polymer Branch
Nonmetallic Materials Division

GEORGE F. SCHMITT, Assistant Director
Nonmetallic Materials Division

If your address has changed, if you wish to be removed from our mailing list, or if the addressee is no longer employed by your organization, please notify WL/MLBP, Wright-Patterson AFB, OH  45433-6533, to help us maintain a current mailing list.

Copies of this report should not be returned unless return is required by security considerations, contractural obligations, or notice on a specific document.

Unclassified
SECURITY CLASSIFICATION OF THIS PAGE

| REPORT DOCUMENTATION PAGE | Form Approved OMB No. 0704-0188 |
|---|---|

| 1a. REPORT SECURITY CLASSIFICATION Unclassified | 1b. RESTRICTIVE MARKINGS |
|---|---|

| 2a. SECURITY CLASSIFICATION AUTHORITY | 3. DISTRIBUTION/AVAILABILITY OF REPORT |
|---|---|
| 2b. DECLASSIFICATION/DOWNGRADING SCHEDULE | Approved for public release; distribution is unlimited |

| 4. PERFORMING ORGANIZATION REPORT NUMBER(S) | 5. MONITORING ORGANIZATION REPORT NUMBER(S) WL-TR-92-4002 |
|---|---|

| 6a. NAME OF PERFORMING ORGANIZATION Virginia Polytechnic Institute and State University | 6b. OFFICE SYMBOL (If applicable) | 7a. NAME OF MONITORING ORGANIZATION Materials Directorate Wright Laboratory |
|---|---|---|

| 6c. ADDRESS (City, State, and ZIP Code) Department of Chemistry Blacksburg, VA 22209 | 7b. ADDRESS (City, State, and ZIP Code) WL/MLBP Wright-Patterson AFB, OH 45433-6533 |
|---|---|

| 8a. NAME OF FUNDING/SPONSORING ORGANIZATION DARPA | 8b. OFFICE SYMBOL (If applicable) | 9. PROCUREMENT INSTRUMENT IDENTIFICATION NUMBER F33615-85-C-5153 |
|---|---|---|

| 8c. ADDRESS (City, State, and ZIP Code) 1400 Wilson Blvd. Arlington, VA 22209 | 10. SOURCE OF FUNDING NUMBERS |||||
|---|---|---|---|---|

| PROGRAM ELEMENT NO. | PROJECT NO. | TASK NO. | WORK UNIT ACCESSION NO. |
|---|---|---|---|
| 62102F | 5456 | 00 | 01 |

11. TITLE (Include Security Classification)

Microwave Processing of Polymeric Materials

12. PERSONAL AUTHOR(S)
J. McGrath, J. Graybeal, T. Ward, J. Wolfe, and G. Wilkes

| 13a. TYPE OF REPORT Final | 13b. TIME COVERED FROM Sep 85 TO Jul 91 | 14. DATE OF REPORT (Year, Month, Day) April 1992 | 15. PAGE COUNT 290 |
|---|---|---|---|

16. SUPPLEMENTARY NOTATION

| 17. COSATI CODES ||| 18. SUBJECT TERMS (Continue on reverse if necessary and identify by block number) |
|---|---|---|---|
| FIELD | GROUP | SUB-GROUP | |
| 07 | 04 | | |
| 11 | 04 | | |

19. ABSTRACT (Continue on reverse if necessary and identify by block number)

Microwave energy is a potentially fast and efficient means of energy for various materials. The coupling of microwave energy into materials during processing involoves much more than just shortening the heat-up time relative to conventional processing and it has the potentia to provide an additional degree of control over morphology, structure, and mechanical be- havior. This report summarizes a multidisciplinary research program sponsored by the Defens Advance Research Project Agency (DARPA) which has been managed by the Materials Directorate, Wright Laboratory, and the Army Research Office. Many fundamental issues relating to the influence of microwave energy on chemistry and mechanical behavior have been investigated and are reported herein. Technology development has been particuarly focussed on poly- meric and composite materials processing. The research has included efforts at two universities, Virginia Polytechnic Institute and State University and Michigan State University. Research has also been conducted at the Materials Directorate, Wright Laboratory, the Foster Miller Company and the Aerospace Materials Development group at McDonnell Douglas

| 20. DISTRIBUTION/AVAILABILITY OF ABSTRACT ☒ UNCLASSIFIED/UNLIMITED ☐ SAME AS RPT. ☐ DTIC USERS | 21. ABSTRACT SECURITY CLASSIFICATION Unclassified |
|---|---|

| 22a. NAME OF RESPONSIBLE INDIVIDUAL Charles Y-C Lee | 22b. TELEPHONE (Include Area Code) 513-255-9158 | 22c. OFFICE SYMBOL WL/MLBP |
|---|---|---|

DD Form 1473, JUN 86          Previous editions are obsolete.          SECURITY CLASSIFICATION OF THIS PAGE
Unclassified

# FOREWORD

This report covers work performed under Contract No. F33615-85-C-5153 during the period of September 1985 to July 1991. The contract entitled "Microwave Processing of Polymeric Materials" was jointly administered by the Materials Directorate, Wright Laboratory, Air Force Systems Command, Wright-Patterson Air Force Base, Ohio with Dr. Charles Y.-C. Lee as the Materials Directorate Project Engineer and the Army Research Office using DARPA funding. The report was prepared by the Virginia Polytechnic Institute and State University, Department of Chemistry and the NSF Science and Technology Center on High Performance Polymeric Adhesives and Composites with James E. McGrath as the Principal Investigator.

# TABLE OF CONTENTS

# FIGURES

# TABLES

# Summary

Microwave energy has long been known to be a potentially fast and efficient source of energy for heating various materials. It was proposed that coupling of microwave energy into materials during processing involves much more than just shortening the heat-up time relative to conventional processing and it is considered to have the potential to provide an additional degree of control over morphology, structure, and mechanical behavior. This report summarizes a multidisciplinary research program sponsored by the Defense Advance Research Project Agency (DARPA) which has been managed by the Materials Directorate, Wright Laboratory, and Army Research Office. Many fundamental issues relating to the influence of microwave energy on chemistry and mechanical behavior have been investigated and are reported herein. Technology development has been particularly focussed on polymeric and composite materials processing. The research has included efforts at two universities, Virginia Polytechnic Institute and State University and Michigan State University. Research has also been conducted at the Wright Laboratory, the Foster Miller Company and the Aerospace Materials Development group at McDonnell Douglas Research Laboratory. The fundamental aspects of the chemistry and polymeric materials was initiated at Virginia Tech. An initial design of an applicator with a closed loop control was constructed at Michigan State University so that coupling of the microwave energy into polymeric materials could be studied in a controlled manner. As the program evolved, aspects of both areas were studied at the two universities. A major result of this program was the generation of technical papers which have been recently published in the Materials Research Society symposia proceedings, Volume 189, 1991. The proceedings are entitled "Microwave Processing of Materials" and was edited by W. W. Snider, W. A. Sutton, M. F. Iskander, and D. L. Johnson. The papers, which were supported by the DARPA effort, are included in this final as an appendix in an attempt to provide overall continuity. The main part of this report has been organized into sections which describe efforts complementary to the published papers provided in the Appendix.

At Virginia Tech, the co-principal investigators have used the applicator developed at Michigan State for the microwave processing of polymeric materials. Many interesting phenomena were identified. For example, the rates of crosslinking reactions encountered in epoxy, bismaleimide, and nadimide (PMR-15, etc.) curing to generate network or thermoset materials has been investigated. It is invariably much more rapid via microwave relative to traditional thermal processing. It appears possible to obtain rather fully cured epoxy networks, for example, in approximately 10 minutes. The analogous systems under conventional conditions would take hours by comparison. There appears to be the potential for selective chemistry. For example, solution imidization can be preferred relative to acetylene cured network formation, even when both groups are on the same molecule! This is no doubt because of the more polar nature of the imidization reaction. Such effort has potential for providing a major new control dimension over polymer synthesis and processing. The same efforts could be applied to small molecule e.g., monomer chemistry. Some effort in new monomer synthesis was conducted during this program and novel chemistries identified are summarized in the report. The second area of materials development is the generation of ceramers (polymer modified ceramics) and this has been investigated extensively during this program. In general, one can conclude that property development in these important hybrid materials can be accomplished in minutes instead of the traditional "days." Efforts were also generated at understanding the mechanism for heating of thermoplastics. Extensive studies resulted in the definition of the terminology "microwave calorimetry."

# I. INTRODUCTION

Recent advances in space and other technologies have produced a continuing and growing demand for high performance polymeric materials that can withstand prolonged exposures to high temperatures. These materials must possess excellent mechanical properties, solvent resistance and dimensional stability over a wide temperature range. Typically, these materials (usually thermosetting resins) are extremely difficult to process, often requiring slow thermal ramp rates to negate temperature gradients and to control the highly exothermic nature of the polymerization.

A possible solution to these processing problems may be microwave processing. Electromagnetic radiation (EMR) processing results in rapid volumetric heating being due to a combination of the large penetration depth of microwave radiation and to the unique mechanism of microwave absorption (i.e., electric dipolar coupling to permanent dipole moments). Indeed, the utilization of microwave radiation is currently found in many applications including food processing/cooking [1-9], drying of lumber and paper [7,8], the sterilization of medical equipment [1,9], and more recently in the processing of ceramics [9,10], polymers [11-64] and composite materials [37-42].

In the current investigation, the feasibility of utilizing a controlled electromagnetic field in a single-mode microwave applicator to process high performance thermosets and nonreactive thermoplastic blends was examined. The next section describes the processing of both neat and thermoplastic-modified epoxy resin networks as well as functionalized poly(arylene ether ketone)s by microwave and classical thermal treatments. In Chapter Three, the influence of chemical structure on miscibility and physical property behavior in blends of poly(arylene ether ketone) with poly(aryl imide) homo- and copolymers is discussed. In addition, microwave processing of selected blends is utilized to demonstrate the principles of "microwave calorimetry."

# II. MICROWAVE PROCESSING OF HIGH PERFORMANCE POLYMERIC NETWORKS

## 2.0. Introduction

Most molecules are polarizable upon exposure to electromagnetic radiation (Figure 1). At the molecular level there are four possible components of polarization; Figure 2 depicts the general relationship of the dielectric constant and the dielectric loss factor as a function of the applied frequency for a polar molecule. At high frequencies, electronic and atomic polarization occur. Electronic polarization is observed because of a displacement of the electrons around the nuclei in each atom. Typically, the time required for electronic polarization is approximately 10-15 seconds, which corresponds to a frequency of ultraviolet radiation (Figure 1). Atomic polarization, on the other hand, arises from the displacement of the atomic nuclei relative to one another, and occurs in a time frame of 10-13 seconds, corresponding to the frequency of infrared radiation (Figure 1). In heterogeneous systems interfacial polarization (also known as space charge or Maxwell-Wagner polarization) is also possible. Interfacial polarization occurs at very low frequencies and arises from a charge build-up in the interfaces between components [65-72].

The largest dielectric loss transition evident in Figure 2, however, is due to orientation polarization (or dipolar relaxation). Orientation polarization results are due to the interaction of molecules with an electromagnetic field. Under normal conditions, polar molecules possessing permanent dipole moments are randomly oriented. However, in the presence of an electric field, the polar molecules line up with the field. As an alternating field is applied, the polarity of the field is varied at the microwave frequency, and the molecules attempt to align themselves with the changing field as depicted schematically in Figure 3. This results in a rotation of the molecules, and a conversion of the electrical energy into thermal energy (or heat) [1,65,69-71].

With long chain macromolecules the same general mechanism applies; however, the dipolar groups are covalently bonded in either the backbone structure, as pendant groups or as endgroups. Thus, instead of a dielectric loss transition from a single molecule, a dielectric loss dispersion corresponding to the sum of many relaxation processes must be considered. Polymers usually
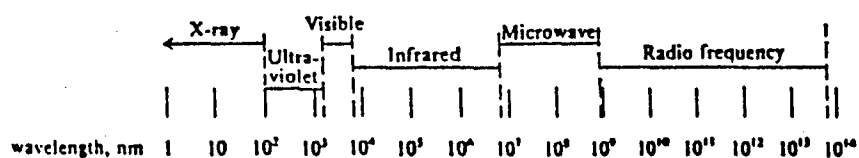
Figure 1.  Electromagnetic spectrum.
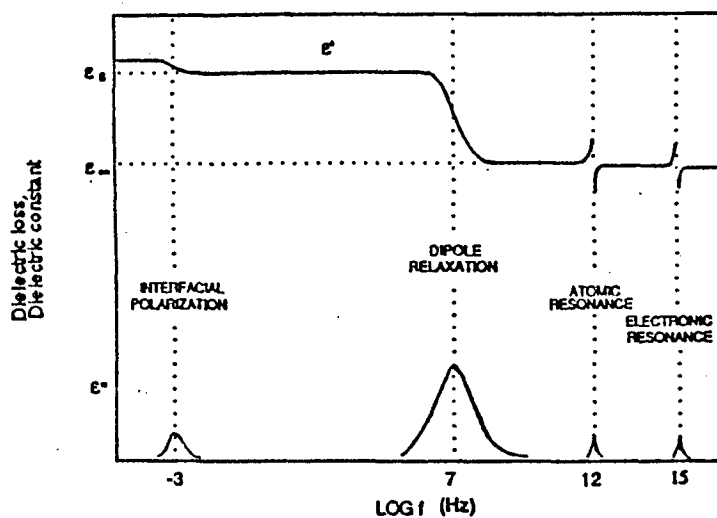


Figure 2.  Schematic diagram representing the dielectric
spectra for a polar molecule [71].
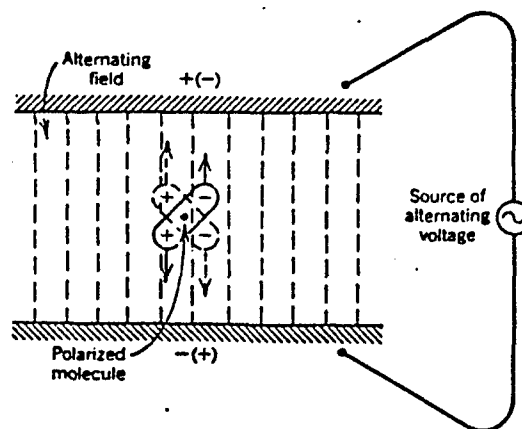


Figure 3.  A molecular dipole in an alternating
electrical field [65].

3

exhibit more than one dielectric loss dispersion; the largest dielectric loss transition is generally the α transition (i.e. primary dispersion). This dispersion involves the co-operative motion of main-chain segments associated with the glass transition. Other relaxation transitions may be found at lower temperatures (or higher frequencies) where the segments of the main-chain are practically immobile. These are called secondary dispersions and are designated by β, etc., in order of decreasing temperature (or increasing frequency). The β transition is associated with smaller more mobile polymeric units such as side chains, chain ends, or even individual atomic groups (e.g. polar substituents) [66-69]. All dielectric loss transitions are a function of both temperature and frequency; this dependency will be addressed in detail in Section 3.2.4..

The dielectric power absorption of a material is given by the equation:

$$ P = K f E^2 \varepsilon'(T) \tan \delta(T) \tag{1} $$

where P is the power dissipation, K is a constant, f is the applied frequency, E is the electric field strength, $\varepsilon'$ is the relative dielectric constant and $\tan \delta$ is the loss tangent. The electromagnetic field energy dissipated as heat per unit volume is seen to be a function of both the properties of the energy source (i.e., field strength and frequency) and material properties (i.e., dielectric constant and loss tangent). Increasing the values of any of these factors increases the amount of energy converted [1,65].

If convection losses and conductive heating effects are ignored, the heating rate of a nonreactive material placed in an electromagnetic field can be described by the relationship:

$$ \frac{dT}{dt} = \frac{K f E^2 \varepsilon'(T) \tan \delta(T)}{\rho \, C_V} \tag{2} $$

where $\rho$ is the density of the material, $C_V$ is the specific heat and the other parameters are the same as in Equation 1. Therefore, the heating rate, dT/dt, of a material is directly dependent on the square of the electric field strength, the applied frequency and the dielectric loss factor ($\varepsilon' \tan \delta$) of the material, which is a function of temperature [1,4-6,65].

Because of the unique mechanism of microwave heating, a number of advantages for microwave processing exist over conventional thermal processing techniques, particularly when thick cross-sectioned parts are involved. In such cases, very slow temperature increases are conventionally utilized to negate thermal gradients through the material during processing. When microwave radiation is used, however, the absorption of energy is more uniform with depth, and thus the polymer can be heated significantly faster while maintaining good thermal uniformity. Processing of this type may result in a reduction of residual stress and superior mechanical properties. Other advantages with microwave processing include: significantly reduced cure cycles in thermosets, increased throughput, and substantially reduced capital and operating costs (since only the sample is heated rather than the surrounding air, oven walls, etc.). And, there is the possibility of selective chemistry because of the nature of microwave absorption.

2.1. Literature Review
2.1.1. Microwave Processing
2.1.1.1. Epoxy Resin Networks

The majority of the literature dealing with the utilization of microwave radiation to process polymer materials has emerged in the past 10 years. The most highly investigated systems are thermosetting epoxy resin networks [11-28]. Gourdenne [62] and co-workers have examined the influence of both continuous and pulsed electromagnetic radiation (EMR) on the crosslinking of the diglycidyl ether of bisphenol A (DGEBA) with 4,4'-diaminodiphenylmethane (DDM) [11-14]. Employing continuous microwave radiation, Gourdenne et al. demonstrated that epoxy resin networks could be effectively cured with efficiency at least equivalent to classical heating. Pulsed

4

EMR processing, however, demonstrated accelerated reaction rates over both the continuous and classical heating techniques. Temperature and dielectric loss as a function of time demonstrated that both the heating rate and time to gelation were enhanced over the continuous processing technique (at the same average power). This suggested that the discontinuous (i.e., pulsed) radiation coupled with the sample more effectively than the continuous radiation. Gourdenne et al. proposed a double relaxation mechanism to explain this phenomenon. The double relaxation postulate suggests a synergistic effect between the electromagnetic field, which couples with the dipoles, and the pulse emission frequency, which induces a dielectric relaxation in the oligomeric epoxy (associated with the motions of short chain segments) [11-14].

In order to investigate the double relaxation postulate, Gourdenne et al. varied both the frequency [13] and length [14] of the pulsed electromagnetic emissions. The results indicated that, indeed, the acceleration of the heating process was dependent on pulse frequency since the heating rate was found to be more highly activated at certain frequencies. A pulse length dependency was also discovered. Gourdenne and co-workers identified a critical pulse length/pulse period (i.e., the inverse of pulse frequency) ratio of 1/5 which they proposed corresponds to a compromise between the dipolar (continuous mode) and segmental (pulsed mode) relaxations. Experimental results demonstrated that if the ratio was significantly lower than 1/5, the accelerated heating effect was diminished. They attributed this to a delayed diffusion of the localized heating effect (i.e., dipolar heating) through the resin/curing agent mixture, because of the shortness of the pulse. At very high pulse length/pulse period ratios (greater than 1/5), the pulsed radiation behaved in a manner analgous to continuous microwave radiation where heating was purely dipolar in nature [13,14].

Jullien [44] and co-workers have also investigated the processing of epoxy resin networks with both continuous and pulsed microwave radiation. They obtained results similar to those of Gourdenne et al., demonstrating that pulsed EMR was more effective than continuous microwave radiation in crosslinking epoxy resin networks at the same average power [15,16]. Jullien et al. discovered that network conversion was more dependent on specific pulse frequencies and lengths rather than the actual cure temperature during EMR processing. Indeed, some of their highest conversions were achieved at the lowest microwave cure temperatures, thus suggesting more efficient energy transfer to the dipolar sites at certain pulse frequencies and lengths [15,16].

Jullien and co-workers attributed the enhanced curing rates achieved with the pulsed microwave radiation to homopolymerization of the DGEBA epoxy reactant. They proposed that the pulsed radiation actually catalyzed the homopolymerization of the DGEBA epoxy reactant over the more traditionally activated epoxide/diamine reaction, as shown in Figure 4, such that a combination of the two reactions occurred during network formation [15,16]. Evidence for the existence of homopolymerization in the crosslinked networks was provided by FTIR and solid state $^{13}$C NMR characterization [15,16].

Researchers at Michigan State University demonstrated, utilizing stress-strain evaluation, that continuous microwave radiation may be employed to achieve mechanical properties comparable to conventional thermal curing techniques in epoxy resin networks [17,18]. More recently, Jow and Hawley [40] have shown that the highly exothermic nature of epoxy resin reactions may be controlled through computer-pulsed microwave processing [19,20]. This technique is significantly different from the previously discussed pulsed EMR experiments, since both the pulse length and period are many orders of magnitude larger (i.e., on the order of a few seconds) with this experimental arrangement. Hawley et al. [21] demonstrated that the typical temperature rise that is due to the exotherm of polymerization may be essentially eliminated with the slow-pulse EMR technique. This is highly advantageous as it allows for higher cure temperatures without thermal degradation, and thus provides the possibility of achieving a higher Tg in the cured component. Jow and Hawley have also developed a dielectric analysis technique, using a single-mode microwave applicator, to measure the dielectric properties (permittivity and dielectric loss factor) of the sample during cure at microwave frequencies. This in situ characterization technique provides essential information about how the dielectric properties of the sample vary with cure at a frequency of 2.45 GHz [19,21,22].
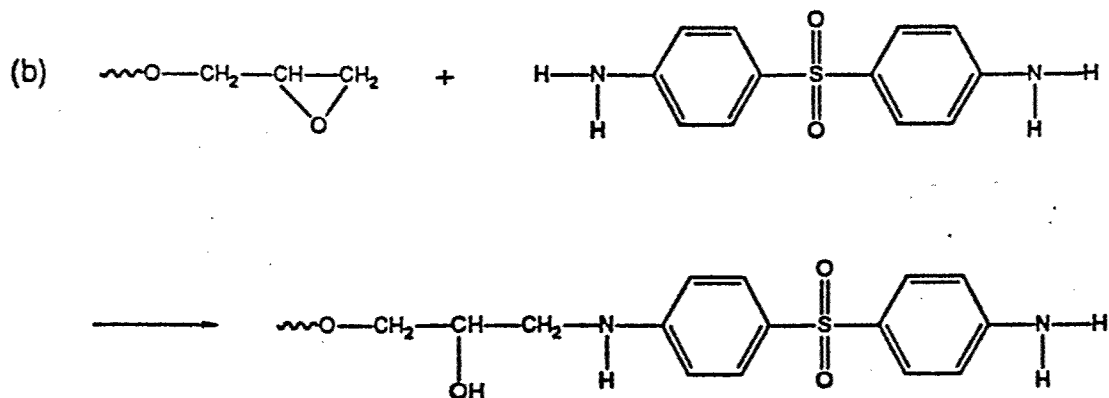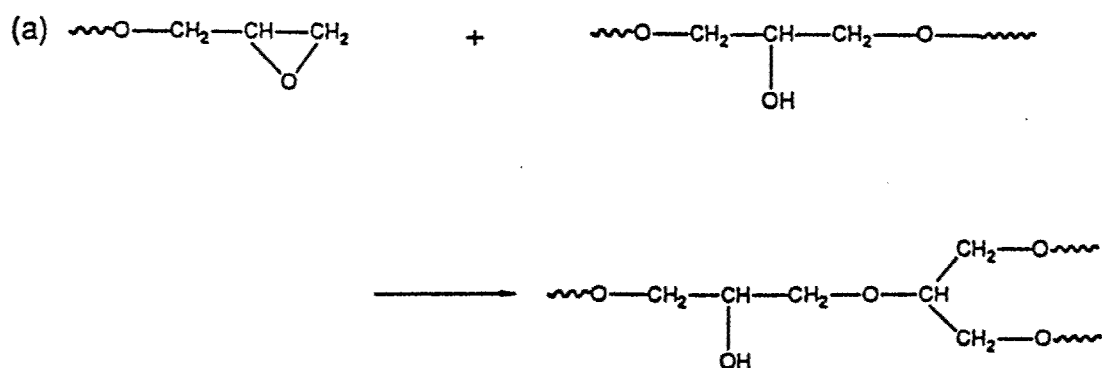
Figure 4.   Polymerization of epoxy resin networks.   (a) Homopolymeriza-
tion of the DGEBA epoxy reactant.   (b) The more common and
highly activated epoxide/diamine reaction.

6

## 2.1.1.2. Epoxy Resin Composites

The microwave processing of epoxy resin composites is another highly active area of research [29-42]. The influence of fillers/structural supports on the EMR processability of epoxy resins is dependent on whether or not the additive is conductive. Gourdenne [29] and co-workers demonstrated that nonconductive dopants, such as glass fibers, behave as diluents and actually reduce the rate of reaction by delaying the exotherm of polymerization. However, this is not the situation for conductive dopants. Raj [30] demonstrated that the rate of heating in microwave processed epoxy resins may be accelerated by the incorporation of iron powder. The microwave heatability of a neat epoxy resin mixture composed of DGEBA with diaminodiphenylsulfone and several epoxy/iron (powder) composites as a function of iron composition is shown in Figure 5. The general shape of the temperature-time cure given in Figure 5 was the same in all cases (although varying in magnitude significantly). Three observable regions were evident corresponding to the heating of the reactants, followed by a rapid temperature increase with the reaction exotherm, and finally by a cooling period and leveling off effect as energy loss by convection and heating because of microwave absorption reached an equilibrium state in the sample. The heating rates shown in Figure 5 were enhanced as the percentage of iron powder increased. This was attributed to a combination of dipolar effects (orientation polarization) and conductive heating effects, due to the interaction of the electric field with the iron powder. The magnitude of the conductive effect was a function of iron composition in the resin as is shown in Figure 5 [30]. Similar results have been reported by Gourdenne [31-35] et al. with other conductive dopants such as aluminum [31-33], copper [34] and carbon black [35].

The EMR processing of continuous carbon fiber reinforced composite laminates have also been investigated. However, because of the conductive nature of the continuous graphite fibers, processing is considerably more complicated. Indeed, numerous processing problems have been reported such as arcing and localized exotherms. Lee and Springer [36-38] conducted a systematic investigation of the interaction of microwave radiation with composite laminates. Utilizing glass fibers as reinforcement, processing control was reported to be relatively straightforward [36-38]. However, when carbon fiber reinforcement was employed, the ability of the microwave radiation to interact with the laminate was dependent on the ply orientation and the polarization angle of the EMR field [36-38]. Utilizing a polarized transverse electromagnetic wave (TEM wave) in a rectangular wave guide, Springer [36-38 et al. observed that the electromagnetic wave must be perpendicular to the alignment of the fiber orientation (i.e., possess a polarization angle of 90°C), as shown in Figure 6, to obtain maximum penetration and absorption of the electromagnetic radiation. Orientation of the fibers parallel to the transverse wave (i.e. polarization angle of 0°) resulted in complete reflectance, while polarization angles between 0°C and 90°C provided varying degrees of absorption. Additionally, it was observed that multidirectional composite laminates were not effectively cured by microwaves [36-38].

Recent results obtained by Chen and Lee [39] and Hawley et al. [40,41], however, demonstrated that the reflectance problem associated with the fiber/EMR wave orientation may be overcome by utilizing a standing wave generated in a single-mode applicator [39,40,41]. Hawley [40, 41] et al. reported that 3-inch square, 24 ply, unidirectional composite laminates have been successfully processed using this technique. Furthermore, it has been suggested by Drzal [42] et al. that selective heating of the fiber over the epoxy resin matrix caused by dissimilar dielectric properties between the conductive carbon fibers and the epoxy resins, actually improves interfacial adhesion. However, experimental methods still need to be devised for the application of pressure to the laminate during EMR processing to optimize mechanical property performance [40,41].

## 2.1.1.3. Polyurethane Polymerizations

Gourdenne [43] et al. have reported synthesizing polyurethanes from diisocyanates and polyethertriol prepolymers utilizing continuous microwave radiation. The polyurethane networks
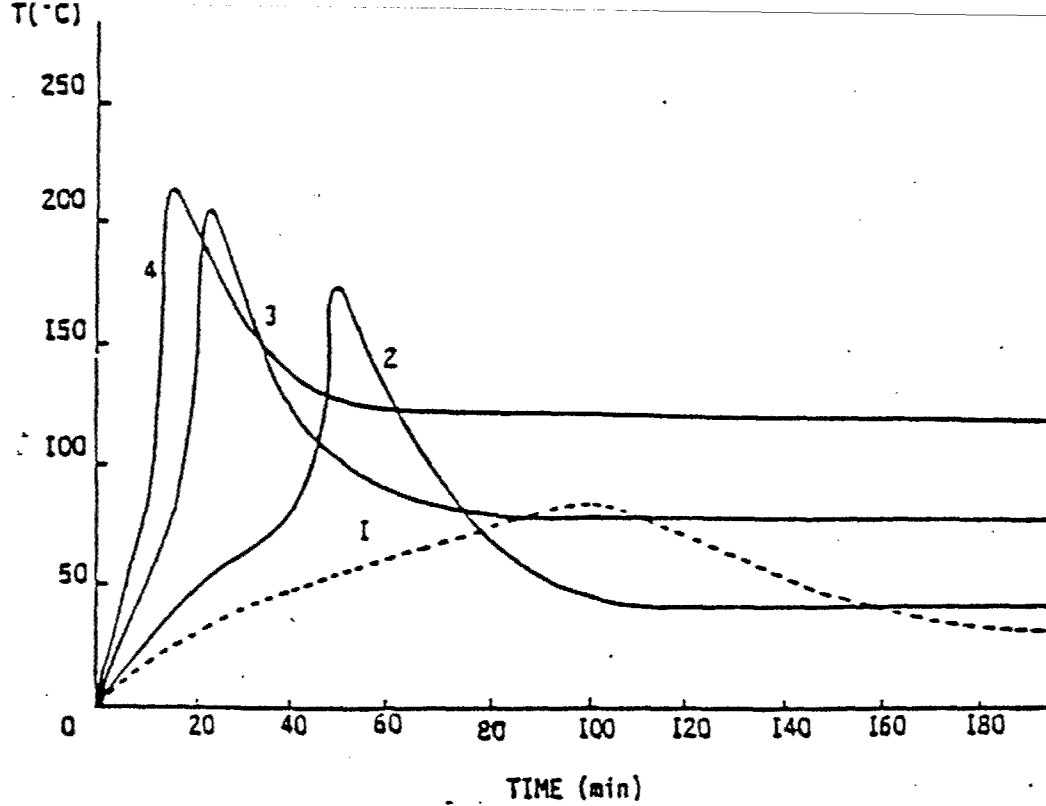
Figure 5. Effect of iron powder concentration on the heating rates of epoxy/iron composites at a constant powder of 20 watts ((1) neat resin (2) 20%, (3) 40% and (4) 60% by weight iron) [30].
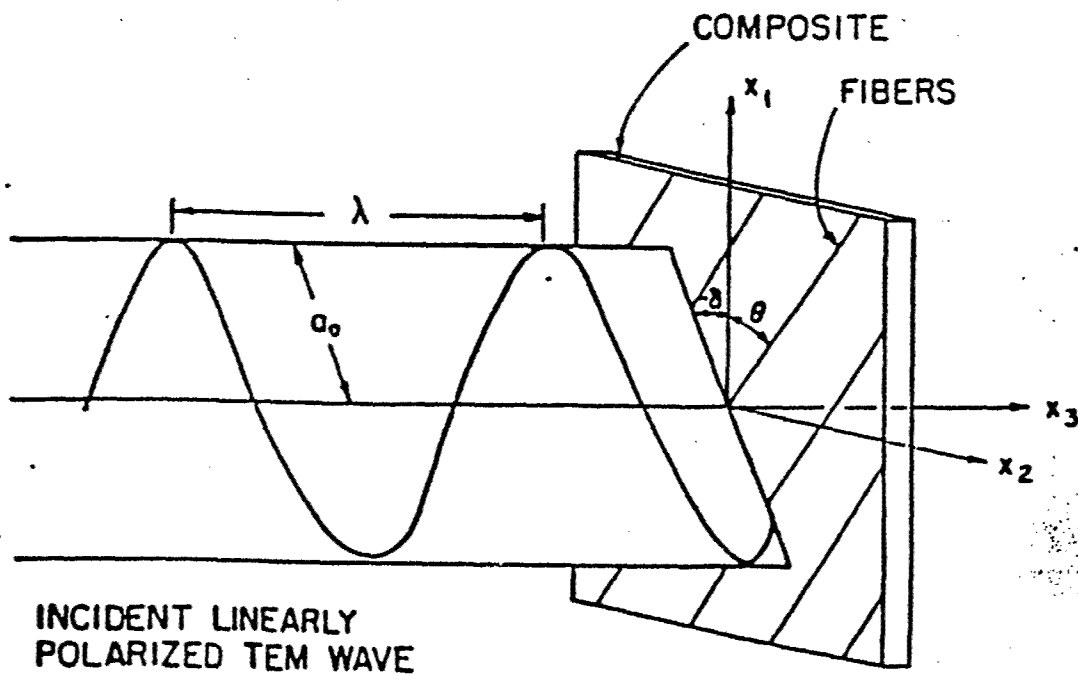


Figure 6. Schematic representation of a polarized electromagnetic wave intersecting a unidirectional graphite fiber composite laminate perpendicular to the alignment of the fiber orientation (i.e. at a polarization angle of 90°) [37].

8

generated demonstrated equivalent mechanical properties (as measured by the elastic compression modulus) to networks cured with classical thermal treatments [43].

Polyurethane curing by pulsed microwave fields has also been reported [44]. Jullian and Valot [44] investigated the curing behavior of polyurethane prepolymers in ethyl acetate solutions (25% solids content). Pulsed microwave radiation was employed to rapidly evaporate the ethyl acetate and cure the remaining thin film. Interestingly, Jullien [44] et al. found that both the energy transfer and hardness of the cured films correlated with the pulse frequency. At specific pulse repetition frequencies the energy transfer in the thin films was enhanced. Jullien et al. attributed the enhancement to the excitation of a low-frequency dielectric relaxation in the polyurethane induced by the microwave pulse modulation, in a fashion similar to that proposed by Gourdenne [11-14] et al. with regard to epoxy resin networks. The correlation of film hardness with the pulse frequency, independent of cure temperature, was suggested by Jullian et al. [44] to be due to either a higher extent of reaction or possibly to the formation of a different polymeric structure, since the EMR processed resins exhibited higher film hardness values than urethane networks cured with conventional thermal treatments.

## 2.1.1.4. Synthetic Rubbers

In the early 1970's microwave processing was explored as a possible technique for the continuous vulcanization of synthetic rubber [45-50]. Electromagnetic radiation is the only suitable means of curing thick rubber sections rapidly. Schwarz et al. [45,46] and Ippen et al. [47] performed extensive investigations on the effects of compounding (i.e., the additions of clay, carbon black, monomeric reagents, etc.) on the microwave absorption characteristics of the synthetic rubber. Their results demonstrated that microwave absorptivity could be effectively controlled by judicous selection of the compounding ingredients. Indeed, several synthetic rubber formulations were cured quickly and efficiently, giving mechanical and electrical properties equivalent to those obtained by traditional curing techniques [45-47].

## 2.1.1.5. Microwave Heat-Drawing

Another unique application of microwave processing employs electromagnetic radiation heating in combination with tensile drawing to orient semicrystalline polymers. The experimental apparatus utilized with this technique is depicted schematically in Figure 7. Unoriented semicrystalline polymeric tapes are drawn through a circular microwave waveguide at a specific strain rate and electric field strength at ambient temperature. Nakagawa [51-59] et al. have studied several different homo- and copolymers subjected to microwave heat-drawing including: poly(oxymethylene) [51-57], poly(ethylene terephthalate) [58], poly(vinyl alcohol) and ethylene-vinyl alcohol copolymers [59] and poly(ethylene terephthalate-co-p-oxybenzoate) [58]. The results of these investigations have shown that ultra high-modulus polymers are generated in comparison to traditional drawing techniques (e.g., tensile drawing, hydrostatic extrusion and die drawing). For instance, microwave heat-drawing of poly(oxymethylene) has resulted in a Young's modulus of 60 GPa; this value is approximately double the modulus value achievable with traditional orienting techniques. Nakagawa et al. suggested the ultra high-moduli generated with microwave heat-drawing is because the fact that the applied tensile stress is more effective at orienting the molecular chains in the amorphous regions of the polymers, since these regions are preferentially heated over the crystalline regions during microwave irradiation [56,57].

## 2.1.1.6. Radical Polymerizations

Gourdenne [60-62] et al. have demonstrated that vinyl monomers possessing sufficient polarity may be polymerized using electromagnetic radiation heating. Both 2-hydroxyethyl
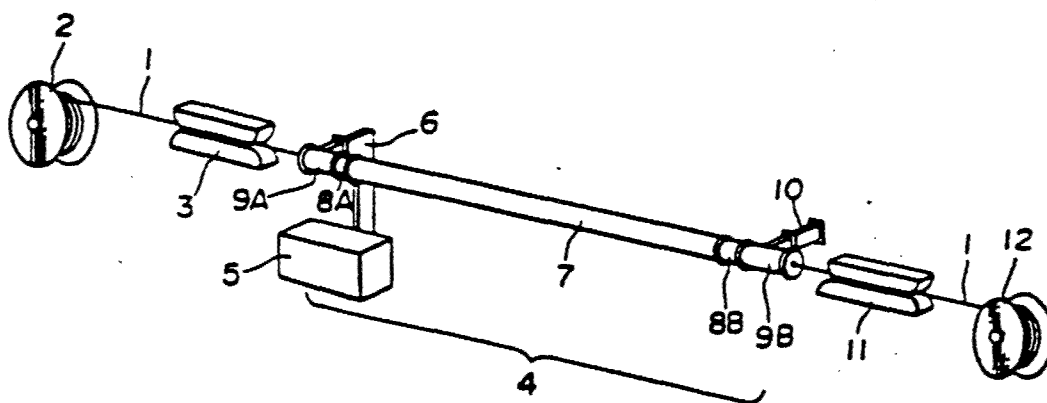
**Figure 7.** Apparatus for drawing under microwave heating: (1) drawing
sample, (2) feed reel, (3) belt feeder, (4) microwave
heating apparatus, (5) microwave power source, (6) rect-
angular waveguide for jointing, (7) circular waveguide for
microwave heating, (8A, 8B, 9A and 9B) circular waveguides
for impedance matching, (10) dummy load, (11) belt take-up
machine, and (12) take-up reel [51].

methacrylate [60,61] and mixtures of unsaturated polyesters/styrene [61,62] have been reported to undergo free radical reactions in bulk without initiators using microwave processing. Polymerization was attributed to thermal activation of unsaturated sites and not to bond cleavage from microwave irradiation.

## 2.1.1.7. Imidization Reactions

Lewis [63-64] et al. have demonstrated that polyamic acids based on 3,3'-diaminodiphenylsulfone (3,3'-DDS) and benzophenone tetracarboxylic dianhydride (BTDA) may be imidized from N-methylpyrrolidinone/cyclohexylpyrrolidinone solutions utilizing microwave radiation as depicted in Figure 8. In fact, kinetic studies from FTIR experiments demonstrated that the reaction rate was accelerated 20 to 34-fold compared with thermal reactions at equivalent temperatures. Furthermore, the activation energy, generated from an Arrhenius plot (Figure 9), was found to be reduced from $105 \pm 14$ kJ mole$^{-1}$ to $57 \pm 5$ kJ mole$^{-1}$ when microwave radiation was employed [63,64].

Rather than a true reduction in the activation energy, Lewis et al. proposed that the "effective temperature" of the dipole moments, which couple with the electromagnetic field, was higher than the bulk temperature measured by the fiber optic temperature sensor. By comparing the reaction rate constants for the microwave and thermal reactions and assuming the activation energy to be the same for both cases, the temperature enhancement at the reactive dipoles was calculated to be approximately 50°C [63,64]. This postulate provides a possible explanation for the accelerated reaction rates observed with continuous microwave radiation.

## 2.1.2. Polymeric Networks
## 2.1.2.1. Toughened Epoxy Resin Networks

Epoxy resins are currently used in structural applications as high performance adhesives and composite matrix resins in both the aerospace and electronic industries. In the cured state, epoxy resins are highly crosslinked, amorphous thermoset polymers which possess excellent thermal and dimensional stability, high modulus and strength, and outstanding adhesive properties [73,74]. However, these materials are also relatively brittle. Several methods have been proposed to increase the toughness of epoxy resins, the most common of which involves modification with a second phase component [75,76].

Typically, epoxy resins are modified with functionalized rubbers, such as carboxyl-terminated butadiene-acrylonitrile copolymers (CTBN). When incorporated into epoxy resins, CTBN produces a two phase morphology consisting of relatively small (~0.1 to 1 μm) rubbery particles dispersed in, and bonded to, an epoxy matrix. The toughness of modified epoxy resin networks is dependent on the properties of the original epoxy, the particle size, particle volume fraction, interfacial bonding, and the properties of the elastomeric component [77].

A major drawback to toughening epoxy resins with rubbers, such as CTBN, is that the increased toughness can only be achieved at the expense of high temperature performance. Because of the low glass transition temperature of the rubbery phase, rubber modification often lowers both the use temperature and modulus of the resulting network. This limitation has been recently overcome with thermoplastic modification [78-93]. Thermoplastic modifiers are tough, ductile engineering polymers possessing high glass transition temperatures. The degree of toughening obtained in these systems may appear to be relatively modest compared to a CTBN modified network; however, the enhanced toughness is achieved without sacrificing the high-modulus or thermal stability of the network.

Selection of a suitable modifier is crucial since its compatibility with the epoxy determines the extent and type of phase separation. The CTBN modifier, for instance, is ideal since it initially forms a homogeneous mixture with the epoxy resin before undergoing an *in situ* phase separation process during network formation. Compatibility of the CTBN modifier can be controlled by
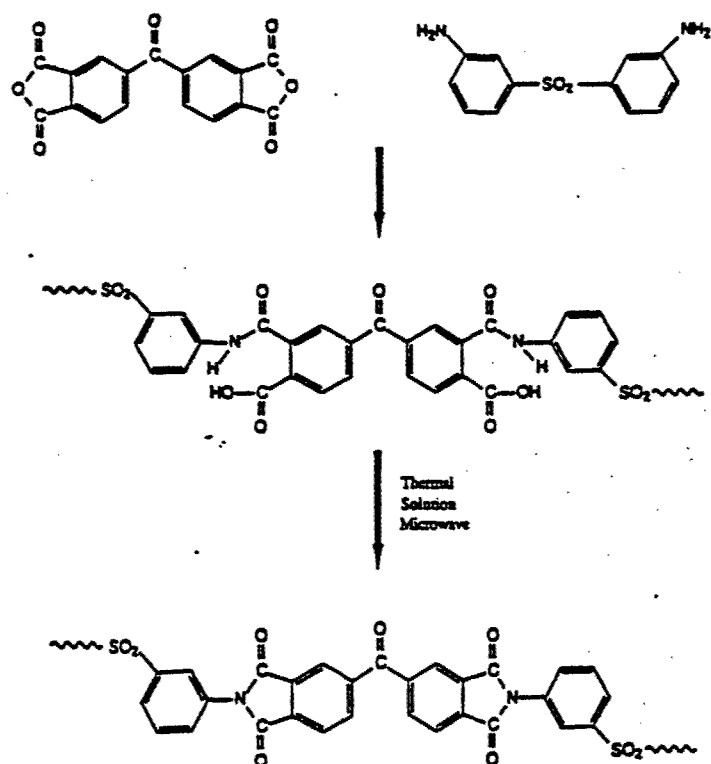
Figure 8. Reaction scheme depicting the conversion of a polyamic acid into a polyimide [64].
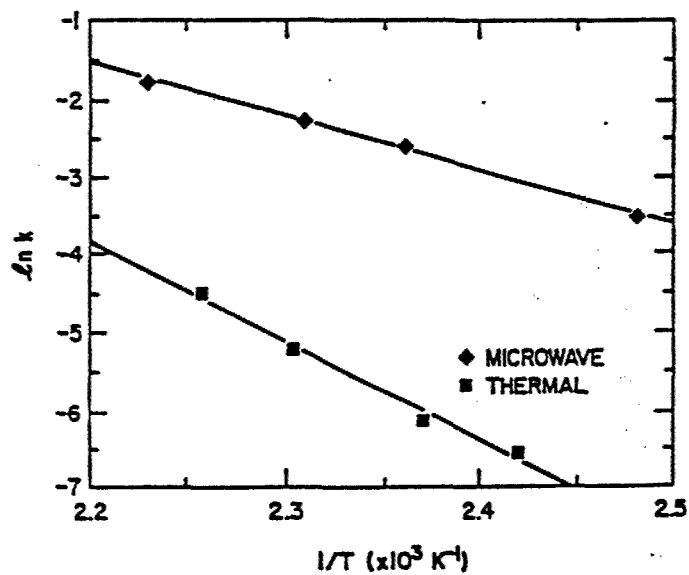


Figure 9. Arrhenius plot for the microwave and thermally induced imidization reactions [64].

varying the acrylonitrile content. CTBN modifiers of higher acrylonitrile content possess a higher polarity and are more compatible with epoxy resins; thus, precipitation is achieved at a later stage of cure to produce smaller phase separated domains [94].

In general, the phase separation behavior in modified epoxy resin networks is controlled by the competing effects of thermodynamics, kinetics, and polymerization rate [94]. In a typical polymer blend, thermodynamics can be utilized to make predictions about the equilibrium state of a binary mixture; however, kinetic factors must also be considered since equilibrium can only be achieved if sufficient time for diffusion is allowed. For thermosetting systems, further complications exist because both molecular weight and viscosity increase with increasing conversion of the epoxy resin network. Once the development of the network structure reaches the stage of gelation, phase separation is halted and the morphology is fixed. Thus, from a single rubber- or thermoplastic-modified epoxy resin formulation a variety of different phase-separated morphologies can be generated by accelerating the approach to the gel point and halting morphological development before complete phase separation [94,96].

### 2.1.2.1.1. Polymer-Polymer Miscibility

Two materials are considered miscible if they exhibit single-phase behavior (i.e., a single glass transition temperature) upon blending. In order for two materials to be miscible two thermodynamic criteria must be met. The first is that the Gibbs free energy of mixing, $\Delta G_m$, must be negative, that is,

$$\Delta G_m = \Delta H_m - T\Delta S_m < 0 \tag{3}$$

where $\Delta H_m$ is the enthalpy of mixing, $\Delta S_m$ is the entropy of mixing and $T$ is absolute temperature. The second condition is

$$\frac{\delta^2 \Delta G_m}{\delta \phi_2^2}\bigg|_{P,T} > 0 \tag{4}$$

where $\phi 2$ is the volume fraction of component 2 [97-106]. Figure 10 demonstrates three possible ways in which the free energy of mixing, $\Delta G_m$, may vary with composition. Curve A represents an immiscible mixture since $\Delta G_m$ is always positive, and the first thermodynamic condition is not satisfied. Complete miscibility is obtained in curve B since both thermodynamic conditions are satisfied at all compositions. Curve C represents a situation where partial miscibility is achieved. A miscibility gap exists because the second thermodynamic condition (Equation 4) is not satisfied over certain compositional ranges [104].

Phase separation behavior can be better understood by simultaneously examining the dependence of free energy of mixing and temperature on composition as shown in Figure 11 [97]. The lower diagram in Figure 11 is the same as curve C in Figure 10. The two minima in this curve occurring at compositions $\phi B$ and $\phi B'$ represent the most thermodynamically stable compositions for the mixture at $T_1$. Also labeled are compositions $\phi S$ and $\phi S'$ which intersect the $\Delta G_m$ versus composition plot at the two points of inflection; these compositions may be thermodynamically defined as:

$$\frac{\delta^2 \Delta G_m}{\delta \phi_2^2}\bigg|_{T,P} = 0 \tag{5}$$

13
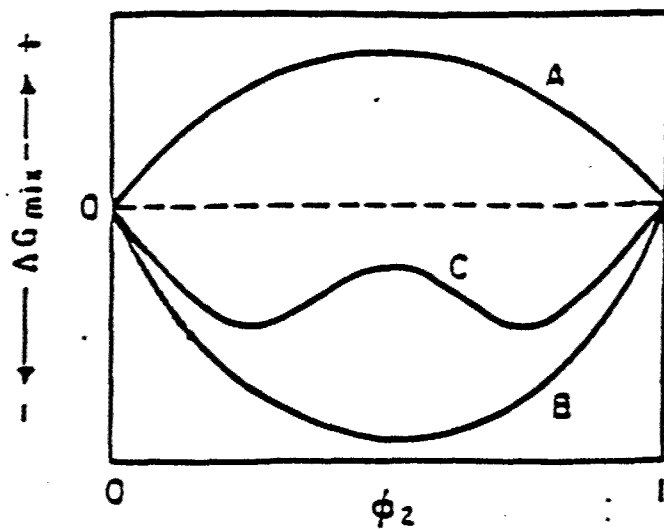
Figure 10. Free energy of mixing for binary mixtures which are completely immiscible (A), completely miscible (B), and partially miscible (C) [104].
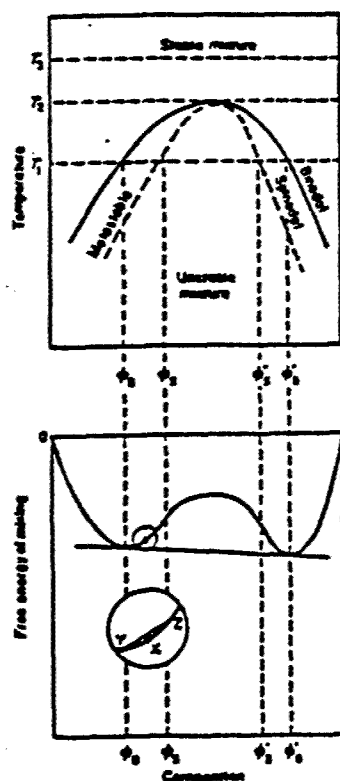


Figure 11. Phase diagram for a binary mixture exhibiting upper critical solution temperature (UCST) behavior [97].

14

Between $\phi S$ and $\phi S'$ at $T_1$, the second thermodynamic condition for miscibility (Equation 4) is not satisfied and the system is unstable. Concentration fluctuations in this region give rise to negative free energy changes, thus phase separation can take place spontaneously by spinodal decomposition. Spinodal decomposition is a kinetic process involving the generation of a highly interconnected phase-separated structure through the spontaneous and continuous growth of a phase within an unstable mother phase. The growth originates, not from nuclei, but from small amplitude composition fluctuations which are always present in the equilibrium state [98,99].

Between the point of inflection (spinodal point) and tangential point (binodal point) in the lower diagram of Figure 11, a metastable compositional region exists. This region of metastability between $\phi B$ and $\phi S$ and between $\phi B'$ and $\phi S'$ arises from any small composition fluctuation that produces an increase in free energy which acts as a barrier to phase separation. This is illustrated in the inset of Figure 11; if composition X phase separates to a mixture of Y and Z then the average free energy will be higher. If phase separation takes place in the metastable regions, it can only occur by a process of nucleation and growth [97].

The upper portion of Figure 11 represents a phase diagram for polymer-polymer mixtures exhibiting upper critical solution temperature (UCST) behavior. Most high molecular weight polymers and thermosets, however, exhibit lower critical solution temperature (LCST) since they are typically less miscible at higher temperatures or conversions. A phase diagram is created by plotting a series of $\Delta Gm$ versus $\phi_2$ curves as a function of temperature for blends or conversion for networks. It provides a very useful map to predict the presence and type of phase separation as a function of temperature and composition in a binary mixture [97-104]. There are several regions of importance in the phase diagram. The critical temperature, $T_c$, occurs at the intersection of the binodal and spinodal curves and can be determined from the expression:

$$\frac{\delta^3 \Delta G_m}{\delta \phi_2{}^3} \bigg|_{T,P} = O \tag{6}$$

Since the phase diagram in Figure 11 demonstrates UCST behavior, above $T_c$ the system is miscible in all proportions [98].

The spinodal curve in the phase diagram of Figure 11 defines the position where spontaneous phase separation (spinodal decomposition) occurs. The binodal curve defines another region of phase separation commonly referred to as nucleation and growth. The area between the binodal and spinodal curves represents the metastable region of temperature and composition where only nucleation and growth occur. Generally with UCST behavior, as temperature is lowered, phase separation occurs by nucleation and growth mechanisms unless the critical point is traversed or the nucleation and growth region is rapidly crossed to reach the spinodal region [98-104]. An example of this is a thermoplastic blend at temperature $T_3$ (Figure 11) which is rapidly quenched into the spinodal region. In an analgous manner, if the temperature axis of Figure 11 is replaced with conversion and LCST behavior is assumed, a thermoset system can be quenched by accelerating the approach to the gel point.

## 2.1.2.1.2. Flory-Huggins Equation

In modified thermosets the enhanced toughness is related to the morphology of the cured network [77]. In most rubber- or thermoplastic-toughened epoxy resin systems the modifier initially forms a homogeneous mixture with the uncured epoxy resin before undergoing an in situ phase separation process during network formation. Demixing of the homogeneous binary mixture occurs when the Gibbs free energy changes sign, from negative to positive, as molecular weight increases with conversion of the network structure. Analysis of the Flory-Huggins equation provides an explanation for this demixing process [106].

The Flory-Huggins equation for the Gibbs free energy of mixing states:

$$\Delta G_m = V(\delta_1 - \delta_2)^2 \phi_1 \phi_2 + RT[(\phi_1/i_1)\ln \phi_1 + (\phi_2/i_2)\ln \phi_2] \tag{7}$$

where V is the molar volume, $\delta_1$ and $\delta_2$ are the solubility parameters of the two components, $\phi_1$ and $\phi_2$ are the volume fractions, and $i_1$ and $i_2$ are the respective degrees of polymerization. By definition the Flory-Huggins equation only predicts UCST behavior; thus the left hand term in Equation 7, representing the enthalpy of mixing, $\Delta H_m$, is always positive. The magnitude of this term is controlled by the differences in the solubility parameters squared, $(\delta_1 - \delta_2)^2$. Using the Hildebrand approach, this term approximates the Flory-Huggins interaction parameter, $x_{12}$. The $x_{12}$ parameter is related to the enthalpy of interaction between the two components comprising the binary mixture. It is a function of temperature, composition, and molecular weight. Since the miscibility of most polymer mixtures is determined by enthalpic effects, the $x_{12}$ parameter strongly influences the type and degree of phase separation [98]. As polymerization progresses during a thermoset reaction $\Delta H_m$ is relatively uneffected, except for free volume effects which are small in comparison to the entropic contribution [97-106].

The entropic effect of mixing two components is represented by the right-hand term in Equation 7, which is always negative since $\Delta S_m$ is positive. As molecular weight and thus the degree of polymerization, i, increase the magnitude of the negative entropic contribution to $\Delta G_m$ decreases. This results in a removal of the entropic driving force for miscibility and results in demixing and phase separation [97-106].

### 2.1.2.1.3. Time-Temperature-Transformation Diagram

During an isothermal cure of a thermosetting system there are two phenomena of critical importance that can occur: gelation and vitrification. Gelation generally occurs first and is characterized by the formation of a material of infinite molecular weight. The gel point can be calculated as a function of the reactivity, functionality, and stoichiometry of the reactants. Prior to gelation, the system is soluble and fusible; however, after gelation the polymer does not flow and is no longer processable. Vitrification occurs when the glass transition temperature of the growing polymer coincides with the cure temperature. At vitrification the system is transformed from a viscous liquid or elastic gel to a glass. Further curing in the glassy state is extremely slow since the reaction shifts from chemical control to diffusion control; thus, for all practical purposes, vitrification brings an abrupt halt to curing. However, vitrification is a reversible transition; therefore,reheating above the Tg devitrifies the partially cured thermoset and allows for further curing of the network [107-109].

Using torsional braid analysis (TBA), Gillham [107-109] has modeled these phenomena with an isothermal time-temperature-transformation (TTT) cure diagram. A TTT diagram, shown schematically in Figure 12, is a plot of the isothermal cure temperature ($T_{cure}$) versus the times to gelation and vitrification. The diagram displays the different states encountered in the thermosetting process. These states include liquid, sol/gel rubber, gel rubber, ungelled glass, gelled glass, and char. Three critical temperatures are also shown: $T_{go}$, gel $T_g$, and $T_{g\infty}$. $T_{go}$ is the glass transition temperature of the uncured reactants. Below Tgo no significant reaction of the uncured resin mixture occurs. The point at which gelation and vitrification occur simultaneously is known as gel $T_g$. Between $T_{go}$ and gel $T_g$ the system vitrifies before gelling, thus quenching the chemical reaction. However, when curing between gel $T_g$ and $T_{g\infty}$ (i.e., the minimum cure temperature required to achieve complete cure), gelation precedes vitrification and the material, initially a liquid, reacts to form a crosslinked rubbery network. This crosslinked rubbery network consisting of finite molecular weight sol fraction and infinite molecular weight gel fraction reacts until the Tg of the system reaches the cure temperature. At this point vitrification occurs and further chemical reaction is halted [107-109].
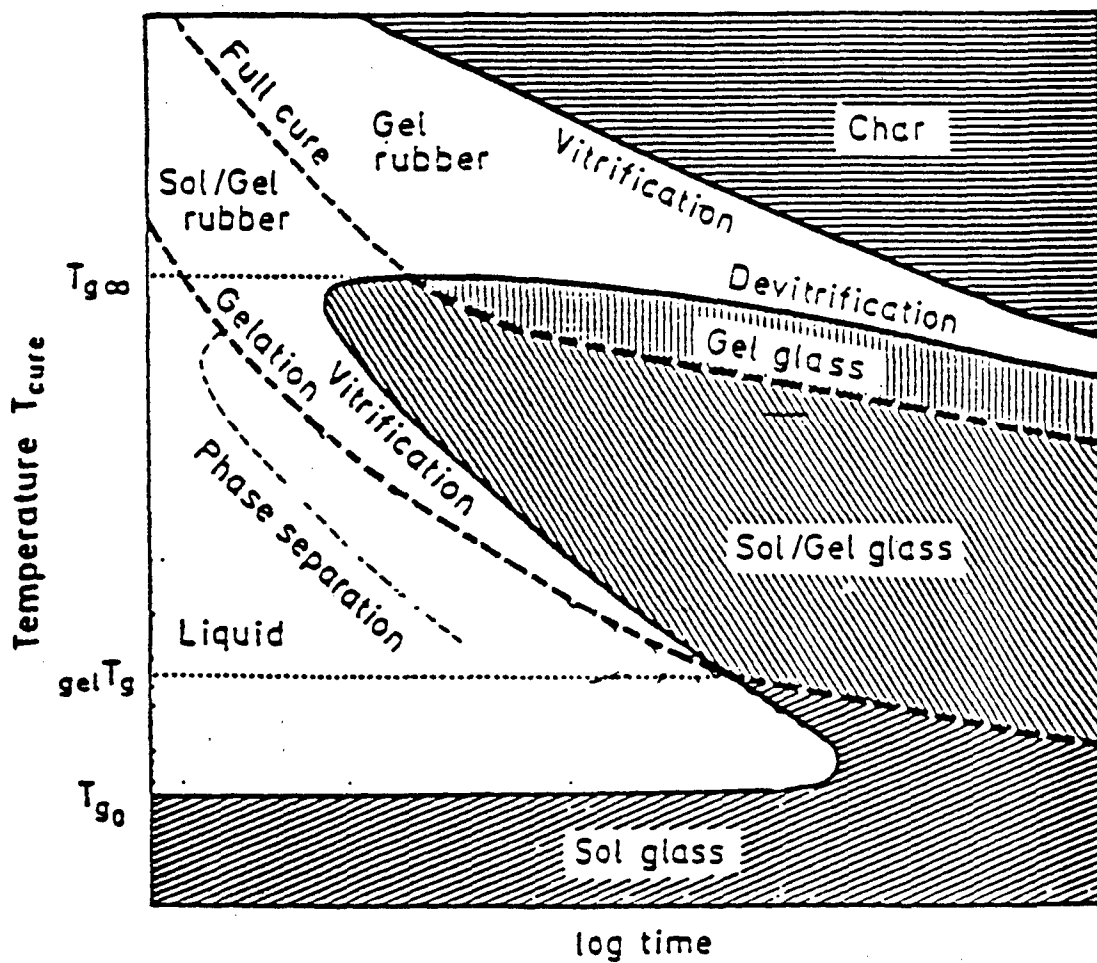
**Figure 12.** Time-temperature-transformation (TTT) isothermal cure diagram for thermosetting polymeric systems [107].

17

The full cure line shown in Figure 12 indicates the time required at any given cure temperature, for the $T_g$ to equal $T_{g\infty}$. In the absence of full cure, the vitrified region formed between gel $T_g$ and $T_{g\infty}$ contains both soluble and insoluble fractions. For systems where $T_{g\infty}$ can be attained in the absence of degradation, curing above $T_{g\infty}$ is the most direct method for achieving full cure. However, for high $T_g$ systems, where curing above $T_{g\infty}$ would lead to thermal degradation, the full cure line provides an alternative method for achieving complete cure [107-109].

The TTT diagram can be extended to include phase separation, viscosity, thermal degradation, and extent of conversion. The generalized TTT diagram in Figure 12 has been extrapolated to take into account phase separation by combining the TBA results with cloud point observations from a rubber-modified thermoset. The cloud point results predict the onset of phase separation while the gelation line predicts the end of phase separation, thus providing a "window of phase separation" on the TTT diagram [107].

The time-temperature-transformation diagram has great utility in commercial applications. The TTT diagram plays a very important role in composite prepregging applications where the time-temperature paths of cure necessary to achieve appropriate viscosity levels for good tack and drape are extremely important. It is also employed with high Tg epoxy resin compositions so that cure cycles can be developed to control shrinkage and degradation. In conclusion, the TTT diagram permits time-temperature paths of cure to be chosen so that gelation, vitrification, and phase separation occur in a controlled manner, hence producing reproducible and predictable material properties in thermosetting systems [107-109].


## 2.1.2.1.4. Toughening Mechanisms in Rubber-Modified Epoxy Resin Thermosets

A great deal of controversy exists on the nature of the toughening mechanisms in modified epoxy resin networks. Much of the dispute is centered around whether the modifier or the matrix absorbs most of the fracture energy, and whether the matrix undergoes crazing, void formation or shear yield deformation. The issue is extremely important because once the mechanisms responsible for increased toughness are clearly identified, then design parameters can be modified to optimize properties and performance [110-111].

In general, the deformation of glassy polymers can be divided into two categories: elastic and plastic deformation. Elastic deformation is recoverable in a finite time while plastic deformation, which takes into account shear yielding, crazing, and void formation, is irrecoverable [75,76].

The appearance of what seems to be small microcracks in stressed thermoplastics such as polystyrene or high-impact polystyrene (HIPS) is known as crazing. Crazes are voids in plastically deformed polymers which when sufficiently stressed can create a crack and lead to fracture. Crazes usually grow normal to the direction of the applied tensile stress and reflect light; this explains the stress-whitening observed in HIPS and other plastically deformed thermoplastics. Unlike cracks, however, crazes are load-bearing entities that are due to the web of stretched microfibrils that span the space between the walls of what would otherwise be called cracks. As a result of this ability to bear a substantial load, a craze growing adjacent to another will pass by as though the other were not there. In contrast, a crack tends to veer and terminate perpendicular into the neighboring crack, eventually leading to failure [112-114].

Shear yielding is another form of plastic deformation which includes both diffuse shear yielding and localized shear band formation. It occurs under an applied stress when the material is restrained in two dimensions. In contrast to crazing, shear deformation consists of a change of shape without significant change of volume. Shear yielding is a very important deformation mechanism for two reasons. First, it is the factor which limits the strength of the polymer if brittle fracture can be suppressed. Second, under plane strain conditions where brittle fracture is prevalent, shear yielding in the form of localized shear band formation is the major energy dissipative process in the vicinity of the crack tip; it blunts the sharp crack and increases toughness [75,76,113].

A typical representation of a shear band is shown in Figure 13. Shear bands are thin planar regions of high shear strain. They are initiated in regions where there are inhomogeneities of strain because of internal or surface flaws, or to stress concentrations. The slip plane, usually less than 1 μm in thickness, occurs at a 45° angle to the perpendicular of the applied tensile stress on a plane of maximum shear stress [75,113].

Several mechanisms have been proposed to account for the increased toughness observed in rubber-toughened epoxy resin networks. These mechanisms include: crazing, shear yielding and crazing, rubber tearing, and voiding and shear yielding. Sultan and McGarry [115] investigated the behavior of CTBN modified epoxy resin networks under a biaxial stress field and have proposed microcavitation at the crack tip, which they identified as crazing, to be the principal toughening mechanism. McGarry et al. [115] supported these results with observations of stress-whitening and decreased macroscopic density from volume dilation measurements.

Riew et al. [77] supported the conclusions of Sultan and McGarry in their investigations of CTBN modified epoxy resin thermosets. In fact, Riew et al. further proposed that: shear deformations are dominant in networks toughened with small rubber particles (<0.5 μm); crazing is dominant in networks toughened with large rubber particles (1-5 μm); and, maximum toughening is obtained under conditions of combined shear and craze deformations when both large and small particles are present in the network.

Using tensile creep dilatometry, Bucknall et al. [75,106] found that in rubber-modified epoxies volume strain and toughness increased with rubber content. Assuming that shear flow creates no volume change, Bucknall et al. attributed the volume strain to crazing and proposed, as did Riew et al., that massive crazing and shear flow are the two energy absorbing mechanisms in rubber-modified plastics.

The existence of crazing in highly crosslinked materials, such as epoxy resin networks, is currently under much debate. Other investigators [110,111] have found that volume dilation cannot be unambiguously and exclusively attributed to crazing since void formation can also cause volume dilation. Recent theoretical studies by Donald and Kramer [116] have shown that in glassy thermoplastics there is a transition from crazing to a shear yielding mechanism as the length of the polymer chain between physical entanglements decreases. Kinloch et al. [111] suggested that crazing in epoxy resins is questionable because thermosets possess high crosslink density and therefore short chain lengths between crosslinks, which would inhibit craze deformation. In summary, the investigations discussed above do not provide conclusive evidence that crazing is a major toughening mechanism in modified epoxy resin networks.

A theory which attributes the toughening solely to the rubber particles was proposed by Kunz et al. [117,118] in 1981. This theory, better known as the crack-bridging theory, suggests as shown in Figure 14 that the crack advances through the rubber particles so that as the crack opens, the particles are stretched between the crack surfaces, and eventually tear before the crack can extend further. It is proposed that the particle is entirely responsible for the enhanced toughness of rubber-modified epoxy resin networks. Several studies [117-119] have demonstrated some evidence supporting this theory; however, numerous inconsistencies between this theory and experimental observations still exist. The crack-bridging theory cannot explain stress-whitening or the large amount of plastic deformation that occurs in the epoxy resin phase. Furthermore, this theory cannot theoretically account for the high fracture toughness values achieved in rubber-modified epoxy resins based solely on the tear energy of the rubber particles [111]. Hence, while the rubber tear mechanism may make a contribution to the toughening effect, it is probably not the major toughening mechanism in highly toughened epoxy resin systems [110,111].

Bascom et al. [120,121] and Hunston et al. [122] proposed that the mechanism of rubber toughening involves plastic flow combined with dilation and void formation in either the particles or at the particle-matrix interface. They hypothesized that cavitation of the rubbery particles caused by the triaxial tension ahead of the crack tip increases the size of the plastic zone, thus blunting the sharp crack. Furthermore, they proposed that both shear yielding of the epoxy matrix and elongation of the rubber particles significantly contribute to toughening. Kinloch et al. [111] presented TEM and SEM micrographs which support the findings of Bascom et al. and Hunston et al. The micrographs demonstrate that both cavitation and plastic shear yielding are the
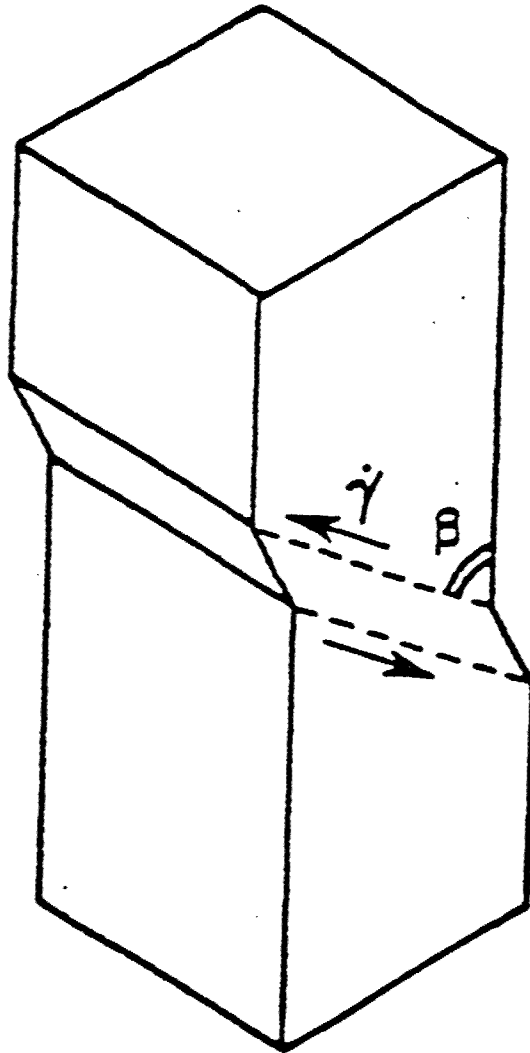
Figure 13. Schematic representation of shear band formation [113].
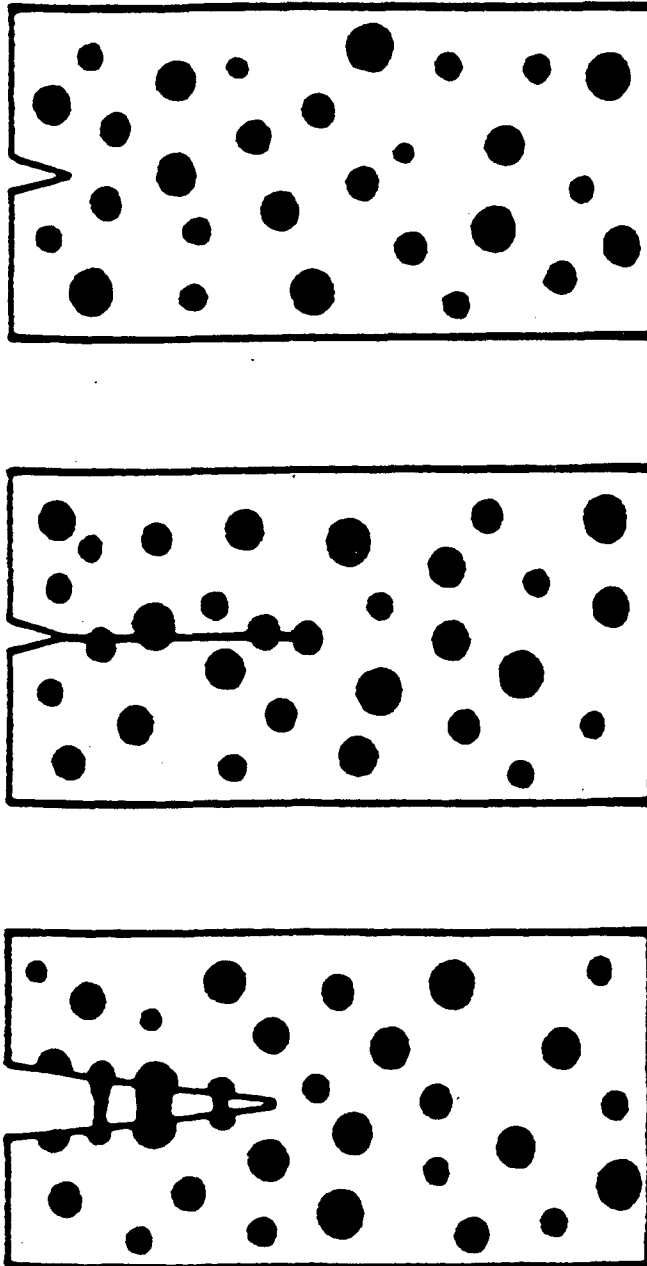
Figure 14.   Crack-bridging model proposed by Kunz et al. [117].

microdeformation mechanisms occuring in the vicinity of the crack tip that dissipate energy and produce the toughening effect. Kinloch et al., however, proposed that the main source of energy dissipation in this mechanism is the plastic shear yielding of the epoxy resin matrix.

Recently, Yee and Pearson [110] provided further evidence for the mechanism proposed by Bascom et al. and Hunston et al. Using optical microscopy of thin sections of a rubber-toughened epoxy perpendicular to the fracture surface, they were able to discern that cavitation of the particles occurred prior to shear yielding in the matrix. Yee et al. [110] proposed that the toughening effect is achieved as the rubber particles cavitate and subsequently promote shear deformation, thus creating a large plastic zone and blunting the sharp crack as demonstrated schematically in Figure 15.

In general, it is accepted by most workers in the field that deformation in the matrix resin is the major energy absorbing mechanism in rubber- toughened thermosets. Thus, the ability of the matrix to undergo plastic deformation should be directly related to the amount of energy it can dissipate. Currently, many investigators [123-125] are studying the effect of matrix crosslink density on toughness enhancement in rubber-modified thermosets.

Yee and Pearson [123] investigated the variation of matrix crosslink density in a series of CTBN modified diglycidyl ether of bisphenol A (DGEBA) based epoxies utilizing diaminodiphenylsulfone (DDS) as a curing agent. Variation in the molecular weight between crosslinks $\overline{M_c}$ was achieved by employing DGEBA resins which ranged in epoxide equivalent weight from 174 to 1800 grams per equivalent. The dependence of fracture toughness upon monomer (DGEBA) molecular weight in both the modified (10 weight percent CTBN) and neat resin networks is shown in Figure 16. This plot demonstrated that the fracture toughness increased dramatically with increasing monomer molecular weight in the modified networks; however, only modest increases were observed for the neat resin networks. Yee et al. [123] attributed the significant increases in toughness in the modified networks to an enhancement of the process zone in front of the crack tip which effectively blunts the sharp crack and increases the fracture energy. Furthermore, Yee et al. [123] proposed that the ability weight between crosslinks with increasing monomer molecular weight.

Kinloch et al. [124] also investigated the fracture behavior of rubber-modified epoxy resins as a function of increasing molecular weight between crosslinks $\overline{M_c}$ in the epoxy matrix phase. By employing different cure schedules they demonstrated that the degree of crosslinking and thus $\overline{M_c}$ could be changed without significantly altering the morphology of the resulting network. The molecular weight between crosslinks, determined from the equilibrium rubbery modulus by DMA, was varied from ~600 g/mole to 5000 g/mole. Fracture toughness results demonstrated substantial (two-fold) increases in both the unmodified and modified networks as $\overline{M_c}$ was increased from ~600 g/mole to 5000 g/mole. Kinloch et al. [124] attributed the enhanced toughness to the ability of the epoxy matrix to undergo plastic deformation, because of the increased ductility obtained with a greater chain length between crosslinks.

In both of these investigations, where $\overline{M_c}$ was increased either by choice of epoxide or curing schedule, there was a corresponding reduction in the $T_g$ of the network, thus effectively raising the test temperature relative to $T_g$. In order to attribute fracture toughness solely to $\overline{M_c}$, measurements at temperatures relative to $T_g$ are necessary to isolate the $\overline{M_c}$ effect. These types of measurements are currently being conducted by Yee; however, the results have not been published yet.

## 2.1.2.1.5. Thermoplastic Modification of Epoxy Resin Networks

Numerous engineering thermoplastics have been employed to toughen epoxy resin networks over the past decade. The actual toughening mechanism involved with thermoplastic modification is greatly debated. The proposals which have been put forward are often conflicting. Some investigators proposed no increase in toughness with thermoplastic modification [84,85] while others reported a linear increase in fracture toughness with increasing thermoplastic content,

22
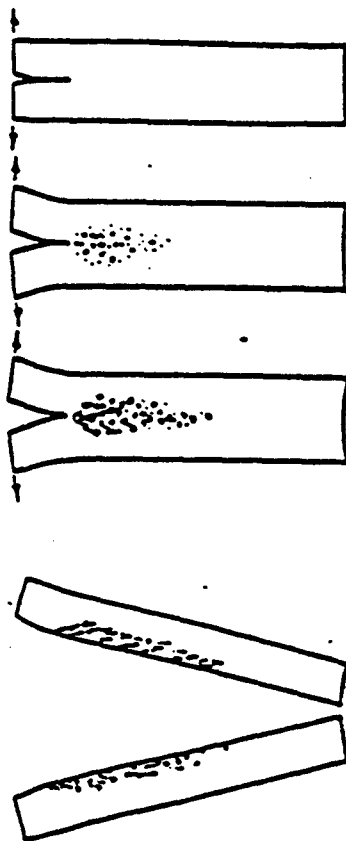
Figure 15.  Toughening mechanism in rubber-toughened epoxies proposed by Yee and Pearson [110].
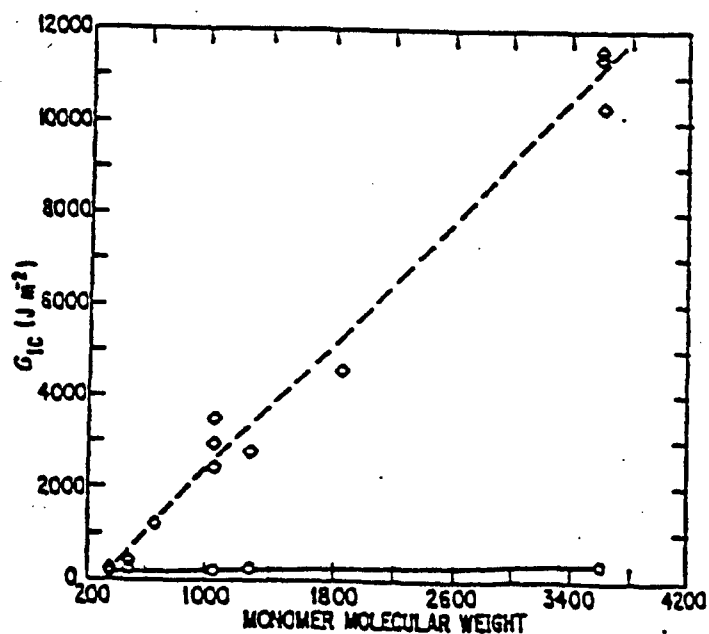


Figure 16.  Plot of fracture toughness ($G_{Ic}$) versus increasing DGEBA equivalent weight demonstrating the effect of $<M_c>$ (matrix) on toughness in both rubber modified ( ) and neat (o) epoxy resin networks [123].

23

independent of morphology [86,90], and even others suggested a maximum in toughness at intermediate compositions resulting from a co-continuous morphology [87,88].

The first reports in the literature concerning the utilization of thermoplastics to toughen epoxy resins appeared in the early 1980's. Raghava [84] and Bucknall [85] both employed polyethersulfone (PES), Vitrex 100P (ICI), as a toughening agent in epoxy resins and observed no increase in the fracture toughness of the corresponding networks. Bucknall et al. [85], however, conclusively demonstrated the existence of phase separation in this system by dynamic mechanical analysis (DMA) and scanning electron microscopy (SEM). They also showed that the type and stoichiometry of the resin and curing agent strongly influenced the resulting morphology of the PES modified system. In a later publication, Raghava attributed the lack of toughening in the modified networks to poor adhesion between the phase separated components.

One of the first reported studies in the open literature of chemically reacting a thermoplastic polymer into an epoxy resin network was reported by J. L. Hedrick et al. [78,79]. In this investigation a phenolic hydroxyl terminated bisphenol-A polysulfone (PSF) was incorporated into an epoxy resin system based on Epon 828 and diaminodiphenylsulfone (DDS). The PSF was pre-reacted with a large excess of the epoxy resin using a quaternary ammonium catalyst to functionalize the PSF oligomers with epoxide groups prior to the addition of the curing agent. The concentration and molecular weight of the PSF modifier was varied to investigate their effect on the properties of the resulting networks. Mechanical property results demonstrated that the fracture toughness ($K_{Ic}$) of the cured networks increased substantially (from 0.6 to 1.7 $Nm^{-3/2}$) when both the concentration and the molecular weight of the PSF modifier were increased. Furthermore, the fracture toughness increased without significantly decreasing the modulus, thermal stability or solvent resistance of the resulting network.

Hedrick et al. [78-80] also investigated the morphology of the polysulfone-toughened epoxies with scanning electron microscopy. At low weight percent incorporations (10% to 15%), the polysulfone modifier phase separated into a well defined, two-phase morphology consisting of a relatively homogeneous distribution of PSF spheres in the epoxy resin matrix. As the concentration of the PSF was increased (20% to 30%) a phase inversion resulted; and, the morphology consisted of a continuous polysulfone matrix surrounding discrete spheres of epoxy resin.

Chu and Jabloner [89] patented the thermoplastic modification of epoxy resin networks in 1986. They demonstrated that epoxy resin networks could be effectively toughened with amino functionalized thermoplastics (polyethers, polysulfones or polyethersulfones) possessing molecular weights in the range of 2,000 to 10,000 g/mole and glass transition temperatures between 125°C and 250°C. Multiphase morphologies were observed along with significant enhancements in fracture toughness; however, no toughening mechanisms were proposed.

Brown and Kim [93] utilized SEM, DMA, and optical microscopy to investigate the morphology and toughening mechanisms in the commercially available Hercules thermoplastic-modified epoxy resin system. The morphological development in these materials was observed to be similar to that found in rubber-toughened materials with a phase inversion occurring at a composition between 10% and 30% of the modifier. Fracture toughness, however, exhibited a continuous change as a function of oligomer content despite morphological changes. Brown et al. attributed this to different toughening mechanisms which operate at different compositions. They proposed that at low weight percent incorporations (10%) of the modifier where the morphology consists of a continuous epoxy matrix with discrete PSF spheres dispersed within, the toughening mechanism involved localized yielding in the epoxy matrix initiated upon the deformation of the discrete modifier particles. At high weight percent incorporations (30%), above the phase inversion composition, the toughening mechanism was attributed to the ductile yielding of the oligomeric modifier phase (i.e., the continuous phase) [93].

Recently, Bucknall and Gilbert [90] demonstrated that polyetherimides (PEI) can also be utilized to effectively toughen epoxy resin networks. Fracture toughness results demonstrated a linear increase with increasing PEI incorporation up to 25 weight percent with only modest reductions in Young's modulus. The linear correlation between fracture toughness and increasing

modifier incorporation in thermoplastic-modified epoxy resin networks is greatly debated. McGrail et al. [87] and Recker et al. [88] proposed that an optimum morphology exists at intermediate compositions where a maximum in fracture toughness is achieved.

McGrail and co-workers [87] proposed that the co-continuous morphology, characteristic of spinodal decomposition, results in enhanced fracture toughness in polyethersulfone-toughened thermosets. Furthermore, they observed that this morphology better translated the increased toughness into composite structures. They achieved spinodal decomposition in the thermoplastic-modified epoxy resin networks by systematically varying the backbone structure of the thermoplastic while holding other variables such as the cure schedule, molecular weight, and concentration of the modifier constant.

Recker and co-workers [88] investigated thermoplastic-modified epoxy neat resins and composite laminates to correlate fracture toughness with damage tolerance. Fracture toughness as measured by $G_{Ic}$ and $G_{IIc}$ was studied as a function of the modifier molecular weight and concentration. They discovered that $G_{Ic}$ was directly proportional to molecular weight up to a number average molecular weight of approximately 10,000 g/mole. Beyond 10,000 g/mole, toughness was found to be independent of molecular weight. They further reported that the toughness demonstrated a linear dependence on the modifier concentration except at intermediate concentrations (~25% by weight), where a maximum was observed. These results have generated great interest by other investigators to study morphological control in toughened thermosets.


2.1.2.1.6. Control of Phase Separation in Toughened Epoxy Resins

From a single rubber- or thermoplastic-modified epoxy resin formulation a variety of different phase separated morphologies can be achieved. The phase separation behavior in these systems is controlled by the competing effects of thermodynamics, kinetics, and polymerization rate [94-96,106]. As discussed previously (Section 2.1.2.1.1.), thermodynamics can be utilized to make predictions about the equilibrium state of the resin-modifier mixture; however, kinetic factors must also be considered since equilibrium can only be reached if sufficient time and diffusion exist. For thermosetting systems, further complications exist because both molecular weight and viscosity increase with increasing conversion of the network structure. Once the development of the network reaches the stage of gelation, phase separation is halted and the morphology is fixed [94-96].

Recently, many investigators have explored the effect of chemical composition of the modifier, the temperature of cure and the gelation time on the resulting morphology and mechanical properties of toughened epoxy resin networks. Gillham et al. [94] investigated the thermomechanical transitions and the extent of phase separation in CTBN modified epoxies as a function of the acrylonitrile content of the modifier and the temperature of cure. They demonstrated that as the acrylonitrile content in the CTBN modifier was increased the solubility parameter increased substantially because of the rise in polarity. At a constant rubber content of 10 parts per hundred rubber, the CTBN toughened networks exhibited a significant decrease in particle size with increasing acrylonitrile content because of enhanced compatibility.

The effect of increasing cure temperature was more complicated. As the isothermal cure temperature was varied, Gillham et al. [94] observed a maximum in the size of the phase separated particles at an intermediate cure temperature. They attributed this to the competition of thermodynamic and kinetic effects on the rate of nucleation and growth. At low temperatures, nucleation of the dispersed CTBN phase was favored thermodynamically but diffusion to nucleating sites was reduced because of the high viscosities and low temperatures. At high temperatures, the nucleation rate was low, but the low viscosity and high temperatures facilitated the diffusion.

Recently, Inoue and co-workers [126,127] modeled the phase separation behavior of both thermoplastic- and elastomeric-modified epoxy resins by utilizing curing agents of different reactivity. Inoue et al. achieved control of the morphology by accelerating the approach to the gel point, thus halting morphological development before complete phase separation. The proposed

25

model of phase separation is shown in Figure 17. Inoue [126, 127] et al. demonstrated that if morphological development was rapidly quenched the co-continuous morphology, characteristic of spinodal decomposition, was achieved, and if the system was cured at slower rates phase separation proceeded via a nucleation and growth mechanism, characteristic of binodal phase separation.

The results of both Gillham et al. [123] and Inone et al. correlate quite well with a theoretical model developed by Williams et al. [123]. The model was developed to predict the mean radius and volumetric concentration of the dispersed phase in a phase separated thermoset as a function of network conversion. The model also predicts the location of the binodal and spinodal curves on a phase diagram by analyzing of the Flory-Huggins equation (Section 2.1.2.1.3.) for the Gibbs free energy of mixing.

## 2.1.2.2. High Performance Thermosetting Polymeric Resins
### 2.1.2.2.1. Introduction

Recent advances in the aerospace and electronic industries have produced a continuing and growing demand for high performance polymeric materials. These polymers must possess excellent mechanical properties, solvent resistance, and dimensional stability over a wide temperature range. For instance, when polymers are employed as adhesives and composite matrix resins on high-speed aircraft, temperatures as high as 200°C are encountered at the wing fronts. Adhesives utilized in such applications must be designed to withstand these temperatures for thousands of hours without degredation or loss of performance. Furthermore, these polymers must possess solvent resistance to chlorinated solvents such as methylene chloride so that the aircraft can be painted, solvent stripped, etc. These requirements have led to the development of several heat-resistant thermosetting resins.

The most common high temperature thermosetting polymers commercially available, excluding the epoxy resin systems discussed previously, include bismaleimides, acetylene-terminated resins, and bisnadimides [128-131]. Bisbenzocyclobutenes and allylphenyl imide resins have recently received much attention in the open literature [132-136] but have not yet been commercially developed. A recurring theme in all of these resin systems is the ability to undergo homopolymerization. The polymerization usually proceeds via a free radical mechanism from terminal unsaturation.

## 2.1.2.2.2. Bismaleimides

Bismaleimides are one of several polymer classes under evaluation as matrix resins for high temperature fiber-reinforced composites. In 1964 Grundschober [137] first reported their thermally induced homo- and copolymerizations to yield highly crosslinked networks. Bismaleimide networks possess good physical properties, thermal stability, and processability, thus making them highly competitive with the conventional epoxy resin systems.

One of the major advantages of the bismaleimide system is its ability to undergo an addition polymerization with no volatile by-product formation at relatively low temperatures [128,131]. The proposed crosslinking mechanism proceeds via a free radical route as exemplified in Figure 18. Support for this mechanism has been provided by Brown et al. [138,139] using electron spin resonance (ESR) measurements and by Lind et al. [140] and Carduner et al. [141] using carbon 13 nuclear magnetic resonance (NMR). The high reactivity of the maleimide double bond is a consequence of the electron-withdrawing nature of the two adjacent imide carbonyl groups. Polymerization occurs just above the crystalline melting temperature of the bismaleimide monomer to form a highly crosslinked network. The curing rate can be accelerated by the addition of peroxides or anionic catalysts [142,143] or decreased by the addition of free radical inhibitors such as hydroquinone [144].

26
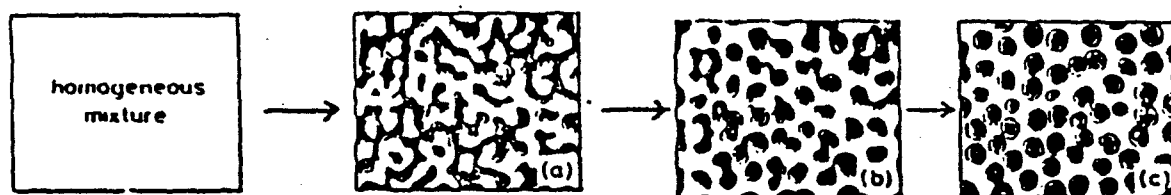
Figure 17.   Schematic representation of the stages of phase separation
in modified epoxy resin networks as modeled by Inoue et al.
[126].
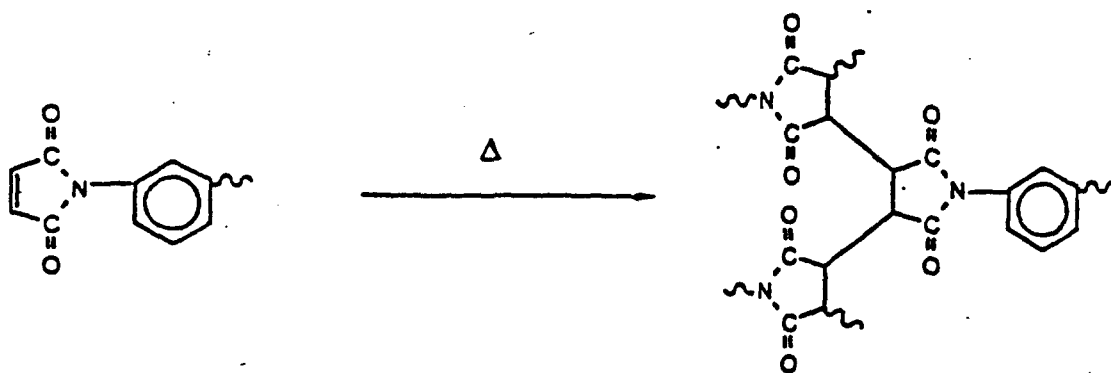


Figure 18.   Proposed thermally-induced free radical crosslinking reaction
responsible for network formation in bismaleimides [138].

The most widely utilized bismaleimide monomer is 4,4'-bismaleimidodiphenylmethane (BMI) primarily because of the low cost of the starting materials, 4,4'-diaminodiphenylmethane and maleic anhydride.

However, in principle, every aromatic diamine or amine-terminated prepolymer can be employed in the synthesis of bismaleimides [128]. The chemical structure of the backbone between the terminating maleimide groups is responsible for several cured resin properties [145].

McGrath et al. [146,147] demonstrated that the mechanical properties of simple bismaleimides can be significantly enhanced by the incorporation of poly(arylene ether sulfone) and poly(arylene ether ketone) oligomeric backbones. In this investigation amine-terminated oligomers of controlled molecular weight (2-10,000 g/mole) were converted to bismaleimides by reaction with maleic anhydride. Substantial increases in the fracture toughness of the resulting networks were observed relative to monomeric bismaleimides. The enhanced toughness was attributed to both the increased molecular weight between crosslinks and the $\beta$-relaxation of the matrix. Similar results utilizing poly(ether sulfone)s have been reported by Kwiatkowski et al. [148].

Another approach to improve the fracture toughness and processing characteristics of bismaleimides involves copolymerization of simple BMI resins with comonomers. Several different comonomers have been developed, the most common of which include: Diels-Alder comonomers, allylphenyl comonomers, aromatic diamines, and bisbenzocyclobutenes [128]. Indeed, the commercially available Compimide from Technochemie GmbH-Verfahrenstechnik is based on this technology. Compimides consist of a blend of monomeric bismaleimides with alkenyl-terminated poly(arylene ether ketone) oligomers. This system possesses enhanced toughness and reduced moisture absorption without significant reductions in flexural modulus [149,150]. Similar investigations were conducted at V.P.I. and S.U. by Senger et al. [151,152], where maleimide functionalized poly(arylene ether ketone) oligomers of controlled molecular weight were blended with bismaleimidodiphenylmethane. Mechanical property and swelling results demonstrated that the fracture toughness, crosslink density, and rubbery modulus of the co-cured networks were effectively controlled by variation of the blend composition.

The most common method of enhancing the processability of BMI involves copolymerization and chain extension with aromatic diamino compounds such as diaminodiphenylmethane (DDM) [128-131,153]. Bismaleimides and aromatic diamines polymerize via a Michael addition as described in the literature [130]. In most instances the bismaleimide is employed in excess to produce low molecular weight maleimide functionalized prepolymer. The final cured resin properties such as toughness, crosslink density, and processability are controlled by the structures and ratios of the starting reactants (i.e., the bismaleimide and aromatic diamine). A similar approach to enhance processability is utilized in the Ciba-Geigy Matrimid 5292 A/B system; however, in this case BMI is polymerized with a diallyl bisphenol A comonomer [154,155].

## 2.1.2.2.3. Bisnadimides

In the early 1970's, Lubowitz discovered that bisnadimides undergo an addition polymerization via a reverse Diels-Alder reaction to form highly crosslinked networks. The discovery led to the NASA developed PMR-15 polyimide resin. The PMR (Polymerization of Monomeric Reactants) technology evolved to solve the processing difficulties encountered with high performance heterocyclic polymers. The PMR approach (Figure 19) involves dissolving a dialkyl ester of an aromatic tetracarboxylic acid, an aromatic diamine, and the monoalkylester of 5-norbornene-2,3-dicarboxylic acid in a low boiling alcohol. The stoichiometry is controlled to obtain a molecular weight of approximately 1,500 g/mole. The solution is utilized to impregnate reinforcing carbon fibers. Composite laminates are then cured between 150 and 200°C in stages to allow the monomers to undergo an in situ cyclodehydration reaction to form a norbornene endcapped, low molecular weight prepolymer. Further processing at higher temperatures (≥300°C) is employed to form an insoluble network [128,156,157].
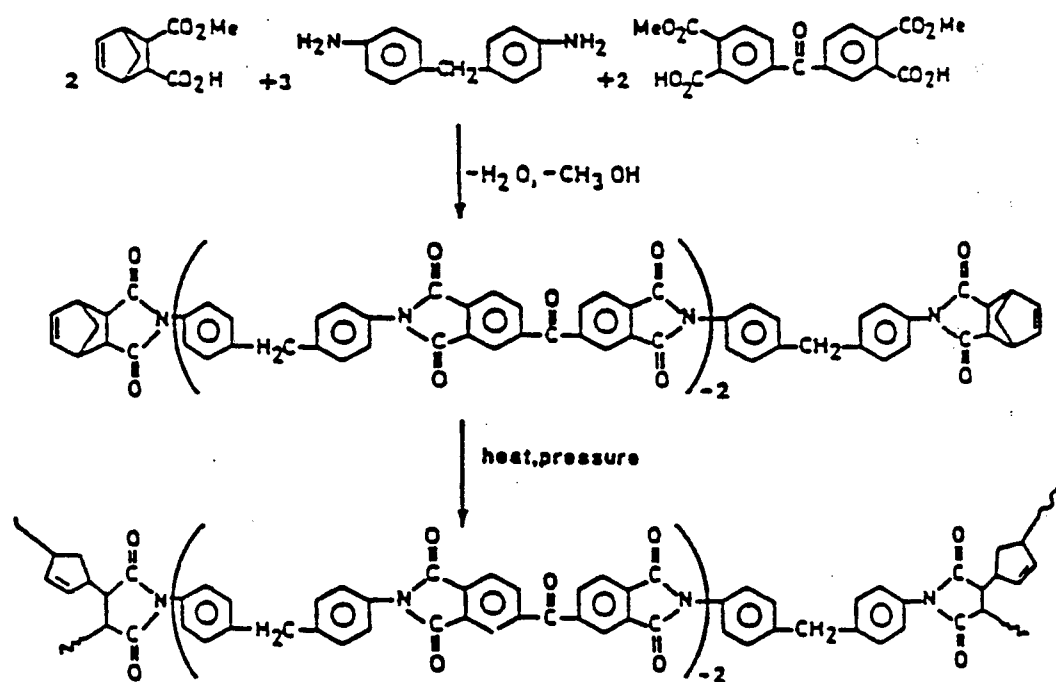
Figure 19. Synthesis of PMR-15 [156].

The crosslinking mechanism of the PMR resins is generally accepted to proceed via the reverse Diels-Alder reaction of the norborneyl endgroups to generate the maleimide moiety and cyclopentadiene. The highly activated maleimide unsaturation immediately proceeds to copolymerize with cyclopentadiene and unrearranged norbornenyl groups to produce a crosslinked network as shown in Figure 20. Evidence to support this mechanism has been provided by Wilson et al. [156,159] and Ritchey et al. [160-162] using model compound studies with N-phenylnadimide. The model reagent was molded at various temperatures and the resulting soluble polymers were characterized by proton and carbon NMR and FTIR.

The PMR approach has overcome the tack and drape problems common to most high temperature resin systems; however, the release of cyclopentadiene in the final cure stage has caused considerable compound investigations [156] difficulties. McGrath et al. [163] demonstrated using thermogravimetric analysis (TGA) coupled with mass spectroscopy (MS) that approximately 60% of the theoretical amount of cyclopentadiene from the reverse Diels-Alder reaction is volatilized at atmospheric pressure. In industrial applications of PMR-15 resins long, complex cure cycles and high processing pressures are required to achieve void-free composite laminates. Presumably, pressure prevents the loss of cyclopentadiene.

### 2.1.2.2.4. Acetylene-Terminated Resins

Acetylene containing materials, particularly oligomers and polymers, represent another important class of high performance structural resins. The thermal reaction of the acetylenic group is very complex and many reaction paths are possible. However, it is generally accepted that the acetylenic group undergoes a thermally-induced free radical addition polymerization at temperatures in excess of 300°C. The properties and processing characteristics of the resin are strongly dependent on the backbone structure of the diacetylene starting reactant [164].

The acetylene moiety has been incorporated into several different systems. Acetylene-terminated phenylene oligomers were introduced in 1974 by Hercules under the trade name of H-Resin [165]. Potential areas of application contemplated for H-Resin were corrosion-resistant coatings, structural composites, and molded electronic components. However, because of an unfavorable combination of price, processability, and performance, the H-Resin was not successfully commercialized.

Acetylene-terminated imide oligomers were first reported in the early 1970's [166]. These materials were synthesized by reacting 2 moles of an aromatic tetracarboxylic acid dianhydride with 1 mole of an aromatic diamine to yield an anhydride-terminated amic acid oligomer. Subsequent reaction with an ethynyl substituted aromatic amine followed by chemical or thermal cyclodehydration converted the amic acid to the acetylene-terminated imide oligomer (ATI). Since their initial discovery, many ATI's have been synthesized from different combinations of aromatic dianhydrides, aromatic diamines, and ethynyl substituted aromatic amines. In fact, the commercial resin HR-600 is based on the ATI technology. The HR-600 resin system has been incorporated into graphite fiber-reinforced composites. Mechanical property results demonstrated excellent flexural and interlaminar shear strengths along with outstanding thermal stability [164].

Major processing problems have plagued ATI's as well as many other acetylene-terminated heterocyclics. The ethynyl groups begin to react and inhibit flow and fiber-wetting prior to the formation of a complete melt. One approach taken to improve the flow and solubility characteristics has been to convert the ethynyl-terminated amic acid oligomers to isoimide oligomers by chemical cyclodehydration using dicyclohexylcarbodiimide. This approach improved processability while maintaining comparable composite and adhesive properties to conventional ATI's. Furthermore, since the isoimide moiety rearranges to the imide structure in the final stage of cure at elevated temperatures, there exist no structural differences in the fully cured resins [167].
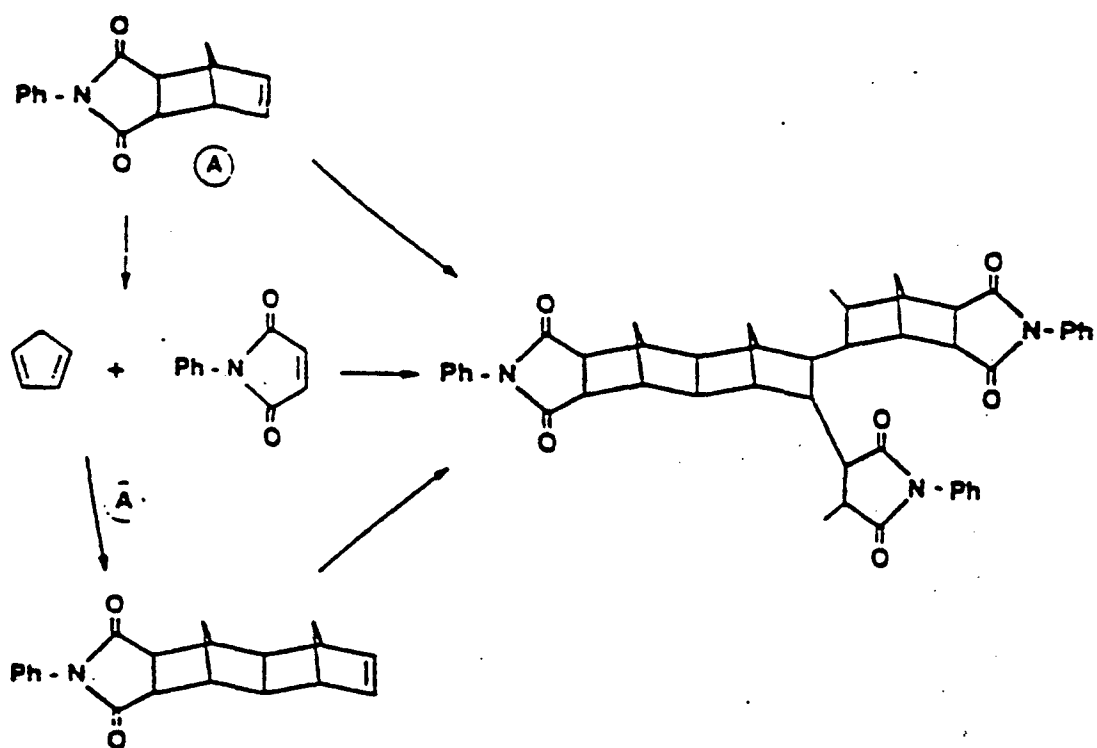
Figure 20. Proposed polymerization scheme for bisnadimides from model compound investigations [156].

## 2.1.2.2.5. Bisbenzocyclobutenes

Recently a new class of high performance thermosets known as bisbenzocyclobutenes has emerged in the literature [132-135]. Bisbenzocyclobutenes, like the previous systems discussed, undergo an addition polymerization at elevated temperatures (≥250°C). Homopolymerization proceeds through the thermally initiated ring opening of benzocyclobutene to yield an o-xylylene intermediate. The o-xylylene functionality can polymerize to form a crosslinked network or undergo a cycloaddition Diels-Alder reaction in the presence of a suitable dienophile [132-135] as shown in Figure 21.

Arnold et al. [132,135] have investigated the bisbenzocyclobutene resin system as a candidate for high temperature composite applications. They demonstrated that the bisbenzocyclobutene system exhibits excellent thermal stability up to 260°C. Furthermore, it was shown that the benzocyclobutene moiety can be blended and co-cured with acetylene functionalized systems to widen the processing window and enhance mechanical property performance.

Denny et al. [133] have demonstrated similar results utilizing bisbenzocyclobutene functionalized imide prepolymers. They showed that bisbenzocyclobutene resins can be copolymerized with bismaleimide resins, such as bismaleimidodiphenylmethane, via a Diels-Alder cycloaddition reaction. In theory an eight-membered ring structure should result and linear polymer molecules should be formed with no branching or network formation. In reality, however, a combination of both homo- and copolymerization reactions take place during cure and an insoluble network is created

## 2.1.2.2.6. Ketimines

Another novel class of high performance thermosets, based on amino functionalized poly(ether ketone)s, has recently been introduced in the literature. Mohanty et al. [168] reported crosslinking in aromatic amine-terminated poly(arylene ether ketone) (PEK) oligomers when processed above 220°C. Crosslinking occured via attack of the amine endgroups at the ketone groups along the polymer backbone to form ketimine linkages as shown in Figure 22. Mohanty et al. [168] reported that the resulting lightly crosslinked networks possessed good thermal stability and excellent mechanical properties.

The crosslinking mechanism shown in Figure 22 is significantly different than the previously discussed addition polymerizations. The amine endgroups react with the ketone groups by a Schiff base reaction and release water; thus, network formation occurs through a condensation polymerization. The rate of polymerization is relatively slow in comparison to the free radical systems; however, it is accelerated tremendously under reduced pressures.

Thompson and Farris [169] recently reported that semicrystalline poly(ether ether ketone) (PEEK) can be crosslinked by reaction with 1,4-phenylenediamine in a similar manner to that reported by Mohanty et al. [168]. The objective was to decrease high temperature creep in PEEK by increasing the glass transition temperature and the high temperature modulus. Indeed, upon reacting a tenfold excess of diamine with respect to the theoretical amount of carbonyl groups in the PEEK backbone, the glass transition temperature of PEEK was increased from 143°C to greater than 280°C. However, the commercial viability of this process is questionable since the release of volatiles during cure often results in void formation in composite laminates.

## 2.2. Experimental Techniques
## 2.2.1. Polymer Synthesis and Blend Preparation
## 2.2.1.1. General Considerations of Step-Growth Polymerization

Step-growth polymerization involves the stepwise condensation (and in some cases addition) of functional monomers to form high molecular weight polymers. All step-growth polymerizations fall into two categories depending on the type of monomer(s) employed. The first, an A-B system,

**Figure 21.** Proposed benzocyclobutene-terminated resin cure
mechanism [132].



**Figure 22.** Proposed crosslinking mechanism for amine-terminated
poly(arylene ether ketone)s [168].
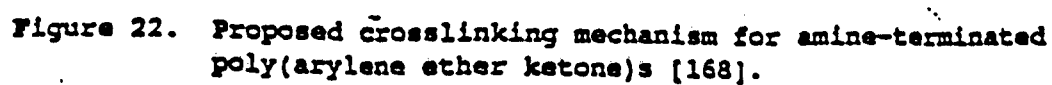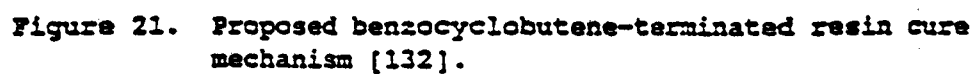
involves a single monomer unit which contains both types of functional endgroups. The second, an A-A/B-B system, involves two different bifunctional monomers in which each monomer possesses only one type of functional group.

In order to synthesize high molecular weight linear polymers, several criteria must be satisfied. First, a perfect stoichiometric balance of the two difunctional monomers must be introduced. Second, a high degree of monomer and solvent purity is necessary. And third, the reaction responsible for the polymerization must reach a very high conversion with the absence of side reactions.

In homopolymer syntheses, control of molecular weight and endgroup functionality are crucial. The mechanical and thermal properties of a polymer depend primarily on molecular weight and molecular structure. The mechanical properties increase dramatically up to the point at which the critical molecular weight for the development of entanglements, $M_e$, is reached and then level off with increasing molecular weight. As molecular weight advances above $M_e$, the melt viscosity dependency on molecular weight increases to the 3.4 power making melt processing very difficult. Consequently, a compromise between processability and optimum polymer properties must often be achieved.

The following section deals with the purification of the various monomers and solvents along with the experimental techniques for oligomer syntheses and their subsequent post reactions. Furthermore, a discussion on control of molecular weight and endgroup functionality, via the use of a monofunctional reagent and the Carothers equation, is described.

## 2.2.1.2. Solvent Purification

A variety of solvents were employed in the preparation of the functionalized oligomers. Table 1 lists the structures and suppliers for the most commonly used solvents. The solvents for synthetic reactions were stirred over finely ground calcium hydride for at least 24 hours, refluxed for approximately 1 hour, and then fractionally distilled. Some distillations, particularly for high temperature boiling solvents, were conducted under reduced pressure. Distillations which did not require vacuum were conducted with a low nitrogen flow through the apparatus. In all cases the initial fraction (approximately 5% by volume) was discarded and the constant boiling fraction was collected in a round bottom flask. The flask was sealed with a rubber septum and the solvent was utilized within 24 hours or it was redistilled.
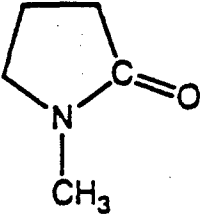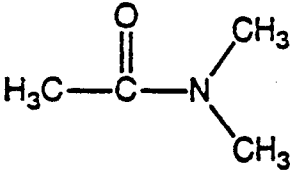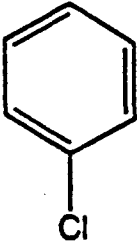
## 2.2.1.3. Monomer Purification

2,2-Bis(4-hydroxyphenyl)propane (Bisphenol-A)

|  |  |
|---|---|
| Source: | Dow Chemical |
| Empirical Formula: | C15H16O2 |
| Molecular Weight: | 228.27 |
| Melting Point (pure), °C: | 154-155 |
| Structure: | Table 1 |

Purification: Bisphenol-A was added to reagent grade toluene in a 25 w/v percent ratio into an erlenmeyer flask. The solution was heated to 100°C with stirring until complete dissolution and 2 grams of activated charcoal were added. The dark solution was stirred for 20 minutes and filtered through a porcelain buchner funnel using CeliteTM to remove the charcoal. The clear, colorless solution was reheated to dissolve the bisphenol-A and to reduce the volume by approximately 10 percent. The solution was slowly cooled to room temperature to yield white crystals. The crystals were isolated by filtration and then dried under vacuum at 50°C for 12 hours. The dried crystals were crushed and dried for an additional 12 hours at 80-90°C under vacuum to remove any trapped or residual solvent.

**Table 1. Common solvents utilized in the preparation of functionalized oligomers.**

| Structure | Solvent | Supplier |
|---|---|---|
| | 1-Methyl-2-Pyrrolidinone (NMP) | Fisher Scientific or Aldrich |
| | N,N-Dimethyl-acetamide (DMAc) | Fisher Scientific or Aldrich |
| | Chlorobenzene | Fisher Scientific or Aldrich |
| | Toluene | Fisher Scientific |

4,4'-Dichlorodiphenylsulfone (DCDPS)
| | |
|---|---|
| Source: | AMOCO Chemicals |
| Empirical Formula: | C12H8Cl2O2S |
| Molecular Weight: | 287.16 |
| Melting Point (pure), °C: | 147-148 |
| Structure: | Table 2 |

Purification: DCDPS was added to reagent grade toluene in a 60 w/v percent ratio into an erlenmeyer flask. Two grams of activated charcoal were added and the solution was heated with stirring to boiling. After 20 minutes the dark colored solution was filtered through CeliteTM using a porcelain buchner funnel. The clear filtrate was boiled to reduce the volume, and then slowly cooled to room temperature. White crystals were isolated by filtration and washed with cold toluene. The crystals were dried under vacuum at 80°C for 8 hours, then crushed and dried again under vacuum at 90°C for 12 hours.

m-Aminophenol (mAP)
| | |
|---|---|
| Source: | Aldrich |
| Empirical Formula: | C6H7NO |
| Molecular Weight: | 109.129 |
| Melting Point (pure), °C: | 125-126 |
| Structure: | Table 2 |

Purification: mAP was sublimed twice under reduced pressure to produce highly pure, white crystals.

4,4'-Difluorobenzophenone (DFBP)
| | |
|---|---|
| Sources: | ICI or Amoco Chemical Company |
| Empirical Formula: | C13H8OF2 |
| Molecular Weight: | 218.12 |
| Melting Point (pure), °C: | 123-124 |
| Structure: | Table 2 |

Purification: DFBP was received as a highly pure, white powder and was used without further purification.

Maleic Anhydride (MA)
| | |
|---|---|
| Source: | Aldrich |
| Empirical Formula: | C4H2O3 |
| Molecular Weight: | 98.06 |
| Melting Point (pure), °C: | 54-56 |
| Structure: | Table 2 |

Purification: MA was sublimed twice under reduced pressure to produce highly pure, white crystals.

5-Norbornene-2,3-dicarboxylic Anhydride (NA)
| | |
|---|---|
| Source: | Aldrich |
| Empirical Formula: | C9H8O3 |
| Molecular Weight: | 164.16 |
| Melting Point (pure), °C: | 165-167 |
| Structure: | Table 2 |

Purification: NA was sublimed under reduced pressure to produce highly pure, white crystals.

3,3'-Diaminodiphenylsulfone (3,3'-DDS)

|  |  |
|---|---|
| Source: | Kennedy and Klim |
| Empirical Formula: | C12H12N2O2S |
| Molecular Weight: | 248.30 |
| Melting Point (pure), °C: | 172-173 |
| Structure: | Table 2 |

Purification: 3,3'-DDS was added to a 25 w/v percent methanol solution in an erlenmeyer flask. The methanol was deoxygenated prior to use by purging with nitrogen for 5 hours. The solution was heated with stirring to approximately 60°C. Upon dissolution it was filtered through fluted filter paper. The clear filtrate was reheated to 60°C with stirring and deoxygenated distilled water (approximately 2 v/v percent) was added (to induce the precipitation). The solution was allowed to slowly cool to room temperature. White crystals were isolated by vacuum filtration, washed with cold deoxygenated methanol, and dried at 60°C in a vacuum oven for 8 hours. The crystals were crushed and dried again at 60°C for 12 hours.

4,4'-Diaminodiphenylsulfone (4,4'-DDS)

|  |  |
|---|---|
| Source: | Aldrich |
| Empirical Formula: | C12H12N2O2S |
| Molecular Weight: | 248.30 |
| Melting Point (pure), °C: | 177-178 |
| Structure: | Table 2 |

Purification: 4,4'-DDS was recrystallized by the same procedure as utilized for 3,3'-DDS.

Diglycidylether of Bisphenol-A (DGEBA)

|  |  |
|---|---|
| Source: | Dow Chemical (DER 332) |
| Empirical Formula: | C21H24O4 |
| Molecular Weight: | 340.42 |
| Melting Point (pure), °C: | 45-46 |
| Structure: | Table 2 |

Purification: DGEBA was recrystallized from a 60/40 mixture of methyl isobutyl ketone and 2-ethoxyethyl ether. The solution was refrigerated for approximately 3 days with frequent stirring. White crystals eventually precipitated out and were isolated by filtration. The crystals were washed once with cold methanol and several times with hexanes and then dried under reduced pressure for 72 hours at 20-25°C.

Epon 828

|  |  |
|---|---|
| Source: | Shell Chemical Company |
| Molecular Weight: | ~372 |
| Structure: | Figure 2 |

Purification: Epon 828 was received as a viscous liquid and was used without further purification.

Bismaleimidodiphenylmethane (BMI)

|  |  |
|---|---|
| Source: | Technochemie-GmbH |
| Empirical Formula: | C21H14N2O4 |
| Molecular Weight: | 358.36 |
| Melting Point (pure), °C: | 157-158 |
| Structure: | Table 2 |

Purification: BMI was used as received without further purification.

Figure 22a. **Structures of the various monomers utilized to prepare the functionalized oligomers and crosslinked networks.**
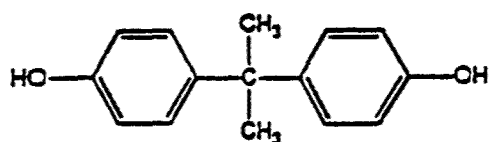


Bisphenol A
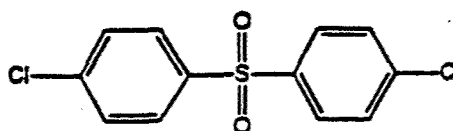
DCDPS
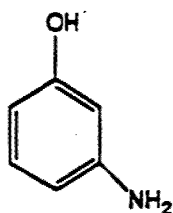
mAP
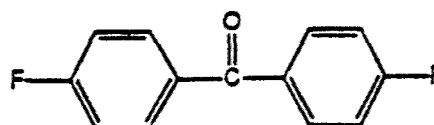
DFBP

MA

ND
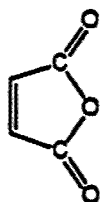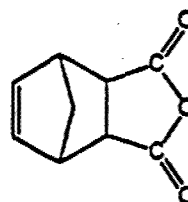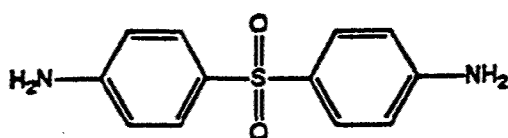
4,4' - DDS
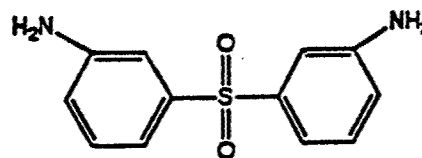
3,3' - DDS
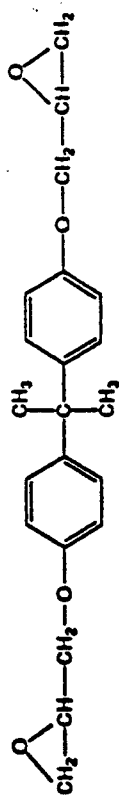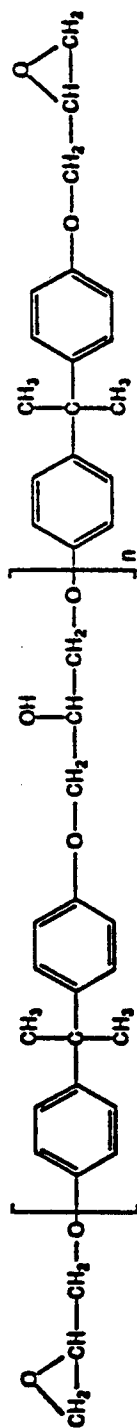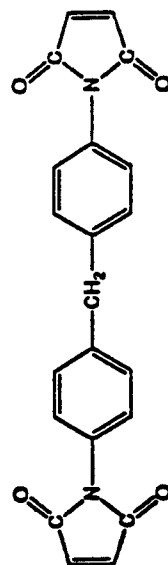
Figure 22a. (Continued)

39

## 2.2.1.4. Synthesis of amino functionalized Poly(arylene ether sulfone) oligomers

Reaction:



where DPS =
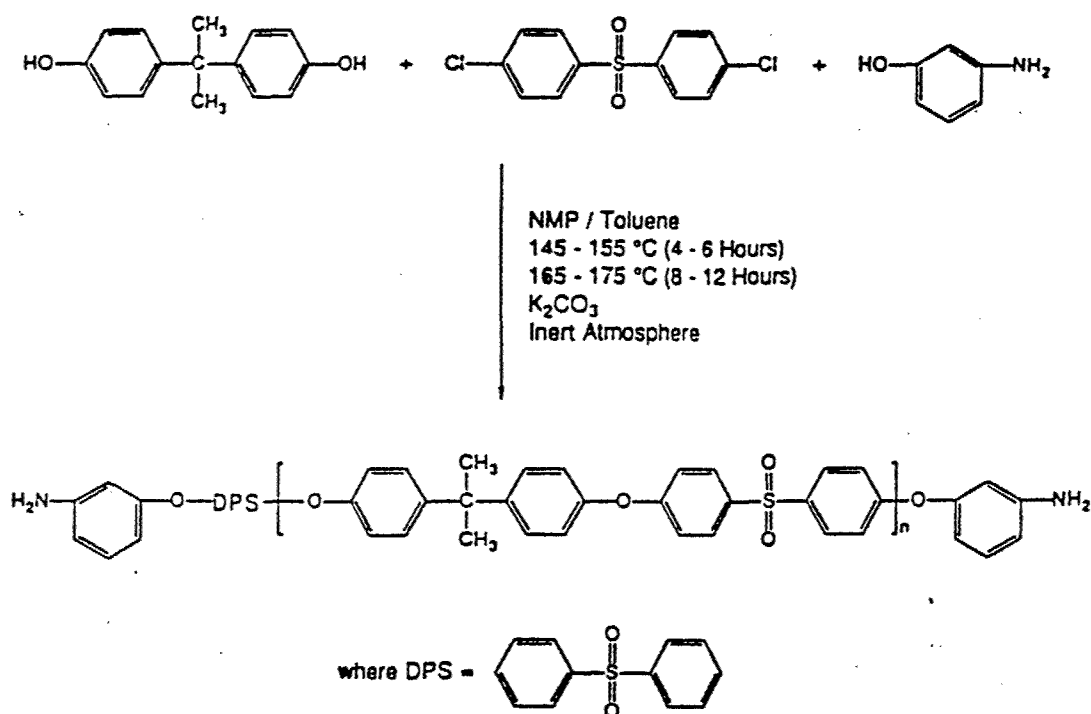


Procedure:

Purified Bisphenol A, 4,4'-dichlorodiphenylsulfone (DCDPS), and m-aminophenol (mAP) were charged into a four-neck flask equipped with a mechanical stirrer, gas inlet, thermometer and Dean Stark trap fitted with a condensor and drying tube as shown in Figure 23. The stoichiometry of the reactants was varied according to the Carothers equation (Section 2.2.1.) to achieve oligomers of controlled molecular weight. The reactants were dissolved in NMP (70%) and toluene (30%) to 15% solids concentration. Potassium carbonate ($K_2CO_3$) base was added in a 20 molar percent excess and the mixture was heated until the toluene began to reflux (approximately 140°C-150°C). The water released during phenoxide formation was collected in the Dean Stark trap. The solution was refluxed until complete dehydration was achieved (approximately 4-6 hours depending on the quantities of the reactants). Toluene was drawn from the Dean Stark trap until the reaction temperature reached 165°C-170°C. The system was then allowed to react for 8-12 hours, resulting in a viscous, dark green solution. After cooling to approximately 80°C, the reaction mixture was filtered to remove the inorganic salts. The reaction solution was acidified with glacial acetic acid and then precipitated into a tenfold volume of alcohol. Isopropanol was used for low molecular weight oligomers ($M_n < 5,000$ g/mole); and methanol was utilized for higher molecular weight oligomers ($M_n \geq 5,000$ g/mole). The precipitated oligomer (tan powder) obtained by filtration was washed several times with alcohol and allowed to dry. It was then stirred in hot water (90°C-95°C) for 4-8 hours to remove any trapped salts, refiltered, washed with more alcohol, and dried under vacuum for at least 8 hours at 60°C-80°C. After drying the oligomer was redissolved in methylene chloride and the precipitation, filtration and washing procedures were repeated. Finally, the oligomer was dried under vacuum at 100°C-120°C to constant weight.

40

Motor  Drying tube

Condenser

Gas inlet

Dean Stark trap

Thermometer

Reaction flask

Stir paddle
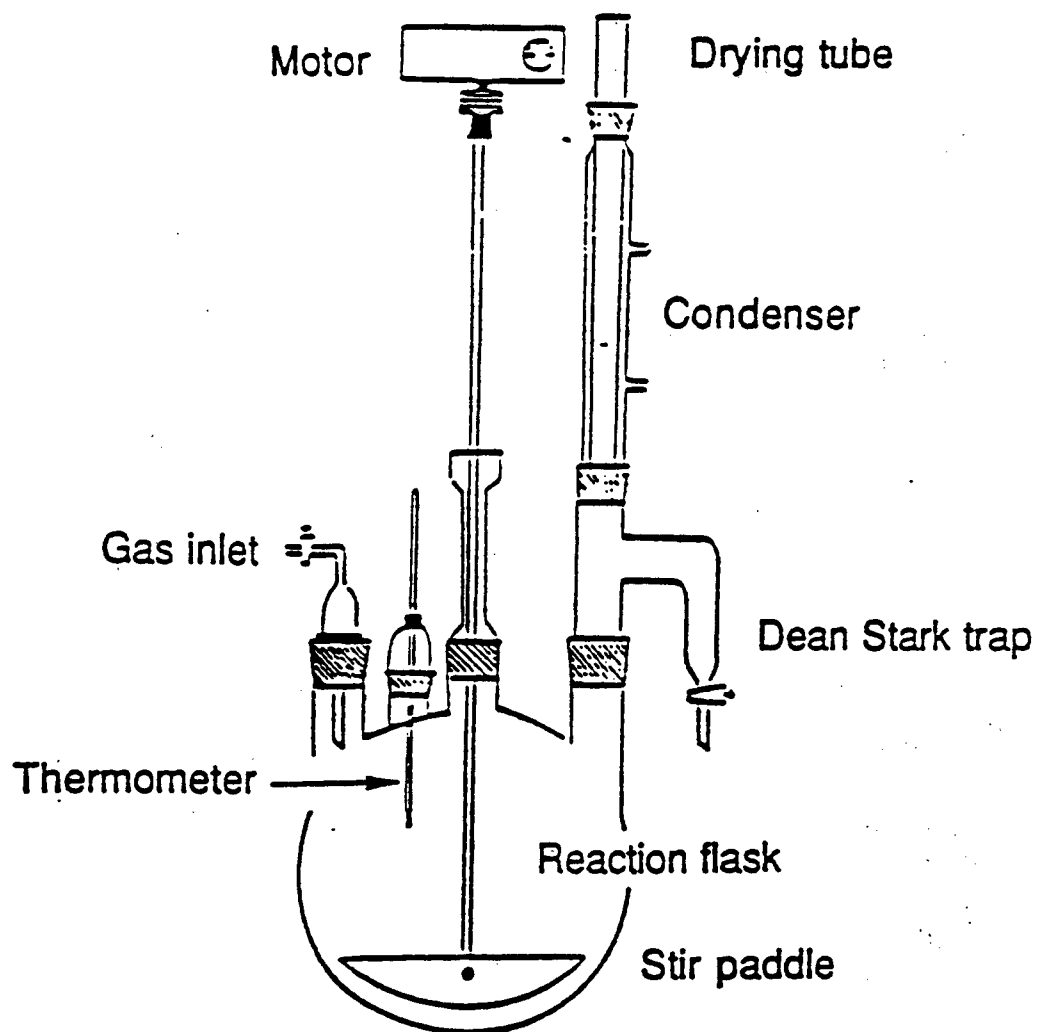
Figure 23. Reaction apparatus utilized for the synthesis of the step-growth polymers.

41

## 2.2.1.5. Synthesis of amino functionalized poly(arylene ether ketone) oligomers

Reaction:



DMAc / Toluene
140 - 145 °C (4 - 6 Hours)
155 - 160 °C (8 - 12 Hours)
$K_2CO_3$
Inert Atmosphere

$H_2N$ - PEK - $NH_2$

where BP =
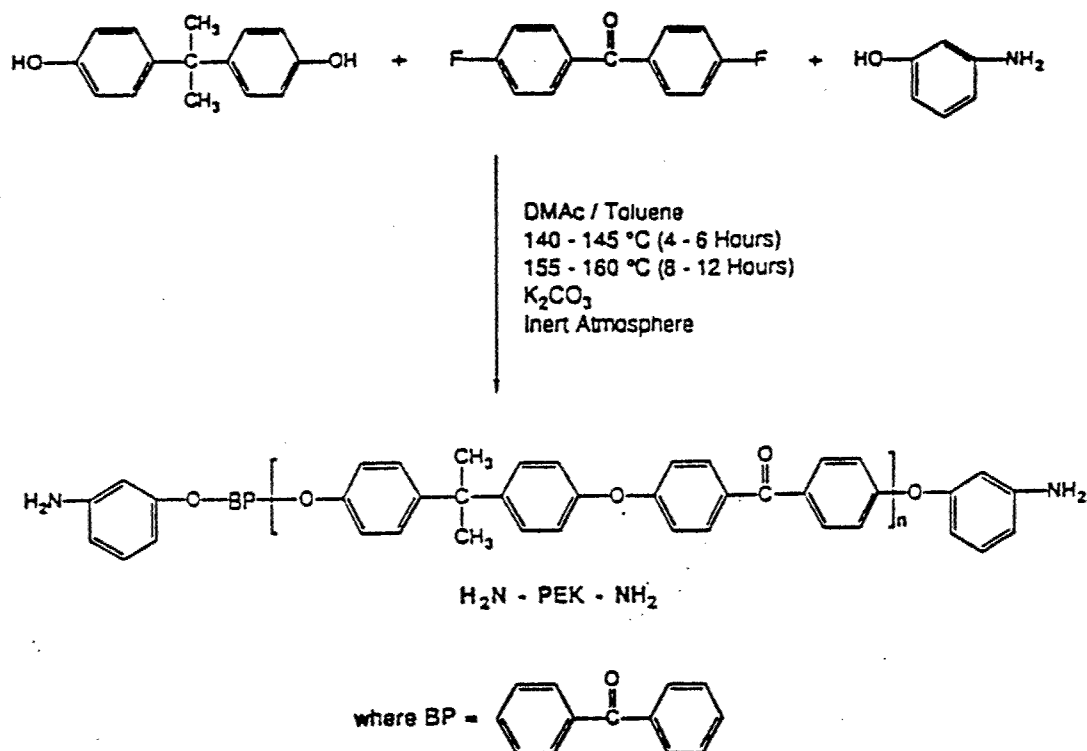
Procedure:

The same synthetic procedure utilized in the synthesis of the amino functionalized poly(arylene ether sulfone)s was employed. However, 4,4'-difluorobenzophenone (DFBP) was substituted for 4,4'-dichlorodiphenylsulfone (DCDPS), and DMAc was used instead of NMP.

## 2.2.1.6. Molecular weight and endgroup control in step-growth polymerizations via the Carothers equation

As previously discussed (Section 2.2.1.1.), molecular weight and endgroup functionality play a major role in the mechanical and thermal properties of a polymer. In order to properly control molecular weight and endgroup functionality, a stoichiometric imbalance of the difunctional monomers must be utilized or a monofunctional monomer must be employed. The Carothers equation provides the theoretical means to vary the stoichiometry to achieve control of molecular weight and functionality in step-growth polymerizations. A derivation of the most useful equations for the condensation of activated dihalides with bisphenols is presented below. A more complete derivation of the Carothers equation is described in basic polymer texts [170-172].

The Carothers equation relates the number average degree of polymerization, $X_n$, to the extent of reaction, p, and average functionality, $F_{av}$, of the polymerizing system:

$$X_n = \frac{2 N_o}{(2 N_o - N_o p F_{av})} = \frac{2}{(2 - p F_{av})} \tag{8}$$

42

where $N_0$ is the initial moles of monomer units. Assuming $F_{av}$ is 2.0 for completely difunctional starting reactants, the above equation simplifies to:

$$X_n = \frac{1}{1 - P} \qquad (9)$$

which illustrates that at very high extents of reaction, as p approaches 1, molecular weight approaches infinity.

In the polymerization of difunctional monomers A-A and B-B, such as dihalides and bisphenols, the number average degree of polymerization is twice the number of repeat units in the polymer molecule, DP, because

$$X_n = 2\,DP = 2\;\frac{\text{Desired Molecular Weight}}{\text{Mol. wt. of the repeat unit}} \qquad (10)$$

each repeat unit contains the residue of two monomers. Molecular weight can be related to the stoichiometric imbalance, r, by the expression:

$$X_n = \frac{(1 + r)}{(1 - r)} \qquad (11)$$

The stoichiometric imbalance is defined to have a value equal to or less than unity. The stoichiometric imbalance can be systematically varied to control Xn. The stoichiometry can be offset by the incorporation of a monofunctional reagent or by the excess addition of either the bisphenol or dihalide. When excess difunctional B monomer is used to offset the stoichiometry and achieve B endgroups,

$$r = \frac{N_A}{N_B} \qquad (12)$$

where NA and NB are the moles of difunctional A and B monomers, respectively. Alternatively, if a monofunctional reagent with a B endgroup is incorporated,

$$r = \frac{N_A}{N_B + 2N_B{'}} \qquad (13)$$

where $2N_B{'}$ is the total number of moles of the monofunctional reagent. This approach dictates that the number of A functional groups equals the number of B functional groups, with the polymer endgroups determined by the nature of the monofunctional reagent. The coefficient 2 in front of NB' is required, since one mole of B has the same quantitative effect as one excess mole of B-B on limiting the growth of the polymer chain.

Solutions of equation 13 were achieved by arbitrarily assigning the moles of difunctional A monomer as 0.1. The moles of difunctional B monomer were then defined as r, and the moles of monofunctional B monomer required to limit molecular weight were obtained by substitution of NA and NB into equation 13. To obtain a sufficient total batch size, the values were scaled

accordingly. For specific information regarding sample reactions or other synthetic issues the reader is referred to the work of Mohanty [173] and Jurek [174,175].

2.2.1.7. Synthesis of maleimide- and nadimide-terminated poly(arylene ether ketone) oligomers

Reaction:
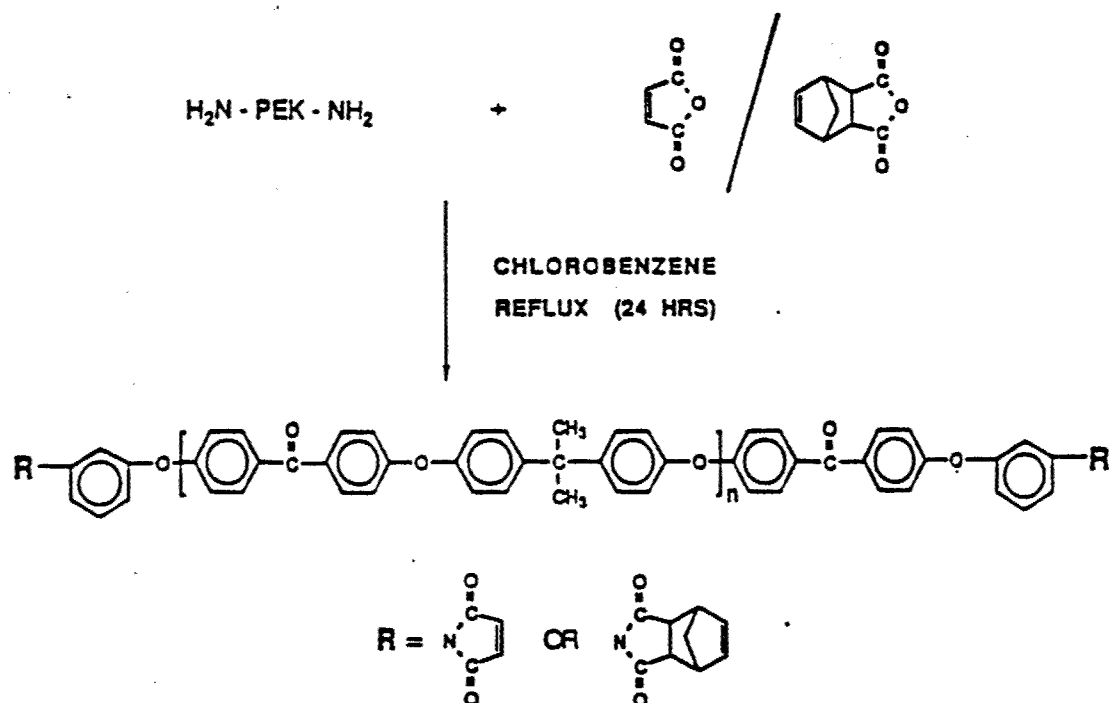


Procedure:

A two-step procedure was utilized in the synthesis of the maleimide-and nadimide-terminated poly(arylene ether ketone) (PEK) oligomers. The amine-terminated PEK oligomer (Section 2.2.1.5.) was titrated to determine the number average molecular weight. A 20-50 molar percent excess of either maleic anhydride or norbornene dicarboxylic anhydride along with the amine-terminated PEK oligomer was added to a four-neck round bottom flask equipped with a nitrogen inlet, mechanical stirrer, thermometer and Dean Stark trap (Figure 23). The reactants were dissolved in chlorobenzene to 15% solids concentration, purged with nitrogen and stirred at room temperature for 4 hours to form the maleamic acid precursor. The solution was then refluxed at $132^\circ$C for 24 hours to allow for imidization. Chlorobenzene served as both a solvent and azeotropic medium. The solution was cooled to room temperature and precipitated into a tenfold excess of methanol. The endcapped oligomers were dried under vacuum at 80°C for 24 hours before redissolving in chloroform and precipitating from methanol. Finally, the oligomeric tan powder was dried under vacuum at 100°C to constant weight. Both infrared measurements and titration of potentially uncyclized amic acid groups suggested that the derivatization was quantitative [146,147].

2.2.1.8. Crosslinking of Functionalized Poly(arylene ether ketone)s

Certain functionalized poly(arylene ether ketone)s (PEK) are known to undergo crosslinking reactions at elevated temperatures as previously described (Section 2.1.2.2). Samples of amino, maleimide and nadimide functionalized PEK oligomers were cured isothermally for various time

44

intervals in a forced air convection oven (Blue M). The samples were in the form of thin (~1 mm in thickness) discs (~2 cm in diameter) weighing one to two grams.

## 2.2.1.9. Preparation of modified epoxy resin networks

Reaction:



DGEBA

OR

EPON 828

+



AMINE - TERMINATED POLYSULFONE

EPOXY - CAPPED POLYSULFONE

+

EXCESS DGEBA (OR EPON 828)

+



3,3'- OR 4,4'- DDS

CROSSLINKED NETWORK
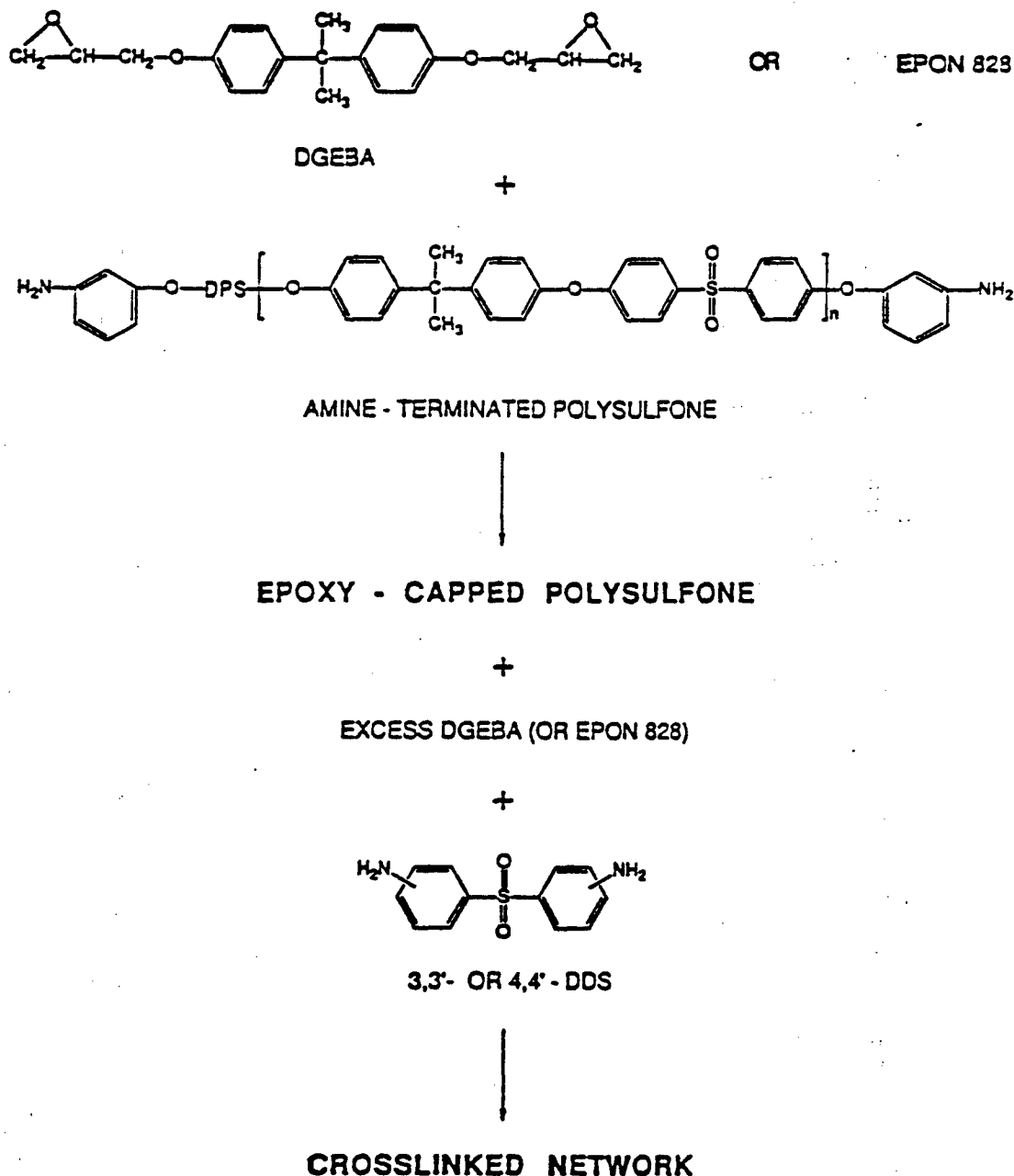
Procedure:

The epoxy resin, either DGEBA or Epon 828, and the amine-terminated poly(arylene ether sulfone) (PSF) oligomer were carefully weighed in a two-neck round bottom flask. The flask, equipped with a gas inlet and mechanical stirrer, was placed in a silicone oil bath as shown in Figure 24. The mixture was heated to 90°C with stirring under vacuum to degas the epoxy resin. In approximately 0.5-1.5 hours, the homogeneous light brown mixture ceased bubbling, indicating that all of the moisture and dissolved gasses were removed. The reaction temperature was then raised to 130°C and the curing agent, either 3,3'- or 4,4'-diaminodiphenylsulfone (DDS), was

45
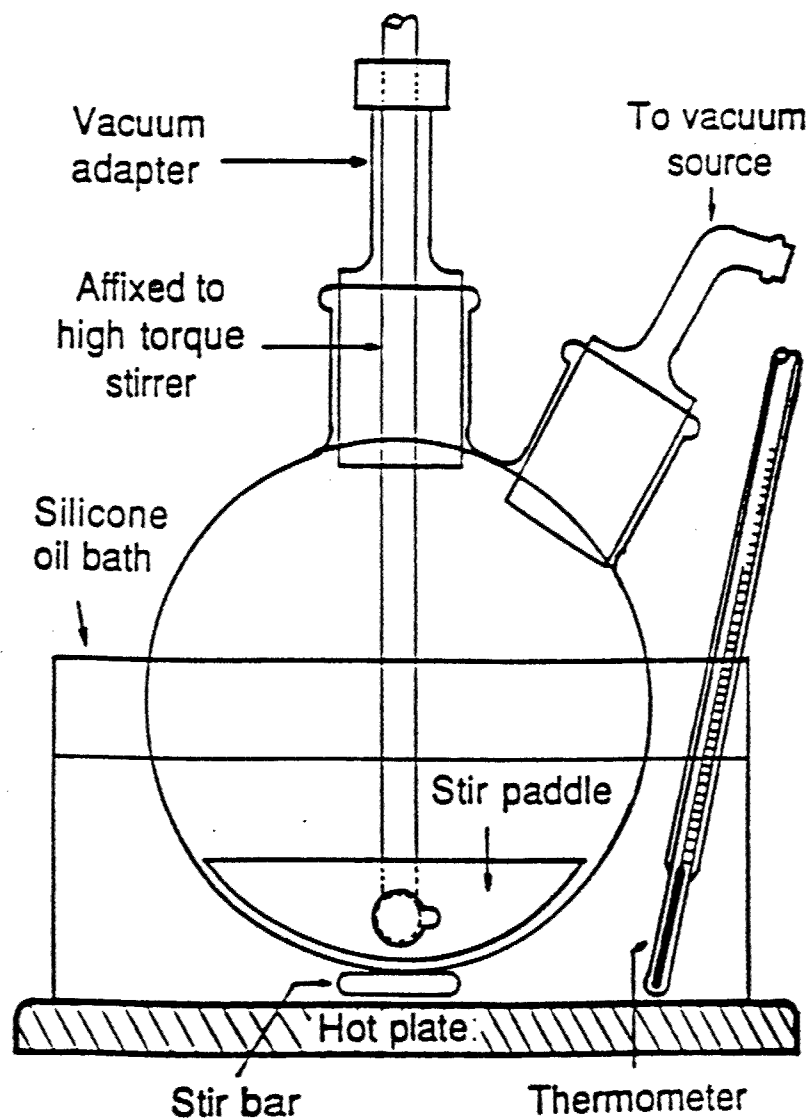
**Figure 24.** Reaction apparatus used in the preparation of the modified epoxy resin networks.

added. The stoichiometry was controlled such that the difunctional epoxide was reacted in a 2:1 molar ratio with respect to the tetrafunctional PSF and DDS. Upon dissolution of the DDS into the epoxy resin/PSF mixture (approximately 20 to 30 minutes) a transparent, homogeneous solution was formed. The homogeneous solution was poured into a preheated RTV silicone rubber mold (Dow Corning 3120 RTV and Dow Corning catalyst RTV-S), covered with a sheet of 0.01 mil Teflon and weighted down. The mold was then placed into a forced-air convection oven and cured at the desired temperature profile. The Epon 828/3,3'-DDS system was cured at 140°C for 2 hours and then postcured at 180°C for 1 hour. The Epon 828/4,4'-DDS and DGEBA/4,4'-DDS systems were cured in a similar manner; however, the chosen cure temperatures were 170°C to 210°C and 190°C to 240°C, respectively.

### 2.2.1.10. Preparation of maleimide-terminated poly(arylene ether ketone)/ bismaleimidodiphenylmethane blends

Blend system:



+



$\Delta$

### CROSSLINKED NETWORK
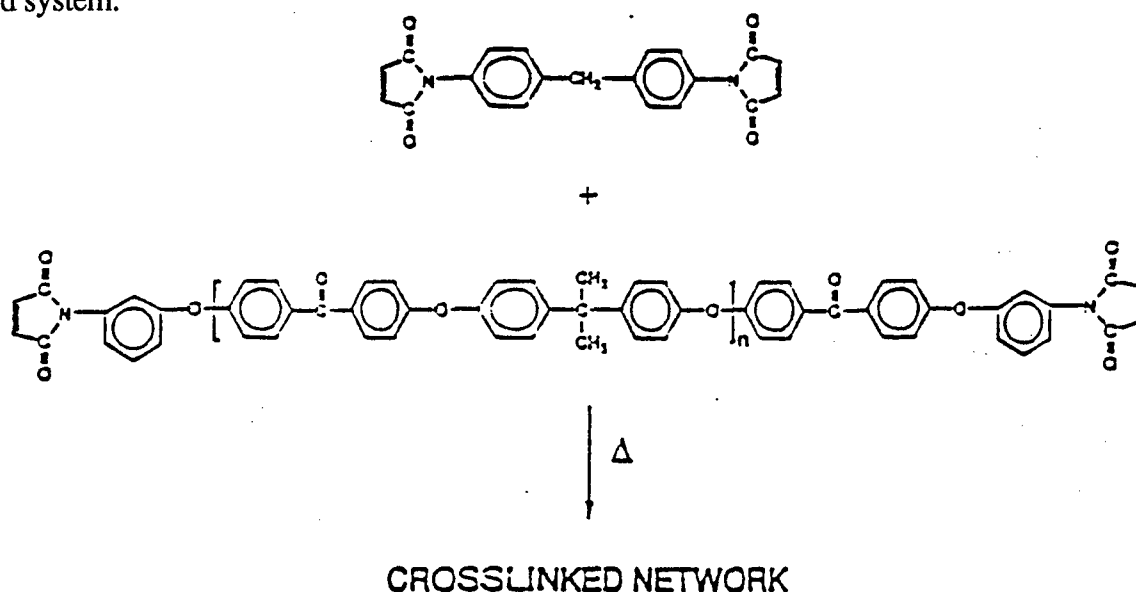
Procedure:

Blends of bismaleimidodiphenylmethane and maleimide-terminated poly(arylene ether ketone) oligomers were prepared in a 10 w/v percent chloroform solution. Each component was weighed into an erlenmeyer flask, dissolved in chloroform and coagulated in hexanes using an explosion-proof blender. The blend was isolated by filtration and dried under vacuum at 80°C to constant weight. The resulting light yellow powder was cold pressed into small discs (approximately 2 cm in diameter and 1 mm in thickness) weighing 1 to 2 grams. The blend was then cured in a forced air convection oven (Blue M Model DCI-146C) at 220°C for various time intervals.

### 2.2.2. Microwave Processing
### 2.2.2.1. Microwave Instrumentation

The equipment utilized for microwave processing is shown in Figure 25 and further described in Table 2. It consists of a Raytheon magnetron operating at a frequency of 2.45 GHz, coaxial transmission lines, a circulator, a directional coupler, power sensors, power meters and a tunable cavity. Table 2 provides the model numbers and suppliers of the various components. In this experimental set-up the microwave power generated by the Raytheon magnetron was
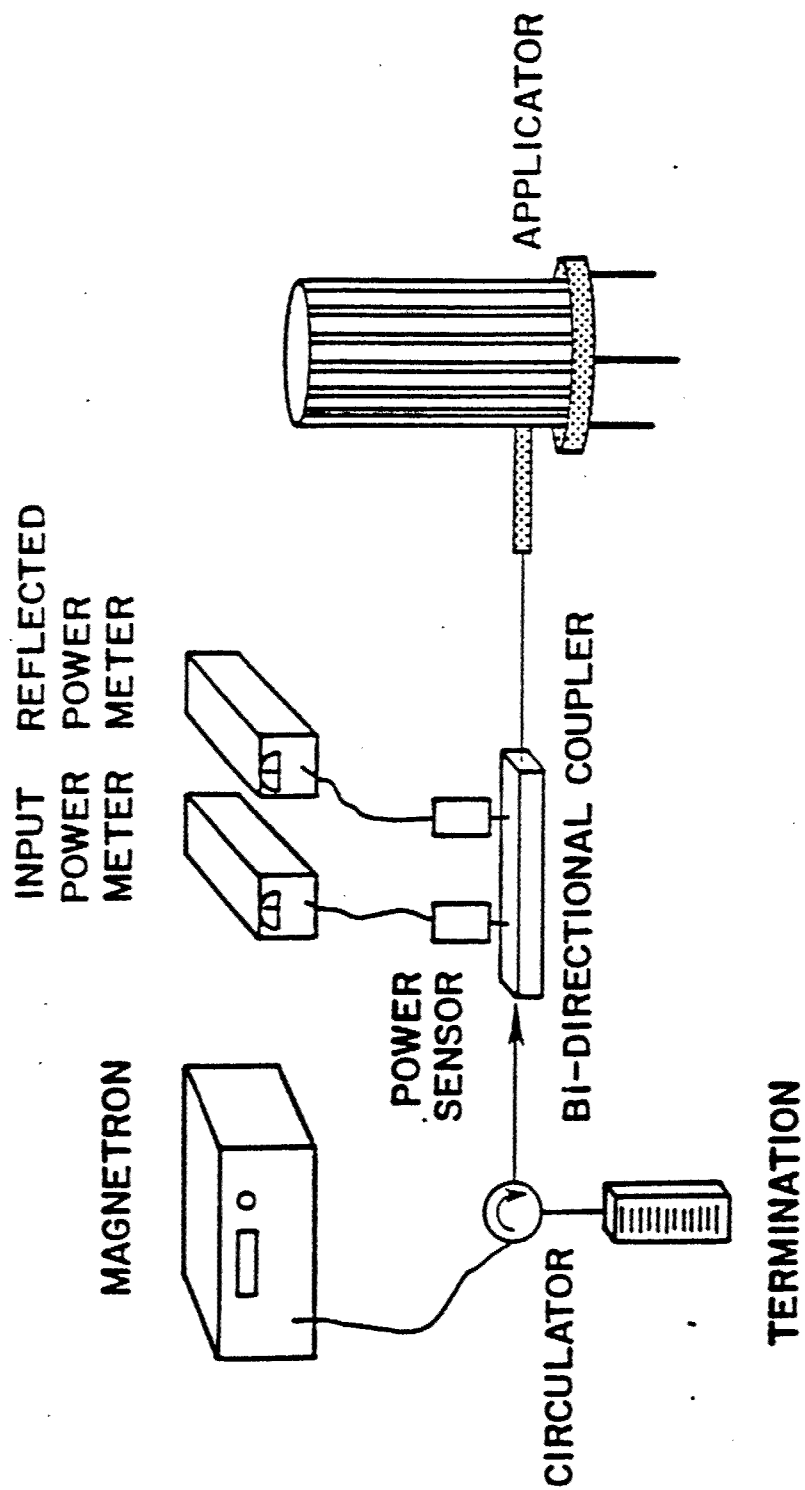
Figure 25. Schematic representation of the instrumentation used for microwave processing.

Table 2. **Components of the microwave instrumentation.**

| Component | Company | Model |
|---|---|---|
| Magnetron, 0-120 watts | Raytheon | PGM-10X1 |
| Coaxial Cable, modified | Raytheon | 57111G2E |
| Circulator | Ferrite Control | 2620 |
| Coaxial Cable (RG-214) | Coax Connection | CC2547-36 |
| Termination, 175 watts | NARDA | 369BNF |
| Termination, 40 watts | NARDA | 376BNF |
| Directional Coupler, dual (20dB | NARDA | 3022 |
| Directional Coupler (20dB) | NARDA | 3003 |
| Adapter | NARDA | 614A |
| Adapter | Hewlett Packard | S281A |
| Attenuators (20dB) | Weinschel | 49-20-43 |
| Power Sensors | Hewlett Packard | 8481B |
| Power Meter | Hewlett Packard | 435B |
| Frequency Meter | Hewlett Packard | 536A |
| Coaxial Cable | Maury Microwave | 8913C-36 |

*Components in 50 ohm and/or coaxial form.

transmitted through a coaxial transmission line to a circulator which protected the magnetron from reflected power by dissipating it at an external termination site. A directional coupler was utilized to divert power so the incident and reflected radiation could be monitored via power sensors and meters. The tunable cavity was a 17.8 cm diameter, cylindrical brass applicator.

The electromagnetic applicator (Figure 26) was designed and constructed by Michigan State University for the purpose of either materials processing or plasma generation [176,177]. It operates in a single-mode capacity and has a distinct advantage over multimode applicators; the impedance mismatch between the external circuit and the applicator because of changes in the dielectric properties of the loaded material during processing can be corrected by manually tuning the applicator [176,177]. This allows for the reproducible, uniform curing of polymeric materials in a controlled electromagnetic field. Several defined modes can exist in this cavity by adjusting the cavity length and coupling probe depth. The TE111 mode was chosen to process the polymers described in this dissertation. The field distributions of the two-dimensional $TE_{11}$ mode and the three-dimensional $TE_{111}$ mode are shown schematically in Figure 27. The $TE_{111}$ is the lowest mode in this cavity, existing at a theoretical cavity length of 6.69 cm. Determination of the mode was made by inserting a microcoax electric field probe into the cavity wall as shown in Figure 26.

Cure temperature was monitored via a Luxtron fluoroptic thermometry system (Model 750). Electrically nonconductive fiber optic probes (one to four) were placed into the sample through the circular opening in the top of the applicator. The probes were frequently placed into thin pyrex glass capillaries (Fisher Scientific melting point tubes) to protect the fragile tips from damage. The cure temperature was monitored every second with an accuracy of $\pm 1.0°C$. The Luxtron fluoroptic thermometry system and the Hewlett Packard power meters were interfaced with an IBM personal computer. The computer was programmed to simultaneously record the powers and temperature as a function of time during the processing experiments.

## 2.2.2.2. Epoxy Resins

The epoxy resin was prepared as previously described (Section 2.2.1.8.). The homogeneous epoxy/curing agent mixture was allowed to cool to room temperature in the reaction flask. The solution was then heated to approximately 100°C as needed using a hot air gun to allow for the pouring of the resin into silicone rubber molds. Prior to electromagnetic processing, the reaction proceeded to approximately 8 to 10 percent conversion by differential scanning calorimetry. Selection of the proper molding compound was very important; General Electric's RTV 664 was selected because it was free of electrically conductive fillers. Molds were fabricated to yield either four three-point bend fracture toughness specimens (Section 2.2.3.8.) or two flexural modulus specimens (Section 2.2.3.9.). The outer dimensions of the molds were approximately 4 cm x 4 cm x 1 cm. Preheating of the mold was necessary prior to the addition of the epoxy resin mixture to prevent void formation in the cured resins.

The preheated mold was placed in the center of the cavity. An additional empty silicone rubber mold was stacked underneath the mold to raise the height of the samples to 2.5 cm. The mold was oriented so that the length of the fracture toughness or flexural modulus specimens was perpendicular to the coupling probe inside the applicator. Uniformity of the temperature over the sample specimens was confirmed by placing multiple fiber optic temperature probes in the resin. The sample temperature was relatively uniform ($\pm 2°C$) except at the very outermost edges of the specimens which was slightly cooler (approximately 5-10°C) because of heat dissipation into the mold.

The neat epoxy resins were cured at a constant power of 21-22 watts. The power varied slightly depending on the condition (Q factor) of the microwave applicator. The modified epoxy resins were cured at slightly higher processing powers (27-28 watts) because of their higher viscosity and reduced mobility. To investigate the control of morphology in the modified epoxy resin networks variable-power processing was utilized. A maximum temperature of 20°C above the maximum achievable glass transition temperature, $Tg_{\infty}$, was reached in all the thermoset systems. The Epon 828/4,4'-DDS system achieved a maximum temperature of approximately

50
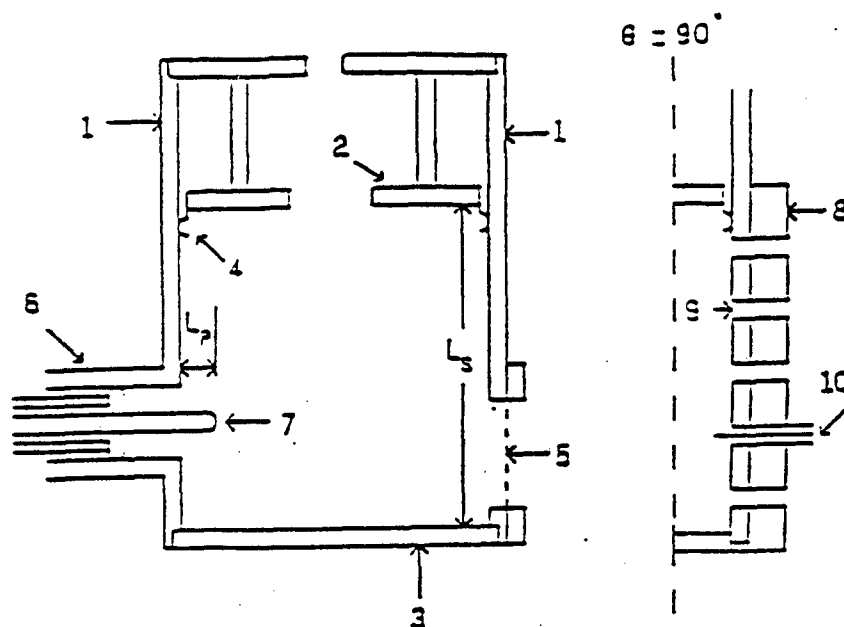
Figure 26. Cross-sectional view of the cylindrical microwave applicator. Full cross-section is the θ=0°C plane passing through the input probe. Partial cross-section θ=90°C displays the microcoax inputs. The numbered pieces are: (1) conducting cylindrical shell, (2) sliding short, (3) end plate, (4) silver finger stock, (5) screened viewing port, (6) coaxial input, (7) adjustable coupling probe, (8) brass microcoax probe holder, (9) diagnostic holes, and (10) microcoax electric field probe [173].



$E$ ——— $H$ ------
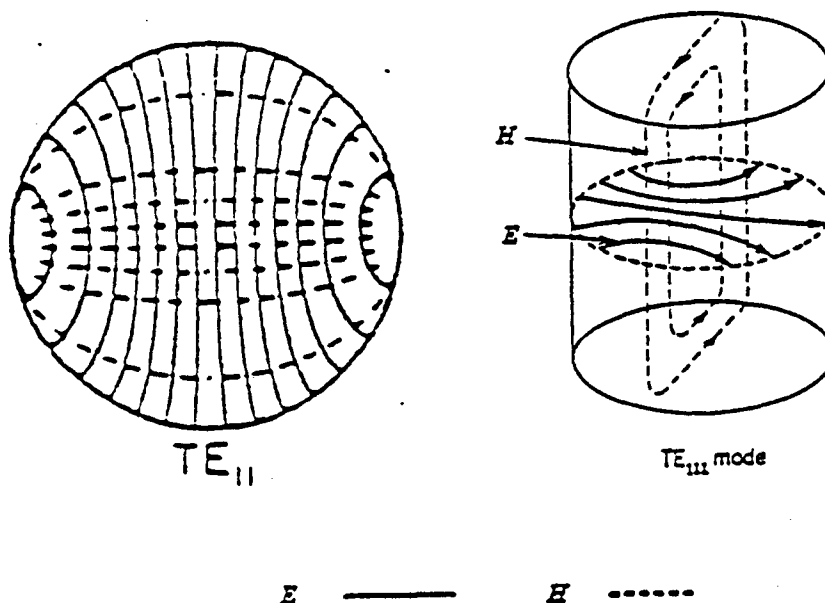
Figure 27. Field lines for the two-dimensional $TE_{11}$ mode and three-dimensional $TE_{111}$ mode.

51

220°C, while the Epon 828/3,3-DDS and DGEBA/4,4'-DDS systems achieved maximum temperatures of 190°C and 250°C, respectively. In most instances the epoxy resin mixture was approximately 50°C prior to the application of the radiation. When heated from room temperature (20°C-25°C) higher processing powers (27-33 watts) were needed to properly cure the resins because of the reduced dielectric loss of the resin at the lower temperature.

### 2.2.2.3. Functionalized Poly(arylene ether ketone)s

The maleimide, nadimide and amino functionalized poly(arylene ether ketone)s (PEK) were cured from cold pressed, one gram discs (approximately 2 cm in diameter and 1 mm in thickness). The samples were cured from room temperature in a cylindrical teflon sample holder, possessing an inner diameter of 2 cm and an outer diameter of 2.5 cm, in the geometric center of microwave applicator. Two pieces of silicone rubber (2 cm x 2 cm x 1.2 cm) were utilized to elevate the teflon sample holder to the center of the $TE_{111}$ mode. An additional piece of silicone rubber was placed on the top of the sample holder in order to secure the fiber optic temperature probes and to insulate the sample to prevent heat convection losses from the specimen. The samples were cured isothermally at various temperatures by controlling the electric field strength around the specimen. An initial input power of 60 watts was utilized to reach the desired cure temperature. The cure temperature was then held constant (±1°C) by either reducing the input power or detuning the microwave cavity.

### 2.2.2.4. Blends of Bismaleimidodiphenylmethane and Maleimide-terminated Poly(arylene ether ketone)

Bismaleimidodiphenylmethane and maleimide-terminated poly(arylene ether ketone) blends were prepared as previously described (Section 2.2.1.10.). The blends were then cold pressed and processed in an analgous manner to the functionalized poly(arylene ether ketone)s (Section 2.2.2.3.).

### 2.2.3. Characterization
### 2.2.3.1. Potentiometric Endgroup Titration

Titrations of functional monomers and oligomers were performed on either a Fisher Scientific Titrimeter II or MCI GT-5 (COSA Instruments Corporation) automatic potentiometric titrator. Samples were accurately weighed into a 150 ml beaker, dissolved with 60 ml of solvent and stirred to dissolution. Sample quantities were chosen to require approximately 2 to 4 ml of titrant. After complete dissolution, the electrodes were inserted into the solution and the titration was started. The endpoint was determined from the maximum in the first derivative plot of the titration curve. A blank titration (solvent only) was performed with the same titrant and solvent volume. The blank volume was subtracted from the endpoint value.

Amine-terminated poly(arylene ether ketone) and poly(arylene ether sulfone) oligomers were dissolved with a 70/30 (v/v) mixture of chlorobenzene (freshly distilled) and glacial acetic acid. Upon complete dissolution the mixture was titrated with 0.02 N anhydrous hydrogen bromide (HBr) in glacial acetic acid. Monomeric and oligomeric epoxides were titrated by a technique reported by Fritz [178]. The epoxide was weighed into a 150 ml beaker along with 2 grams of cetyltrimethylammonium bromide. The mixture was then dissolved in glacial acetic acid and titrated with 0.1 N perchloric acid in glacial acetic acid. Both titrants were standardized by titrating potassium hydrogen phthalate in glacial acetic acid. The molecular weights reported were based on an average of a minimum of three titrations.

## 2.2.3.2. Intrinsic Viscosity

The intrinsic viscosity, [η], of the functionalized oligomers was determined in chloroform at 25°C using a Cannon-Ubbelohde viscometer. A minimum of four concentrations were used for the measurements. The intrinsic viscosity results are reported in units of deciliters per gram.

## 2.2.3.3. Fourier Transform Infrared Spectroscopy (FTIR)

A Nicolet IODX spectrophotometer was utilized for obtaining the infrared spectra on the functionalized oligomers and monomers. The functionalized oligomers were analyzed in the form of thin films cast from dilute chloroform solutions. Monomers were examined as potassium bromide pellets.

## 2.2.3.4. Differential Scanning Calorimetry

Glass transition temperatures, melting points and epoxy network curing investigations were determined on either a Perkin-Elmer DSC-4 or a DuPont 912 connected to a DuPont 2100 Thermal Analyst. The baseline was checked for flatness and temperature calibration was accomplished using a two-point calibration procedure with indium and lead standards. The heating rate was 10°C per minute with reported values being obtained from either the first or second scan, as indicated. The glass transition temperature was defined as the midpoint of the slope change from the baseline. The extent of cure in the epoxy resin networks was determined by taking the ratio of the difference between the total enthalpy of polymerization and the exotherm of the partially cured network to the total enthalpy of polymerization. The total enthalpy of polymerization was 385 J/g for Epon 828 and 4,4'-DDS. It was determined by dissolving Epon 828 and DDS in acetone, followed by vacuum drying at ambient temperature to ensure no reaction prior to DSC analysis. All scans were run in a nitrogen atmosphere.

## 2.2.3.5. Percent Gelation from Solvent Extractions

The percent gelation in the crosslinked maleimide, nadimide and amino functionalized poly(arylene ether ketone)s was determined from solvent extractions. Cellulose fiber extraction thimbles were utilized with one to two gram samples in soxhlet extraction apparatus. The samples were extracted with chloroform for 5 days. In order to obtain very precise and accurate results weighing was performed on an analytical balance and great care was taken in the pretreatment and drying of the extraction thimbles. Pretreatment of the thimbles involved soaking in chloroform for 24 hours, then drying under vacuum for 3 hours at 20°C, 15 hours at 120°C, and finally 4 hours at 20°C. The thimbles were removed from the vacuum oven and weighed immediately. A known amount of sample was then added to the thimble and extracted. After the extraction the same drying and weighing procedure was repeated and the percent gelation was determined from the equation below:

$$\text{Percent Gelation} = \frac{w_i - w_f}{w_i} \times 100 \tag{14}$$

where $w_i$ and $w_f$ are the initial and final weights of the sample, respectively.

### 2.2.3.6. Scanning Electron Microscopy

Scanning electron microscopy (SEM) was utilized to study the phase separation behavior in the thermoplastic-modified epoxy resin networks. Two different instruments were utilized in the SEM investigations. An International Scientific Instrument Model SX-40 was used to examine the surface topography up to a magnification of 10,000X, and a Phillips EM-420 Scanning Transmission Electron Microscope (STEM) was utilized for higher magnifications (up to 100,000X). Fracture surfaces were mounted on either copper or aluminum substrates using a conductive silver paint as an adhesive. The specimens were then coated with approximately Å of gold using a Bio-Rad Polaron (Model E5400) high resolution sputter coater to improve conductivity and prevent charging. The fracture surfaces were examined with an electron beam voltage of 15,000 volts and a tilt angle of 0° to 30°.

### 2.2.3.7. Dynamic Mechanical Thermal Analysis

Dynamic mechanical thermal analysis (DMTA) was utilized to investigate the degree of phase separation in the thermoplastic-toughened epoxy resin networks. A Polymer Laboratories Mark II instrument was used at a frequency of 1 Hz and a strain amplitude of 20 μm. Sample specimens possessing dimensions of 3.0 mm x 6.5 mm x 30 mm were mounted in a dual-cantilever clamp and evaluated at a heating rate of 5°C per minute over a 30°C-350°C temperature range.

### 2.2.3.8. Fracture Toughness

The fracture behavior of the thermoplastic-modified epoxy resin networks was examined according to the procedures described by the American Society for Testing and Materials specification (ASTM E399). Three-point bend specimens (Figure 28) possessing dimensions of 3.2 mm x 6.5 mm x 38 mm were cast into silicone rubber molds as previously described (Section 2.2.1.9.). The specimens were prepared for the testing by notching (approximately 0.5 mm deep) the sample in the middle with a reciprocating saw. A sharp crack was then initiated at the base of the notch by carefully tapping a fresh razor blade in the slot. To insure an infinitesimally sharp crack the razor blade was previously chilled by submersion in liquid nitrogen. Care was taken to insure that the crack propagated evenly about midway through the thickness of the specimen. The specimen was then placed into the three-point bend apparatus (depicted in Figure 29), which was affixed to an Instron testing machine (Model 1123). Samples were tested at a crosshead speed of 0.5 mm per minute (or 0.02 in per minute) until failure. Upon failure, the various specimen geometries were measured with a dial caliper and the critical stress intensity to cause catastrophic failure in mode I (tensile) opening was calculated by:

$$K_{Ic} = \frac{P.S}{b.W^{3/2}} \; [2.9(a/w)^{1/2} - 4.6(a/w)^{3/2} + 21.8(a/w)^{5/2} \qquad (15)$$
$$- 37.6(a/w)^{7/2} + 38.7(a/w)^{9/2}]$$

where P = load at failure
S = span between supports
b = thickness
W = width
a = crack length

The calculated results were reported in units of $N/m^{3/2}$.
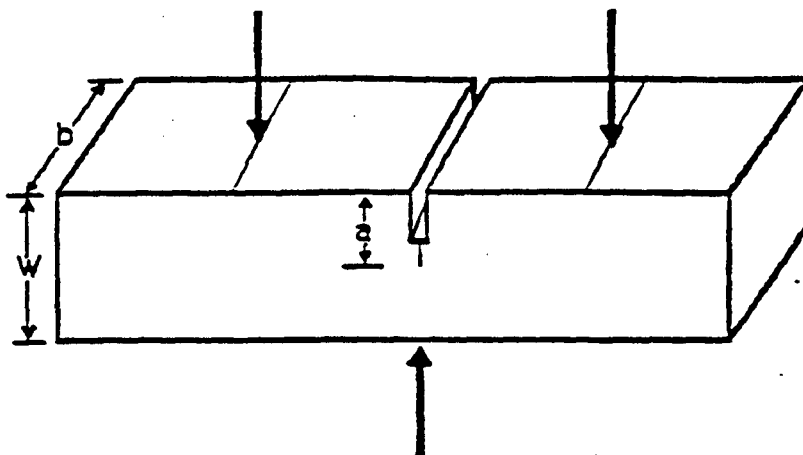
Figure 28. Three-point bend specimen utilized to determine fracture toughness.
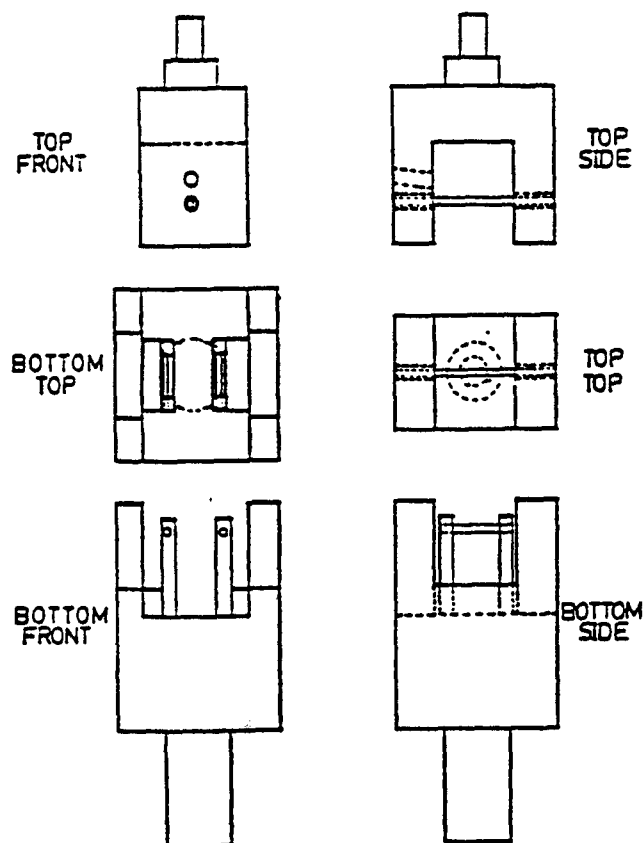


Figure 29. Schematic of the three-point bend fixture used for determining both fracture toughness and flexural modulus.

## 2.2.3.9. Flexural Modulus

The flexural modulus of the epoxy resin networks was evaluated according to the standards of the American Society for Testing and Material specification (ASTM E966). Three-point bend specimens possessing dimensions of 1.5 mm x 13 mm x 52 mm were tested in the apparatus depicted in Figure 29 with an Instron testing machine (Model 1123) at a constant displacement of 1 mm per minute until failure. The flexural modulus was then calculated from the load versus crosshead displacement plot and the following equation:

$$E_f = \frac{4.01 \times 10^{10} \, P \, D}{W \, T^3 \, C} \tag{16}$$

where P = load
D = crosshead displacement
W = width
T = thickness
C = chart speed

The calculated results are reported in units of Pascals.

## 2.3. Results and Discussion
## 2.3.1. Epoxy Resin Networks
## 2.3.1.1. Introduction

Epoxy resin networks have gained wide acceptance in electrical and structural applications because of their exceptional combination of properties such as high strength, adhesion, chemical resistance, thermal stability and superior electrical properties. However, in many structural applications, such as composite matrix resins, their application is limited by the extensive curing cycles required to develop optimum mechanical properties. In this investigation microwave radiation was utilized to cure epoxy resin networks to determine if the long, complex cure cycles required to achieve optimum mechanical properties could be reduced. These cycles usually consist of slow thermal ramp rates to assure uniform temperatures throughout the material, with long time periods at plateau temperatures to allow the reaction to reach completion in a controlled manner and to avoid excessive heat buildup, because of the highly exothermic nature of the process. The application of electromagnetic radiation to this area of processing is ideal because of the large penetration depth of microwave radiation, which provides rapid and uniform heating rates.

## 2.3.1.2. Microwave Processing

The interaction of microwave radiation with dielectric materials has been previously discussed (Section 2.0.). The net result is the conversion of electromagnetic energy into thermal energy or heat. The heating rate is a function of several parameters as described by the equation below:

$$\frac{dT}{dt} = \frac{K \, f \, E^2 \, \epsilon'(T) \, \tan\delta(T)}{\rho \, C_v} \tag{17}$$

where K is a constant, f is the applied frequency, E is the electric field strength, $\rho$ is the density, $C_V$ is the specific heat, $\varepsilon'$ is the dielectric constant and $\tan\delta$ is the dielectric loss tangent. The heating rate equation (Equation 2) provides a qualitative representation of the variables that influence the microwave heating rates of polymeric materials when subjected to an electromagnetic field. However, it only accounts for heating that is due to the interaction of the microwave radiation with the material; it ignores convection and conduction losses as well as heating effects that are due to conductivity and the heat of reaction (if applicable).

The heating rate equation was examined by evaluating the temperature-time profile of various weights of neat Epon 828 (a nonreactive liquid epoxy resin) as shown in Figure 30. Neat Epon 828 can undergo homopolymerization at temperatures in excess of 300°C; however, under the conditions utilized in this investigation it can be considered nonreactive. The general shape of the curves shown in Figure 30 was representative of most nonreactive systems. An initial large rise in temperature was observed, followed by a decrease in the heating rate and an eventual approach to a constant value (i.e. slope of the curve approximately equal to zero). The reduction in the heating rate and the corresponding leveling off effect can be attributed to a thermal equilibrium state that was achieved as the rate of heat dissipation to the environment became equivalent to the rate of sample heating because of microwave energy absorption. Equation 17 can be utilized to predict the initial heating rate of the curves in Figure 30; however, beyond this, additional terms are required to account for heat losses to convection and thermal transfer to the mold.

In general, the factors that influence the shape of temperature-time profiles include: (i) the dielectric loss behavior of the sample, (ii) the incident power and position of the sample within the cavity, (iii) the sample size, (iv) the sample geometry, and (v) the heat capacity of the polymer and mold.

The dielectric loss factor is the most important parameter effecting the heating rate of a polymer. The dielectric properties are a function of temperature; thus, as temperature increases both $\varepsilon'$ and mobility increase, and the ability of the polymer to couple with the electromagnetic field is enhanced. Chen et al. [179] has defined a variable known as the critical temperature $T_c$ for microwave heating. Above $T_c$, polymers heat up very rapidly when subjected to electromagnetic radiation, and below $T_c$ the heating rate is very slow. $T_c$ is a function of the dielectric loss behavior of the sample at microwave frequencies. With polymeric materials the dielectric loss dispersion shifts to higher temperatures as frequency is increased. The degree to which the dispersion shifts at a frequency of 2.45 GHz may be estimated by analyzing sample mass. The properties of the polymer in the dielectric frequency range using dielectric thermal analysis (DETA). The principles of this technique will be explained in greater detail in a later section of this dissertation, where the technique of microwave calorimetry has been applied to nonreactive thermoplastic blends (Section 3.2.4.).

The input power and the position of the sample in the cavity both make significant contributions to the initial slopes of the curves in Figure 30. The heating rate (Equation 17) is proportional to the electric field strength squared; thus, as input power is increased for a constant mass of sample, the heating rate is accelerated. Furthermore, since the power density stored in the microwave applicator is not constant throughout, the position of the sample within the cavity has a strong bearing on the heating rate.

According to Equation 17, the heating rate should increase as the sample mass of a nonreacting sample is reduced. This theory was examined by heating various weights of neat Epon 828 at a constant input power with the microwave applicator critically coupled in the $TE_{111}$ mode. Indeed, the results demonstrated (as shown in Figure 30) that the heating rate, as evaluated by the initial slope of the temperature-time profile, increased as the mass of the nonreactive sample (neat Epon 828) decreased.

The sample geometry and the heat capacity of the polymer and the mold also influence the shape of the curves in Figure 30. Convection losses to the environment decrease as the volume/surface area ratio of the sample increases. And the heat capacity, being a measure of the ability of a substance to heat, not only influences the rate of temperature increase, but also the rate of temperature decrease.
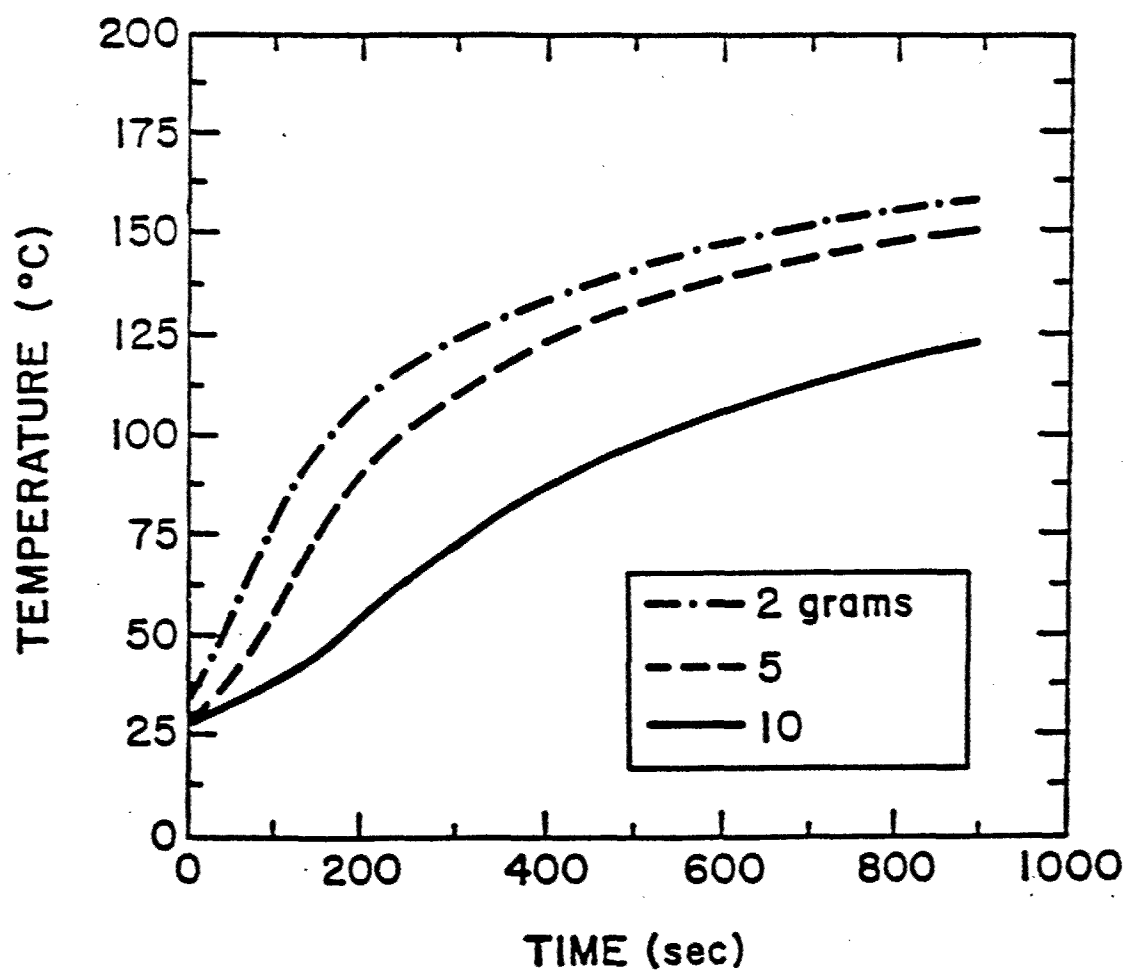
Figure 30. Temperature-time profile for neat Epon 828 as a function of sample mass.

The temperature-time profile of a thermosetting epoxy resin system was much more complicated than that of neat Epon 828. This can be attributed to both the reaction exotherm and the changing dielectric loss behavior of the resin with network formation. A typical temperature-time profile for an electromagnetically processed epoxy resin comprised of Epon 828 and 4,4'-DDS is given in Figure 31. Three distinct regions were observed in Figure 31 corresponding to (I) heating of the monomers, (II) the reaction exotherm, and (III) cooling of the cured system. These results were consistent with previously published observations by Gourdenne et al. [11-14].

In region I of Figure 31, the temperature-time curve obeyed the heating rate equation (Equation 17) in a similar manner to neat Epon 828. In region II a decrease in the heating rate was observed because of heat loss to the environment, followed by rapid heating (3 to 5°C/second) with the onset of the reaction exotherm. In contrast to nonreactive systems, sample mass not only influences the initial heating rate but also determines the maximum temperature reached during processing, since this is governed by the magnitude of the reaction exotherm. In region III of the temperature-time curve cooling was observed because of a combination of the completion of the reaction exotherm and to lower microwave absorption with network formation. With increasing network conversion, corresponding decreases in both mobility and dielectric loss of the resin result, and, microwave absorption is reduced. Furthermore, when the network reaches the stage of vitrification, the $T_g$ of the network becomes equivalent to the cure temperature, thus restricting motion and hampering the ability of the electromagnetic field to effectively couple with the dipoles.

In summary, the temperature-time profiles discussed in this section are a function of numerous parameters, because of the complexity of the microwave absorption process. Defining the variables needed to obtain good process control is crucial. After the processing parameters have been identified, they can be varied in a systematic fashion to control the rate of heating and effectively process polymers.

## 2.3.1.3. Thermal Analysis

Glass transition temperatures and the extent of cure in the microwave and thermally cured epoxy resin networks were determined using differential scanning calorimetry (DSC). DSC provides a simple method for monitoring the extent of reaction by observing the residual exotherm of polymerization. A DSC heating trace (first heat) for a partially cured Epon 828/4,4'-DDS epoxy resin sample processed with microwave radiation is given in Figure 32. A Tg of 165°C and a reaction exotherm indicating that a degree of cure of 98% was achieved during microwave processing can be ascertained from this scan. Typically, microwave processed samples exhibited a Tg of approximately 180°C and a degree of cure in excess of 99%. The second DSC heating scan for the microwave cured network demonstrated a higher Tg of 199°C (as shown in Figure 33) because of completion of the reaction after being heated to 330°C during the first scan. This value was in agreement with that obtained for conventional thermal processing.

The glass transition temperature results in Table 3 shows that incomplete conversion of 1 or 2 percent can depress the $T_g$ of the network up to 25°C. In general, for isothermal cure temperatures below the minimum temperature required to achieve complete cure, $T_{g\infty}$, reaction proceeds to the point at which the $T_g$ corresponds to the cure temperature. At this point vitrification occurs and further curing at or below the same isothermal cure temperature is very slow. At vitrification the reaction shifts from chemical control to diffusion control and, for all practical purposes, further curing is halted. For isothermal cure temperatures equal to or greater than $T_{g\infty}$, essentially complete conversion was obtained as can be shown in Figure 34. When EMR constant power processing was employed, the samples were exposed to the temperature-time profile shown in Figure 31. Thus, the incomplete conversion (approximately 1 to 2 percent) exhibited by the microwave processed epoxy resins may be attributed to the relatively short period of time that the samples remained above $T_{g\infty}$.

A conversion versus time plot for the microwave and conventional isothermally cured epoxy resin networks (based on Epon 828/4,4'-DDS) is shown in Figure 34. This plot demonstrates the enormous capability of electromagnetic radiation (EMR) processing. The EMR processed
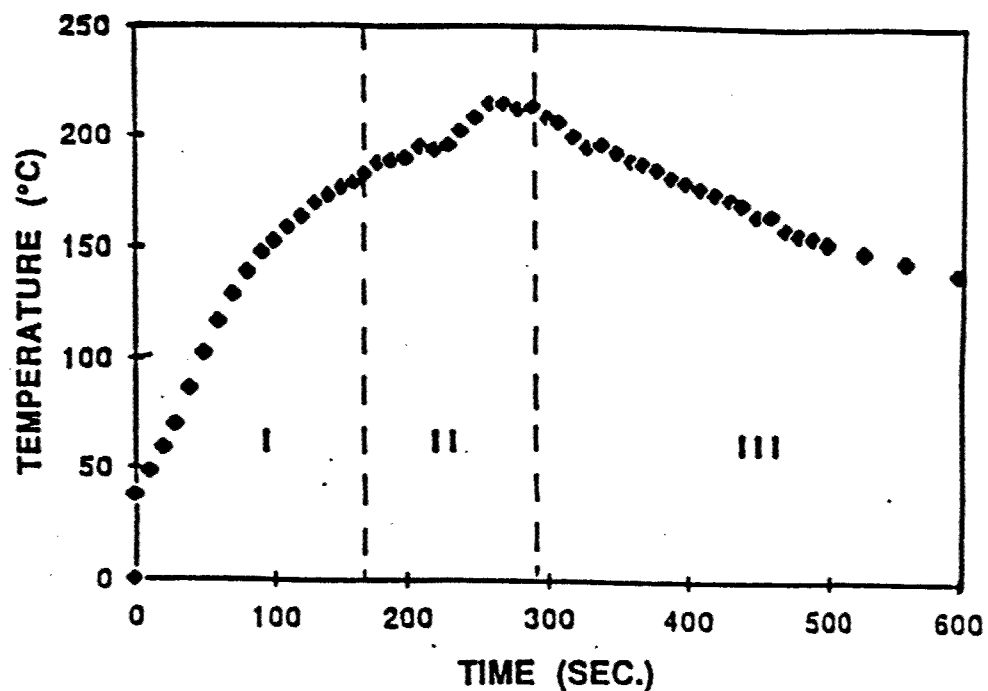
Figure 31. Temperature-time profile for microwave processed
Epon 828/4,4'-DDS epoxy resin.
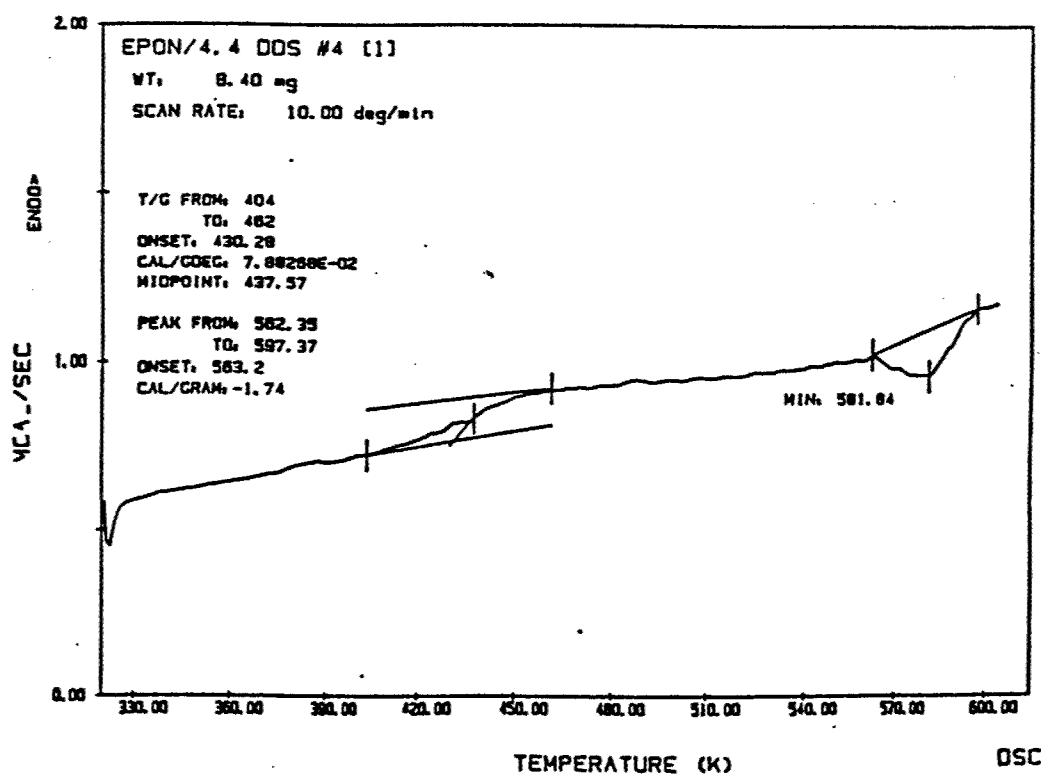


Figure 32. First DSC heating scan for an electromagnetically processed epoxy resin network
(approximately 98% cured).

60
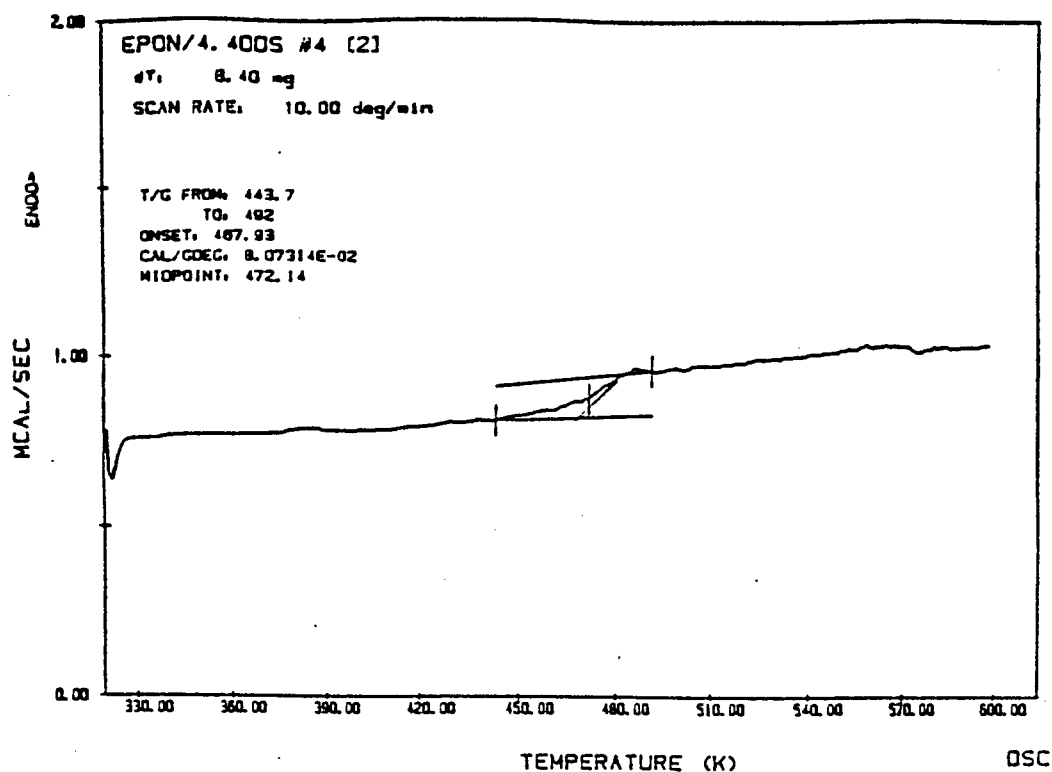
Figure 33.   Second DSC heating scan for an electromagnetically processed epoxy resin network.
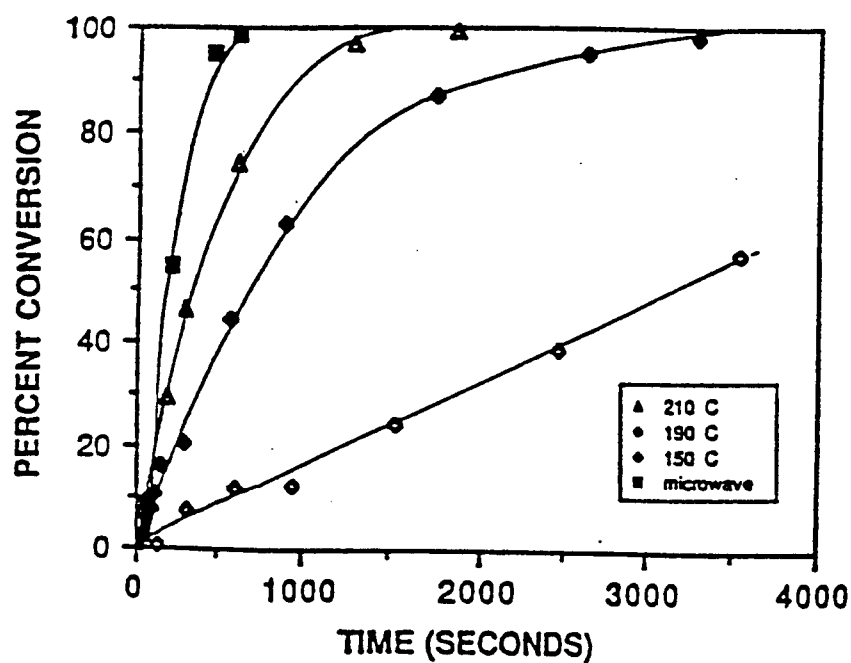


Figure 34.   Microwave and thermal curing behavior of an epoxy resin network based on Epon 828/4,4'-DDS (from Dallas et al. [180]).

61

Table 3. **Glass transition temperatures for the microwave and thermally processed epoxy resin networks.**

| Network System | Microwave | | Thermal | |
|---|---|---|---|---|
| | First Heat | Second Heat | First Heat | Second Heat |
| Epon 828/4,4'-DDS | 180 | 199 | 199 | 199 |
| Epon 828/3,3'-DDS | 155 | 170 | 170 | 170 |
| DGEBA/4,4'-DDS | 212 | 230 | 230 | 230 |

materials achieved 98% to 100% conversion in less than 600 seconds (10 minutes). Samples cured isothermally in a forced-air convection oven at 210°C and 190°C took significantly longer to reach this same degree of conversion (approximately 30 to 60 minutes, respectively). This represents a three- to sixfold reduction in the time required to cure these networks. The mechanism of the accelerated curing rate is uncertain. Two proposals have been put forth to explain the reduced curing times. The first attributes the acceleration to the novel mechanism of energy transfer with EMR processing [11-14]. And, the second proposal, put forward by Lewis et al. [63,64] attributes the accelerated reaction rates to localized heating on the molecular level, as previously discussed (Section 2.1.1.7).

### 2.3.1.4. Mechanical Properties

Several investigators have employed microwave radiation to cure thermosetting epoxy resins as previously discussed (Section 2.1.1.1.). The results of these investigations indicated an acceleration of the curing process upon exposure to the electromagnetic field. However, until the current investigation, the influence of EMR processing on the mechanical properties of the cured epoxy resin networks were unknown. Mechanical property evaluation of these networks is crucial, especially since these materials are targeted for high performance structural applications.

The mechanical properties of the microwave and thermally processed epoxy resin networks are given in Table 4. The results were based on an average of 15 to 20 samples for each fracture toughness value and 8 to 10 samples for each flexural modulus value with a reported error of two standard deviations. Fracture toughness provides a measure of the brittleness of the material, and flexural modulus gives an indication of the strength of the cured network. The results shown in Table 5 as a function of processing were essentially identical within experimental error. This indicated that accelerated microwave processing had no adverse effects on either the toughness or strength of the cured networks.

### 2.3.2. Thermoplastic-Modified Epoxy Resin Networks
### 2.3.2.1. Introduction

Thermoplastic-toughened epoxy resin networks are currently being utilized as high performance composite matrix resins and adhesives in the aerospace and aircraft industries. These systems possess a distinct advantage over the neat resin networks; damage tolerance as measured by compression after impact (CAI) testing is significantly enhanced by the presence of the phase-separated thermoplastic toughener. Thermoplastic modifiers are tough, ductile engineering polymers possessing high glass transition temperatures. When incorporated into thermosets enhanced toughness can be achieved without compromising the high-modulus or thermal stability of the network, contrary to rubber-toughened systems.

Selection of a suitable modifier is crucial since its compatibility with the epoxy determines the extent and type of phase separation. The thermoplastic modifier must be initially soluble in the epoxy resin before undergoing an in situ phase separation process during network formation. The compatibility of the modifier in the epoxy resin varies with chemical composition, endgroup functionality, molecular weight, and percent incorporation. The thermoplastic modifier chosen in this investigation was an amino functionalized poly(arylene ether sulfone) (PSF) oligomer. Amino functionalization of the polysulfone served two purposes. First, it allowed the PSF to actually chemically react with the epoxy, thus maintaining the solvent resistant character of the network. Second, it enhanced the compatibility between the polysulfone and epoxy resin.

Both microwave and conventional thermal processing techniques were employed to cure the thermosetting systems. Microwave radiation was utilized to determine if the long, complex cure cycles required to achieve optimum mechanical properties in these networks could be reduced. And, variable-power microwave processing was employed to determine if the morphology of the modified thermosets could be controlled in a systematic fashion. The fracture toughness and

63

Table 4. Mechanical properties of microwave and thermally cured epoxy resin thermosets.

| Polymer System | Microwave Cure | | Thermal Cure | |
|---|---|---|---|---|
| | $K_{Ic}/10^6 Nm^{-3/2}$ | $E_f/10^9 Pa$ | $K_{Ic}/10^6 Nm^{-3/2}$ | $E_f/10^9 Pa$ |
| Epon 828/4,4'-DDS | 0.6 ± 0.2 | 2.6 ± 0.3 | 0.8 ± 0.2 | 2.5 ± 0.3 |
| Epon 828/3,3'-DDS | 0.7 ± 0.2 | 3.1 ± 0.4 | 0.8 ± 0.2 | 3.0 ± 0.3 |

morphology of the thermoplastic-toughened epoxy resin networks were examined to evaluate the feasibility of microwave processing. The toughened networks were also investigated as a function of the molecular weight and percent incorporation of the polysulfone modifier.

## 2.3.2.2. Preparation of Thermoplastic Modified Thermosets

Amine-terminated poly(arylene ether sulfone) oligomers were successfully synthesized by a nucleophilic aromatic substitution reaction utilizing N-methylpyrrolidinone as a solvent and potassium carbonate as a weak base as described in Section 2.2.1.4. The Carothers equation (Section 2.2.1.6) was utilized to calculate the amount of m-aminophenol required to achieve controlled molecular weight and amine termination. Table 6 provides the theoretical and titrated molecular weights as well as the intrinsic viscosities and glass transition temperatures of the oligomers utilized in this investigation. As demonstrated by Table 5, as molecular weight increased, corresponding increases in the viscosity and Tg of the oligomers were observed. The fully characterized amine-terminated polysulfone oligomers were then utilized together with diaminodiphenylsulfone to cure DGEBA (Section 2.2.1.9.) to form the thermoplastic-toughened epoxy resin networks.

## 2.3.2.3. Morphology

Scanning electron microscopy (SEM) micrographs of actual fracture surfaces of the thermoplastic-modified epoxy resin networks are shown in Figures 35 through 40 as a function of molecular weight, percent incorporation, and processing technique. Each figure in this series is shown at two magnifications (5,000x and 10,000x) with the thermally processed samples on the left-hand side of the figure and the electromagnetically processed samples on the right-hand side. The fracture surfaces for 15 and 30 weight percent incorporation of a 6.0 kg/mole PSF oligomer are shown in Figures 35 and 36, respectively. The SEM results for the 10.9 and 16.2 kg/mole PSF oligomers at 15 and 30 weight percent incorporations are shown in Figures 37 through 40.

## 2.3.2.2.1. Effect of Modifier Molecular Weight

The influence of increasing the molecular weight of the thermoplastic modifier upon the phase separation behavior may best be explained by analyzing the Flory-Huggins equation (Equation 7). Generally, as molecular weight (or the degree of polymerization) of one or both components in a binary mixture increase, the mutual solubility of the two polymers decrease. This may be attributed to a reduction in the combinatorial entropy term in Equation 7, which decreases the magnitude of the negative entropic contribution (i.e., the driving force for miscibility) to the Gibbs free energy of mixing [98,102].

The effect of molecular weight of the polysulfone modifier in the current investigation may be observed by evaluating Figures 35, 37, and 39, where at a constant composition (15 weight percent) molecular weight of the PSF was increased from 6.0 to 10.9 to 16.2 kg/mole, respectively. Comparison of Figures 35, 37, and 39 demonstrate that the morphology of the toughened networks was strongly influenced by the PSF molecular weight. As molecular weight increased, phase separation (for both the thermal and microwave processed systems) became more pronounced and defined, generating a two-phase morphology.

With the addition of 15% of a 6.0 kg/mole PSF oligomer, the SEM micrographs in Figure 35 demonstrated no significant topographical features, thus suggesting that the PSF was highly soluble in the epoxy resin at this molecular weight. However, as molecular weight was increased to 10.9 or 16.2 kg/mole (Figures 37 and 39, respectively), the PSF phase-separated into a well-defined, two-phase morphology consisting of uniformly dispersed spheres of PSF in an epoxy resin matrix for both the electromagnetically and thermally processed materials. The size of the

Table 5.**Characterization of the amine-terminated polysulfone oligomers utilized as thermoplastic toughening agents.**

| Theoretical $<M_n>$ (kg/mole) | Titrated $<M_n>$ (kg/mole) | $T_g(°C)$ [•] | 25°C $[\eta]$ $CH_2Cl_2$ |
|:---:|:---:|:---:|:---:|
| 5.0 | 6.0 | 166 | 0.13 |
| 10.0 | 10.9 | 178 | 0.18 |
| 15.0 | 16.2 | 180 | 0.22 |

[•]Determined by second heating scan from DSC.

THERMAL CURED        MICROWAVE CURED
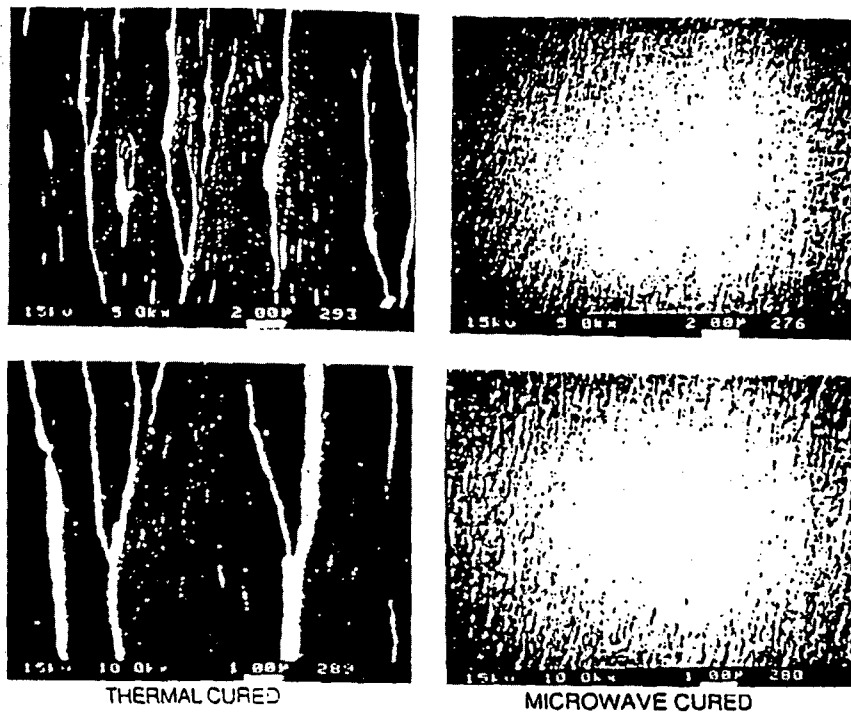
**Figure 35.** Fracture surface of thermal and microwave processed epoxy resin networks containing 15% polysulfone (<Mn> = 6.0 k).



THERMAL CURED        MICROWAVE CURED
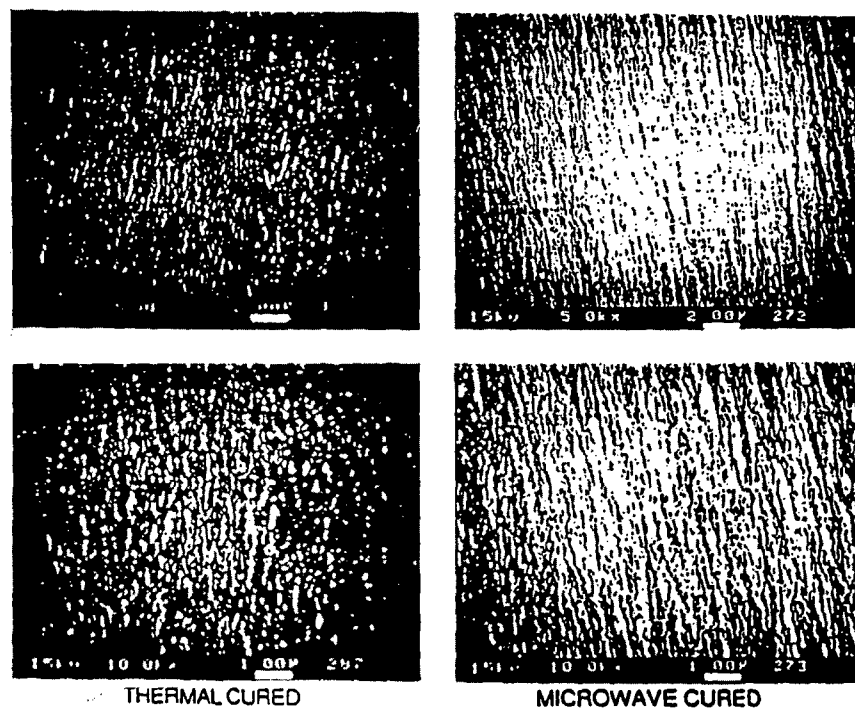
**Figure 36.** Fracture surface of thermal and microwave processed epoxy resin networks containing 30% polysulfone (<Mn> = 6.0 k).

67

THERMAL CURED        MICROWAVE CURED
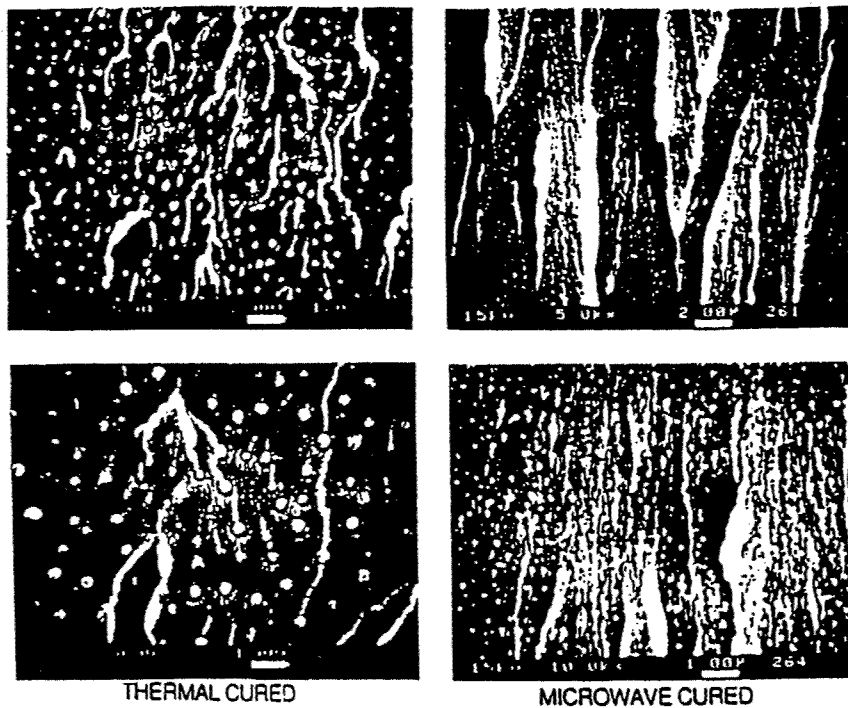
Figure 37. Fracture surface of thermal and microwave processed epoxy resin networks containing 15% polysulfone (<Mn> = 10.9 k).



THERMAL CURED        MICROWAVE CURED
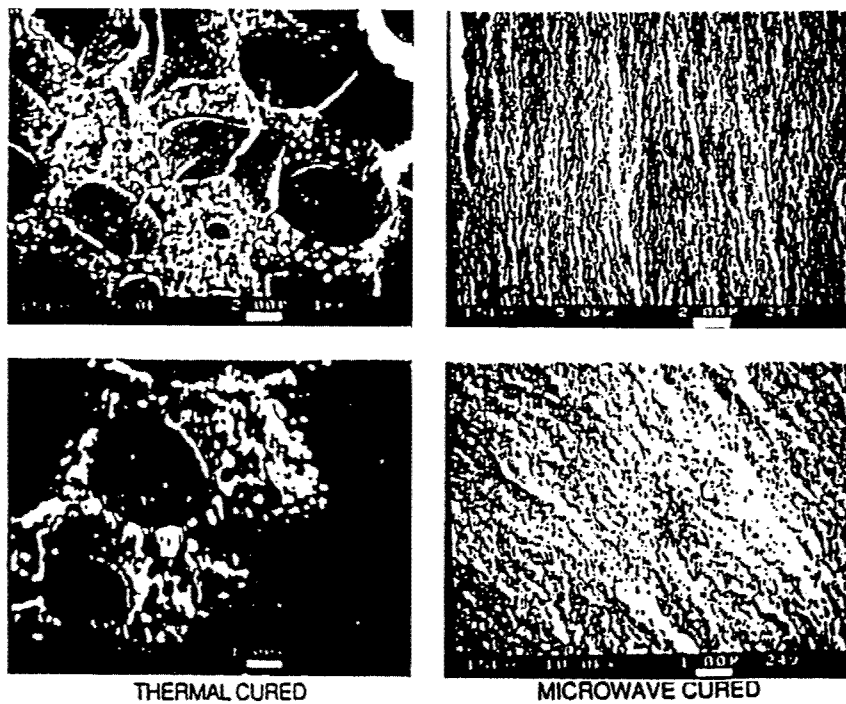
Figure 38. Fracture surface of thermal and microwave processed epoxy resin networks containing 30% polysulfone (<Mn> = 10.9 k).

68

THERMAL CURED        MICROWAVE CURED
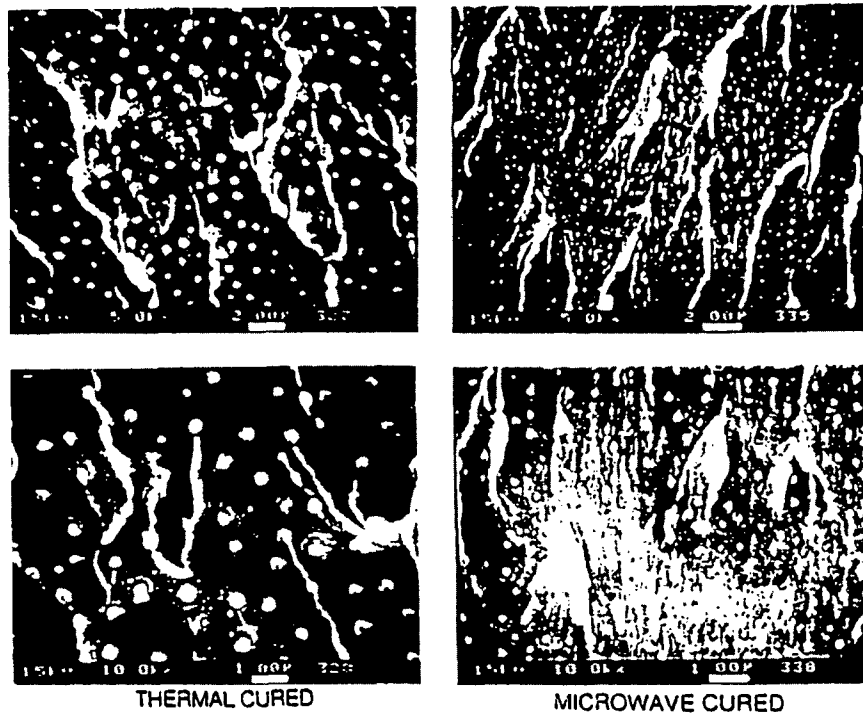
**Figure 39.** Fracture surface of thermal and microwave processed epoxy resin networks containing 15% polysulfone (<Mn> = 16.2 k).



THERMAL CURED        MICROWAVE CURED
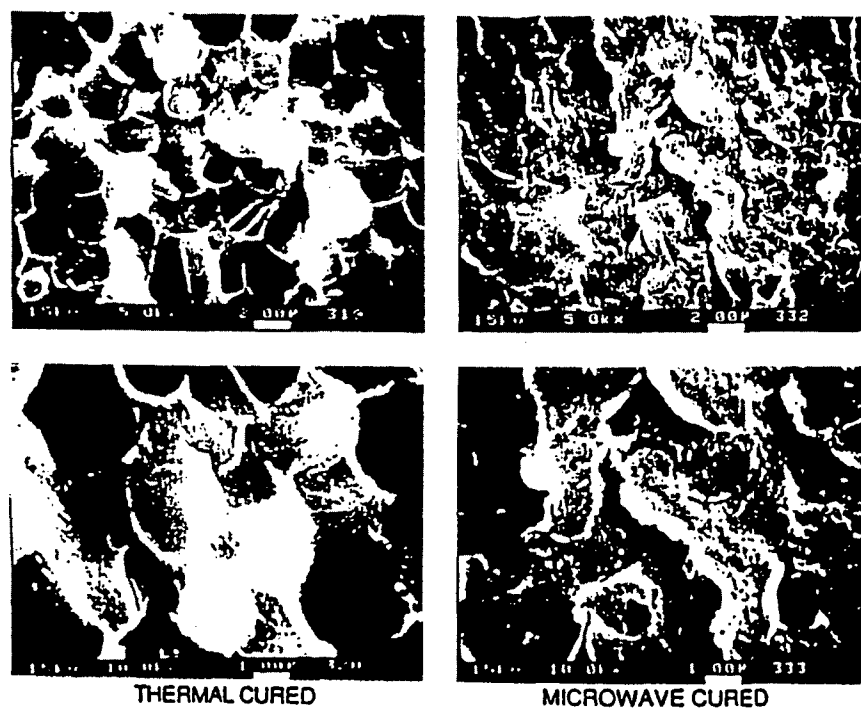
**Figure 40.** Fracture surface of thermal and microwave processed epoxy resin networks containing 30% polysulfone (<Mn> = 16.2 k).

69

spheres was approximately 0.5 to 0.7 μm in diameter for the thermally cured systems and 0.1 to 0.2 μm for the electromagnetically processed materials. The effect of molecular weight was even more pronounced at 30% incorporation as shown in Figures 36, 38, and 40. With the addition of the 6.0 kg/mole oligomer, both the microwave and thermally cured networks exhibited only surface roughness as shown in Figure 36. However, as molecular weight was increased to 10.9 or 16.2 kg/mole (Figures 38 and 40, respectively), the effect of molecular weight upon the solubility of the PSF in the epoxy resin became more evident, especially for the thermally cured networks. The SEM micrographs in Figure 38, for instance, displayed two phases, the lighter continuous phase was polysulfone and the large, dark irregular spheres (4-10 μm in diameter) were composed of epoxy resin. The development of this phase-inverted network became more distinct with the incorporation of 16.2 kg/mole PSF oligomer as shown in Figure 40. The "honeycomb" structure shown in Figure 40, for the thermally processed network, was composed of spheres of epoxy resin embedded in a continuous PSF matrix.

### 2.3.2.3.2. Effect of Composition

The effect of composition on the phase separation behavior of thermoplastic-modified epoxy resin networks can best be explained by analyzing the phase diagram shown in Figure 11. A phase diagram is created by plotting a series of $\Delta G_m$ versus $\phi_2$ curves as a function of temperature for blends or conversion for networks. The generalized phase diagram shown in Figure 11 exhibits upper critical solution temperature (UCST) behavior. Most high molecular weight polymers and thermosets, however, exhibit lower critical solution temperature behavior since they are typically less miscible at higher temperatures or conversions.

In analyzing a phase diagram to determine the effect of composition, the position at which the critical temperature, $T_c$, occurs is extremely important. The critical temperature occurs at the intersection of the binodal and spinodal curves and may be determined from Equation 6. At $T_c$, $\phi_2$ equals the critical composition, $\phi_c$. The physical significance of Tc is that at compositions below $\phi_c$, phase separation generally occurs via a nucleation and growth mechanism characteristic of binodal phase separation. When $\phi_2$ equals $\phi_c$, phase separation occurs by spinodal decomposition. And, finally, when $\phi_2$ is greater than $\phi_c$, a phase inversion results and phase separation, once again, generally takes place by binodal phase separation.

In the polysulfone-modified epoxy resin networks utilized in this investigation the critical composition has been reported to occur at a composition of approximately 25 to 27 weight percent polysulfone [78-81]. Thus, in the thermally cured systems in Figures 37 through 40, where the molecular weight of the PSF was high enough to induce observable degrees of phase separation by SEM, drastically different morphologies were obtained as a function of composition. At 15 weight percent incorporation, phase separation appeared to occur via a nucleation and growth mechanism characteristic of binodal phase separation. The morphology of these networks exhibited a well-defined, two-phase morphology consisting of PSF spheres in an epoxy resin matrix. However, at 30 weight percent incorporation, above $\phi_c$, a phase inversion resulted and the morphology contained a polysulfone-rich continuous phase surrounding large spheres (3 to 4 μm in diameter) of epoxy resin.

### 2.3.2.2.3. Microwave versus Thermal Processing

The thermally and electromagnetically processed polysulfone-modified epoxy resin networks demonstrated significantly different morphologies. This was most evident with the higher molecular weight oligomers as shown in Figures 37 through 40. At 15 weight percent PSF incorporation both the size and concentration of the phase separated PSF domains were found to be highly dependent on processing as demonstrated in Figures 37 and 39. Specifically, the thermally cured materials possessed domains measuring approximately 0.5 to 0.7 μm in diameter. The

morphology of the EMR processed networks contained a greater concentration of smaller (0.1 to 0.2 μm) phase separated domains.

The dependency of the phase separation behavior on processing was also evident at 30 weight percent incorporation as shown in Figures 38 and 40. The phase inversion, that typically occurs in this system at PSF compositions in excess of 27% incorporation, was clearly evident for the thermally cured networks. However, the morphology of the EMR processed materials was not as well-defined. The EMR cured network shown in Figure 38 demonstrated only surface roughness (at least at these magnifications), and the phase inversion, although appearing to commence in Figure 40, was not developed to the same extent as in the thermally cured systems.

In toughened networks the modifier (i.e., polysulfone) is dissolved into the epoxy resin forming a homogeneous mixture before undergoing an in situ phase separation process during network formation. Demixing of the homogeneous binary mixture occurs when the Gibbs free energy of mixing changes sign, from negative to positive, as molecular weight increases with conversion of the network structure. Phase separation is thermodynamically favored; however, it is controlled by the competing effects of the kinetics of phase separation and the reaction rate. Kinetics control the rate of nucleation and growth, and are highly dependent on both temperature and viscosity. Reaction rate dictates the extent of phase separation, since phase separation is halted at gelation as the viscosity of the mixture approaches infinity, ceasing further diffusion in the binary mixture.

When conventional thermal processing was employed to cure the modified networks a cure cycle consisting of 2 hours at 30°C below the ultimate glass transition temperature (230°C), $T_{g\infty}$, and a postcure for 1 hour at 10°C above $T_{g\infty}$ was employed. This cure cycle allowed for sufficient time and diffusion for complete phase separation to occur, as revealed in the SEM micrographs shown in Figures 35 through 40. Conversely, the EMR processing cycle lasted for only 10 minutes because of the accelerated nature of microwave curing. During this cycle, the network was only above $T_{g\infty}$ for approximately 3 minutes. The morphology of these networks revealed (as shown in Figures 35 through 40) that the extent of phase separation, although developed to some degree, was not as well-defined as in the thermally processed materials. This may be attributed to an accelerated approach to the gel point. Microwave processing, as previously discussed (Section 2.3.1.2), results in a three-to sixfold enhancement in the reaction rate of epoxies; thus gelation is achieved prior to complete phase separation. Since the phase separation process stops at gelation, the network becomes "locked" into a phase-mixed morphology indicative of incomplete phase separation.

To determine if the morphology of the EMR processed networks was, in fact, "locked" into the phase-mixed microstructure, the microwave cured specimen shown in Figure 39 was postcured at 240°C for 1.5 hours in a forced-air convection oven. The morphology was then evaluated using a high-resolution Phillips STEM (in the SEM mode) at a magnification of 50,000x. Direct comparison of the microwave processed networks, with and without the postcure, to a thermally cured network revealed (as shown in Figure 41) that the extent of phase separation in the microwave cured material did not change significantly. Indeed, the size of the phase- separated PSF domains in the microwave cured networks was not affected by the thermal postcure.

2.3.2.3.4. Generation of Controlled Morphology with Variable-Power Processing

In general, the phase separation behavior in modified epoxy resin networks is controlled by the competing effects of thermodynamics, kinetics and polymerization rate [94,95]. In a typical polymer blend, thermodynamics can be utilized to make predictions about the equilibrium state of a binary mixture; however, kinetic factors must also be considered since equilibrium can only be reached if sufficient time for diffusion is allowed. For thermosetting systems, further complications exist because both molecular weight and viscosity increase with increasing conversion of the epoxy resin network. Once the development of the network reaches the stage of gelation, phase separation is halted and the morphology is fixed. Thus, from a single thermoplastic-modified epoxy resin formulation a variety of different phase-separated

71

# THERMOPLASTIC MODIFIED EPOXY RESIN NETWORKS
### (15% w/w NH$_2$-PSF Into DGEBA/4,4'-DDS)



Thermally Processed
Bar=0.5µm (100,000x)

Microwave Processed
Bar=0.5µm (100,000x)

Microwave Processed w/
Thermal Postcure (1.5 hr @ 240°C)
Bar=0.5µm (100,000x)
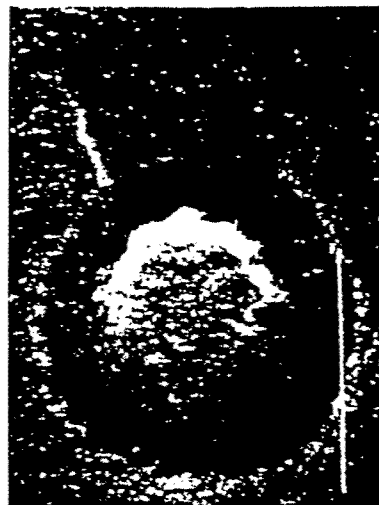
Figure 41. Fracture surfaces of a thermoplastic-modified epoxy resin network (15% w/w of a 16.2 kg/mole PSF oligomer) comparing a conventional thermal cure to microwave processing with and without a postcure.

morphologies can be generated by accelerating the approach to the gel point and terminating morphological development before complete phase separation [94,95]. This has been demonstrated with rubber-modified thermosets by Gillham et al. [94] by varying the initial cure temperature and by Inoue et al. [126,127] through the utilization of highly reactive curing agents.

In the current investigation, variable-power microwave processing was employed to accelerate the curing rate of the thermoplastic-modified epoxy resin networks to control the phase separation behavior. SEM micrograph results for a sample with a composition of 30 weight percent polysulfone (16.2 kg/mole) clearly demonstrated that morphological control with variable-power processing is feasible in Figure 42. Indeed, in comparing low-power (7.5 watts) EMR processing to a conventional thermally cured network the phase-inverted morphology, characteristic of 30 weight percent incorporation of PSF, was observed in both networks. This suggested that an equivalent degree of phase separation was achieved with the two processing techniques. However, as power was increased, for example to 15, 25 or 35 watts, the degree of phase separation became less defined. The networks cured at 35 watts for 2 minutes showed little to no phase separation, while the networks cured at powers of 15 and 25 watts demonstrated intermediate degrees of phase separation by SEM.

Very similar results were obtained at 15 weight percent incorporation of polysulfone as shown in Figure 43. Low-power (7.5 watts) EMR processing yielded networks exhibiting morphologies that were analogous to the thermally cured systems with approximately 0.6 µm spheres of PSF evenly dispersed in the epoxy resin matrix. And, as power was increased, an entire range of phase-separated morphologies was observed. In one particular instance, at a processing power of 32 watts a co-continuous morphology, characteristic of spinodal decomposition, was obtained as shown by high-resolution SEM in Figure 44 (at two different magnifications). This co-continuous microstructure consisted of two interconnecting phases as shown schematically in Figure 45. The development of the phase separation depicted in Figures 43 and 44 for 15 weight percent incorporation of PSF is consistent with the model (Figure 17) proposed by Inoue et al. [126,127]. This model suggests that morphological development proceeds from a homogeneous mixture to spinodal decomposition and eventually to a nucleation and growth mechanism (e.g., binodal phase separation) depending upon the rate of cure.

Spinodal decomposition can best be explained by analyzing the phase diagram in Figure 11. Generally with UCST behavior, as temperature is lowered, there are only two pathways to achieve spinodal decomposition. The first is to transverse the phase diagram (Figure 11) at the critical point; and, the second is to rapidly cross the nucleation and growth region (binodal curve) to reach the spinodal region [100]. An example of this is a thermoplastic blend at temperature $T_3$ (Figure 11) which is rapidly quenched into the spinodal region. In an analgous manner, if the temperature axis of Figure 11 is replaced with conversion and LCST behavior is assumed, a thermoset system can be quenched by accelerating the approach to the gel point.

In summary, toughness enhancement is strongly related to the morphological structure of the modified network. The co-continuous morphology has been reported [87] to yield superior mechanical properties, especially fracture toughness. Furthermore, the co-continuous microstructure has been reported [87] to translate the enhanced fracture toughness into composite structures better than other types of phase separation. Thus, morphological control via variable-power microwave processing may be very important to the optimization of mechanical property performance in toughened epoxy resin networks.

## 2.3.2.4. Thermal Analysis

Thermal analysis techniques, specifically differential scanning calorimetry (DSC) and dynamic mechanical thermal analysis (DMTA), were utilized to investigate the degree of phase separation in the thermoplastic-modified epoxy resin networks. The DSC results for the thermally cured networks displayed, for both 15% and 30% incorporation of polysulfone ($\overline{M}_n$ = 16.2 kg/mole), two Tg's at 180°C and 230°C for the PSF and epoxy resin phases, respectively, as

# CONTROL OF PHASE SEPARATION USING MICROWAVE PROCESSING

### (30% w/w Polysulfone into DGEBA / 4,4'-DDS)
### Scanning Electron Microscopy Micrographs (12,500x, Bar=0.5µm)
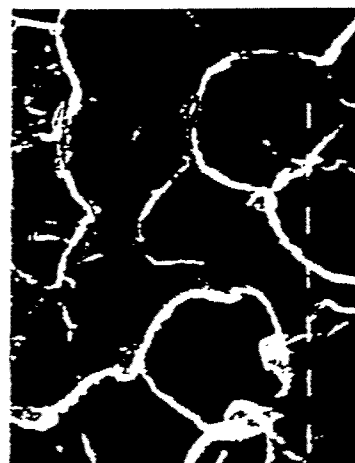


Thermally Cured
(2 hrs. @ 190°C, 1 hr. @ 240°C)
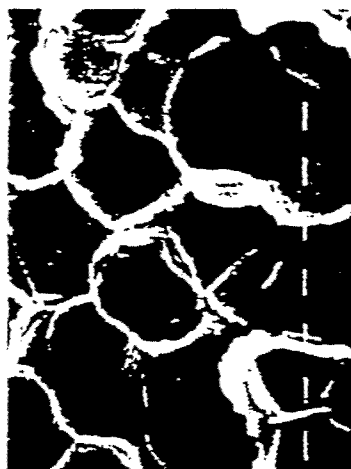
Microwave Cured
(1 hr. @ 7.5 watts)

Microwave Cured
(12 min. @ 15 watts)
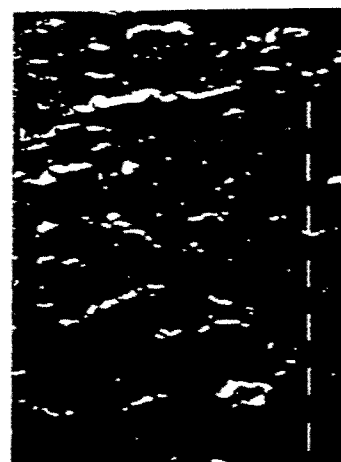
Microwave Cured
(4 min. @ 25 watts)
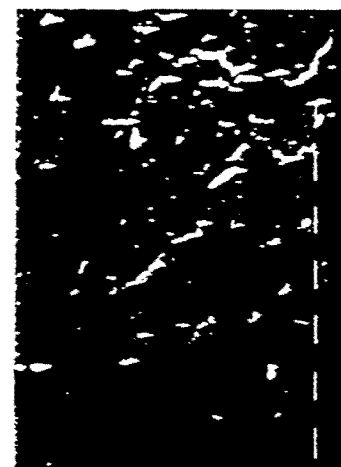
Microwave Cured
(2 min. @ 35 watts)

Figure 42.  Fracture surfaces demonstrating control of phase separation using variable power microwave processing with thermoplastic-modified epoxy resin networks (30% w/w of a 16.2 kg/mole PSF oligomer).

74

# CONTROL OF PHASE SEPARATION USING MICROWAVE PROCESSING
### (15% w/w Polysulfone into DGEBA / 4,4'-DDS)
Scanning Electron Microscopy Micrographs (50,000x, Bar=0.5μm)

Microwave Cured
(1 hr. @ 7.5 watts)

Thermally Cured
(2 hrs. @ 190°C, 1 hr @ 240°C)

Microwave Cured
(4 min. @ 25 watts)

Microwave Cured
(2 min. @ 35 watts)

Microwave Cured
(12 min. @ 15 watts)
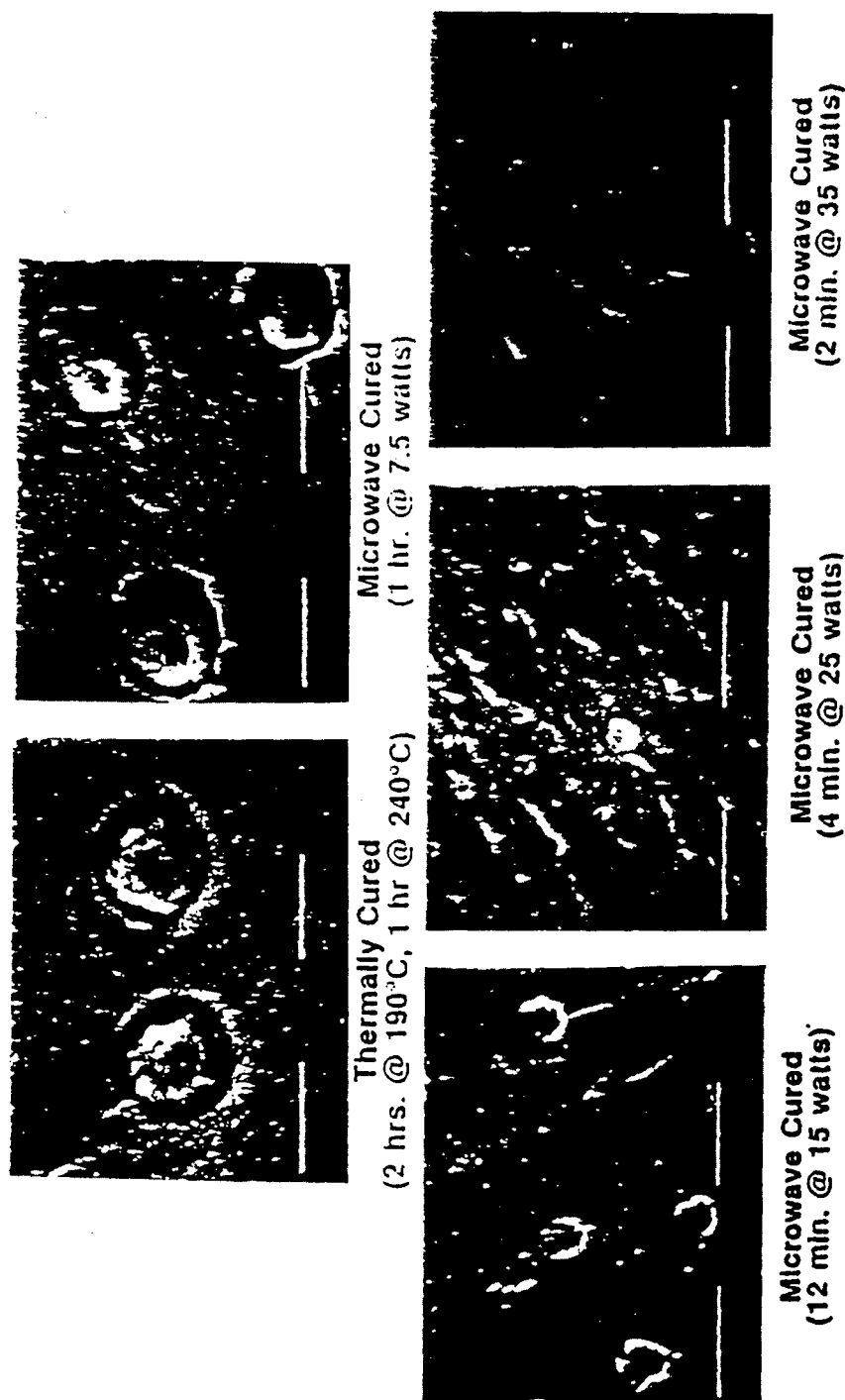
Figure 43. Fracture surfaces demonstrating control of phase separation using variable power microwave processing with thermoplastic-modified epoxy resin networks (15% w/w of a 16.2 kg/mole PSF oligomer).

75

BAR = 0.5 μm (50,000x)
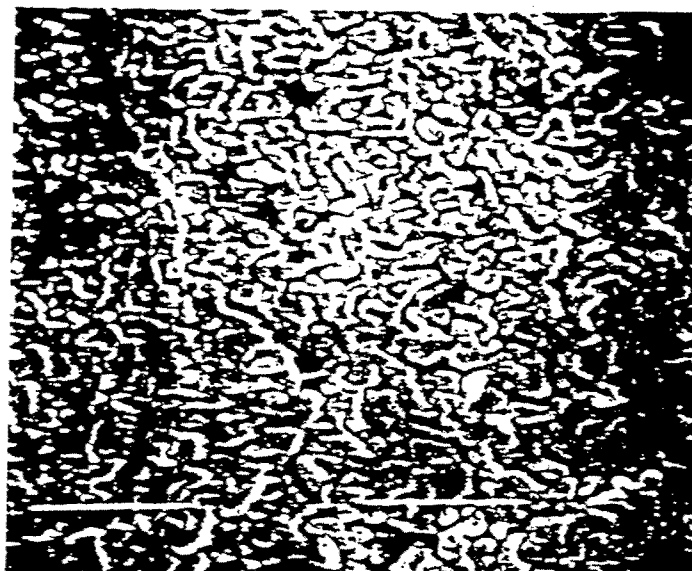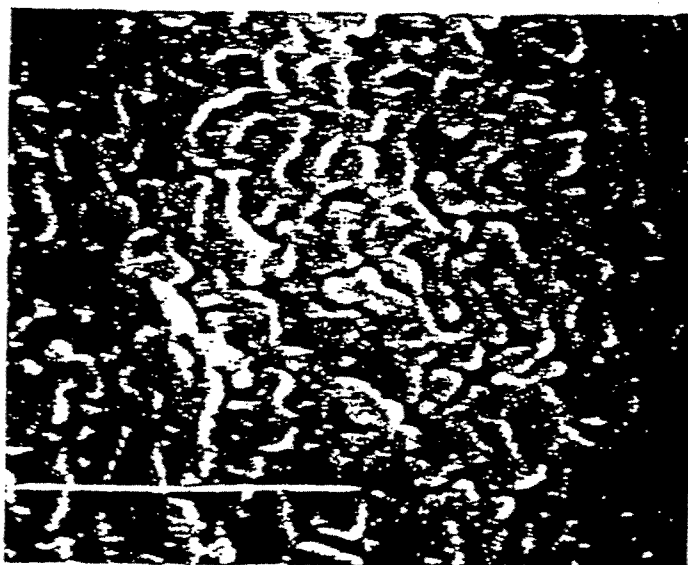


BAR = 0.5μm (100,000x)

Figure 44    Fracture surface of a microwave processed (32 watts) thermo-plastic-modified epoxy resin network (1.5% w/w of a 16.2 kg/mole PSF oligomer) demonstrating spinodal decomposition
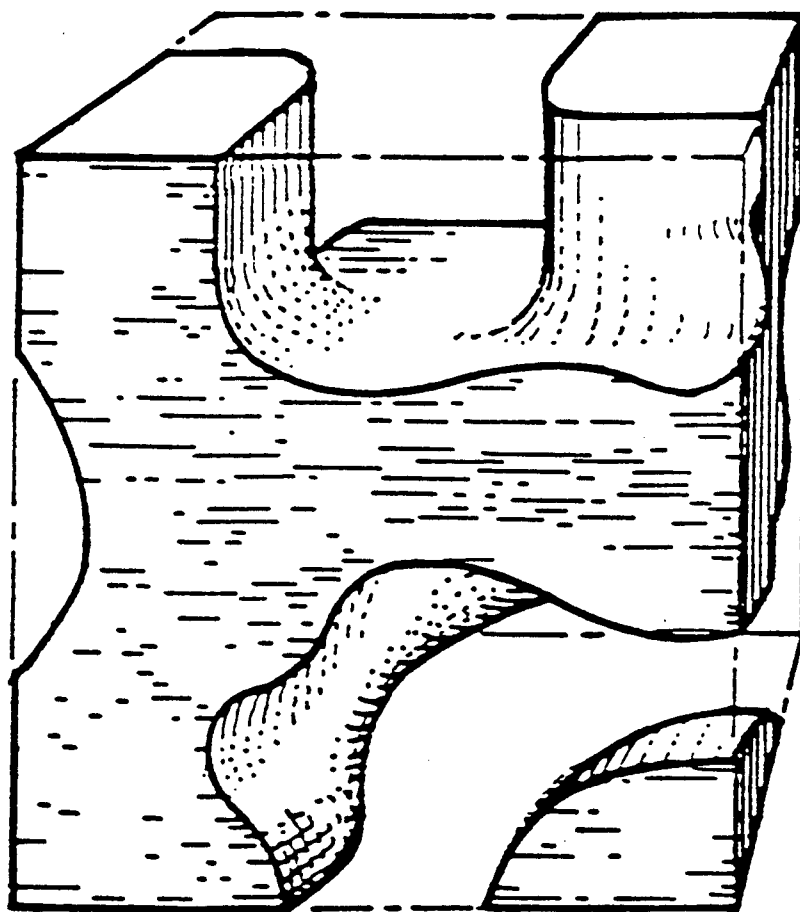
Figure 45. Schematic representation of the co-continuous morphology characteristic of spinodal decomposition [102].

77

shown in Table 6. These glass transition temperatures are the same as the pure homopolymers; thus, suggesting the development of two essentially pure phases following thermal processing. The electromagnetic radiation (EMR) processed networks, however, exhibited (Table 6) $T_g$'s at 179°C and 200°C for the PSF and epoxy resin phases, respectively. The lower glass transition temperature at 179°C was approximately the same as that for the polysulfone oligomer, indicating the existence of an essentially pure PSF phase. The upper $T_g$ at 200°C, however, was significantly depressed from the $T_g$ of the pure epoxy resin phase (230°C), indicating plasticization of the epoxy resin $T_g$. Plasticization of this type is indicative of phase-mixing in modified epoxy resin networks [94].

To determine if the morphology of the EMR processed networks was, in fact, "locked" into the phase-mixed microstructure, the microwave cured specimen (containing 30% of the 16.2 kg/mole PSF oligomer) was postcured at 240°C for 1.5 hours in a forced-air convection oven. Direct comparison of the EMR processed networks, with and without the postcure, to a thermally cured network revealed (as shown in Figure 46) that the extent of phase separation in the microwave cured material never achieved the same degree of phase separation as the conventional thermally cured networks. The upper $T_g$ of the EMR cured network increased from 200°C to 213°C (probably because of further reaction); however, the $T_g$ was still 17°C lower than the thermally cured network indicating plasticization and phase-mixing of the epoxy resin phase. These results correlated well with the SEM analysis shown in Figure 41, where the size of the phase-separated polysulfone discrete phase remained unchanged after a thermal postcure. The dynamic mechanical thermal analysis (DMTA) results for the thermally and microwave cured epoxy resin networks containing 30% polysulfone (Mn = 16.2 k) are shown in Figures 47 and 48, respectively.

The DMTA for the thermally processed network demonstrated a two-step decrease in modulus and two clearly defined damping peaks (from the log tan δ trace) corresponding to $T_g$'s at 190°C and 230°C for the pure PSF and epoxy resin phases, respectively. This indicated that the phase separation in the thermally cured network was essentially complete prior to gelation. The EMR processed material (Figure 48), conversely, displayed a single sharp decrease in the modulus and a single, broad damping transition with a shoulder; this was indicative of phase-mixing. Furthermore, the upper $T_g$ was at 201°C as opposed to 230°C for the thermally cured network, again indicating that the epoxy resin phase was plasticized by the presence of polysulfone. These findings correlated well with the SEM analysis shown in Figures 37 and 39, where the volume fraction of the phase-separated polysulfone phase appeared to decrease with EMR processing.

In order to determine the extent of phase-mixing in the microwave processed networks, the theoretical glass transition temperature for a miscible polysulfone/epoxy resin phase was calculated by the well-known Fox equation:

$$\frac{1}{T_g} = \frac{w_1}{T_{g1}} + \frac{w_2}{T_{g2}} \tag{18}$$

where $w_1$ and $w_2$ are the weight fractions, and $T_{g1}$ and $T_{g2}$ are the glass transition temperatures of the component polymers, respectively. At 30% incorporation of polysulfone where $T_{g1}$ and $T_{g2}$ were 180°C and 230°C for the PSF and epoxy resin phases, respectively, the theoretical glass transition temperature for a miscible binary mixture was calculated to be 214°C. This value was in agreement with the glass transition temperature obtained for the postcured microwave sample at 213°C from Figure 46. The excellent correlation between the experimental and theoretical glass transitions suggested the existence of a miscible PSF/epoxy resin phase in the microwave networks.

Table 6. Glass transition temperatures of the thermoplastic-modified epoxy resin networks.

| Network System | $T_{g1}$ (°C) | $T_{g2}$ (°C) |
|---|---|---|
| Control (DGEBA/4,4'-DDS) | | |
| Thermal | --- | 230 |
| Microwave | --- | 212 |
| | | |
| 15% w/w PSF-NH$_2$ ($\overline{M_n}$ = 16.2 k) | | |
| Thermal | 180 | 230 |
| Microwave | 179 | 200 |
| | | |
| 30% w/w PSF-NH$_2$ ($\overline{M_n}$ = 16.2 k) | | |
| Thermal | 180 | 230 |
| Microwave | 179 | 203 |

•Determined from DSC-first scan at 10°C/minute.
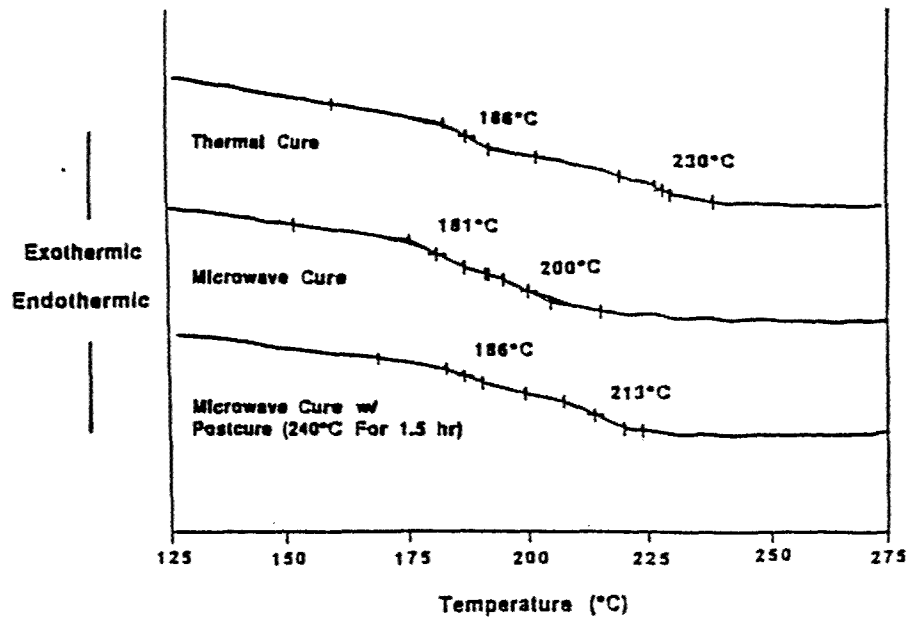
Figure 46. Glass transition temperatures of the thermoplastic-modified epoxy resin networks containing 30 weight percent of the 16.2 kg/mole polysulfone oligomer.
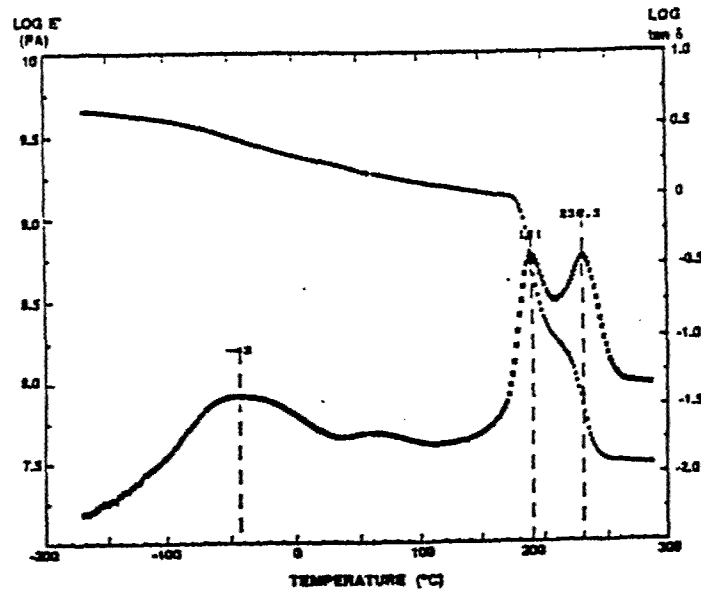


Figure 47. Dynamic mechanical thermal analysis behavior of a thermally cured thermoplastic-modified epoxy resin network (30% w/w of a 16.2 kg/mole polysulfone oligomer).
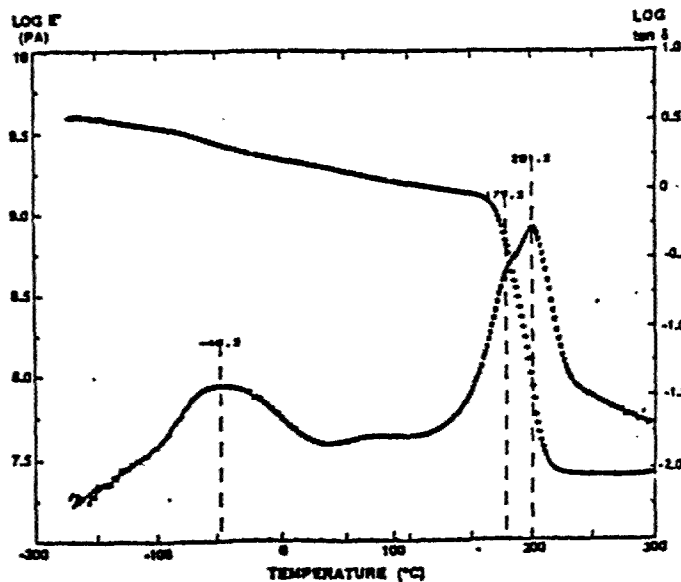


Figure 48. Dynamic mechanical thermal analysis behavior of an EPR cured thermoplastic-modified epoxy resin network (30% w/w of a 16.2 kg/mole polysulfone oligomer).

80

## 2.3.2.5. Fracture Toughness

Typically, brittle epoxy resin networks are toughened by the incorporation of a second component which phase separates during network formation. Toughness enhancement is dependent on the properties of the original epoxy, the particle size, particle volume fraction, interfacial bonding, and the properties of the modifier [106]. Thus, the resulting morphology of the phase separated networks is strongly related to the fracture toughness behavior. In the current investigation, thermoplastic-toughened epoxy resin networks were examined as a function of the molecular weight and percent incorporation of the modifier. Furthermore, comparisons were made between the EMR and thermal processing techniques to evaluate the effect of an accelerated microwave cure on the fracture toughness behavior of the networks.

Fracture toughness, as measured by $K_{Ic}$, was found to increase as a function of both molecular weight and percent incorporation of the modifier with both processing techniques as shown in Table 7. For instance, at 30 weight percent incorporation of the 16.2 kg/mole modifier in the thermally cured networks, the fracture toughness increased from 0.98 to 1.43 to 1.76 Nm-3/2 as molecular weight increased from 6.0 to 10.9 to 16.2 kg/mole, respectively. In the thermally cured networks modified with the 10,900 g/mole PSF oligomer, fracture toughness increased from 1.02 to 1.43 Nm$^{-3/2}$ as the incorporation of the modifier was increased from 15 to 30 percent, respectively. These fracture toughness values are substantially higher than the control resin (neat DGEBA/4,4'-DDS), which possessed a KIc value of 0.88 Nm$^{-3/2}$. Similar results were obtained for the microwave processed systems as shown in Table 7.

The actual toughening mechanism involved with thermoplastic modification is greatly debated. The proposals which have been put forward are often conflicting. Some investigators have proposed a linear increase in fracture toughness with increasing thermoplastic content, independent of morphology [86,90], and others such as McGrail, et al. [87] have suggested a maximum in toughness at intermediate compositions resulting from a co-continuous morphology. The results in the current investigation correlated well with the findings of Brown and Kim [93]. Brown et al. found that fracture toughness in thermoplastic-modified epoxy resin networks demonstrated a continuous change as a function of oligomer content despite morphological changes. They attributed this to different toughening mechanisms which operate at different compositions. Brown et al. proposed that at low weight percent incorporations (10%) of the modifier where the morphology consists of a continuous epoxy matrix with discrete PSF spheres dispersed within, the toughening mechanism involved localized yielding in the epoxy matrix initiated upon the deformation of the discrete modifier particles. Indeed, examination of the fracture surfaces for 15 weight percent incorporation of the 16.2 kg/mole PSF oligomer (shown in Figure 39) revealed that the phase-separated PSF particles were plastically deformed. The polysulfone composite particles in the thermally cured networks appear to be pulled away from the surface. The dark rings around these particles are indicative of excellent interfacial adhesion between the phases and are characteristic of localized yielding in the epoxy resin matrix [93].

At high weight percent incorporations (30%), above the phase inversion composition, Brown and Kim attributed toughening to the ductile yielding of the oligomeric modifier phase (i.e., the continuous phase). This observation appears to be analgous with the findings in the current investigation. Examination of the fracture surfaces for the thermally processed networks with 30% incorporation of the 16.2 kg/mole polysulfone modifier (shown in Figure 40) revealed extensive plastic yielding (or tearing) of the continuous polysulfone oligomeric phase. This was most evident in the 16.2 kg/mole oligomer because the polysulfone was above the critical molecular weight needed to develop entanglements (i.e., ductile behavior).

Surprisingly, the fracture toughness values (based on an average of 15 to 20 samples and reported with an error of two standard deviations) were essentially identical for the two processing techniques with the high molecular weight modifiers (10.9 and 16.2 kg/mole) as shown in Table 7. Indeed, this was not anticipated since the morphologies of the networks were significantly different. The thermally cured systems possessed a well-defined two-phase morphology with essentially two pure phases. The EMR cured networks, alternatively, demonstrated a substantial

81

Table 7. Fracture toughness results obtained with the polysulfone-modified epoxy resin networks.

| Network System | | $K_{fc}/10^6$ ($Nm^{-3/2}$) | |
|---|---|---|---|
| | | Thermal | Microwave |
| Control (DGEBA/4,4'-DDS) | | 0.88 ± 0.10 | 0.84 ± 0.15 |
| $\overline{M_n}$ = 6.0 kg/mole | 15% | 0.91 ± 0.12 | 0.72 ± 0.09 |
| | 30% | 0.98 ± 0.16 | 0.75 ± 0.05 |
| $\overline{M_n}$ = 10.9 kg/mole | 15% | 1.02 ± 0.18 | 1.02 ± 0.23 |
| | 30% | 1.43 ± 0.20 | 1.25 ± 0.32 |
| $\overline{M_n}$ = 16.2 kg/mole | 15% | 1.06 ± 0.12 | 1.15 ± 0.19 |
| | 30% | 1.76 ± 0.19 | 1.72 ± 0.22 |

degree of phase-mixing and were shown (by both SEM and thermal analysis results) to possess an essentially pure polysulfone phase and a phase- mixed PSF/epoxy resin phase.

The analogous fracture toughness results may be attributed to similar but slightly different toughening mechanisms operating in each system. At 15% incorporation of the 16.2 kg/mole PSF modifier, where the morphology consists of discrete spheres of PSF evenly distributed in the epoxy resin matrix, the ductile tearing of the polysulfone spheres in the EMR cured networks may not contribute to the toughening effect as significantly as in the thermally cured systems because of their decreased size. However, the localized plastic yielding of the matrix phase will be enhanced because of the increased ductility ascertained in the phase-mixed PSF/epoxy resin phase. As previously discussed (Section 2.1.2.1.5.), the ability of the matrix to undergo plastic deformation in highly crosslinked networks has a tremendous effect on the resulting toughness of the network [123-125]. At 30% incorporation of the modifier, the morphology of the EMR cured networks resembled the phase-inverted morphology of the thermally processed system; however, it was clearly not as well-developed. The enhanced toughness in these networks can be attributed to the ductile tearing of both the continuous PSF phase and the PSF/epoxy resin discrete phase. This is slightly different than in the conventionally cured networks, where the discrete phase is substantially pure epoxy resin, thus contributing very little to the enhanced toughness. For the low molecular weight modifier (6.0 kg/mole) the fracture toughness values for the thermally processed networks at both 15% and 30% incorporation were slightly higher than those obtained for the microwave cured systems. In comparing the SEM results in Figures 35 and 36, the morphology of the networks was similar in that neither the microwave nor the thermally cured networks exhibited a detectable degree of phase separation (at least at these magnifications). However, the general appearence of the surface topography of the EMR processed material was "smooth" in comparison to the thermally cured system, which exhibited a "rougher" texture. This suggested that additional energy absorbing mechanisms took place during the fracture of the conventionally processed network. In either case, the absence of noticable degrees of phase separation by SEM explains the lack of a substantial increase in fracture toughness. Indeed, it has been reported that single-phase binary networks generally do not possess enhanced toughness [75,94].

### 2.3.3. Functionalized Poly(arylene ether ketone)s
### 2.3.3.1. Introduction

The demand for high performance polymeric materials that can withstand prolonged exposures to high temperatures is continually growing, because of the needs of the aerospace and electronic industries. These materials must possess excellent mechanical properties, solvent resistance and dimensional stability over a wide temperature range. These requirements have led to the development of several heat-resistant thermosetting resins. The most common of these resins, excluding the epoxy resin systems previously discussed, include bismaleimides, acetylene-terminated resins and bisnadimides [128]. A reoccurring theme in all of these resin systems is the ability to undergo homopolymerization; polymerization usually proceeds via a free radical mechanism from terminal unsaturation. The physical properties of the resulting networks are controlled by the chemical structure of the backbone between the reactive endgroups. The curing rate or reactivity of the oligomers is a function of the endgroup chemistry, the chemical structure and molecular weight of the repeat unit, and the cure temperature.

Lyle et al. [146,147] has demonstrated that tough, ductile engineering thermoplastics functionalized with reactive endgroups, specifically maleimide-terminated poly(arylene ether ketone) (PEK) oligomers, can be transformed into solvent-resistant networks. The rationale was to combine the outstanding mechanical properties of a PEK thermoplastic with the solvent and creep resistance of a thermoset. The molecular weight of the maleimide functionalized PEK oligomer was varied to control the fracture toughness behavior, thermal stability, solvent resistance and high temperature modulus of the resulting networks. The thermal and mechanical properties of the PEK based bismaleimide thermosets as a function of molecular weight are shown in Table 8. Lyle et al. [146,147] reported that as the molecular weight of the starting reactant (i.e., maleimide-terminated PEK oligomer) increased, fracture toughness was substantially enhanced while the Tg

Table 8. **Glass transition temperatures and fracture toughness results for a series of PEK networks as a function of oligomer molecular weight (from Lyle et al. [146,147]).**

| $\overline{M_n}$ (kg/mole) | $Tg(°C)$ [*] | $K_{Ic}/10^6$ $(Nm^{-3/2})$ |
|---|---|---|
| 2.5 | 179 | 1.8 ± 0.2 |
| 5.0 | 175 | 2.0 ± 0.2 |
| 10.0 | 169 | 3.3 ± 0.2 |

[*]Determined from differential scanning calorimetry.

of the cured network decreased slightly (because of the increased molecular weight between crosslinks). Similar findings have been reported by Mohanty et al. [168] and Wu et al. [163] with amine-terminated and nadimide-terminated PEK's, respectively.

The most widely utilized bismaleimide is based on bismaleimidodiphenylmethane (BMI). BMI networks possess excellent thermal stability and strength; however, they are susceptible to failure in impact situations because of their brittle character. BMI resins are normally toughened by chain extension via a Michael addition with an aromatic diamine; but, toughness enhancement is small, with KIc values only increasing from ~0.2 to ~0.6 N/m3/2 [130]. Recently, Senger et al. [151,152] demonstrated that BMI's may be toughened by the chemical incorporation of a reactive thermoplastic which phase-separates during polymerization. The rationale, to introduce a second thermoplastic phase which acts as a stress concentrator for propagating cracks, was analgous to that employed in toughened epoxy resin systems. Maleimide-terminated poly(arylene ether ketone) (MI-PEK) oligomers were utilized as toughening agents. Fracture toughness (Table 9), as evaluated by both $K_{Ic}$ and $G_{Ic}$ measurements in the co-cured networks increased with increasing MI-PEK content; however, swelling in chlorinated solvents also increased along with a reduction in high temperature modulus (Figure 49) (because of the increased molecular weight between crosslinks). Intermediate blend compositions, however, demonstrated a synergistic effect since enhanced toughness was achieved while retaining adequate high temperature stiffness.

In the current investigation microwave radiation was employed to cure maleimide, nadimide and amino functionalized poly(arylene ether ketone) oligomers of controlled molecular weight. Typically, high performance thermoset resins require extensive and complex processing cycles to develop the optimum mechanical properties. The objective was to evaluate the feasibility of using electromagnetic radiation to reduce the time needed to achieve fully cured networks. The crosslinking reaction kinetics of the microwave and thermally cured PEK based thermosetting resins were investigated to determine the influence of endgroup functionality, molecular weight, and cure temperature. Lastly, blends of maleimide-terminated PEK with BMI were examined with both processing techniques.

## 2.3.3.2. Synthesis of Functionalized Poly(arylene ether ketone) oligomers

The two-step procedure utilized in the synthesis of the functionalized poly(arylene ether ketone) oligomers was well-established by Mohanty et al. [168] and Lyle et al. [146,147]; for specific information regarding synthetic issues, the reader is referred to their work. The properties of the amine-terminated PEK oligomers are given in Table 10. As molecular weight increased, corresponding increases in the viscosity and Tg of the oligomers were observed as shown in Table 10. The intrinsic viscosities of the PEK oligomers were determined before and after imidization to assure that no premature crosslinking had occurred during the endcapping reaction to form the maleimide-terminated and nadimide-terminated PEK oligomers. The results shown in Table 11 confirmed that the oligomers did not increase in molecular weight following reaction, thus suggesting that chain extension during the two-step synthetic procedure was not prevalent. The maleimide and nadimide functionalized oligomers were analyzed by FTIR and potentiometric titrations for residual amic acids. Both infrared measurements and titration of potentially uncyclized amic acid groups suggested that the derivatization of the amic acid to the imide was quantitative [146,147].

## 2.3.3.3. Microwave versus Thermal Processing

A typical temperature-time profile demonstrating isothermal microwave curing at 260°C for a maleimide-terminated poly(arylene ether ketone) (MI-PEK) oligomer, possessing a number average molecular weight of 2.5 kg/mole, is shown in Figure 50. The temperature of the EMR processed MI-PEK oligomer, as demonstrated by Figure 50, increased at a heating rate of

Table 9. Fracture toughness and swelling results for bismaleimido-
diphenylmethane/maleimide-terminated PEK blends as a
function of composition (from Senger et al. [151,152]).

| Weight Percent BMI/MI-PEK (5.4K) | $K_{Ic}$ $(MN/m^{3/2})$ | $G_{Ic}$ $(kJ/m^2)$ | Percent Swelling |
|---|---|---|---|
| 0/100 | 3.9 | 8.9 | 360 |
| 5/95 | 3.0 | 7.5 | 200 |
| 25/75 | 2.1 | 3.7 | 50 |
| 50/50 | 0.9 | 0.8 | 2 |
| 75/25 | 0.4 | 0.4 | 1 |
| 100/0 | <0.2 | <0.1 | — |

Table 10. Characterization of the amine-terminated poly(arylene ether ketone) oligomers.

| Theoretical $\langle M_n \rangle$ (kg/mole) | Titrated $\langle M_n \rangle$ (kg/mole) | $T_g(°C)$ [*] | 25°C $[\eta]$ CHCl$_3$ |
|---|---|---|---|
| 2.5 | 3.4 | 126 | 0.10 |
| 5.0 | 6.3 | 140 | 0.25 |
| 7.5 | 8.3 | 156 | 0.32 |

[*] Determined by differential scanning calorimetry.

Table 11. Intrinsic viscosities of the functionalized poly(arylene ether ketone) oligomers.

| Theoretical $\overline{M_n}$ (kg/mole) | 25°C $[\eta]$ CHCl$_3$ |
|---|---|
| **Amine-terminated PEK** | |
| 2.5 | 0.10 |
| 5.0 | 0.25 |
| 7.5 | 0.32 |
| **Maleimide-terminated PEK** | |
| 2.5 | 0.09 |
| 5.0 | 0.26 |
| 7.5 | 0.31 |
| **Nadimide-terminated PEK** | |
| 2.5 | 0.12 |
| 5.0 | 0.25 |
| 7.5 | 0.33 |
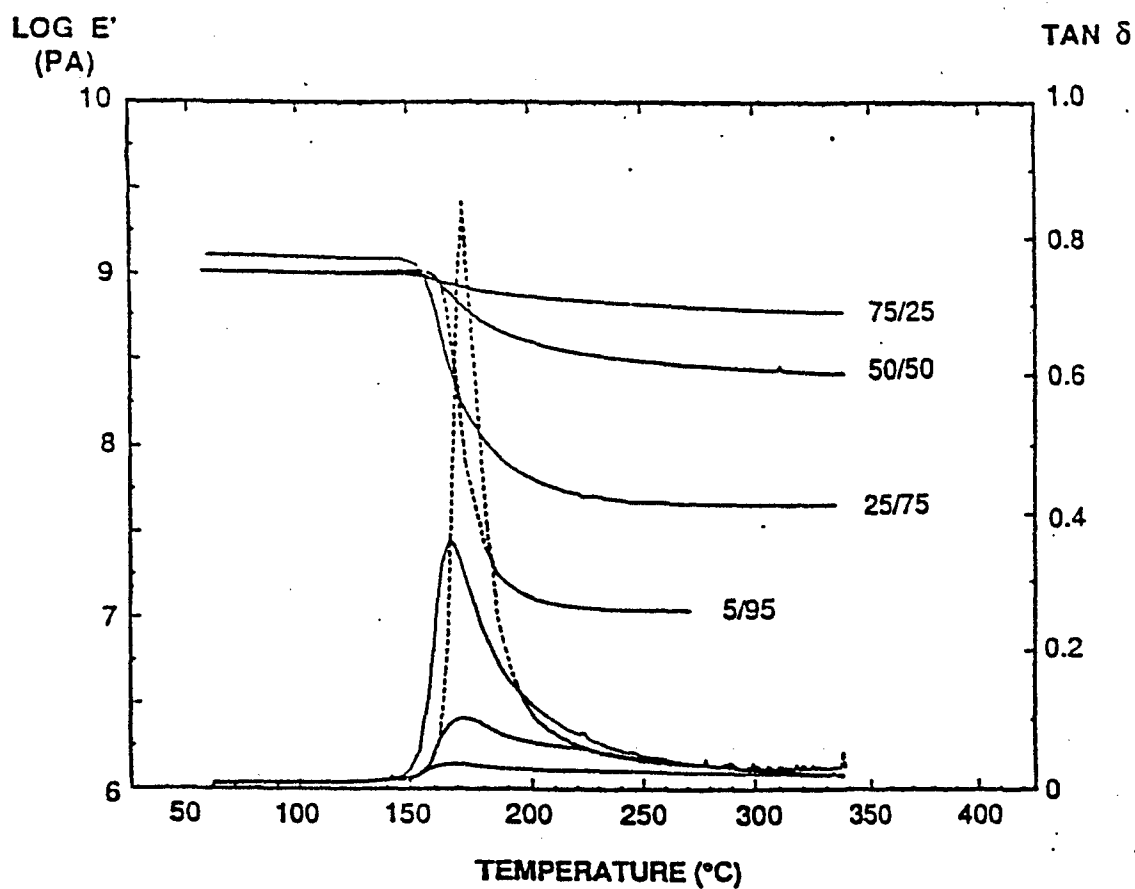
Figure 49.  Dynamic mechanical behavior (1 Hz) of co-cured blends of
            bismaleimidodiphenylmethane and maleimide-terminated PEK
            oligomers as a function of blend composition (from Senger
            et al. [151,152]).
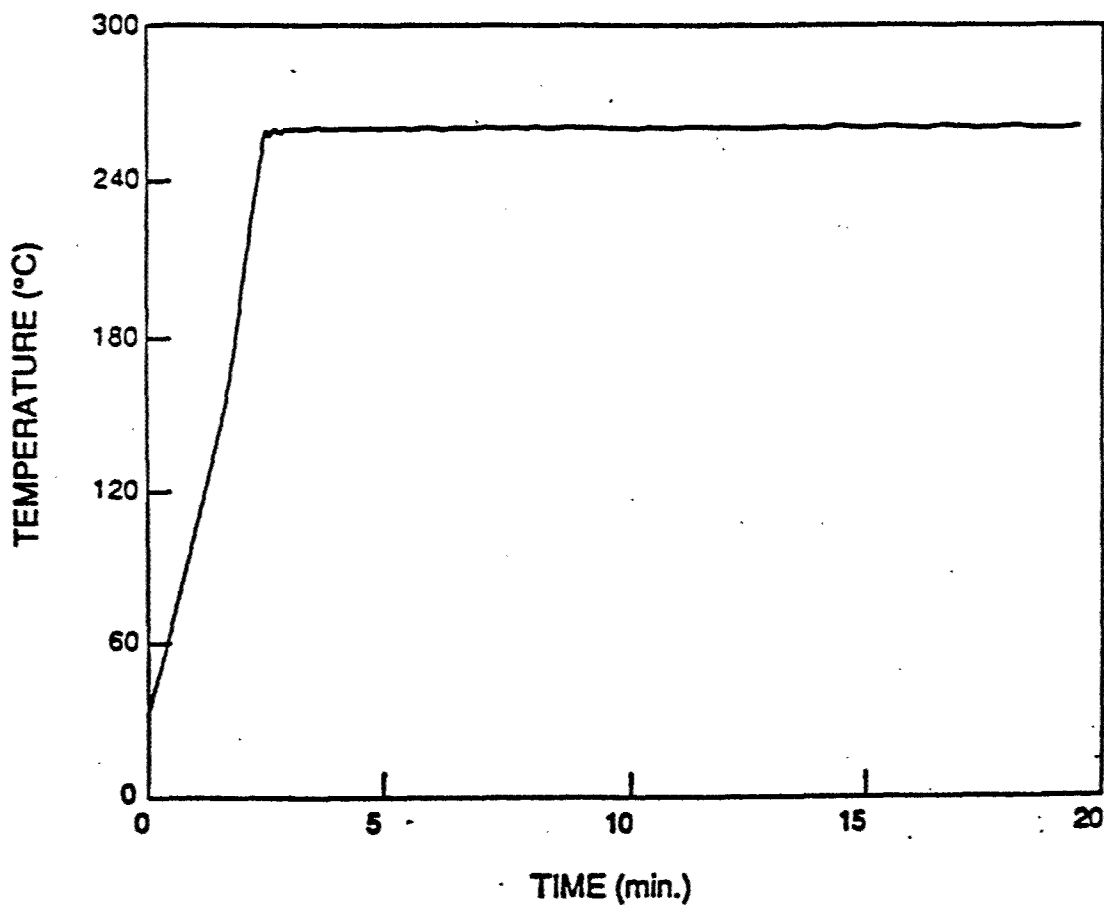
Figure 50.   Temperature-time profile demonstrating the isothermal
             (260°C) microwave curing of a maleimide-terminated PEK
             ($<M_n>$ = 2.5 k).

90

approximately 1°C to 2°C per second until the $T_g$ of the oligomer was reached. At this temperature a fivefold increase in the heating rate was observed to approximately 5°C to 10°C per second. This transition was evident from the changing slope of the initial temperature-time curve.

It may be attributed to the enhanced ability of the polar ketone groups in the PEK backbone and the reactive endgroups to couple with the electromagnetic field. Once the sample achieved the desired isothermal cure temperature the electric field strength was reduced by either detuning the cavity or decreasing the input power to maintain constant temperature. The microwave input power needed to heat the functionalized PEK's was considerably higher (60 watts) in comparison to the epoxy resin precursors (21-28 watts) previously discussed. The increased power was required to compensate for the lower dielectric loss of the PEK materials. The general shape of the temperature-time curve in Figure 50 was representative of all the functionalized PEK's processed. However, the initial time period to reach the 260°C isothermal cure temperature varied with both molecular weight and endgroup functionality. As molecular weight increased the initial time to reach 260°C increased; for instance, with the MI-PEK oligomer the time increased from 2.5 to 4.5 to 6.5 minutes as molecular weight increased from 2.5 to 5.0 to 7.5 kg/mole, respectively, holding all other variables such as input power, sample size, etc. constant. And, at a constant molecular weight, the initial time to reach 260°C was most rapid for the MI-PEK's followed by the ND-PEK's and lastly the NH2-PEK's. However, the influence of endgroup functionality on the initial heating time was not as dramatic as molecular weight. These observations suggested that the initial time to reach the desired isothermal cure temperature was a function of the variables which influenced the ability of the oligomer to couple with the electromagnetic radiation, such as the chemical structure and the type and concentration of the endgroup. This initial heating time was neglected in the curing plots, since there was relatively low conversion at this point, as indicated by the polymer being completely soluble.

## 2.3.3.3.1. Effect of Endgroup Functionality

The influence of endgroup functionality on the isothermal (260°C) microwave curing behavior of a series of functionalized PEK's, possessing a number average molecular weight of 2.5 kg/mole, is shown in Figure 51 for the three different functionalities (maleimide, nadimide, and amine). The maleimide-terminated PEK cured most rapidly, reaching essentially 100% gelation in only 35 minutes. The nadimide-terminated and amine-terminated poly(arylene ether ketone) (ND-PEK and NH2-PEK, respectively) oligomers, alternatively, contained only 92% and 70% gel formation, respectively, after 60 minutes. The differences in the reaction rates may be attributed to the dissimilar crosslinking reactions that occur during network formation.

As previously discussed (Section 2.2.2.2.), the NH2-PEK oligomers react via a Schiff base reaction as the amine endgoups attack ketone groups along the polymer backbone to form an imine linkage as shown in Figure 22. Since water is released during the polymerization, network formation is considered to occur via a condensation polymerization [168]. In contrast, the MI-PEK and ND-PEK oligomers undergo a thermally induced free radical crosslinking reaction as shown in Figures 18 and 20, respectively. Thus, it was expected that the MI-PEK and ND-PEK oligomers would cure considerably faster, since free radical reactions are typically more rapid than condensation polymerizations [170].

The high reactivity of the maleimide moiety is a consequence of the electron-withdrawing nature of the two adjacent imide carbonyl groups. The MI-PEK oligomers undergo an addition polymerization with no volatile formation at relatively low temperatures. In fact, polymerization usually occurs just above the crystalline melting point or Tg of the bismaleimide precursor [138,139]. The crosslinking reaction of nadimide-terminated systems is more complex and less understood; it is postulated that a reverse Diels-Alder reaction of the norbornenyl endgroups occurs to generate the maleimide moiety and cyclopentadiene. The highly-activated maleimide unsaturation is then proposed to copolymerize with cyclopentadiene and unrearranged norbornenyl groups via an addition polymerization as depicted in Figure 20 [156,159]. The release of cyclopentadiene during cure has caused considerable difficulties with commercial resins based on

91

bisnadimides (i.e., PMR-15 resins) [156]. Long, complex cure cycles and high processing pressures are required to achieve void-free composite laminates [156]. Indeed, in the current investigation where the ND-PEK was processed at atmospheric pressure, void formation was clearly evident, presumably because of the release of cyclopentadiene. The curing rate of the nadimide-terminated PEK's was slower than that of the comparative maleimide functionalized oligomers (Figure 51); it is postulated that the decreased reactivity may be attributed to the reverse Diels-Alder reaction, which is presumably the rate determining step in the polymerization of the norbornenyl endgroups [156,159].

A major advantage of microwave processing over conventional thermal processing is illustrated by the plot shown in Figure 52, depicting the microwave and thermal curing behavior of a 7.5 kg/mole MI-PEK oligomer at 220°C. This plot exemplifies the tremendous capabilities of microwave processing; a fully cured network was achieved in only 35 minutes as opposed to over 10 hours with a conventional thermal cure. This represents a twentyfold reduction in the processing time at the same isothermal cure temperature. The importance of this capability in the processing of high performance polymers is enormous; EMR processing may be utilized to reduce the long-term high temperature conditions (which might lead to degradation) normally employed in the fabrication of structural components or coatings.

Similar reductions in the EMR cure time were observed for the nadimide-terminated and amine-terminated PEK's as shown in Figures 53 and 54, respectively. Figures 53 and 54 depict the isothermal (260°C) microwave and thermal curing behavior of ND-PEK and NH2-PEK oligomers, respectively, possessing molecular weights of 2.5 kg/mole. Higher processing temperatures were required to achieve complete cure in the thermal reactions of the ND-PEK and NH2-PEK oligomers in a 7- to 10-hour time frame, compared with the MI-PEK. This, again, emphasized the fact that the maleimide-terminated oligomer was the most reactive of the three functionalities. The microwave processed PEK's in Figures 53 and 54 were not cured to completion because of instrument limitations; the high power (60 watts) processing requirement for the low loss PEK oligomers overheated the microwave generator after 1 hour of continuous use. However, "high power" is relative to the generator utilized; commercial microwave ovens for heating food typically operate at 700 watts. Thus, the actual power required to process both the epoxy resin precursors and the functionalized PEK oligomers was quite low.

As previously discussed (Section 2.0.), the mechanism of the accelerated curing rate is uncertain. Two proposals have been put forth to explain the reduced curing times. The first attributes the acceleration to the novel mechanism of energy transfer with EMR processing [11,14], and the second proposal attributes the accelerated reaction rates to the localized deposition of microwave energy to functional groups possessing permanent dipole moments (i.e., the ketone moieties and the maleimide endgroups in PEK based bismaleimides). It has been postulated that these "high energy regions" may be manifested as regional high temperature (on the molecular level) or ensembles where there is an enhanced reactivity, either of which may result in increased reaction rates [63,64].

## 2.3.3.3.2. Effect of Molecular Weight

The influence of molecular weight on the curing behavior of the PEK oligomers was investigated with the maleimide-terminated systems. A plot of the percent gelation versus curing time in minutes for a series of three different molecular weight MI-PEK oligomers cured isothermally at 220°C with EMR processing is shown in Figure 55. Fully insoluble networks were achieved with all three oligomers in less than 40 minutes. Furthermore, the curing rate was enhanced by decreasing the molecular weight of the oligomers. This may be attributed to a combination of two factors. First, as the molecular weight of the MI-PEK oligomer decreased from 7.5 to 5.0 to 2.5 kg/mole, the weight percent (i.e., relative concentration) of the reactive functional endgroups increased from 2.3% to 3.0% to 5.5%, respectively. And second, as molecular weight decreased, the melt viscosity decreased, thus increasing mobility during curing. Both of these factors are extremely important in a thermosetting reaction; however, they are
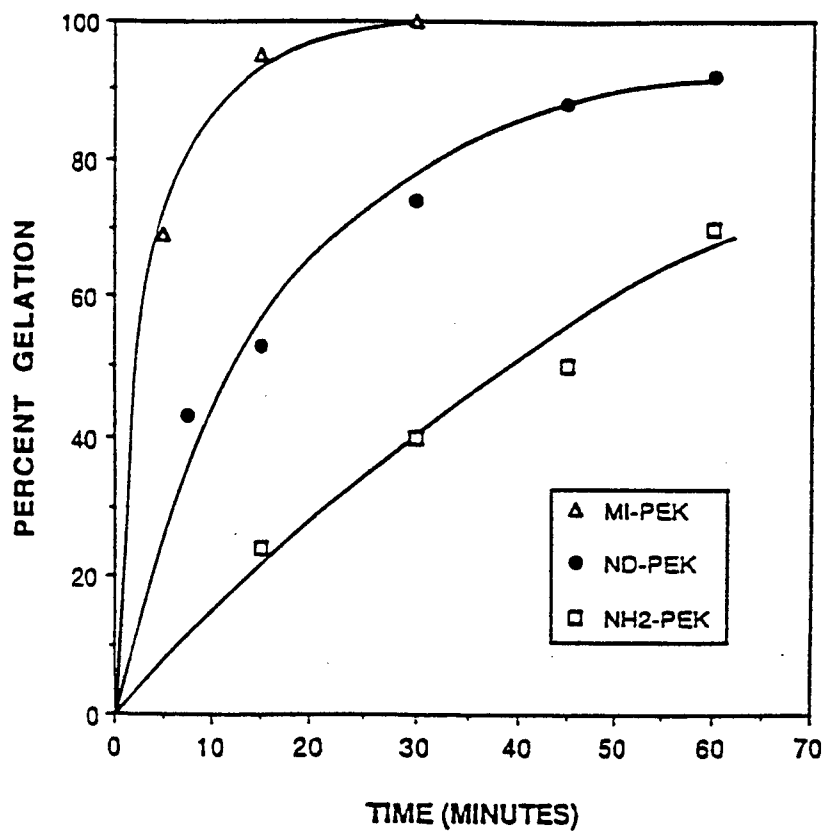
Figure 51. Isothermal (260°C) microwave curing behavior of thermo-
setting poly(arylene ether ketone) oligomers as a function
of endgroup functionality.
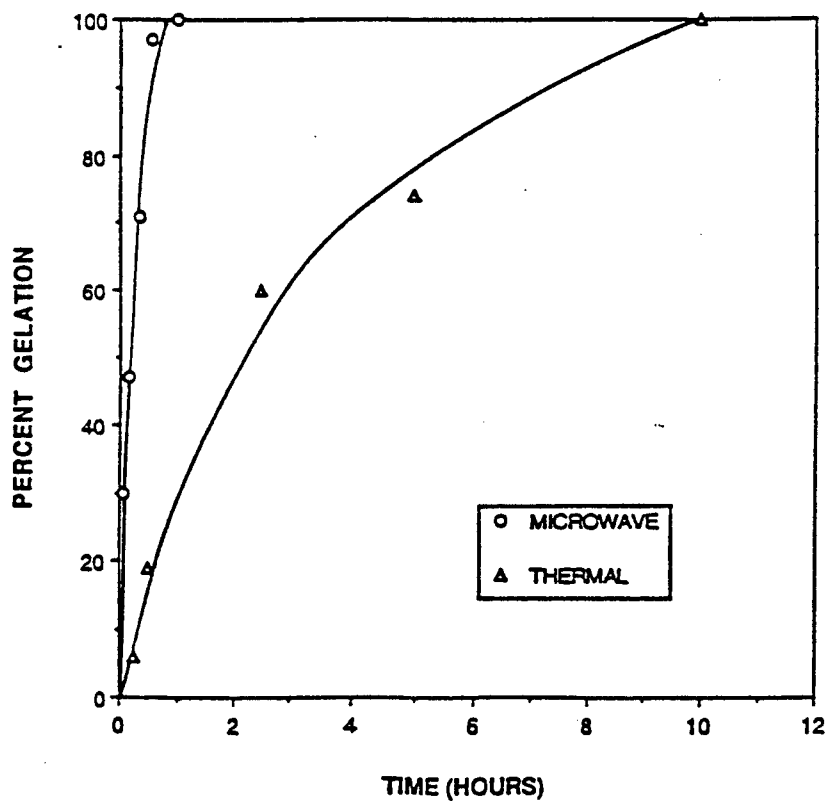


Figure 52. Comparison of EMR and thermal curing behavior of a
maleimide-terminated PEK at 220°C.
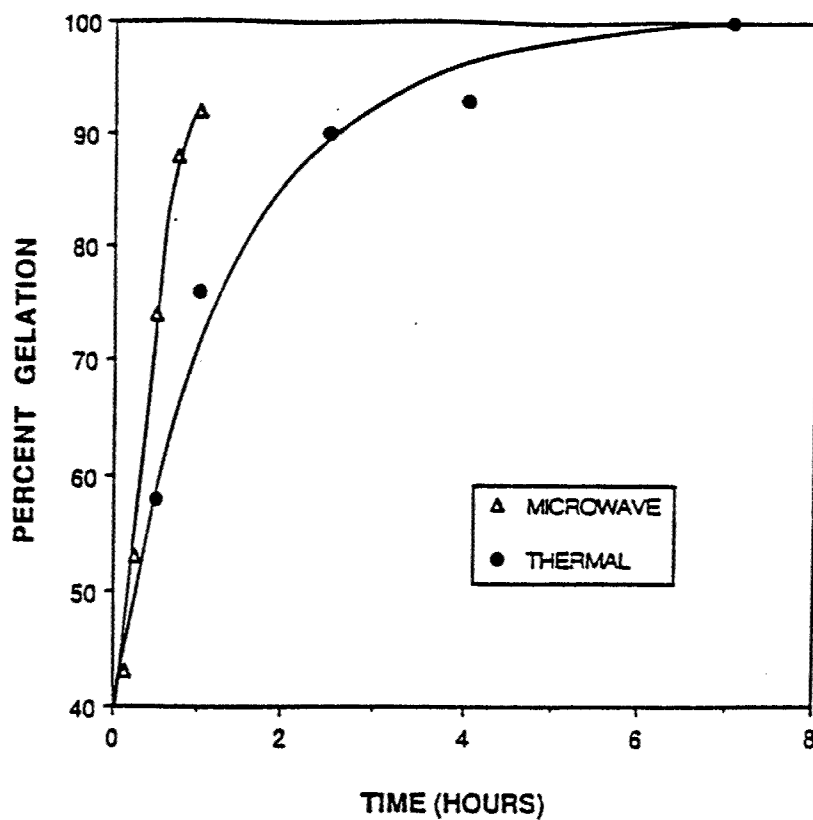
Figure 53. Comparison of EMR and thermal curing behavior of a nadimide-terminated PEK at 260°C.
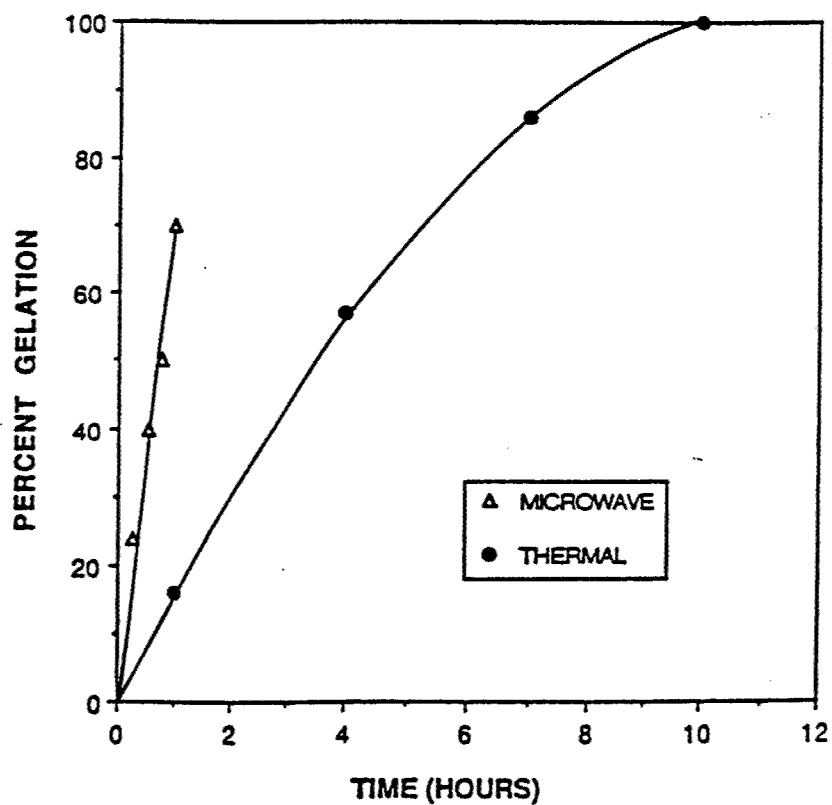


Figure 54. Comparison of EMR and thermal curing behavior of an amine-terminated PEK at 260°C.

94
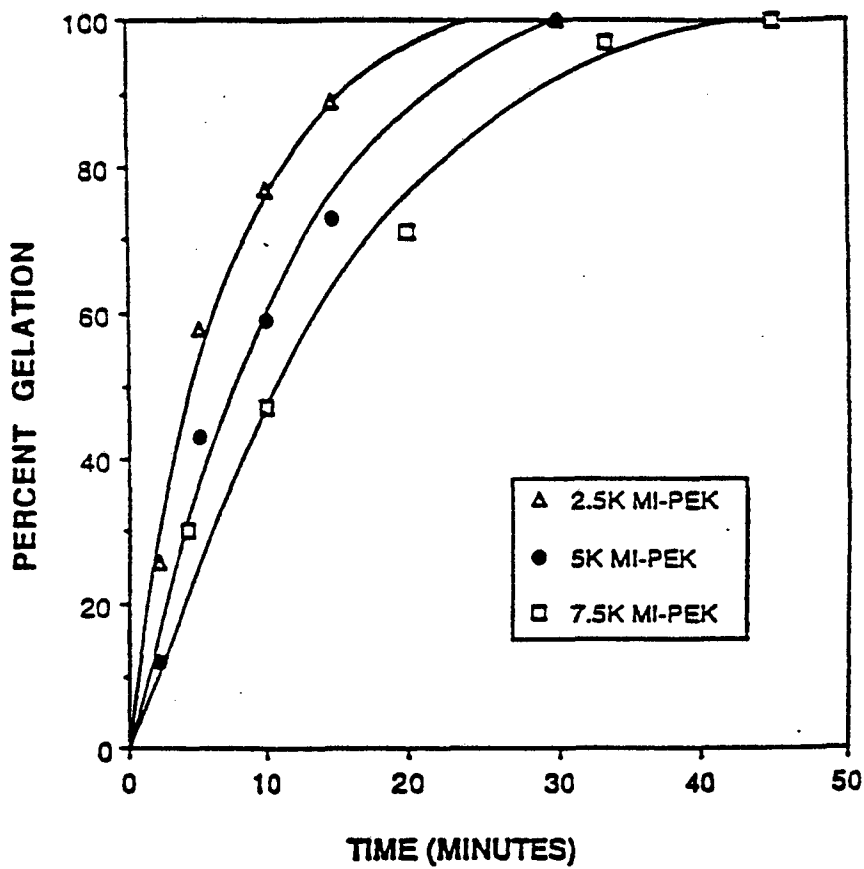
Figure 55. Isothermal (220°C) microwave curing behavior of a series of maleimide-terminated PEK's as a function of molecular weight.

95

especially significant with EMR processing since microwave absorptivity increases with both a higher concentration of polar groups (i.e. maleimide endgroups) and enhanced mobility.

The effect of molecular weight was also investigated with the thermally cured MI-PEK oligomers (5.0 and 7.5 kg/mole) as shown in Figure 56. The same trend was observed as in the EMR cured resins; however, the thermal cures took significantly longer to reach completion.

### 2.3.3.3.3. Effect of Cure Temperature

The influence of cure temperature on the reaction rates of the functionalized PEK's was illustrated with the microwave processed maleimide-terminated PEK (2.5 kg/mole) as shown in Figure 57. The effect of cure temperature with this oligomer was minimal; indeed, upon increasing the cure temperature 80°C, from 220°C to 300°C, only a slight reduction in the cure time was observed (Figure 28). Complete curing plots were not generated for the comparative thermally cured oligomer; however, it was demonstrated that complete cure was achieved in approximately 4 hours at 220°C and 1 hour at 300°C. Thus, the effect of cure temperature with the thermally processed oligomers was quite significant. This suggested that as cure temperature increased the difference between the microwave and thermal cure times appeared to decrease.

### 2.3.3.3.4. Blends of Maleimide-Terminated Poly(arylene ether ketone) with Bismaleimidodiphenylmethane

The isothermal (220°C) microwave and thermal curing behavior of bismaleimidodiphenylmethane (BMI), maleimide-terminated PEK and their 50/50 weight percent blend is shown in Figures 58 and 59, respectively. As demonstrated by these plots, the simple BMI resin cured most rapidly, followed by the blend and, lastly, by the MI-PEK oligomer for both processing techniques. Furthermore, as in previous situations, the microwave cured resins (Figure 58) cured much more rapidly than the corresponding thermally processed oligomers (Figure 59).

The effect of blending the simple BMI resin with the maleimide-terminated PEK oligomers was analogous to decreasing the molecular weight of the PEK oligomer (Section 2.3.3.3.2.). As the BMI content was increased, the weight percent of the reactive functional endgroups increased, thus increasing the relative concentration of the highly activated maleimide endgroups. Furthermore, as BMI content increased, the melt viscosity decreased, thus increasing the mobility of the resin. Both of these factors (increased concentration of reactive endgroups and enhanced mobility) have a strong influence on both microwave absorptivity and the curing rates in thermosetting reactions.

## III. CONCLUSIONS

Microwave processing has been demonstrated to have a number of real and potential advantages relative to thermal processing. The rapidity of the process plus the ability to control morphology in multiphase materials is unique and should be further studied and commercialized in selected areas. One of the early applications appears to be in the filament winding of thermoplastic composites as discussed in the appendix by Lind et.al. from McDonnell Douglas. A variety of dielectric studies were conducted on model polystyrene systems, epoxies, PEEK, Ultem, polyimides, polyamides, ethylene vinyl acetate (EVA), polyethylene, PBI/polyimide blends, styrene acrylonitrile (SAN) and nitrile rubber. A consistent view has been developed wherein the polarity of the material influences the processability either into reactive networks or nonreactive thermoplastics. Near the end of the effort, techniques were developed for the in situ dielectric and spectroscopic characterization of the curing material. This would be most valuable for dynamic studies of network formation as well as possibly the generation of smart materials which contained
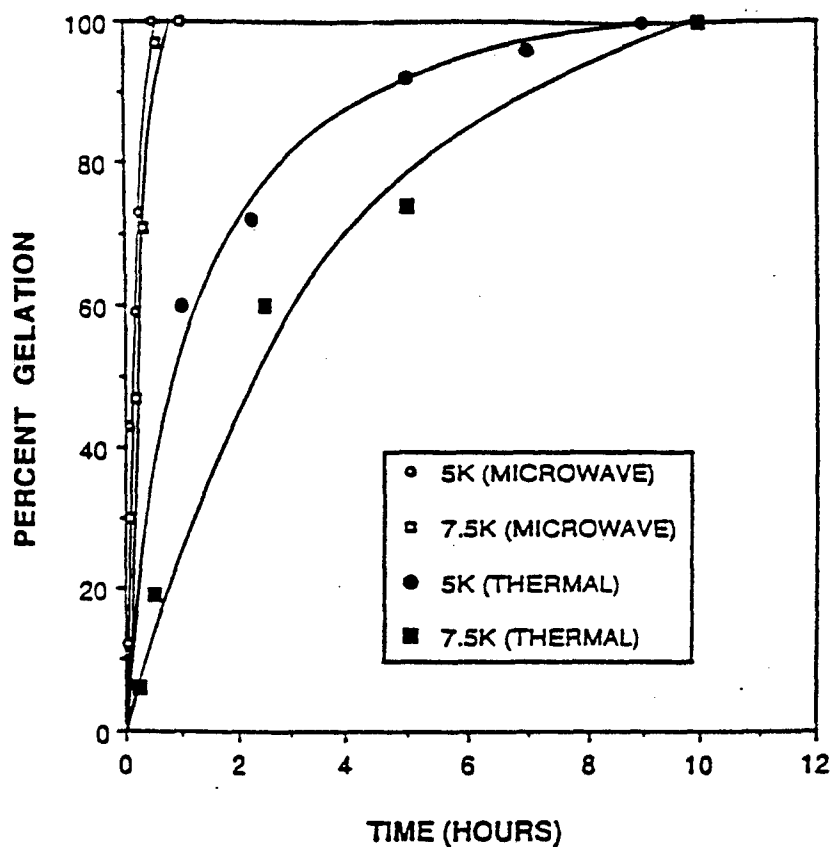
Figure 56. Isothermal (220°C) curing behavior of maleimide-
terminated PEK as a function of processing and molecular
weight.
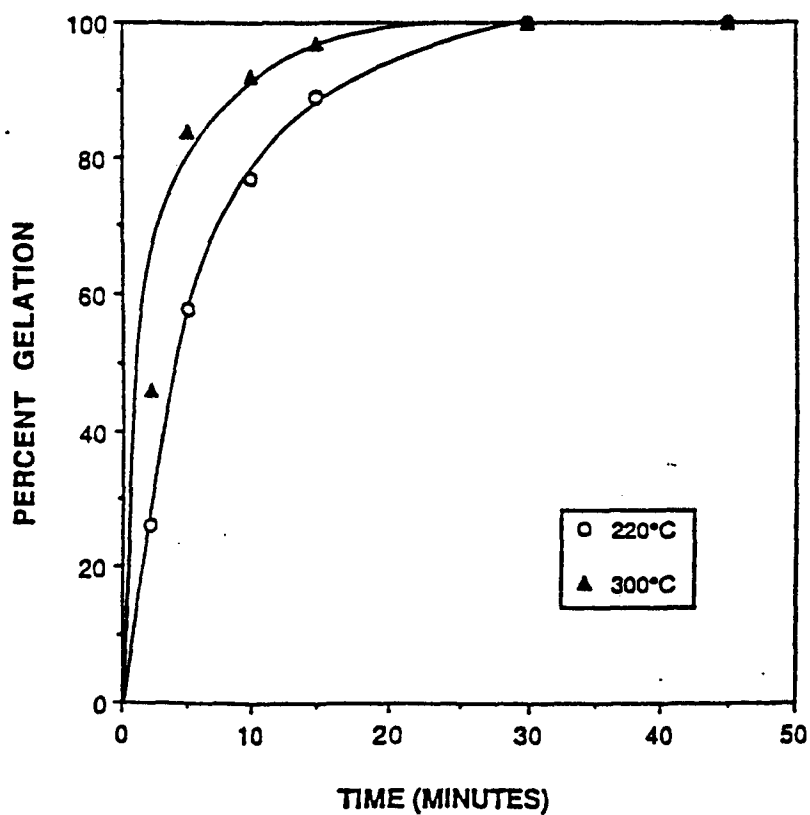


Figure 57. Microwave curing behavior of a maleimide-terminated PEK
(2.5 kg/mole) as a function of cure temperature.

97
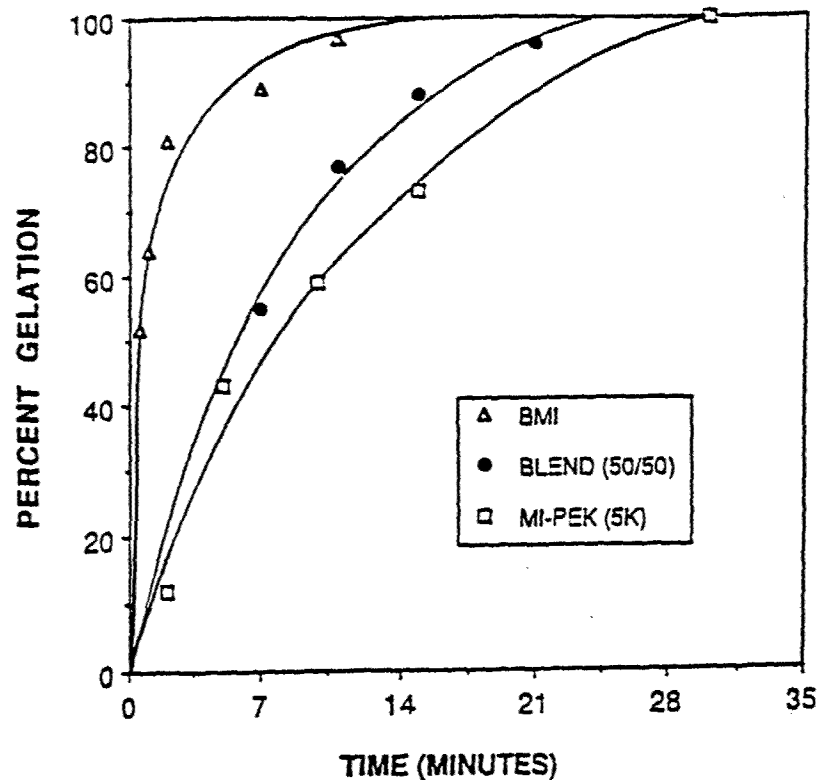
Figure 58. Isothermal (220°C) microwave curing behavior of bis-maleimidodiphenylmethane, maleimide-terminated PEK and their 50/50 weight percent blend.
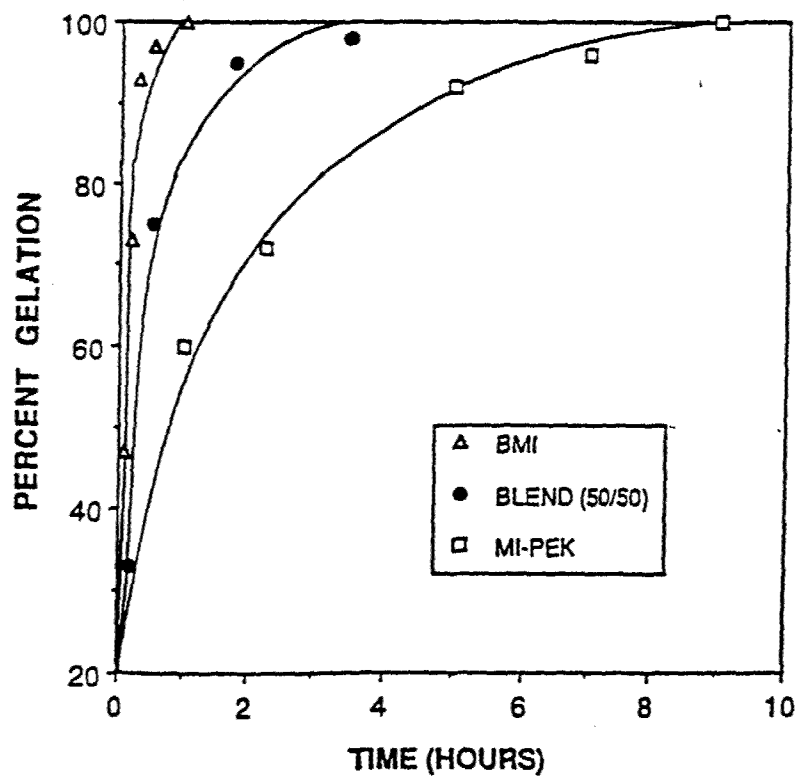


Figure 59. Thermal curing behavior of bismaleimidodiphenylmethane, maleimide-terminated PEK and their 50/50 weight percent blend at 220°C.

98

appropriate sensors. The preliminary results are extremely interesting but are considered a bit premature to include in the main body of this report. Subsequent efforts possibly with alternative or additional support funds could further develop this important processing monitoring area. The concepts of microwave calorimetry are considered extremely important for the processing of thermoplastics. Finally, application of the microwave curing phenomena to inorganic hybrids, e.g., the ceramers, has been demonstrated and could advance this important hybrid area significantly. Most obvious applications would be for high refractive index coating materials, although many others have been suggested and are included in the contribution of Wilkes provided in the appendix.

## IV. RECOMMENDED FUTURE STUDIES

It would be counter productive and really a shame to stop the work at this point, just as a number of potential important applications have been identified. In particular, there is a major need for the scaling of the microwave equipment developed by Michigan State and modified by others. The availability of the equipment will be a major issue in allowing others to build on research reported herein. Thus, it is strongly recommended that equipment development be further pursued, particularly allowing for pressure during fabrication steps.

A whole range of new chemistries could be studied, in particular, the potential for combining metals with polymers or ceramics with polymers should be pursued. It is easy to imagine, for example, the development of major new stealth technology which would couple the rapid processing of low dielectric polymer and ceramic powders with metal derivatives with a view toward obtaining highly damped radar transparent materials. The principal investigator plans to develop such ideas into a proposal for DARPA.

## REFERENCES

1.  A. C. Metaxas and R. J. Meredith, Industrial Microwave Heating, Peter Peregrinus, London, 1983.

2.  R. V. Decareau and R. A. Peterson, Microwave Processing and Engineering, Ellis Horwood, London, 1986.

3.  R. V. Decareau, Microwaves in the Food Processing Industry.

4.  D. A. Copson, Microwave Heating, Avi Publishing, Connecticut, 1975.

5.  E. C. Okress, Microwave Power Engineering, Volume 2: Applications, Academic Press, New York, 1968.

6.  P. Fellows, Food Processing Technology: Principles and Practice, Ellis Horwood, New York, 1988.

7.  M. LeMaguer and P. Jelin, Food Engineering and Process Applications, Volume 1: Transport Phenomena, Elsevier Applied Science Publishers, New York, 1986.

8.  W. A. Geoffrey Voss, IEEE Transactions on Industry and General Applications, 2 (3), 234 (1966).

9. W. H. Sutton, M. H. Brooks, and I. J. Chabinsky Eds., <u>Microwave Processing of Materials</u>, Materials Research Society, Pittsburgh, Vol. 124, 1988.

10. L. M. Sheppard, Ceramic Bull., <u>67</u> (10), 1656 (1988).

11. Q. Le Van and A. Gourdenne, Eur. Polym. J., <u>23</u> (10), 777 (1987).

12. N. Beldjoudi, A. Bouazizi, D. Douibi and A. Gourdenne, Eur. Polym. J., <u>24</u> (1), 49 (1988).

13. N. Beldjoudi and A. Gourdenne, Eur. Polym. J., <u>24</u> (1), 53 (1988).

14. N. Beldjoudi and A. Gourdenne, Eur. Polym. J., <u>24</u> (3), 265 (1988).

15. F. M. Thuillier, H. Jullien, M. F. Grenier-Loustalot, Polym. Comm., <u>27</u>, 206 (1986).

16. S. Aussudre, A. Priou, H. Jullien, M. Delmotte, F. M. Thullier, D. Boulonnais and J. Sailleau, Rech. Aerosp., <u>5</u>, 1 (1988).

17. S. M. Singer, J. Jow, J. D. DeLong and M. C. Hawley, Polym. Mat. Sci. Eng., <u>60</u>, 869 (1989).

18. S. M. Singer, J. Jow, J. D. DeLong and M. C. Hawley, SAMPE Quarterly, <u>20</u> (2), 14 (1989).

19. J. Jow, Ph.D. Dissertation, Michigan State University, East Lansing, Michigan (1989).

20. J. Jow, J. D. DeLong and M. C. Hawley, SAMPE <u>20</u> (2), 46 (1989).

21. J. Jow, M. C. Hawley, M. Finzel and T. Kern, Polym. Eng. Sci., <u>28</u> (22), 1450 (1988).

22. J. Jow, M. C. Hawley, M. C. Finzel and J. Asmussen, Rev. Sci. Instrum., <u>60</u> (1), 96 (1989).

23. L. K. Wilson and J. P. Salerno, <u>Microwave Curing of Epoxy Resins</u>, Report No. 78-46, Avradcom (1978).

24. G. B. Taggart, <u>Electromagnetic Processing of Materials</u>, BDM Corporation, McLean, Virginia, Technical Report, 1984.

25. E. Karmazsin and P. Satre, Thermochimica Acta, <u>93</u>, 305 (1985).

26. N. S. Strand, Modern Plastics, <u>57</u> (10), 64 (1980).

27. N. S. Strand, 35th Annual Technical Conference, 1980, Reinforced Plastics/Composites Institute, The Society of the Plastics Industry, Inc. Section 24-C, 1.

28. N. S. Strand, <u>Microwave Curing of Thermoset Resins</u>, Society of Manufacturing Engineers Technical Paper, EM79-368 (1979).

29. A. Gourdenne and Q. Le Van, ACS Polym. Preprints, <u>22</u> (2), 125 (1981).

30. R. G. Raj, Polym. Mat. Sci. Eng., <u>56</u>, 537 (1987).

31. Y. Baziard and A. Gourdenne, Eur. Polym. J., 24 (9), 873 (1988).

32. Y. Baziard and A. Gourdenne, Eur. Polym. J., 24 (9), 881 (1988).

33. Y. Baziard, S. Breton, S. Toutain and A. Gourdenne, Eur. Polym. J., 24 (6), 521 (1988).

34. R. G. Raj, Polym. Mat. Sci. Eng., 55, 49 (1986).

35. A. Bouazizi and A. Gourdenne, Eur. Polym. J., 24 (9), 889 (1988).

36. W. I. Lee and G. S. Springer, J. Comp. Mat., 18, 357 (1984).

37. W. I. Lee and G. S. Springer, J. Comp. Mat., 18, 387 (1984).

38. W. I. Lee, Ph.D. Dissertation, University of Michigan (1983).

39. Y. Chen and C. Y. Lee, Polym. Mat. Eng. Sci., 60, 680 (1989).

40. J. Jow, M. C. Hawley and J. D. DeLong, Proc. Am. Soc. Composites, Third Tech. Conf., Seattle, Washington, pp. 305-312, 1988.

41. G. L. Vogel, J. Jow, J. D. DeLong and M. C. Hawley, Proc. Am. Soc. Composites, Fourth Tech. Conf., Blacksburg, Virginia, pp. 3-12, 1989.

42. R. Agrawal and L. T. Drzal, J. Adhes., 29 (1), 63 (1989).

43. B. Silinski, C. Kuzmycz and A. Gourdenne, Eur. Polym. J., 23 (4), 273 (1987).

44. H. Jullien and H. Valot, Polymer, 26, 506 (1985).

45. H. F. Schwarz, R. G. Bosisio, M. R. Wertheimer and D. Couderc, Rubber Age, 107 (11), 27 (1975).

46. H. F. Schwarz, R. G. Bosisio, M. R. Wertheimer and D. Couderc, J. Microwave Power, 8, 303 (1973).

47. J. Ippen, Rubber Chem. Technol., 44, 294 (1971).

48. I. J. Chabinsky, Rubber World, 188, 34, April (1983).

49. I. J. Chabinsky, Elastomerics, 115, 17, January (1983).

50. C. L. Lee, in ACS Symp. Series, Vol. 107, Eds., T. L. Vigo and L. J. Nowack, Am. Chem. Soc., Washington D.C., pp. 62-66, 1979.

51. K. Nakagawa, O. Maeda and S. Yamakawa, J. Polym. Sci.: Polym. Lett. Ed., 21, 933 (1983).

52. Y. Takeuchi, F. Yamamoto, K. Nakagawa and S. Yamakawa, J. Polym. Sci.: Polym. Phys. Ed., 23, 1193 (1985).

53. K. Nakagawa, T. Konaka and S. Yamakawa, Polymer, 26, 84 (1985).

54. T. Konaka, K. Nakagawa and S. Yamakawa, Polymer, 26, 462 (1985).

55.    Y. Takeuchi, K. Nakagawa and F. Yamamoto, Polymer, 26, 1929 (1985).

56.    K. Nakagawa and T. Konaka, Polymer, 27, 1030 (1986).

57.    K. Nakagawa and T. Konaka, Polymer, 27, 1553 (1986).

58.    M. Amano and K. Nakagawa, Polymer, 28, 263 (1987).

59.    M. Amano and K. Nakagawa, Polym. Comm., 28, 119 (1987).

60.    M. Teffal and A. Gourdenne, Eur. Polym. J., 19 (6), 543 (1983).

61.    S. Aussudre, A. H. Maassarani, L. Thourel and A. Gourdenne, 9th International Congress on Electroheat, Sect. 4, Comm. III A,3 (1980).

62.    A. Gourdenne, A. H. Maassarani, P. Monchaux, S. Aussudre and L. Thourel, ACS Polym. Preprints, 20 (2), 471 (1979).

63.    D. A. Lewis, J. D. Summers, T. C. Ward and J. E. McGrath, ACS Polym. Preprints, 29 (1), 174 (1988).

64.    D. A. Lewis, J. D. Summers, T. C. Ward and J. E. McGrath, J. Appl. Polym. Sci., submitted.

65.    T. L. Wilson, in Encyclopedia of Polymer Science and Engineering, Ed. J. I. Kroschwitz, John Wiley and Sons, Vol. 5, pp. 1-23, 1986.

66.    S. Matsuoka, in Encyclopedia of Polymer Science and Engineering, Ed. J. I. Kroschwitz, John Wiley and Sons, Vol. 5, pp. 23-36, 1986.

67.    N. G. McCrum, B. E. Read and G. Williams, Anelastic and Dielectric Effects in Polymeric Solids, John Wiley and Sons, New York, 1967.

68.    P. Hedvig, Dielectric Spectroscopy of Polymers, John Wiley and Sons, New York, 1977.

69.    A. R. Von Hippel, Dielectric Materials and Applications, Technology Press of M.I.T. and John Wiley and Sons, New York, 1954.

70.    G. L. Link, in Polymer Science, Ed. A. D. Jenkins, North-Holland Publishing, London, pp. 1282-1295, 1972.

71.    T. G. Parker, in Polymer Science, Ed. A. D. Jenkins, North-Holland Publishing, London, pp. 1297-1327, 1972.

72.    J. I. Kroschwitz, Electrical and Electronic Properties of Polymers: A State of the Art Compendium, John Wiley and Sons, New York, 1988.

73.    W. G. Potter, Epoxide Resins, Springer-Verlag, New York, 1970.

74.    C. A. May and G. Y. Tanaka, Eds., Epoxy Resin Chemistry and Technology, Marcel Dekker, New York, 1973.

75.    C. B. Bucknall, Toughened Plastics, Wiley, New York, 1977.

76. A. J. Kinloch and R. J. Young, Fracture Behavior of Polymers, Applied, Science, London, 1983.

77. C. K. Riew, E. H. Rowe and A. R. Siebert, in Toughness and Brittleness of Plastics, Eds., R. D. Deanin and A. M. Crugnola, Adv. Chem. Ser. 154, American Chemical Society, Washington D.C., pp. 326-343, 1976.

78. J. L. Hedrick, I. Yilgör, G. L. Wilkes and J. E. McGrath, Polym. Bull., 13, 201 (1985).

79. J. L. Hedrick, I. Yilgör, J. C. Hedrick, G. L. Wilkes and J. E. McGrath, Soc. Adv. Mat. Proc. Eng., 30, 947 (1985).

80. J. A. Cecere, J. L. Hedrick and J. E. McGrath, Soc. Adv. Mat. Proc. Eng., 31, 580 (1986).

81. J. A. Cecere and J. E. McGrath, ACS Polym. Preprints, 27, 299 (1986).

82. J. C. Hedrick, D. A. Lewis, G. D. Lyle, T. C. Ward and J. E. McGrath, Proceedings of the American Society for Composites, Fourth Technical Conference, Technomic, Lancaster, pp. 167-176, 1989.

83. J. C. Hedrick, D. A. Lewis, T. C. Ward and J. E. McGrath, ACS Polym. Preprints, 29(1), 363 (1988).

84. R. S. Raghava, Soc. Adv. Mat. Proc. Eng., 28, 367 (1983).

85. C. B. Bucknall and I. K. Partridge, Polymer, 24, 639 (1983).

86. R. S. Raghava, J. Polym. Sci.: Polym. Phys., 25, 1017 (1987).

87. G. R. Almen, R. K. Maskell, V. Molhotra, M. S. Sefton, P. T. McGrail and S. P. Wilkinson, Soc. Adv. Mat. Proc. Eng., 33, 979 (1988).

88. H. G. Recker, T. Allspach, V. Altstadt, T. Folda, W. Heckmann, P. Ittemann, H. Tesch and T. Weber, SAMPE Quarterly, 21(1), 46 (1989).

89. S. G. Chu, H. Jabloner and B. J. Swetlin, European Patent 0193082 (to Hercules Incorporated) (1986).

90. C. B. Bucknall and A. H. Gilbert, Polymer, 30, 213 (1989).

91. N. Odagiri, T. Muraki and K. Tobukuro, Soc. Adv. Mat. Proc. Eng., 33, 272 (1988).

92. J. Diamant and R. J. Moulton, Soc. Adv. Mat. Proc. Eng., 29, 422 (1984).

93. S. C. Kim and H. R. Brown, J. Mater. Sci., 22, 2589 (1987).

94. Manzione, J. K. Gillham and C. A. McPherson, J. Appl. Polym. Sci., 26, 889 (1981); 26, 907 (1981).

95. R.J.J. Williams, J. Borrajo, H. E. Adabbo and A. J. Rojas, in Rubber Modified Thermoset Resins, C. K. Riew and J. K. Gillham, Eds., Adv. Chem. Ser. 208, American Chemical Society, Washington D.C., pp. 195-213, 1984.

96. D. Verchère, H. Sautereau, J. P. Pascault, S. M. Moschiar, C. C. Riccardi and R.J.J. Williams, Polymer, 30(1), 107 (1989).

97. D. J. Walsh, in Comprehensive Polymer Science, C. Booth and C. Price, Eds., Pergamon Press, New York, Vol. 2, pp. 135-154, 1989.

98. O. Olabisi, L. M. Robeson and M. T. Shaw, Polymer-Polymer Miscibility, Academic Press, New York, 1979.

99. O. Olabisi, J. Chem. Ed., 58(11), 944 (1981).

100. L. M. Robeson, in Encyclopedia of Materials Science and Engineering, M. B. Bever, Ed., Pergamon Press, New York, Oxford, pp. 3654-3658, 1986.

101. P. C. Hiemenz, Polymer Chemistry, Marcel Dekker, New York, pp. 505-537, 1984.

102. D. R. Paul, S. Newman, Eds., Polymer Blends, Academic Press, New York, 1978.

103. D. R. Paul, J. W. Barlow and H. Keskkula, in Encyclopedia of Polymer Science and Engineering, J. I. Kroschwitz, Ed., John Wiley and Sons, New York, Vol. 12, pp. 399-461, 1988.

104. D. R. Paul and J. W. Barlow, J. Macromol. Sci.: Rev. Macromol. Chem., 618(1), 109 (1980).

105. L. P. McMaster, Macromolecules, 6, 760 (1973).

106. C. B. Bucknall and T. Yoshii, Brit. Polym. J., 10, 53 (1978).

107. M. T. Aronhime and J. K. Gillham, in Epoxy Resins and Composites IV, Adv. Polym. Sci. 78, Springer-Verlag, New York, pp. 83-113, 1986.

108. J. K. Gillham, in Encyclopedia of Polymer Science and Engineering, J. I. Kroschwitz, Ed., John Wiley and Sons, New York, Vol. 4, pp. 519-524, 1988.

109. R. B. Prime, in Thermal Characterization of Polymeric Materials, E. A. Turi, Ed., Academic Press, New York, pp. 435-565, 1981.

110. A. F. Yee and R. A. Pearson, J. Mater. Sci., 21, 2462 (1986); 21, 2475 (1986).

111. A. J. Kinloch, S. J. Shaw, D. A. Tod and D. L. Hunston, Polymer, 24, 1341 (1983); 24, 1355 (1983).

112. R. P. Kambour, J. Polym. Sci.: Macromol. Rev., 7, 1 (1973).

113. R. N. Haward, The Physics of Glassy Polymers, John Wiley and Sons, New York, 1973.

114. E. J. Kramer and L. L. Berger, in Crazing in Polymers, Vol. 2, Adv. Polym. Sci. 91/92, Springer-Verlag, New York, pp. 1-68, 1990.

115. J. N. Sultan and F. J. McGarry, Polym. Eng. Sci., 13(1), 29 (1973).

116. A. M. Donald and E. J. Kramer, J. Mater. Sci., 17, 1871 (1982).

117.  S. Kunz-Douglass, P.W.R. Beaumont and M. F. Ashby, J. Mater. Sci., 15, 1109 (1980).

118.  S. C. Kunz and P.W.R. Beaumont, J. Mater. Sci., 16, 3141 (1981).

119.  A. G. Evans, Z. B. Ahmad, D. G. Gilbert and P.W.R. Beaumont, Acta. Metall., 34(1), 79 (1986).

120.  W. D. Bascom, R. L. Cottington, R. L. Jones and P. Peyser, J. Appl. Polym. Sci., 19, 2545 (1975).

121.  W. D. Bascom, R. Y. Ting, R. J. Moulton, C. K. Riew and A. R. Siebert, J. Mater. Sci., 16, 2657 (1981).

122.  D. L. Hunston, J. L. Bitner, J. L. Rushford, J. Oroshnik and W. S. Rose, Elast. Plast. 12, 133 (1980).

123.  R. A. Pearson and A. F. Yee, J. Mater. Sci., 24, 2571 (1989).

124.  A. J. Kinloch, C. A. Finch and S. Hashemi, Polym. Comm., 28, 322 (1987).

125.  R. S. Bauer, Soc. Adv. Mat. Proc. Eng., 34, 997 (1989).

126.  K. Yamanaka and T. Inoue, J. Mat. Sci., 25, 241 (1990).

127.  K. Yamanaka, Y. Takagi and T. Inoue, Polymer, 30, 662 (1989); 30, 1839 (1989).

128.  H. D. Stenzenberger, Br. Polym. J., 20, 383 (1988).

129.  H. D. Stenzenberger, M. Herzog, W. Romer, R. Scheiblich, and N. J. Reeves, Br. Polym. J., 15, 2 (1983).

130.  H. D. Stenzenberger, in Structural Adhesives:  Developments in Resins and Primers, ed. A. J. Kinloch, Elsevier, New York, pp. 78-126, 1986.

131.  D. Landman, in Developments in Reinforced Plastics-5, G. Pritchard Ed., Elsevier Applied Sci., New York, pp. 39-81, 1986.

132.  L. S. Tan, E. J. Soloski, and F. E. Arnold, ACS Symp. Ser., 367, 347 (1988).

133.  L. R. Denny, I. J. Goldfarb and M. P. Farr, ACS Symp. Ser., 367, 366 (1988).

134.  L. S. Tan and F. E. Arnold, ACS Polym. Preprints, 26(2), 178 (1985).

135.  F. E. Arnold and L. S. Tan, Soc. Adv. Mat. Proc. Eng., 31, 968 (1986).

136.  H. D. Stenzenberger and P. Koning. High Perform. Polym., 1(2), 133 (1989).

137.  F. Grundschober and J. Sambeth, U.S. Patent 3380964 (to Rhone Poulenc) (1964).

138.  I. M. Brown and T. C. Sandreczki, Macromolecules, 23(1), 94 (1990).

139.  I. M. Brown and T. C. Sandreczki, Polym. Mater. Sci. Eng., 59, 612 (1988).

140.  A. C. Lind and C. G. Fry, Polym. Mater. Sci. Eng., 59, 466 (1988).

141. K. R. Carduner and M. S. Chattha, Polym. Mater. Sci. Eng., 56, 660 (1987).

142. R.C.P. Cubbon, Polym., 6, 419 (1965).

143. Y. Nakayama and G. Smets, J. Polym. Sci.: Part A-1, 5, 1619 (1967).

144. D. O. Hummel, K. U. Heinen, H. D. Stenzenberger, and H. Siesler, J. Appl. Polym. Sci., 18, 2015 (1974).

145. I. K. Varma, G. M. Fohlen, and J. A. Parker, J. Polym. Sci.: Polym. Chem. Ed., 20, 283 (1982).

146. G. D. Lyle, J. S. Senger, D. H. Chen, S. Kilic, S. D. Wu, D. K. Mohanty, and J. E. McGrath, Polymer, 30, 978 (1989).

147. G. D. Lyle, J. C. Hedrick, D. A. Lewis, J. S. Senger, D. H. Chen, S. D. Wu, and J. E. McGrath, in Polyimides: Materials, Chemistry and Characterization, eds. C. Feger, M. M. Khojasteh, and J. E. McGrath, Elsevier, New York, pp. 213-228, 1989.

148. G. T. Kwiatkowski, L. M. Robeson, G. L. Brode, and A. W. Bedwin, J. Polym. Sci.: Poly. Chem. Ed., 13, 961 (1975).

149. H. D. Stenzenberger, P. Koning, M. Herzog, and W. R@mer, Soc. Adv. Mat. Proc. Eng., 32, 44 (1987).

150. H. D. Stenzenberger, W. Romer and M. Herzog, Soc. Adv. Mat. Proc. Eng., 31, 920 (1986).

151. J. S. Senger, G. York, D. Chen, K. Ung, and J. E. McGrath, in the Proceedings of the American Society for Composites, 4th Technical Conference, Technomic, Lancaster, pp. 631-637, 1989.

152. J. S. Senger, Ph.D. Dissertation, Virginia Polytechnic Institute and State University, Blacksburg, Virginia 24061 (1990).

153. I. K. Varma and R. Tiwari, J. Therm. Anal. 32(4), 1023 (1987).

154. K. A. Barrett, M. A. Chaudhari, and B. H. Lee, SAMPE Journal, 25(2), 17 (1989).

155. J. J. King, M. Chaudhari, and S. Zahir, Soc. Adv. Mat. Proc. Eng., 29, 392 (1984).

156. D. Wilson, Br. Polym. J., 20(5), 405 (1988).

157. D. Kumar, G. M. Fohlen, and J. A. Parker, J. Polym. Sci.: Polym. Chem. Ed., 21, 565 (1983).

158. P. N. Preston, I. Soutar, B. Woodfine, and J. N. Hay, High Perform. Polym., 1(2), 161 (1989).

159. J. N. Hay, J. D. Boyle, P. G. James, J. R. Walton, and D. Wilson, in Polyimides: Materials, Chemistry and Characterization, eds. C. Feger, M. M. Khojasteh, and J. E. McGrath, Elsevier, New York, pp. 305-320, 1989.

160. C. N. Sukenik, W. M. Ritchey, V. Malholra, and U. Varde, in <u>High Temperature Polymer Matrix Composites</u>, NASA Conference Publication, No. 2385, pp. 79-90, 1985.

161. A. C. Wong and W. M. Ritchey, Macromolecules, <u>14</u>, 825 (1981).

162. A. C. Wong, A. N. Garroway, and W. M. Ritchey, Macromolecules, <u>14</u>, 832 (1981).

163. S. D. Wu, J. S. Senger, J. C. Hedrick, G. D. Lyle, D. H. Chen, M. Chen, J. D. Rancourt, and J. E. McGrath, Soc. Adv. Mat. Proc. Eng., <u>34</u>, 139 (1989).

164. P. M. Hergenrother, in <u>Encyclopedia of Polymer Science and Engineering</u>, Ed., J. I. Kroschwitz, John Wiley and Sons, New York, Vol. 1, pp. 61-86, 1988.

165. H. Jabloner and L. C. Cessna, J. Elastomers Plast., <u>6</u>, 103 (1974).

166. A. L. Landis, N. Bilow, R. H. Boschan, R. E. Lawrence, and T. J. Aponyi, ACS Polym. Preprints, <u>15</u>(2), 533 (1974).

167. A. L. Landis and A. B. Naselow, Soc. Adv. Mat. Proc. Eng., Tech. Conf. Ser., <u>14</u>, 236 (1982).

168. D. K. Mohanty, J. S. Senger, C. D. Smith, and J. E. McGrath, Soc. Adv. Mat. Proc. Eng., <u>33</u>, 970 (1988).

169. S. A. Thompson and R. J. Farris, J. Appl. Polym. Sci., <u>36</u>, 1113 (1988).

170. G. Odian, <u>Principles of Polymerization</u>, John Wiley and Sons, New York, 1970.

171. A. Rudin, <u>The Elements of Polymer Science and Engineering</u>, Academic Press, Orlando, 1982.

172. F. W. Billmeyer, Jr., <u>Textbook of Polymer Science</u>, 3rd Ed., Wiley-Interscience, New York, 1984.

173. D. K. Mohanty, Ph.D. Dissertation, Virginia Polytechnic Institute and State University, Blacksburg, Virginia 24061 (1983).

174. M. J. Jurek, Ph.D. Dissertation, Virginia Polytechnic Institute and State University, Blacksburg, Virginia 24061 (1987).

175. M. J. Jurek and J. E. McGrath, Polymer, <u>30</u> (8), 1552 (1989).

176. J. Asmussen, H. H. Lin, B. Marring, and R. Fritz, Rev. Sci. Instrum., <u>58</u>(8), 1477 (1987).

177. H. H. Lin, Ph.D. Dissertation, Michigan State University, East Lansing, MI, 1988.

178. J. S. Fritz, <u>Acid-Base Titrations in Nonaqueous Solvents</u>, Allyn and Bacon, Boston, 1973.

179. M. Chen, Ph.D. Dissertation, Virginia Polytechnic Institute and State University, Blacksburg, Virginia 24061 (1989).

# APPENDIX

# BASIC IDEAS OF MICROWAVE PROCESSING OF POLYMERS

M. Chen[1], E. J. Sicchi[2], T. C. Ward* and J.E. McGrath

NSF STC: High Performance Polymeric Adhesives and Composites and
Department of Chemistry
Virginia Polytechnic Institute and State University
Blacksburg, VA 24061-0212

## ABSTRACT

The objective of this effort has been to investigate the relationship between polymer structure and microwave absorptivity. Dielectric loss factor, $\varepsilon''$, loss tangent, $\tan\delta$, and oscillator strength, $(\varepsilon_S - \varepsilon_\infty)$, were used to evaluate potential material processability under applied microwave radiation. Numerous polymeric materials varying in chemical and physical structures were irradiated in a low power ( <100W) electric field at 2.45 GHz. Electromagnetic radiation was applied as either traveling or resonant wave modes in either cylinderical or rectangular waveguides. In general, heatibility was found to be a direct function of the dielectric loss dispersion with temperature and frequency. The dielectric loss factor obtained at low frequency measurements was found to be directly proportional to the heatability of polymers. A WLF plot was used to predict the shift of dielectric loss maxima into or out of the microwave frequency range.

# INTRODUCTION

The application of microwave processing to polymers and composites has been pursued in several laboratories throughout the world over the past two decades. Here, significant impact has been made in the rubber and food industries where processing with microwaves yields substantial advantages. In contrast to conventional thermal treatments, these advantages are rapid volumetric heating, no overheating at the surface, addressable heating, energy saving and low operating costs, increased throughput, and reduced degradation.

Microwave heating of materials stems from dielectric power absorption as described by the following equation:

$$P = KfE^2\varepsilon'\tan\delta \qquad [1]$$

where P is the power dissipation in W/cm$^3$, K is a constant equal to $55.61 \times 10^{-14}$, f is the applied frequency in Hz, E is the electric field strength in V/cm, $\varepsilon'$ is the dielectric constant and $\tan\delta$ is the dielectric loss tangent. Both $\varepsilon'$ and $\tan\delta$ depend upon both the frequency and the sample temperature. The electromagnetic field energy dissipated as heat per unit volume is proportional to the dielectric loss factor ($\varepsilon'\tan\delta$), the square of the field strength ($E^2$) and the frequency (f) of the applied field. In this discussion, it is assumed that influences upon heating rate due to heats of reaction are negligible.

The ratio of the dielectric loss factor, $\varepsilon''$, to the dielectric constant, $\varepsilon'$, is called the loss tangent, $\tan\delta$, for a nonionic material. The dielectric loss factor determines primarily the rate of conversion of electrical energy into thermal energy in the material before phase transition losses. Since the electric field penetrates the material, heat is generated internally. Thus, until convection and conduction losses become important, the dielectric power dissipation is independent of the heat flow through the surface of the material. This is in contrast to conventional thermal heating which is dependent upon the thermal conductivity of the material and, therefore, is much more time consuming.

If convection and conduction losses and heat flux due to chemical reactions are ignored, the heating rate of a material placed in an electromagnetic field depends on several key parameters. These may be described by the relationship:

$$\frac{dT}{dt} = \frac{KfE^2\varepsilon'(T)\tan\delta(T)}{\rho C_v} \qquad [2]$$

110

where $\rho$ is the density of the material, $C_V$ is the specific heat and the other variables are as defined in Equation 1. Again, no chemical reactions are assumed. The heating rate, as Equation 2 indicates, is directly dependent on the dielectric behavior of a polymer. It must be noted that the dielectric behavior is a function of temperature due to the variability of $\varepsilon''$ with temperature. This behavior is determined largely by the charge distribution within bonds, chain conformation, bulk morphology and statistical thermal motion of the polar groups. The most influential factor is its chemical structure. A detailed investigation of dielectric properties would not only permit a better understanding of the polymer structure but would also allow the prediction of an optimum chemical structure for maximizing its coupling with microwave energy. Ultimately, this study would identify those materials which would be most suitable for microwave processing.

A better understanding of the mechanism for coupling microwave energy into a material may be achieved by examining the dependence of dielectric properties upon frequency at fixed temperatures or upon temperature at fixed frequencies. The resultant contour surface of dielectric loss versus log(frequency) and temperature would reveal region of dielectric due to different mechanisms. Interpretation of these mechanisms usually requires information over a wide frequency range along with other material data such as the melting point and the glass transition temperatures. The activation energies of the various relaxations, $\Delta E_a$, can be an important clues for identifying associated molecular motions. Although an optimum frequency for dielectric heating can be selected from knowledge of maximum dielectric loss, the process is actually much more complex.

Numerous techniques for obtaining dielectric properties of polymers dependent upon frequency are available (1). For the measurement of the complex dielectric constant at frequencies below 100 MHz, bridge methods are employed. Above this frequency, the measurement is accomplished by either a reentrant cavity, standing wave, or cavity resonator methods. Above 10 GHz, free space methods are used. It is rare, however, to find high frequency and temperature variation data for polymers in the literature.

The quantity that influences microwave heatability the most is the dielectric loss factor. However, its variation with temperature at 2.45 GHz is difficult to measure. It is more experimentally convenient to obtain dielectric absorption spectra as a function of temperature at various lower frequencies. The variations caused by orientation polarization changes could be observe directly. In addition, since the mechanical

111

properties (polarization and relaxation) of polymers are closely associated with its electrical properties, the techniques for respective properties measurements are complementary in the characterization of structure-property relationships.

## THEORY OF STRUCTURE-PROPERTY RELATIONSHIPS

The general relationship of the dielectric constant and the dielectric loss factor to the applied frequency for a polar molecule is depicted in Figure 1. Electronic polarization is observed at high frequencies corresponding to the uv region, as a result of the displacement of the electrons in the molecules relative to the positive nuclei. This type of polarization occurs in all materials and yields a dielectric constant of about two. Atomic polarization arises from the displacement of atoms relative to one another in the molecule. The movement of heavy nuclei is more sluggish than that of electrons. The time required for atomic polarization is around $10^{-13}$ s and corresponds to the frequency range of infrared radiation. Electronic and atomic polarizations may also be called displacement deformations or distortion polarizations, in which case, the dipole moment so produced is called an induced dipole moment. Both of these rapid events are referred to as "optical polarizations."

If the polar molecules intrinsically possess a permanent dipole moment, the moment will tend to align to the applied field to give a net polarization in that direction. Within the frequency range of dielectric relaxation, the polarizability due to the electronic and atomic polarization remains unchanged. This is due to the time required for the distortion polarization of a molecule to reach equilibrium with the applied field being much shorter relative to that for orientation polarization. At lower frequencies, the contribution of the induced dipole moments becomes negligible compared to the permanent dipole moments of the system. Dipole relaxation is commonly in the frequency range of $10^6$ to $10^{10}$Hz. The static (relaxed) dielectric constant, $\varepsilon_s$, and the high frequency (unrelaxed, or optical) dielectric constant, $\varepsilon_\infty$ are defined in Figure 1 as the maximum and minimum dielectric constant in the dipole relaxation region.

Electronic, atomic, and orientation polarization are due to local changes in atoms, molecules, or the structures of solids and liquids. In contrast, interfacial polarization occurs as a result of the differences in the conductivities and dielectric constants of the materials at interfaces. This accumulation of space charge is responsible for field distortions and dielectric loss, referred to as Maxwell-Wagner charging.

Dielectric relaxation is the exponential decay of the polarization with time in a dielectric material when an externally applied field is removed. Dielectric relaxation

112

causes anomalous dispersion in which the dielectric constant decreases with increasing frequency, as depicted in Figure 1. In the most elementary fashion the decay function can be described in the following relationship:

$$\varnothing_a(t) \; \alpha \; e^{-t/\tau} \tag{3}$$

where $\tau$ is the relaxation time, the time required for the polarization to decay to 1/e of the original equilibrium value. It is time independent but highly temperature dependent. From a structural point view, the dipole relaxation depends on the internal structures of the molecules and on the molecular arrangement or structure of the dielectric material.

In polymeric systems, the relationship shown in Equation 3 is highly simplified. The relaxation time depends on the viscosity of the medium, which in turn depends on the temperature. In gases where the molecular motion is vigorous and rapid, the time required for dipole relaxation is near $10^{-12}$ s. For small molecules in low viscosity liquids, the time required is about $10^{-11} - 10^{-10}$ s, which corresponds directly to the microwave frequency region. For large molecules or viscous liquids, the time required is about $10^{-6}$ s, i.e., radio frequencies. The phase lag between the polarization and the applied field reveals an absorption of energy which will be temperature dependent. Increasing temperature, and thus, mobility of the polymers, allows rapid orientation of polar molecules in the direction of the external electric field. As Equation 3 is inadequate in the case of alternating fields, the polarization may be related to frequency and a distribution of relaxation times as follows in Equation 4. This "stretched" exponential distribution allows for a broader response, such as typical for polymers, through the adjustable parameter $\beta$.

$$\varnothing_b(t) \; \alpha \; e^{(-t/\tau)^{\beta}} \tag{4}$$

As indicated in Figure 2, at high frequencies the greater viscosity of polymer molecules prevents the dipoles from orienting in the rapidly reversing field. Consequently, the dipoles do not influence the a-c characteristics ($\varepsilon'_{\infty}$ and $\varepsilon''_{\infty}$) at high frequencies. As the frequency decreases, the dipoles respond more freely with an associated loss of energy. The loss peaks ultimately decrease when the oscillations of individual units no longer couple. As the frequency is reduced still further, the applied power is no longer converted to heat by viscous transfer. At this point, the dielectric constant possesses its highest static value, $\varepsilon_s$, in relation to the dipole contribution,

and the dielectric loss factor and loss tangent reach a minimum. As the frequency approaches zero, $\varepsilon''$ approaches zero and $\varepsilon'$ approaches the static dielectric constant, $\varepsilon_S$. As the frequency approaches infinity, $\varepsilon'$ approaches $\varepsilon_\infty$, the optical dielectric constant. The optical dielectric constant is defined as the product of the permittivity in free space and the square of the refractive index.

Separating the real and the imaginary parts of Debye equations yields:

$$\varepsilon' = \varepsilon_\infty + \frac{\varepsilon_S - \varepsilon_\infty}{1 + \omega^2 \tau^2} \qquad [5]$$

$$\varepsilon'' = \frac{\left(\varepsilon_S - \varepsilon_\infty\right) \omega \tau}{1 + \omega^2 \tau^2} \qquad [6]$$

where $\omega$ is the frequency ($\omega = 2\pi f$) and $\tau$ is the dielectric relaxation time. As the frequency or the relaxation time is changed via a temperature shift, $\varepsilon''$ yields a maximum value at $(\varepsilon_S - \varepsilon_\infty)/2$ when $\omega \tau = 1$ in the simplified model where one $\tau$ is sufficient. At the same time, $\varepsilon'$ decreases from $\varepsilon_S$ to $\varepsilon_\infty$ with increasing frequency. For polar liquids, this decrease may occur within a 100-fold frequency range.

In the case of polymers, however, this dispersion occurs over a much wider frequency range. Additionally, the maximum value of $\varepsilon''$ is typically lower than that predicted by Equation 6. Polar polymers realistically never follow the simple Debye equations. The real situation may be represented by the superposition of several Debye curves representing a set or distribution of relaxation times. To adequately represent polymer response, measurements should be made over a frequency range of $10^{-3}$ to $10^{10}$ Hz. The high-frequency value of the dielectric constant, $\varepsilon_\infty$, is 2.2 to 2.5 for polymers. The static quantity, $\varepsilon_S$, may have a wide range of values depending on the polymer structure.

In simple liquids, the relationship of dielectric constant and dipole moment has been successfully expressed by the Onsager equation (2). At ordinary temperatures, a polymer molecule in the liquid or even glassy phase will undergo continuous Brownian motion and the moment of the chain will vary continuously in time. However, the Onsager theory is not sufficient to describe the dielectric properties of polymer molecules.

114

In the condensed phase or semidilute solutions, the dipole moments of the molecules or groups interact strongly and result in a decrease of the total dipole moment. This reduction factor, $g_r$, was first defined by Kirkwood (3).

$$g_r = \frac{\mu_{eff}^2 \text{(condensed)}}{\mu_0^2 \text{(gas)}} \qquad [7]$$

where $\mu_0$ is the total dipole moment of the group or molecule and $\mu_{eff}$ is the effective dipole moment measured in the condensed state. The value of the reduction factor is determined by the number and distance of the nearest polar neighbors to the group considered. Typically, the Kirkwood reduction factor is significantly different from unity, even for dilute solutions, due to the intramolecular interactions of the polar units of the macromolecule. Additionally, the Kirkwood coefficient is highly temperature dependent.

Although intramolecular interactions influence the physical properties of bulk polymers in the solid and viscoelastic fluid states, the conformational motions of polymer molecules in bulk are not yet completely understood. It is difficult to determine which specific part of the molecule behaves rigidly during thermal motion in a given temperature range. As such, their corresponding reduction factors have yet to be determined.

Fröhlich (4) modified the Onsager theory by incorporating the Kirkwood reduction factor into the Onsager equation which resulted in the Fröhlich-Kirkwood equation:

$$\varepsilon_s - \varepsilon_\infty = \frac{3\varepsilon_s}{\left(2\varepsilon_s + \varepsilon_\infty\right)} \frac{4\pi N}{3kT} \left(\frac{\varepsilon_\infty + 2}{3}\right)^2 g_r \mu_0^2 \qquad [8]$$

The quantity ($\varepsilon_s - \varepsilon_\infty$) is important in the analysis of dielectric data in terms of molecular structure. It is a measure of the intensity or the strength of the relaxation process. It is proportional to the number of dipoles involved in the relaxation process yet inversely proportional to the temperature. If the dipole moment, $\mu_0$, and the intra- and intermolecular interactions, $g_r$, are not changed in the working temperature range, then the dielectric constant should decrease with increasing temperature. This is the case for dilute solutions and for some polymers in the molten state. However, the dielectric constant of practically all polar polymers increases with increasing

115

temperature, indicating that the dependence is mainly governed by both intra- and intermolecular interactions.

The area beneath the dielectric loss factor versus frequency curve, pictured in Figure 1, is proportional to $(\varepsilon_s - \varepsilon_\infty)$. The maximum dielectric loss factor varies with the distribution of relaxation times, as governed in the following equation:

$$\varepsilon_s - \varepsilon_\infty = \frac{2}{\pi} \int_{-\infty}^{\infty} \varepsilon'' d\ln f \qquad [9]$$

These relationships apply to all dispersions, and are useful in checking the internal consistency of data; they are particularly important in polymer dipolar relaxation related to heating.

Polymers usually exhibit more than one dipolar dispersion, as shown in Figure 2. A prominent feature of polymeric dipolar motions involves complex cooperative movement of multiple chain sections consisting of a large number of monomeric units (segments) at the $T_g$. Besides segments, smaller and more mobile kinetic units are also moving in polymers at appropriate temperatures. Such kinetically-independent units may be side chains, chain ends, or individual atomic groups such as polar substituents. The relaxation time of the orientation movement of such groups is smaller than the relaxation time of main-chain segments allowing them to retain their mobility below the glass transition temperature.

In order to identify and compare the locations of loss peaks in different polymers, the nomenclature first suggested by Deutsch, et al. (5) is used. The relaxation observed at the highest temperature (constant frequency) or lowest frequency (constant temperature) is called the $\alpha$ dispersion. Subsequent dispersions are identified with the remaining relaxation regions in order of decreasing temperature (or increasing frequency) as $\beta$, $\gamma$, and so on. In amorphous polymers, a loss region associated with the glass-rubber transition is observed at or above the "equilibrium", or "zero heating-rate", glass-transition temperature, $T_g$, and is usually labelled the $\alpha$ relaxation. The glass-to-rubber transition in polymers is associated with orientation rotation of multiple backbone chain units of the macromolecule under conditions where segmental movement becomes possible due to increasing free volume. If there are polar groups in the polymer's side chains which are capable of orientation in an electric field independent of one another and which have different relaxation times, additional dipole-group loss maxima will also appear in the $\varepsilon''$ vs. temperature or $\varepsilon''$ vs. frequency curves.

116

The variation of $\varepsilon'$ and $\varepsilon''$ with frequency is shown schematically in Figure 3 and complements the variation of $\varepsilon'$ and $\varepsilon''$ with temperature given in Figure 2. The peak values are identical, but the dispersion shapes are different. The relaxation time of each process can be described by the following equation:

$$\tau_i = \tau_{io} \exp\left(\frac{\Delta E_a}{RT}\right)$$

[10]

where $\tau_{io}$ is the relaxation time of the $i^{th}$ mode of motion in the high temperature limit. The higher the temperature, or the smaller the activation energy, the shorter the relaxation time. In Figure 2, the activation energy of the local chain motion ($\beta$ process) is always less than that of the main chain motion ($\alpha$ process) at a given temperature, usually by one order of magnitude. Therefore, for a given increase in temperature, the $\beta$ relaxation will shift along the abscissa faster than that of an $\alpha$ relaxation. As a result, both relaxations tend to merge as frequency is increased. In the frequency domain (see Figure 3), the shift along the abscissa of the $\alpha$ relaxation is faster than that of the $\beta$ relaxation. Therefore, both relaxations eventually merge as frequency is increased.

There is no single method available for characterizing the dielectric behavior over an extremely wide frequency range, i.e., several orders of magnitude. However, it is easy to monitor the dielectric properties via a thermal cycle at a given fixed frequency up to the 100 kHz range. According to the principle of time-temperature superposition (6-8), the dielectric response in Figure 1 will shift to a higher frequency region by increasing the temperature and maintain the same shape. Merging $\alpha$ and $\beta$ relaxations at higher frequencies, however, will change the shape of the $\varepsilon''$ distribution, but will not affect the values of the oscillator strength, ($\varepsilon_s - \varepsilon_\infty$), over the frequency domain of dipole relaxation. Evaluation of the heatability of polymers by determination of the values of ($\varepsilon_s - \varepsilon_\infty$) for various polymers is suggested.

Orientation polarization due to the presence of permanent dipoles in a molecule is the major energy coupling mechanism available for heating. For polymers containing dipolar groups, the complex dielectric relaxation effects observed are related to coupled orientation of the permanent dipoles subsequent to the application of the electric field. To evaluate the influence that structure-property relationships will have on processability with microwave radiation, it is imperative that the dielectric properties be thoroughly investigated and be correlated with chemical and morphological conformation. One must first examine the relationships between the

dielectric constants of polymers and the effective dipole moments, as described in Equation 8. In considering effective dipole moments, it is helpful to use group moments instead of bond moments. Group moments are the dipole moments of such chemical groups which are known to have a stable configuration even during thermal motion. One may calculate for all polymer structures a "static" dipole per repeat structure and are typically on the order of $10^{-18}$ esu cm (1 Debye). Dipole moments have usually been determined in the gas phase or in a solution of a polar substance dissolved in a nonpolar solvent where, at infinite dilution, the interaction of the polar molecules with each other could be neglected. A. L. McClellan collected all experimentally determined dipole moments reported prior to 1962 (9). The tabulated dipole moments are arranged in the order of decreasing dipole moments and presented in Tables 1 and 2. From the dipole moments of these model molecules, the order of polarity of group moments in polymer structure units is shown in Figure 4.

## EXPERIMENTAL

### MATERIALS

The glass transition temperatures, melting temperatures and the suppliers of the polymers used in this study are summarized in Table 3. All polymers except for the nitrile rubbers were used without further purification. The nitrile rubbers were dissolved in chloroform (3% wt. of solid), filtered through a Whatman No. 1 filter paper, coagulated by dropwise addition of chloroform solution to methanol, and dried in a vacuum oven at room temperature for 12 hours. This purification procedure was repeated to ensure high purity. Purified nitrile rubber containing 2% by weight of dicumyl peroxide (supplied by the Lucidol Division of the Pennwalt Corporation, minimum of 99% purity, used as received) was dissolved in chloroform (6% wt. of solid). Films were prepared by casting the solution into a teflon mold. Upon evaporation of the solvent, the films were dried in a vacuum oven at room temperature for 24 hours. These films were kept in the desiccator until they were used for Dynamic Mechanical Thermal Analysis (DMTA), Dielectric Thermal Analysis (DETA), and the microwave experiments.

Thermally-cured films were prepared in a convection oven at 150°C for 2.5 hours. Specimen preparation methods are summarized in Table 3. For the semicrystalline polymers, some samples were quenched from the melt state into an ice water bath,

118

while others of higher crystallinity were prepared by quenching in the platten press (Pasadena Hydraulics, Inc., model number P210C-X3-5-7-20).

## DISPERSION SPECTROMETER SYSTEMS

Polymer Laboratory's DETA and DMTA instruments were used to provide relaxation information covering the broad frequency range of 0.3 Hz to 100 kHz. Dielectric spectra from -150°C to above $T_g$ or $T_m$ were obtained via DETA at fixed frequencies of 0.1, 1, 10 & 100 kHz. Thermal mechanical spectra from -150°C to $T_g$ or $T_m$ were studied by using the DMTA at frequencies of 0.3, 1, 3, 10 and/or 30 Hz. All samples, except the nitrile rubbers, were tested in the bending mode. The mechanical analyzer was equipped with shear clamps for testing the soft uncured nitrile rubber. A single cantilever bending mode was chosen for the microwave-cured nitrile rubber.

## MICROWAVE INSTRUMENTATION

The travelling wave applicator is depicted schematically in Figure 5. The individual components of the microwave system are described below.

(i)     A Raytheon model PGM-10X1 variable (0-120 watts) power generator operating at 2.45 GHz which was used as the microwave source.

(ii)     A circulator to protect the microwave generator from reflected waves, as well as a matched termination.

(iii)     Coaxial directional couplers, attenuators and power meters which measure the incident power, $P_i$, reflected power, $P_r$, and transmitted power, $P_t$.

(iv)     Adapter that connects the coaxial cable to the WR284 waveguide.

(v)     Samples were separated by teflon sheets of 0.005 in. thick and placed into a 3.3 cm high by 1.27cm inside diameter cylindrical teflon sample holder. The sample holder was placed at the maximum electric field region of the waveguide.

(vi)     An adapter fastened at the other end to couple the coaxial cable to the waveguide for the travelling mode.

(vii)     A Luxtron fluoroptic thermometry system model 750 was used for temperature measurements. The fiber-optic temperature measuring probe was inserted into the center of the sample to measure the sample temperature.

(viii)     An IBM personal computer was used to record powers and temperature versus time, simultaneously.

(ix)   Various starting temperatures for the investigation were induced by external heating of the waveguide with a strip heater.

There is only one mode, $TE_{10}$ (10), which can propagate freely in the rectangular WR284 waveguide.  This mode is characterized by an electric field vector (E) which has one component only, linearly polarized parallel to the narrow faces of the waveguide with a half sinusoidal variation between them, having a maximum value at the midpoint.

Travelling wave applicators are those which apply power from the generator into the waveguide allowing absorption of the energy by one pass of the waves through the sample before being absorbed by a terminator.  This particular waveguide was characterized by a low VSWR (Voltage Standing Wave Ratio) of less than 1.17 for this experiment.  Travelling wave applicators can be operated empty without risk to the generator.  Ideally, the waves cannot be reflected back and forth; therefore, the electric field strength is relatively low.  This wave applicator was used to process the nitrile rubbers with three different percentages of acrylonitrile content.

A cylindrical cavity, resonant wave applicator was used to process the ethylene/vinyl acetate copolymers.  The $TE_{111}$ mode was chosen to process these polymers.  The specimens for microwave processing (1 cm x 1 cm x 0.5 cm) were placed in the cavity of a flexible silicone mold.  The size of the silicone mold was approximately 2 cm x 2 cm x 1.2 cm.  Two more pieces of silicone mold were stacked to support the specimen and to raise the specimen to the center of the $TE_{111}$ mode.  An additional silicone mold was placed on the top of the specimen in order to secure the fiber optical temperature probe in place and to prevent heat convection losses from the specimen.

## RESULTS AND DISCUSSION

## THERMAL RESPONSE FROM DETA AND DMTA

### Polysulfone

The temperature dependence of the log storage modulus and the loss tangent for bisphenol A based polysulfone at 1, 3, 10 and 30 Hz using the DMTA instrument is depicted in Figure 6.  The glass transition temperature of bisphenol-A polysulfone was observed at around 190°C.  The well known low temperature $\beta$ transition is apparent at approximately -70°C.

120

The temperature dependence of the dielectric loss tangent obtained via DETA for polysulfone is illustrated in Figure 7. The loss tangent scale between -60°C and 40°C was expanded 50-fold in order to present the β relaxation. The peak intensity of the α relaxation was about 100 times larger than that of the β relaxation. The intensity of the dielectric absorption depends on the position of the polar bonds in the polymer chain with respect to the specific units involved in the thermal motion. In the case of polysulfone, the highly polar sulfone groups were integral to the main chain. Such polarity, active as a loss mechanism only in the glass transition region, resulted in a large dielectric relaxation. The low dielectric intensity of the β relaxation for polysulfone is consistent with the known ring flips and vibrations of the bis-phenol A moiety which is of lower polarity.

The variation of the dielectric constant and the dielectric loss of polysulfone with temperature is shown in Figure 8. The relative dielectric constant increased by only 0.2 in the β relaxation region, but it increased from 2.9 to 7.65 in the glass transition zone which was evidence for a strong dielectric relaxation. As discussed before, we can consider the inverse of the temperature axis as equivalent to a frequency axis so that the static and high frequency dielectric constants can be identified, as in Figure 8. The static (relaxed) dielectric constant, $\varepsilon_s$, was assigned as the maximum dielectric constant, 7.65 for polysulfone. The high frequency (unrelaxed) dielectric constant, $\varepsilon_\infty$, was assigned as the minimum dielectric constant, 2.7. The maximum value of the dielectric loss factor from Figure 8 and the loss tangent from Figure 7 at 100 kHz are 1.68 and 0.282, respectively.

*Nitrile Rubbers*

The α relaxations of nitrile rubber, with and without dicumyl peroxide, were obtained via DETA at 1, 10 and 100 kHz and are summarized in Table 4. Due to local motions, β relaxations were small and difficult to detect from the linear plot of tanδ versus temperature. Above the glass-transition temperature, ionic conductivity increased due to the increased mobility of the free charges. The maximum values of tanδ were almost the same regardless of the addition of 2% by weight of dicumyl peroxide. This was attributed to the fact that dicumyl peroxide is not a polar peroxide (11).

Crosslinking tends to lower energy absorption associated with thermal motion of polar -CN groups. Crosslinking of polymers results in decreased segmental mobility which increases the relaxation time of dipole-segmental loss, so that the dielectric loss

121

maximum temperature is shifted to a higher temperature. This can be clearly seen in Table 4 for the uncured and cured nitrile rubbers. The maximum loss tangent value of thermally-cured nitrile rubber was reduced to one third of that of uncured nitrile rubber. Nonetheless, even at a loss tangent value of 0.1, the cured nitrile rubber was receptive enough to show good heatability. The maximum value of $\tan\delta$ increased with increasing percentage of polar acrylonitrile. In addition, the corresponding transition temperature shifted to a higher temperature as also shown in Table 4.

The molecular relaxation process in polymers which gives rise to dielectric relaxation, in general, can also be seen in the mechanical spectroscopy analogue. Since $\tan\delta$ peaks in DMTA are biased by a fundamental weighting of different molecular motion processes to give approximately a decade mismatch, comparisons within this frequency region are developed by establishing correlations between loss peaks of loss moduli (G" or E") in DMTA and loss peaks of $\tan\delta$ in DETA. Temperatures for loss maxima obtained from DMTA experiments are given in Table 5. In the case of nitrile rubber with 2% added dicumyl peroxide without curing, it was seen that the $T_{max}$ from the DMTA spectra were shifted +9°C across two orders of frequency range. The DETA spectra revealed a $T_{max}$ value shift of +20°C across three orders of frequency. The width of the $\tan\delta$ peak tended to broaden with increasing frequency. This would indicate a broad distribution of relaxation times having slightly different activation energies. Overall, the base width in these dispersions is larger than 40°C. By increasing frequency from 0.33 Hz to 100 kHz, $T_{max}$ shifted 31°C with $T_{max}$ at 100 kHz at 7°C. On this basis, the tail of the dielectric loss spectra would extend to near room temperature (20°C) when the applied frequency approached the microwave region ($2.45 \times 10^9$ Hz).

*Other Polymers*

The glass transition temperatures for various polymers determined at 0.1, 1, 10 and 100 kHz via a DETA are summarized in Table 6. In the case of the methacrylates, the bold numbers indicate that $\alpha$ and $\beta$ relaxations have merged. The bold italic numbers indicate those transitions which were difficult to obtain for some polymers. For the semicrystalline polymers, the $T_g$'s for both the quenched and the slow-cooled materials were also determined.

The glass transition and melting temperatures and the apparent activation energies calculated from the frequency range of 0.1 kHz to 100 KHz are summarized in Table 7. As frequency increased, the $T_g$'s determined from the peaks of $\tan\delta$ were

122

shifted to higher temperatures. A plot of log(frequency) versus the reciprocal of absolute temperature maximum ($T_g$) for the $\alpha$ relaxation fell on a smooth curve, indicating a continuously changing activation energy with temperature. Placement of a straight line through the data over a narrow frequency range yielded a slope proportional to the activation energy, $\Delta E_a$. These calculated values are summarized in the 4th and 5th columns in Table 7. In general, the activation energies in the 4th column, calculated from the $T_g$'s at 1, 10 and 100 kHz, are smaller than those in the 5th column, calculated from the $T_g$'s at 0.1, 1, 10 and 100 kHz. Although four decades of frequency were not enough to yield a plot of the Williams-Landel-Ferry (WLF) relationship (8), these calculated activation energies fit this trend. These Arrhenius activation energies were useful in predicting the shift of the dielectric loss factor spectra into or out of the 2.45 GHz frequency region. Generally, the stiffer the polymer chain, the higher the $T_g$ and the larger the apparent activation energy. This would result in a slower shift of the dielectric loss spectra and a narrower span between $T_g$ and $T_c$, the critical temperature of dielectric loss.

Merging of $\alpha$ and $\beta$ relaxations has a large influence on the dielectric loss factor. The maximum in dielectric loss as well as the shape of the dielectric loss dispersion depends on the distribution of the relaxation times. The area below the dielectric loss factor curve changes as the relaxations merge; however, the value of ($\varepsilon_s$ - $\varepsilon_\infty$) remains unchanged in the transition region. The square of the dipole moment is closely related to ($\varepsilon_s$ - $\varepsilon_\infty$), as shown in Equation 8, rather than to the distribution of the dielectric loss peak. Evaluating the heatability of polymers using the difference of ($\varepsilon_s$ - $\varepsilon_\infty$) was found to be an easy task using the DETA method.

The dielectric properties of various polymers according to the polarity of their group moments is summarized in Table 8. The values of ($\varepsilon_s$ - $\varepsilon_\infty$) are given in the 2nd column. The peak values of $\varepsilon''$ and tan$\delta$ at the highest frequency, 100 kHz, obtained via DETA are listed in the 3rd and 4th columns and would be used to predict the heatability at 2.45 GHz. In general, the variation of tan$\delta$ is relatively small compared to the variations of ($\varepsilon_s$ - $\varepsilon_\infty$) or $\varepsilon''$. Highly polar polymers in the upper half of Table 8 had dielectric properties that were a stronger function of temperature than the lower polarity polymers. In the majority of the cases, the $\alpha$ peak dielectric loss was higher than the $\beta$ dielectric loss, although the reverse was true for poly(methyl methacrylate) and a few other examples. On this basis, the use of low frequency response of dielectric properties for prediction of behavior at microwave frequencies appears appropriate.

From Table 8, it is proposed that the value of $(\varepsilon_s - \varepsilon_\infty)$ for polymer depended on several factors that can be used for advanced processing methods. These are:

(A) <u>Group dipole moments</u>: Dielectric loss depends on the chemical constitution of polymers. It mimics the trend of polarity of small model molecules, but other factors matter.

(B) <u>Mole percentage of polar groups</u>: The dielectric properties of a copolymer chain composed of different randomly alternating monomeric units depended on the constitution of the monomeric units and on their ratio. The oscillator strength of the dielectric transition $(\varepsilon_s - \varepsilon_\infty)$ and $\varepsilon''$ were found to rise monotonically with increasing content of the polar component. Dilution of the polar components in a acrylonitrile-butadiene copolymer caused the maximum $\varepsilon''$ to decrease with increasing butadiene content as demonstrated in a comparison of dielectric spectra given in Figure 9. Additionally, the effect of mole percentage of polar groups were also observed as a functions of (a) % of -CONH (amide) group in different nylons; (b) % of -Cl (chloride) group in poly(vinyl chloride) and polychloroprene; (c) % of -COOR (ester) group in poly(methacrylates). On the cool side of the maximum dielectric constant, change with the effect of increasing temperature on the value of $(\varepsilon_s - \varepsilon_\infty)$ is less important. Beyond the transition region, $(\varepsilon_s - \varepsilon_\infty)$ decreased with increasing temperature. This phenomenon can be explained by referring to Equation 8 where the dielectric constant is seen to decrease with increasing temperature. The differences between the maximum and minimum dielectric constants, $(\varepsilon_s - \varepsilon_\infty)$ are listed in the 2nd column of Table 8. These DETA results will be used to correlate the heating behavior in the microwave field.

(C) <u>Hydrogen bonding</u>: In nylons, the dielectric properties are mainly determined by inter-molecular and intra-molecular hydrogen bonding. At the glass transition temperature, especially, hydrogen bonds must be broken to allow for large-scale motions of the chains. This results in larger values of $(\varepsilon_s - \varepsilon_\infty)$.

(D) <u>Chemical structure</u>: The nature of the dielectric properties is dependent to a great extent not only on the mole percentage of polar groups, but also on their position in the polymer chain. Polar groups in the main chain are far less mobile than those in side chains. In PVAc, the ester group is on the side chain, whereas in PET, the ester group is in the backbone polymer chain. Contributions to the loss by the effective dipole moment of the polar group is stronger comparatively in the first case than in the second. Additionally, polyvinyl esters, where the side group is linked to the main backbone chain by polar C-O bonds, has a dielectric glass transition more intense

124

than that observed for acrylates and methacrylates, where the linkage is an apolar C-C bond.

(E) Steric effects: Steric hindrance provided by the $\alpha$-methyl group was essential for the occurrence of the $\beta$ dielectric loss maximum in PMMA. The $\alpha$-methyl groups maintain the chain backbone as essentially rigid while the -COCH$_3$ group undergoes hindered rotation, so that the $\alpha$ and $\beta$ peaks were resolved for PMMA at frequencies below 1 kHz. Steric effects can also affect percentage crystallinity and chain mobility.

(F) Percentage of crystallinity: Increased crystallinity tends to decrease the magnitude of the dielectric loss as well as increase the temperature of maximum dielectric loss at a given frequency.

(G) Crosslinking density: Any crosslinking of polymers decreases segmental mobility and increases the relaxation times of the dipole-segmental loss. The temperature and magnitude dependence of the dielectric loss is determined by the density of the crosslinking.

(H) Physical state: The effect of physical state of polymers can be illustrated by the values of dielectric constant. For example, although the percentage of -Cl group in polyvinyl chloride is greater than that in polychloroprene, at room temperature the dielectric constant of polychloroprene is higher than that of PVC. A room temperature, polychloroprene is in its rubbery state; therefore the chain segments can move freely, so that the high value of $\varepsilon'$ is related to the dipole orientation polarization of the chain segments. PVC at room temperature is in the glassy state, its chain segment mobility is limited, and the dipole orientation polarization comes only from the movement of the polar group itself. At sufficiently high temperatures, PVC will transform to the rubbery state, and its dielectric constant will eventually be larger than that for polychloroprene.

Other factors such as stereochemical structure, branching, and orientation also influence the effective dipole moment.

MICROWAVE EXPERIMENTAL RESULTS

On the basis of the survey of dielectric properties of numerous polymeric materials, a limited set of materials was selected for examination of heating and curing behaviors with applied microwave radiation. These materials consisted of ethylene/vinyl acetate copolymers varying in percent vinyl acetate and nitrile rubbers varying in percent nitrile content. Through the addition of dicumyl peroxide, these nitrile rubbers were also examined for the influence of crosslinking upon microwave curing behavior. These materials were selected as they provided the appropriate

125

chemical and physical structures necessary to test the hypotheses presented in the above discussion.

Experiments were first conducted with ethylene/vinyl acetate copolymers. Due to the nonpolarity of PE, the cylindrical cavity applicator was used to process PE/PVAc copolymers of four different percentages of vinyl acetate (0, 18, 28 and 33%). In Figure 10, a typical time-temperature profile for the PE/PVAc copolymers, PE and the silicone flexible mold is displayed. The input power was fixed at 20 watts. In the first 1.5 min., the temperature rose at almost the same rate for all polymers. Beyond 1.5 min., the temperature increments became greater for the copolymers having a higher percentage of acetate. Thus, in the first 1.5 min., the temperature increment was due to the heating of the silicone mold. The heat flowed from silicone mold to the PE/PVAc copolymer specimen via thermal conduction at temperatures below 65°C, the critical temperature, $T_c$, of PVAc. Above the $T_c$ of PVAc, the PVAc absorbed microwave energy because the dielectric loss factor of PVAc was higher than that of the silicone mold. The temperature variation of PE in the silicone mold was almost the same as the empty silicone mold reflecting the low dielectric loss of PE. Thus, the final temperature obtained depended on the mole percentage of the polar PVAc.

A second series examined was the nitrile rubbers with different contents of acrylonitrile (19, 30 and 40%). Microwave curing reactions of nitrile rubbers with 2% dicumyl peroxide were carried out at an input power of 50 watts in the traveling wave applicator. Accurate input, reflected and transmitted powers were obtained by completely calibrating each set of attenuators and cables. In Figure 11, these three power readings are plotted versus time for the nitrile rubbers. The input powers, $P_i$, of 50 watts remained unchanged with time. The transmitted powers, $P_t$ were constant only until the sample began to heat rapidly where $P_t$ decreased and leveled off. The reflected powers, $P_r$, were also constant initially, but increased and then leveled off once the sample began heating rapidly. Increasing the acrylonitrile content from 19% to 40% resulted in the overall decrease in transmitted power and an increase in reflected power. This indicated that the energy absorbed by the nitrile rubber increased with the acrylonitrile content.

The microwave curing reactions of 30% acrylonitrile nitrile rubber with 2% dicumyl peroxide were also carried out at three different constant input power levels (40, 50 & 60 watts). The transmitted powers, $P_t$ were constant only until the sample began to heat rapidly then $P_t$ decreased and finally levelled off. The reflected powers, $P_r$, also were constant initially, but increased and then became constant once the sample began heating rapidly. At the same time, reflected powers, $P_r$, increased to

higher values. Temperature and heating rate versus time curves for these materials is presented in Figure 12. This plot reveals the differential absorption of the nitrile rubbers to the microwave radiation under constant input power. Here, the steeper the slope, the shorter the processing time. Similarly, the power absorption and the power absorption rate versus time is depicted in Figure 13. The plateau of temperature and power absorption, $P_a$, in Figures 12 or 13, increased when the acrylonitrile content was increased from 19% to 40%. The same trend was seen when the input power was increased from 40 to 60 watts *vide infra*. In addition, the maximum rate of power absorption, or rate of heating, was shifted to shorter times. The loss tangent value in cured rubber was found to be less than the loss tangent value of the uncured rubber. This can be explained by examining the loss tangent DETA spectra. Since heating rate is proportional to the magnitude of the dielectric loss, as shown in Equation 2, it was expected that the uncured nitrile rubber would heat faster. The effective dipole moment motion associated with energy loss caused by thermal motion of polar groups decreases with crosslinking. Since the polar -CN group was not involved in curing, the dipolar relaxation of the cured rubber did not disappear completely so that the sample could be heated and maintained at a high temperature by the appropriate input power. Indeed, the power absorption curve increased to a maximum and then decreased to a plateau. This suggested that the microwave energy absorbed by the sample was in equilibrium with the energy conducted away from the sample. Thus, the dielectric loss factor became fixed by thermal equilibrium processes.

The variation of power absorption and power absorption rate with temperature for the three different nitrile rubbers is displayed in Figure 14. Power absorption increased continuously with increasing temperature, but then decreased due to the chemical crosslinking which induced a strong viscosity effect which consequently hindered dipolar relaxation. These results were due to the polar acrylonitrile group absorbing energy by interacting with the microwave field which then heated up the whole of the mass to be crosslinked. As a result of the increasing temperature, the crosslinking peroxide decomposed thereby generating a network so that the heating rate decreased eventually due to restricted mobility.

The variations of temperature and heating rate with time for three input powers are given in Figure 15. This plot reveals the effect of increasing field strength at constant composition, i.e., greater field strengths, greater heating rates, shorter processing times. Here, an interesting phenomenon was revealed; all three maximum points of heating rate vs. time plots intersected at about 140°C on their respective temperature curves. The exothermic curing reaction of dicumyl peroxide might be

responsible for such behavior. However, the same phenomenon occurred when nitrile rubber (30% ACN) without dicumyl peroxide was examined, as shown in Figure 16. Another hypothesis for this behavior involves a transition temperature in the 2.45 GHz region. At the maximum value of $\varepsilon''$, the heating rate is at a maximum and subsequently decreases with the decreasing value of $\varepsilon''$.

The plot of heating rate vs. temperature for nitrile rubber containing 2% dicumyl peroxide is presented in Figure 17. As discussed previously, the heating rate was found to be proportional to the dielectric loss factor, as other factors remained constant (Equation 2). The plot of heating rate vs. temperature at 2.45 GHz looked remarkably similar to a typical DETA experiment. By drawing tangents to the "cool sides" of the heating rate vs. temperature curves, three intercept temperatures were obtained. The intercept temperature for any curve identified with the "critical temperature of dielectric loss". The critical temperatures for these three curves were determined to be between 40 and 45°C. The critical temperature gives a good indication of the point at which the dielectric loss factor, $\varepsilon''$, increases significantly on heating. In other words, the tailing of the dielectric relaxation spectra occurred near room temperature. In order to verify this resultt, various starting temperatures for the examination of 19% acrylonitrile nitrile rubber were induced by externally heating on the waveguide via a strip heater, as shown in Figure 5. The sample temperature vs. time for three different starting temperatures, 26°C, 42°C and 51°C, are displayed in Figure 18. The input power was fixed at 20.5 watts. The heating rate and the final plateau temperatures increased significantly at the higher starting temperatures. This indicated that the dielectric loss dipole dispersion had increased with increasing temperature into the dielectric loss region between room temperature and 51°C.

## CONCLUSIONS

The area beneath the dielectric loss factor-frequency plot was proprtional to ($\varepsilon_s$ - $\varepsilon_\infty$) as shown by Equation 9, and remained unchanged during the merging of the a and b relaxations. The use of DETA provided an easy evaluation of heatibility through the assessing the magnitude of ($\varepsilon_s$ - $\varepsilon_\infty$). The value of ($\varepsilon_s$ - $\varepsilon_\infty$) should be used together with the distribution of relaxation times and activation energies to predict the heatability for microwave power processing. In order to relate the structure-property relationships to the values of ($\varepsilon_s$ - $\varepsilon_\infty$) and chemical and morphological structures, it was useful to examine the relationship between the dielectric constants of polymers and the effective dipole moments. In considering effective dipole moments, it was

appropriate to use group moments instead of bond moments. The polarity follows the sequence of group dipole moment as:

$$SO_2 > CONH > CN > C=O > Cl > CO_2R > O > CO_3 > C-C.$$
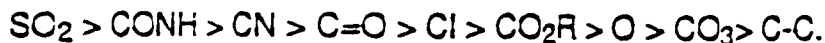
The highly polar -CN group in nitrile rubbers induced a large dipolar relaxation of main chain motions at the glass transition region. From the value of glass transition temperature obtained by DMTA, DETA, and microwave calorimetry, the 'cool side' tail of the dielectric loss spectra was found to extend into the room temperature regime at 2.45 GHz. Nitrile rubbers can be easily heated starting at room temperature. After an initial absorption of microwave energy, the temperature rise caused the dielectric loss factor to increase which, in turn, resulted in a further temperature increase, and so on. The heating rate was found to depend on several factors: (1) the glass transition temperature of nitrile rubber, (2) the percentage of acrylonitrile and (3) the extent of curing. The higher the content of acrylonitrile, the better will be the heatability of the nitrile rubber. However, the glass transition of the nitrile rubber would be higher, too. These two effects therefore lead to the heating rate being essentially independent of the acrylonitrile content which is between 19% to 40%.

In order to avoid trial-and-error experiments in microwave processing, it is necessary to obtain direct and meaningful information about dielectric constant, dielectric loss factor and/or loss tangent as a function of temperature and the degree of curing for crosslinking systems at 2.45 GHz. Interpretation of these dielectric properties usually requires information from a wide frequency and/or temperature range. Therefore, in these experiments where a sufficient range of frequencies was examined, a WLF plot was used to predict the shift of dielectric loss factor into or out of th emicrowave frequency range.

The temperature dependence of loss peaks, in general, follows the well known WLF equation for viscosity and viscoelasticity in polymeric and some nonpolymeric liquids. The applicability of this viscoelastic function to dielectric relaxation data suggests that the temperature dependence of the molecular friction coefficient is common to mechanical and dielectric-relaxation processes. The glass transition temperatures at lower frequencies were obtained from DMTA and DETA spectra and are summarized in Tables 4 and 5. The glass transition temperature at 2.45 GHz was obtained from the temperature at the maximum heating rate. In a typical WLF treatment, Figure 19 shows the plot of the logarithm of the frequency versus the reciprocal of absolute temperature. All a transitions fell on the curve, indicating a

continuously changing activation energy with temperature, as is expected for polymeric materials. A unique characteristic of microwave curing that was taken advantage of in this research was that microwaves penetrate the whole mass instantaneously so that thermal peroxide decomposition starts in every point of the polymer simultaneously, avoiding thermal gradients from conduction. The heating process can be turned on or off instantaneously and therefore curing was controlled more accurately than in conventional thermal methods. Tremendous energy savings can be realized by heating only selected regions of the material with microwave radiation.

## ACKNOWLEDGEMENTS

# REFERENCES

1. B. Silinski, C. Kuzmycz and A. Gourdenne, *Eur. Polym. J.*, 23, 273 (1987)
2. L. Onsager, *J. Am. Chem. Soc.*, 58, 1486 (1936).
3. J. G. Kirkwood, *J. Chem. Phys.*, 7, 911 (1939).
4. H. Fröhlich, "Theory of Dielectrics," Oxford University Press, Oxford (1949).
5. K. Deutsch, E. A. W. Hoff and W. Reddish, *J. Polym. Sci.*, 13, 565 (1954).
6. F. Bueche, *J. Chem. Phys.*, 22, 603 (1954).
7. J. D. Ferry and E. R. Fitzgerald, *J. Colloid Sci.*, 8, 224 (1953).
8. J. D. Ferry and S. Strella, *J. Colloid Sci.*, 13, 459 (1958).
9. J. D. Ferry, "Viscoelastic Properties of Polymers," 3rd Ed., J. Wiley and Sons, New York (1980).
10. D. K. Cheng, "Field and Wave Electromagnetics," Addison-Wesley Publishing Co., Pennsylvania (1983).
11. K. Beiss and G. Menges, "Proc. - Eur. Reg. Tech. Conf.: Plast. Process.", 2nd, 19-1-19-9. Edited by: C. Klason and H. R. Skov, Soc. Plast. Eng. Scand. Sect.: Copenhagen, Den. (1980).

## Table 1
### Dipole moments of small model molecules (9)

| Formula | Compound Name | $\mu$, D | State | $\mu$, D | S |
|---------|---------------|---------|-------|---------|---|
| $CH_4N_2O$ | Urea | | | 4.56 | D |
| $C_2H_6O_2S$ | Dimethyl sulfone | 4.47 | gas | 4.25 | B |
| $C_3H_4O_2$ | ß-Propiolactone | 4.18 | gas | 3.85 | B |
| $C_2H_5NO$ | Acetamide | | | 3.44~3.90 | B |
| | | | | 3.60~3.92 | D |
| $C_2H_3N$ | Acetonitrile | 3.92~4.01 | gas | 3.14~3.54 | B |
| $C_3H_3N$ | Acrylonitrile | 3.89~3.91 | gas | 3.54 | B |
| $C_3H_5NO$ | Ethyl isocyanate | | | 2.84 | B |
| $C_3H_6O$ | Acetone | 2.80~2.97 | gas | 2.40~2.83 | B |
| $C_4H_6O$ | Cyclobutanone | | | 2.76 | B |
| $C_3H_8O_3$ | Glycerol | | | 2.56,2.68 | D |
| $C_2H_6O_2$ | Ethylene glycol | 2.27 | gas | 1.5~2.30 | B |
| | | | | 2.28~2.40 | D |
| $C_3H_{10}N_2$ | 1,3-Diaminopropane | | | 1.96 | B |
| $C_2H_4Cl_2$ | 1,1-Dichloroethane | 2.07~2.63 | gas | 1.8~2.0 | B |
| $CH_3Cl$ | Chloromethane | 1.66~2.02 | gas | 1.69,1.88 | B |
| $CH_4O$ | Methanol | 1.61~1.71 | gas | 1.60~1.78 | B |
| | | | | 1.86~1.93 | D |
| $C_3H_6O_2$ | Methyl acetate | 1.68~1.71 | gas | 1.45~1.75 | B |
| $C_2H_4O_2$ | Acetic acid | 1.4~1.75 | gas | 0.74~1.64 | B |
| | | | | 1.76 | D |
| $CH_5N$ | Methyl amine | 1.00~1.34 | gas | 1.47 | B |
| $C_2H_6O$ | Methyl ether | 1.29~1.33 | gas | 1.25 | B |
| $C_3H_6O_3$ | Dimethyl carbonate | 0.87~1.01 | gas | 0.82~1.07 | B |

S: Solvent, B: Benzene, D: Dioxane

Table 2

Dipole moments of small model molecules (9)

| Formula | Compound Name | μ, D | State | μ, D | S |
|---|---|---|---|---|---|
| $C_3H_8N_2O$ | 1,3-Dimethyl urea | | | 5.1 | B |
| $C_4H_{10}O_2S$ | Diethyl sulfone | | | 4.6,4.8 | D |
| | | | | 4.44,4.50 | B |
| $C_4H_6O_2$ | g-Butyrolactone | | | 3.82~4.15 | B |
| $C_3H_7NO$ | Propionamide | | | 3.30,3.47 | B |
| $C_3H_5N$ | Propionitrile | 4.02~4.06 | gas | 3.85 | D |
| | | | | 3.37~3.69 | B |
| $C_4H_8O$ | 2-Butanone | | | 2.5~2.82 | B |
| $C_5H_8O$ | Cyclopentanone | 3.30 | gas | 2.86~3.03 | B |
| $C_4H_{10}O_3$ | Diethylene glycol | | | 2.69 | D |
| $C_3H_8O_2$ | 1,3-Propanediol | | | 2.37~2.52 | D |
| $C_4H_{12}N_2$ | 1,4-Butanediamine | | | 1.95,2.35 | B |
| $C_3H_6Cl_2$ | 1,2-Dichloropropane | 1.46~1.68 | gas | 1.87 | B |
| | 1,3-Dichloropropane | 2.09 | gas | 2.09,2.10 | B |
| $C_2H_5Cl$ | Chloroethane | 1.76~2.09 | gas | 2.0 | B |
| $C_2H_6O$ | Ethanol | 1.1~1.7 | gas | 1.67~1.80 | B |
| $C_4H_8O_2$ | Ethyl acetate | 1.78 | gas | 1.50~1.88 | B |
| | Methyl propionate | | | 1.70 | B |
| $C_3H_6O_2$ | Propionic acid | 1.76 | gas | 0.63~1.69 | B |
| | | | | 1.51~1.77 | D |
| $C_2H_7N$ | Ethyl amine | 1.00~1.22 | gas | 1.28~1.40 | B |
| $C_3H_8O$ | Methyl ethyl ether | 1.22 | gas | | |
| $C_4H_{10}O$ | Ethyl ether | 1.0~1.19 | gas | 0.74~1.53 | B |
| $C_5H_{10}O_3$ | Diethyl carbonate | 1.07 | gas | 0.91~1.05 | B |

S: Solvent, B: Benzene, D: Dioxane

133

## Table 3

### Thermal properties, sources, and sample preparation in a platten press[a]

| Polymer | $T_g$ °C | $T_m$ °C | Press Temp. °C | Pressure x $10^{-3}$ lb | Source | Thick[b] mm |
|---|---|---|---|---|---|---|
| Polysulfone | 190 | | 245 | 10 | SP2 | 0.36 |
| Nylon6 | 63 | 229 | 230 | 3 | Polysciences | 0.30 |
| Nylon612 | 46 | | 210 | 3 | SP2 | 0.30 |
| Nylon12 | 37 | 178 | 185 | 3 | SP2 | 0.30 |
| Nylon66 | 45 | 254 | | | SP2 | |
| NBR455(40%ACN) | -19 | | | | BF Goodrich | |
| NBR355(30%ACN) | -31 | | | | BF Goodrich | |
| NBR210(19%ACN) | -50 | | | | BF Goodrich | |
| SAN | 101 | | 155 | 10 | Union Carbide | 0.28 |
| PVC | 85 | | 145 | 12 | Polysciences | 0.83 |
| Polychloroprene | -48 | 115 | 115 | 4 | SP2 | 0.46 |
| PVAc | 30 | | 71 | 10 | Aldrich | 0.40 |
| PMMA | 105 | | 180 | 8 | Inland Leidy | 0.46 |
| PEMA | 66 | | 115 | 10 | Inland Leidy | 0.46 |
| PBMA | 20 | | 85 | 10 | Aldrich | 0.46 |
| Polycaprolactone | -60 | 60 | | | Polysciences | |
| PET | 81 | 260 | 265 | 3 | SP2 | 0.27 |
| PEEK | 150 | 334 | 340 | 10 | ICI | 0.32 |
| Polyacetal | -30 | 180 | 180 | 3 | Aldrich | 0.29 |
| PPO | 210 | 268 | 275 | 4 | SP2 | 0.42 |
| PC | 150 | 267 | 270 | 3 | SP2 | 0.23 |
| SBR | | | 110 | 10 | Polysciences | 0.45 |

*SP2: Scientific Polymer Products
a) Pasadena Hydraulics, Inc. model number P210C
b) Sample thickness

134

## Table 4
### Temperatures at the maximum peaks of the loss tangent
### of nitrile rubber at various frequencies from DETA spectra

|  | 0.1kHz | 1kHz | 10kHz | 100kHz |
|---|---|---|---|---|
| Purified nitrile rubber (40% acrylonitrile) | | | | |
| Without curing | -9 | -2 | 5 | 14 |
| Purified nitrile rubber (30% acrylonitrile) | | | | |
| Without curing | -14 | -10 | -4 | 6 |
| w/2% DICUP w/o curing | -13 | -9 | -2 | 7 |
| w/2% DICUP* | -1 | 3 | 10 | 18 |
| Purified nitrile rubber (19% acrylonitrile) | | | | |
| Without curing | -26 | -22 | -15 | -5 |
| w/2% DICUP w/o curing | -26 | -21 | -14 | -4 |
| w/2% DICUP* | -7 | -4 | 2 | 10 |

* Thermally cured at 150°C for 2.5hr

135

## Table 5

### Temperatures at the maximum peaks of the loss moduli of 30% acrylonitrile nitrile rubber* at various frequencies from DMTA spectra

|  | 0.33Hz | 1Hz | 3Hz | 10Hz | 30Hz |
|---|---|---|---|---|---|
| Without curing (G") (Shear) | -24 | -22 | -20 | -17 | -15 |
| Microwave cured at 38 watts for 30min (tanδ) (bending) | -21 | -19 | -17 | -15 | -12 |

* Purified nitrile rubber (30% acrylonitrile) with 2% dicumyl peroxide

Table 6

$T_g$'s from 0.1 kHz to 100 KHz for several polymers

| Polymer | $10^2$Hz | $10^3$Hz | $10^4$Hz | $10^5$Hz | Remark |
|---|---|---|---|---|---|
| Polysulfone | 203 | 208 | 215 | 224 | |
| Nylon6 | 75 | 80 | 85 | 93 | Q in ice water |
| | 72 | 77 | 83 | 91 | Q in press |
| Nylon612 | 66 | 70 | 76 | 87 | Q in ice water |
| Nylon12 | 58 | 62 | 70 | 82 | Q in ice water |
| Nylon66 | 79 | 84 | 87 | 96 | Q in ice water |
| NBR455(40%ACN) | -9 | -2 | 5 | 14 | |
| NBR355(30%ACN) | -14 | -10 | -4 | 6 | |
| NBR210(19%ACN) | -26 | -22 | -15 | -5 | |
| SAN | 123 | 131 | 141 | 153 | |
| PVC | 100 | 105 | 111 | 120 | |
| Polychloroprene | -18 | -14 | -7 | 0 | |
| PVAc | 59 | 67 | 77 | 90 | |
| PMMA | | 90 | 129 | 145 | Partially merge |
| PEMA | 88 | 95 | 110 | 129 | a & b merge |
| PBMA | 52 | 66 | 81 | 102 | a & b merge |
| PET | 92 | 98 | 105 | 111 | Q in ice water |
| | 96 | 105 | 112 | 121 | Q in press |
| PEEK | 152 | 156 | 161 | 165 | Q in ice water |
| | 166 | 168 | 174 | 182 | Cooled in DETA |
| BTDA/APB | | 225 | 235 | 246 | Nondoped imide |
| | | 219 | 229 | 241 | Doped Polyimide |
| Polyacetal | -55 | -44 | -35 | -27 | Q in press |
| PPO | 219 | 228 | 238 | 251 | Q in ice water |
| | 220 | 232 | 239 | 251 | Q in press |
| PC | 163 | 168 | 174 | 182 | Q in ice water |
| | 163 | 168 | 174 | 182 | Q in press |
| SBR | | 78 | 88 | 99 | |

## Table 7

Thermal properties and the apparent activation energies for several polymers

| Polymer | $T_g$,°C | $T_m$,°C | $E_a^*$ | $E_a$# | Remark |
|---|---|---|---|---|---|
| Polysulfone | 190 | | 570 | 640 | |
| Nylon6 | 63 | 229 | 370 | 410 | Q in ice water |
| | | | 350 | 380 | Q in press |
| Nylon612 | 46 | | 270 | 320 | Q in ice water |
| Nylon12 | 37 | 178 | 230 | 270 | Q in ice water |
| Nylon66 | 45 | 254 | 390 | 440 | Q in ice water |
| NBR455(40%ACN) | -19 | | 185 | 190 | |
| NBR355(30%ACN) | -31 | | 170 | 200 | |
| NBR210(19%ACN) | -50 | | 150 | 175 | |
| SAN | 101 | | 300 | 320 | |
| PVC | 85 | | 380 | 420 | |
| Polychloroprene | -48 | | 190 | 220 | |
| PVAc | 30 | | 210 | 220 | |
| PMMA | 105 | | 100 | | Partially merge |
| PEMA | 66 | | 170 | 200 | a & b merge |
| PBMA | 20 | | 130 | 140 | a & b merge |
| PET | 81 | 260 | 420 | 420 | Q in ice water |
| | | | 350 | 340 | Q in press |
| PEEK | 150 | 334 | 790 | 810 | Q in ice water |
| | | | 550 | | Cooled in DETA |
| BTDA/APB | | | 470 | | Nondoped imide |
| | | | 440 | | Doped Polyimide |
| Polyacetal | -30 | 180 | 130 | 110 | Q in press |
| PPO | 210 | 268 | 430 | 460 | Q in ice water |
| | | | 520 | 490 | Q in press |
| PC | 150 | 267 | 550 | 600 | Q in ice water |
| | | | 550 | 600 | Q in press |
| SBR | | | 240 | | |

$E_a$ (kJ/mole) calculated from a) *1, 10 & 100 kHz or b)# 0.1, 1, 10 & 100 kHz

## Table 8
### Dielectric properties at 100 kHz for several polymers

| Polymer | $(\varepsilon_S - \varepsilon_\infty)$ | $\varepsilon''_{max}$ | $\tan\delta_{max}$ | Remark |
|---|---|---|---|---|
| Polysulfone | 4.80 | 1.69 | 0.282 | |
| Nylon6 | 9.60 | 1.41 | 0.184 | Q in ice water |
| | 7.38 | 1.31 | 0.198 | Q in press |
| Nylon612 | 6.72 | 0.75 | 0.147 | Q in ice water |
| Nylon12 | 6.72 | 0.86 | 0.177 | Q in ice water |
| Nylon66 | 4.80 | 0.60 | 0.120 | Q in ice water |
| NBR455(40%ACN) | 14.60 | 5.56 | 0.425 | |
| NBR355(30%ACN) | 10.40 | 3.52 | 0.346 | |
| NBR210(19%ACN) | 5.60 | 1.68 | 0.269 | |
| SAN | 5.25 | 1.59 | 0.269 | |
| PVC | 5.60 | 1.20 | 0.186 | |
| Polychloroprene | 3.45 | 0.99 | 0.185 | |
| PVAc | 5.00 | 1.60 | 0.261 | |
| PMMA | 2.25 | 0.52 | 0.128 | a & b merge |
| PEMA | 1.60 | 0.51 | 0.137 | a & b merge |
| PBMA | 1.50 | 0.49 | 0.127 | a & b merge |
| PET | 2.60 | 0.27 | 0.066 | Q in ice water |
| | 1.40 | 0.08 | 0.024 | Q in press |
| PEEK | 0.85 | 0.22 | 0.064 | Q in ice water |
| | 0.85 | 0.06 | 0.022 | Cooled in DETA |
| BTDA/APB | 1.55 | 0.17 | 0.058 | Nondoped imide |
| | 0.75 | 0.10 | 0.034 | Doped Polyimide |
| Polyacetal | 0.65 | 0.07 | 0.029 | Q in press |
| PPO | 0.50 | 0.01 | 0.005 | Q in ice water |
| | 0.20 | 0.01 | 0.004 | Q in press |
| PC | 1.15 | 0.08 | 0.027 | Q in ice water |
| | 1.10 | 0.07 | 0.027 | Q in press |
| SBR | 0.20 | 0.01 | 0.005 | |
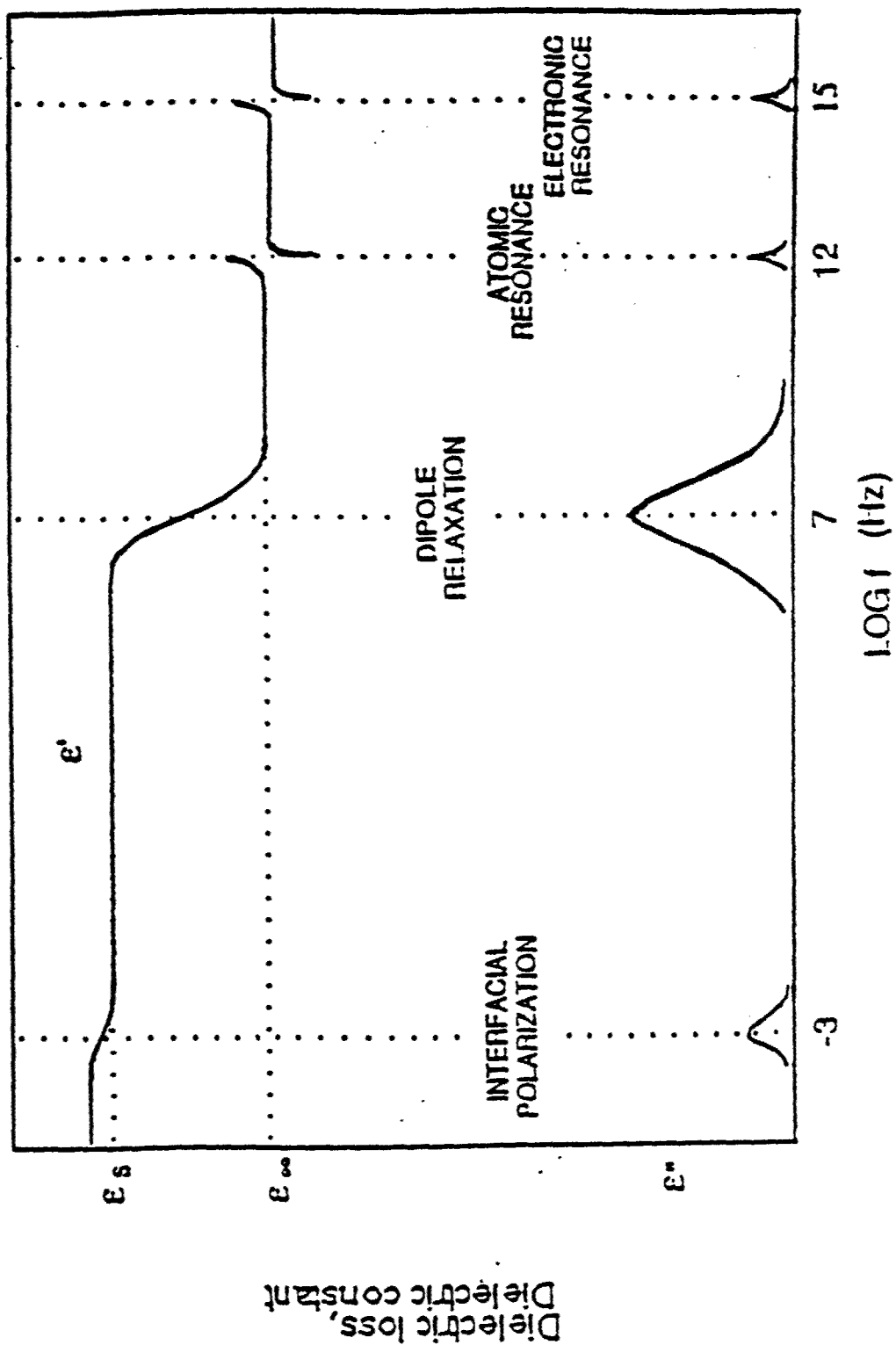
Figure 1.
Schematic diagram of the dielectric spectrum for a polar molecule
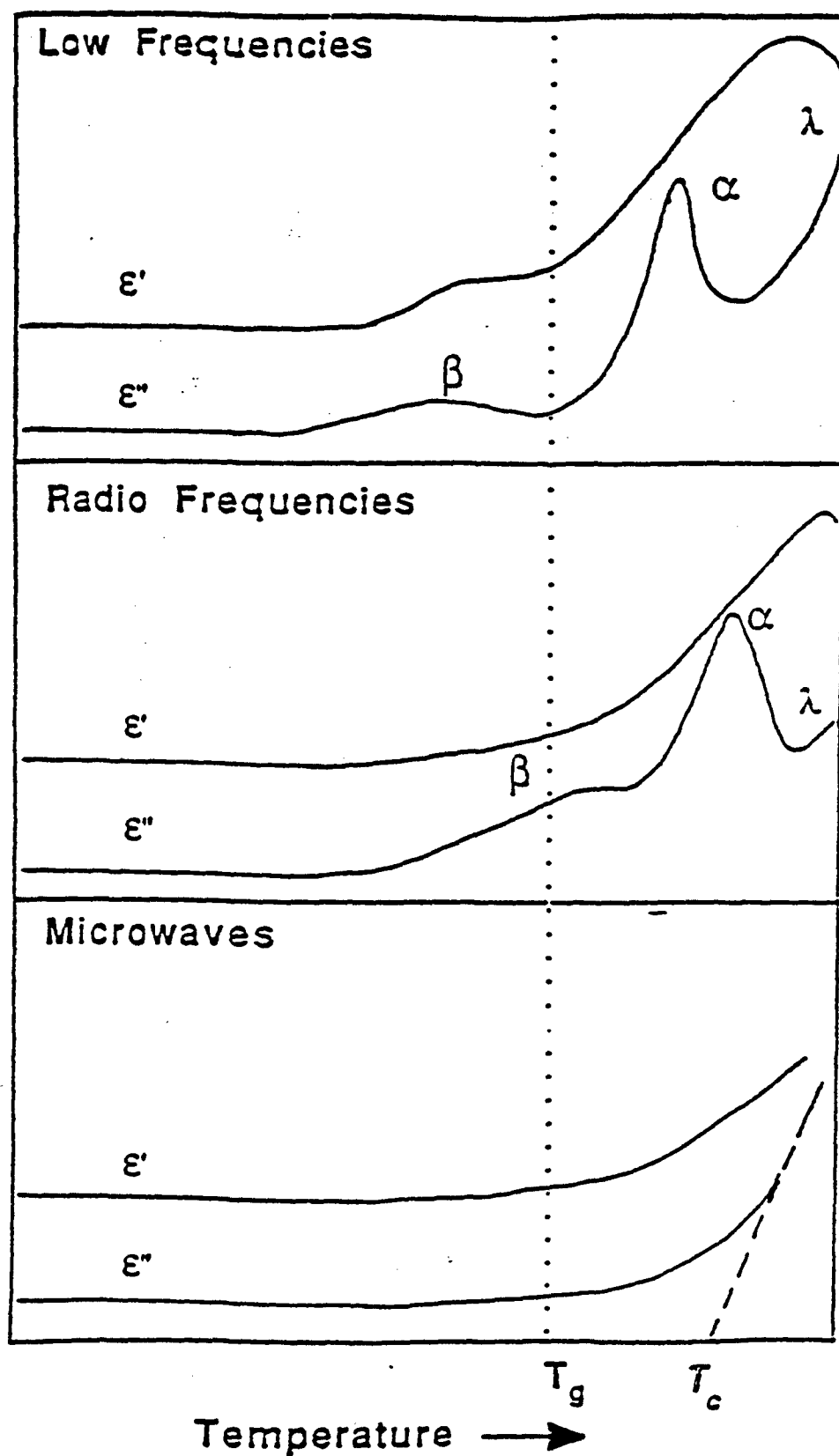
Figure 2.
Schematic representation of the dielectric behavior of
polar polymers at various frequencies

141
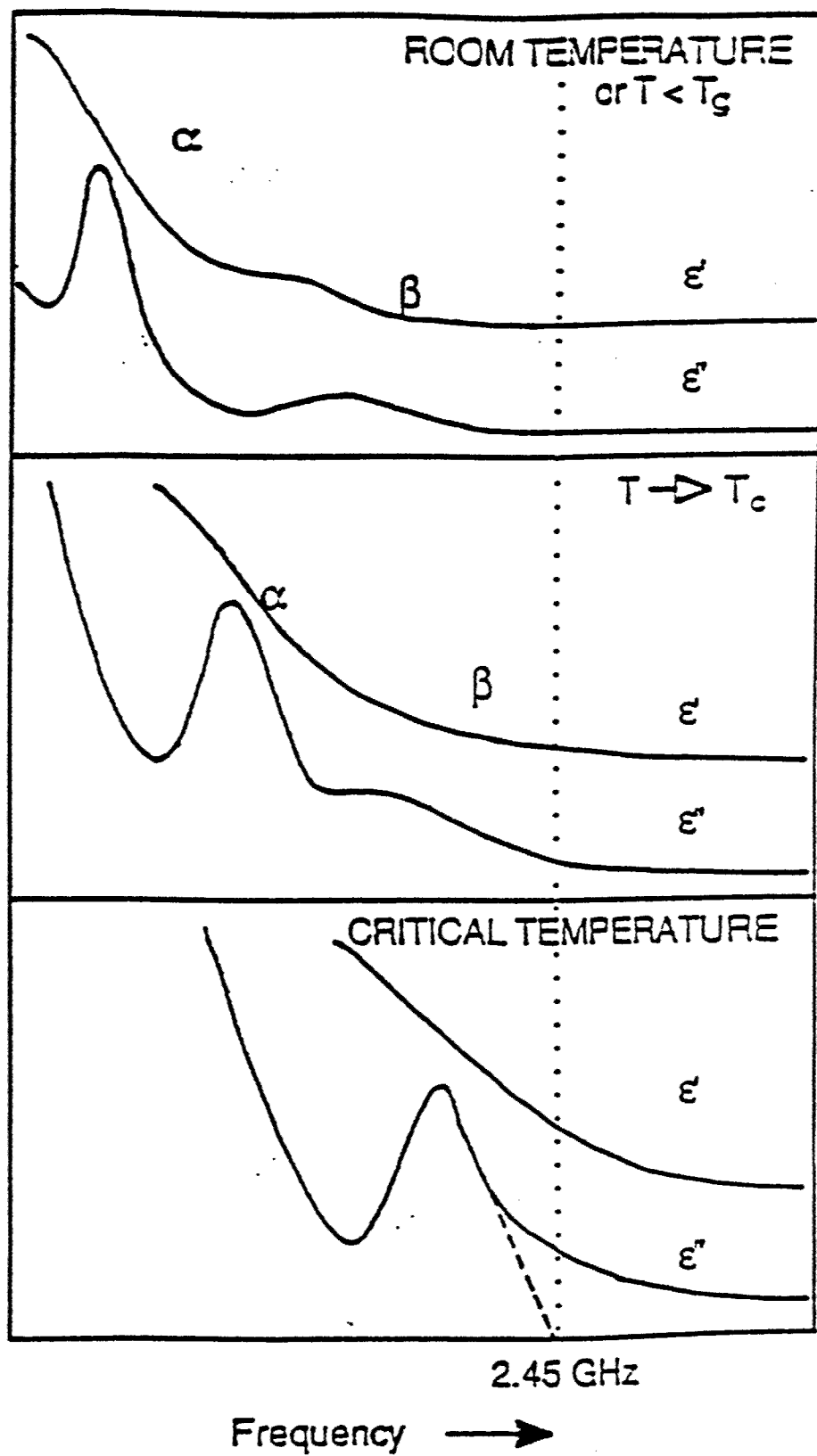
Figure 3.
Schematic representation of the dielectric behavior of polar polymers at various temperatures

142

| Functional Group | | Dipole Moment (Debye) |
|---|---|---|
| O⃦, —NH—C—NH— | Urea | > 4 |
| O⃦, —S—, O⃦ | Sulfone | > 4 |
| O⃦, —C—NH— | Amide | 3-4 |
| —C≡N | Nitrile | 3-4 |
| —N=C=O | Isocyanate | 2-3 |
| O⃦, —C— | Ketone | 2-3 |
| —Cl | Chloride | 1-2 |
| —OH | Hydroxy | 1-2 |
| O⃦, —C—O—R | Ester | 1-2 |
| O⃦, —C—O—H | Acid | 1-2 |
| —NH₂ | Amine | 1-2 |
| —O— | Ether | ~ 1 |
| O⃦, —O—C—O— | Carbonate | ~ 1 |

Figure 4.
The polarity of group dipole moments

143
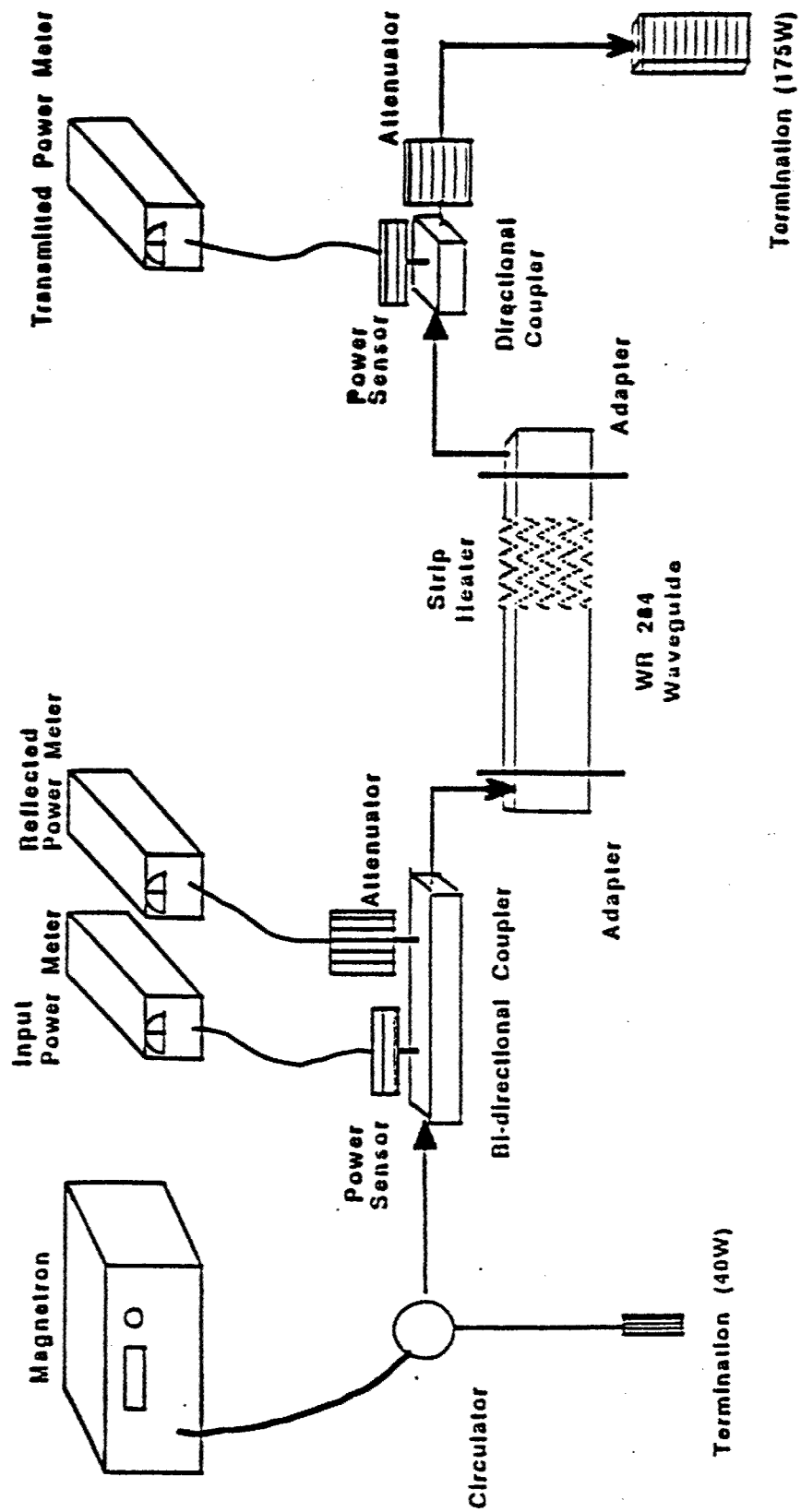
Figure 5.

Schematic of the experimental set-up for the traveling wave applicator with stub tuner

144
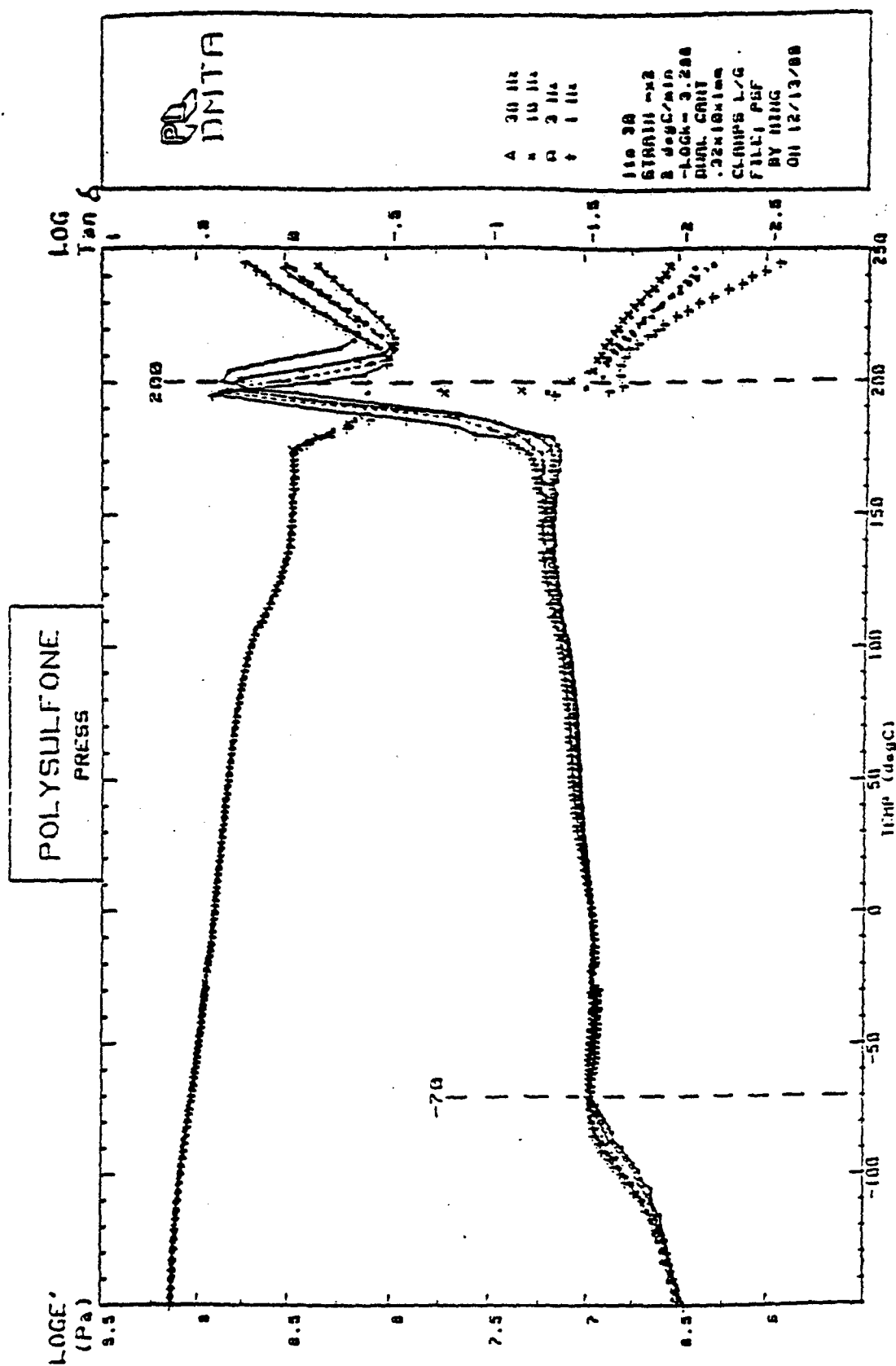
Figure 6.
Temperature dependence of the storage modulus and loss tangent of polysulfone at various frequencies
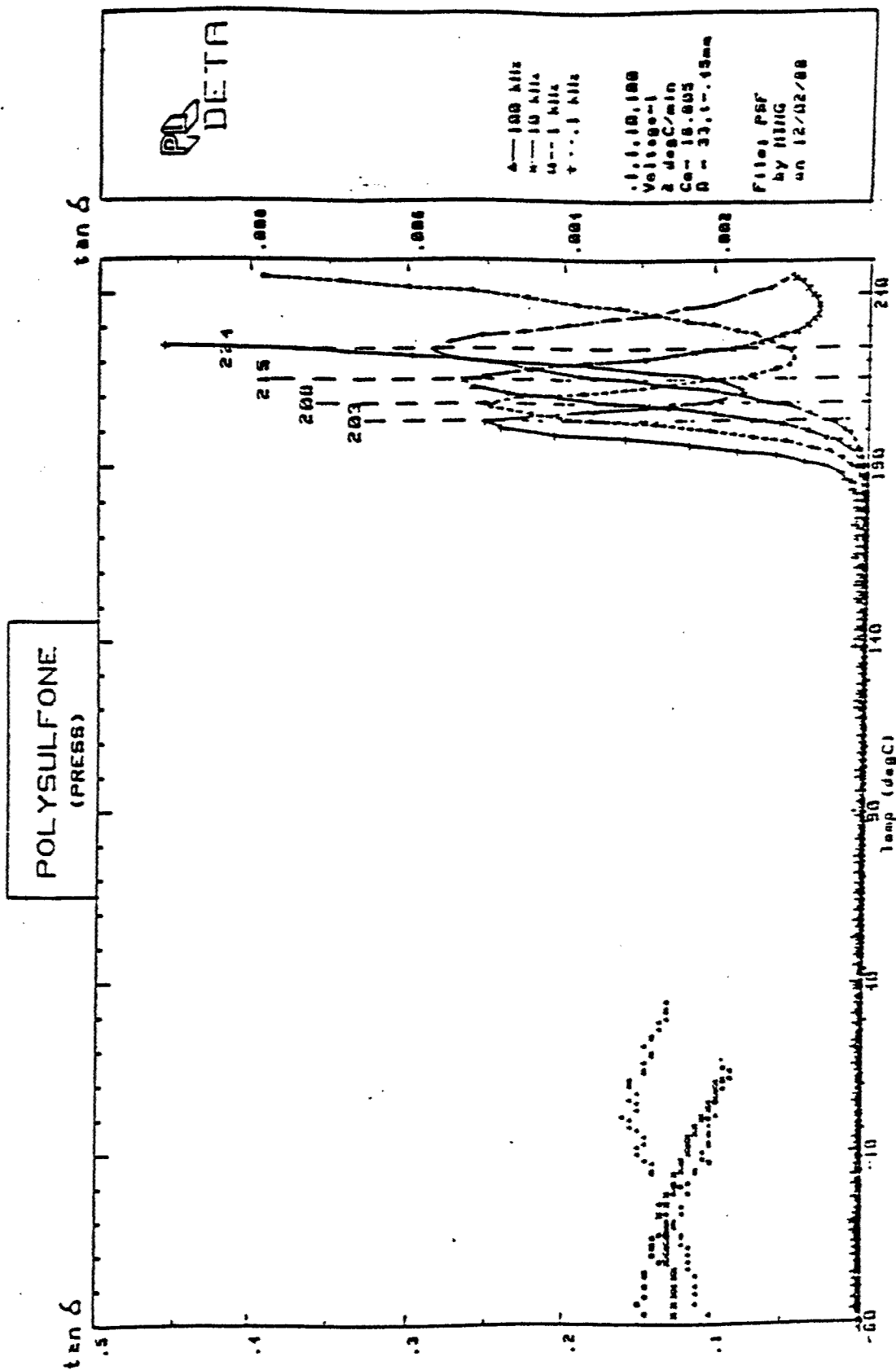
Figure 7.

Temperature dependence of the dielectric loss tangent of polysulfone at various frequencies
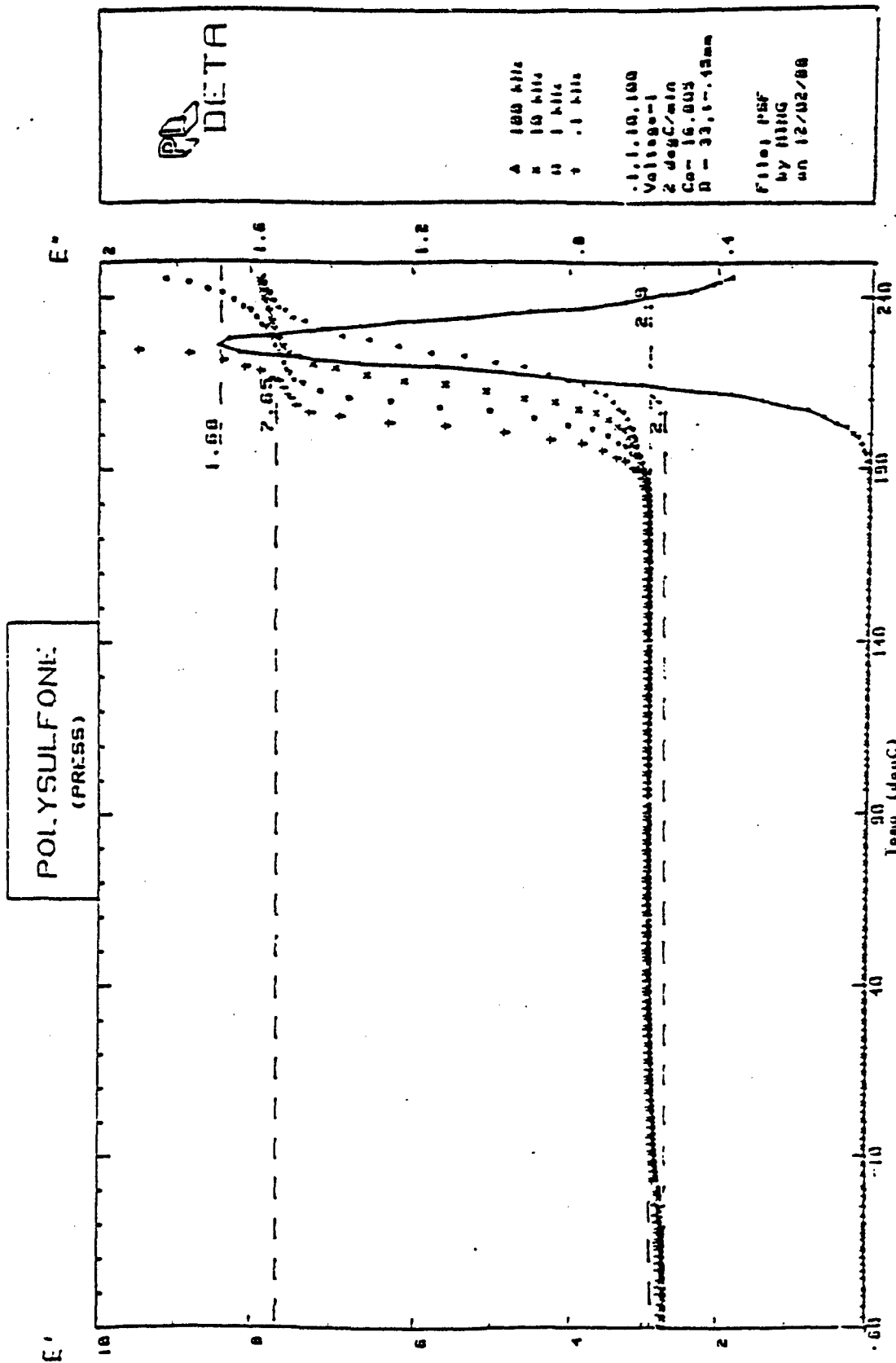
Figure 8.
Temperature dependence of the dielectric constant and the dielectric loss factor of polysulfone at various frequencies

Figure 9.
Comparison of temperature dependences of the dielectric loss factors for nitrile rubbers (40, 30 & 19% acrylonitrile content; top, middle & bottom, respectively) at various frequencies
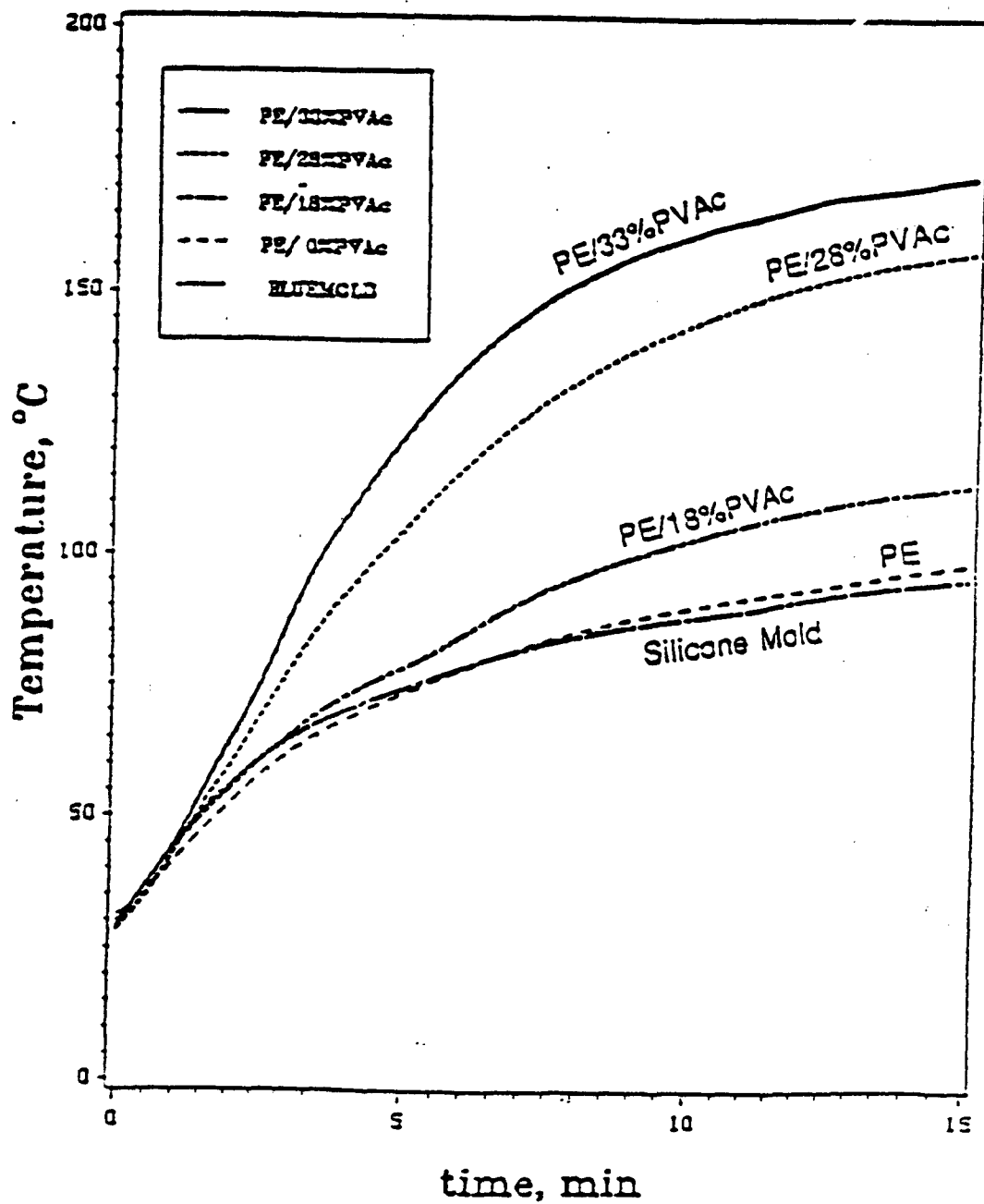
Figure 10.
Variation of the temperature of ethylene/vinyl acetate copolymers and silicone mold
with time in the center of $TE_{111}$ mode of a cylinderical
cavity applicator; input power was 20 W
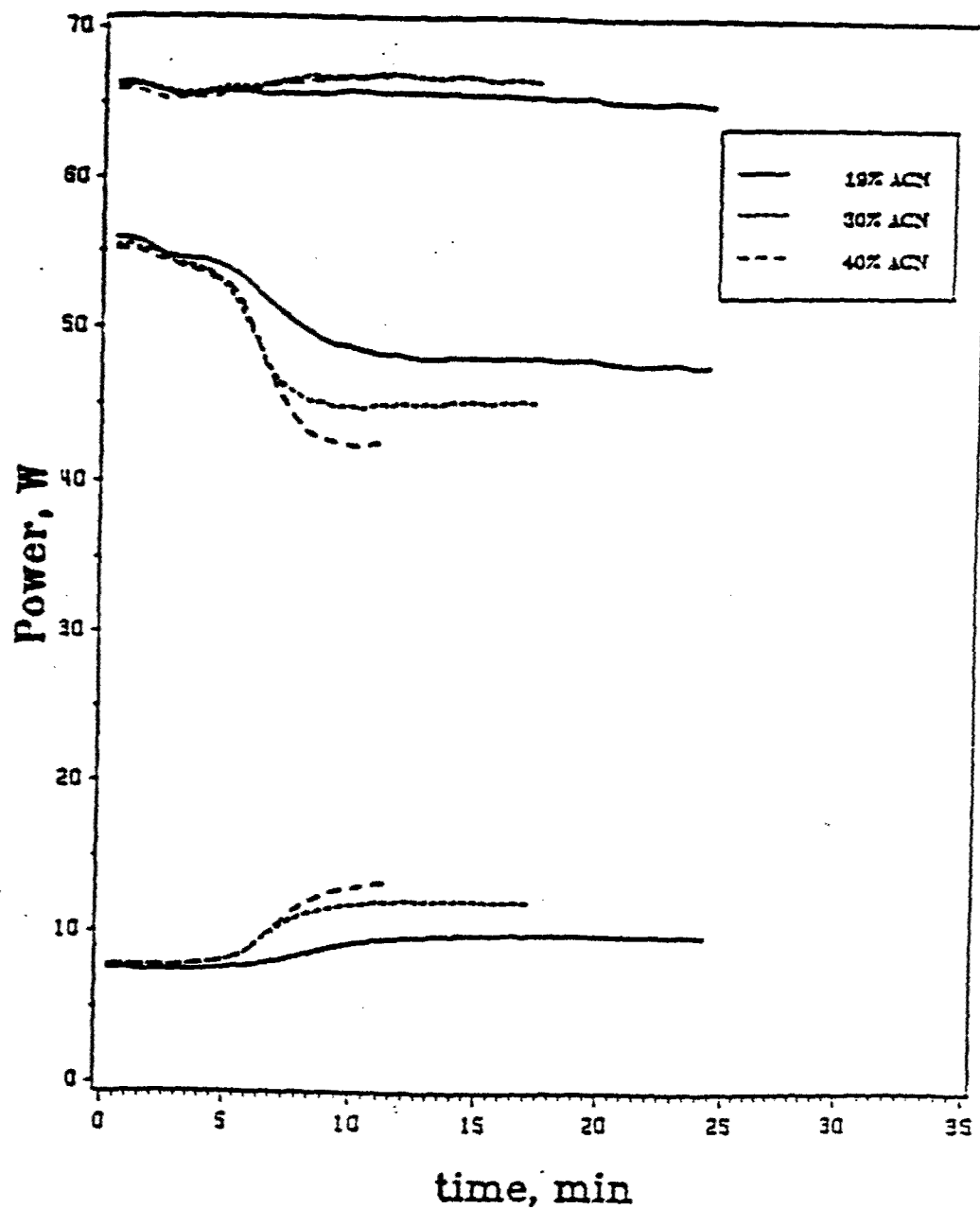
Figure 11.
Variation of the input, transmitted and reflected powers with time for nitrile rubbers (40, 30 & 19% acrylonitrile content) with 2% w/w dicumyl peroxide in a travelling wave applicator
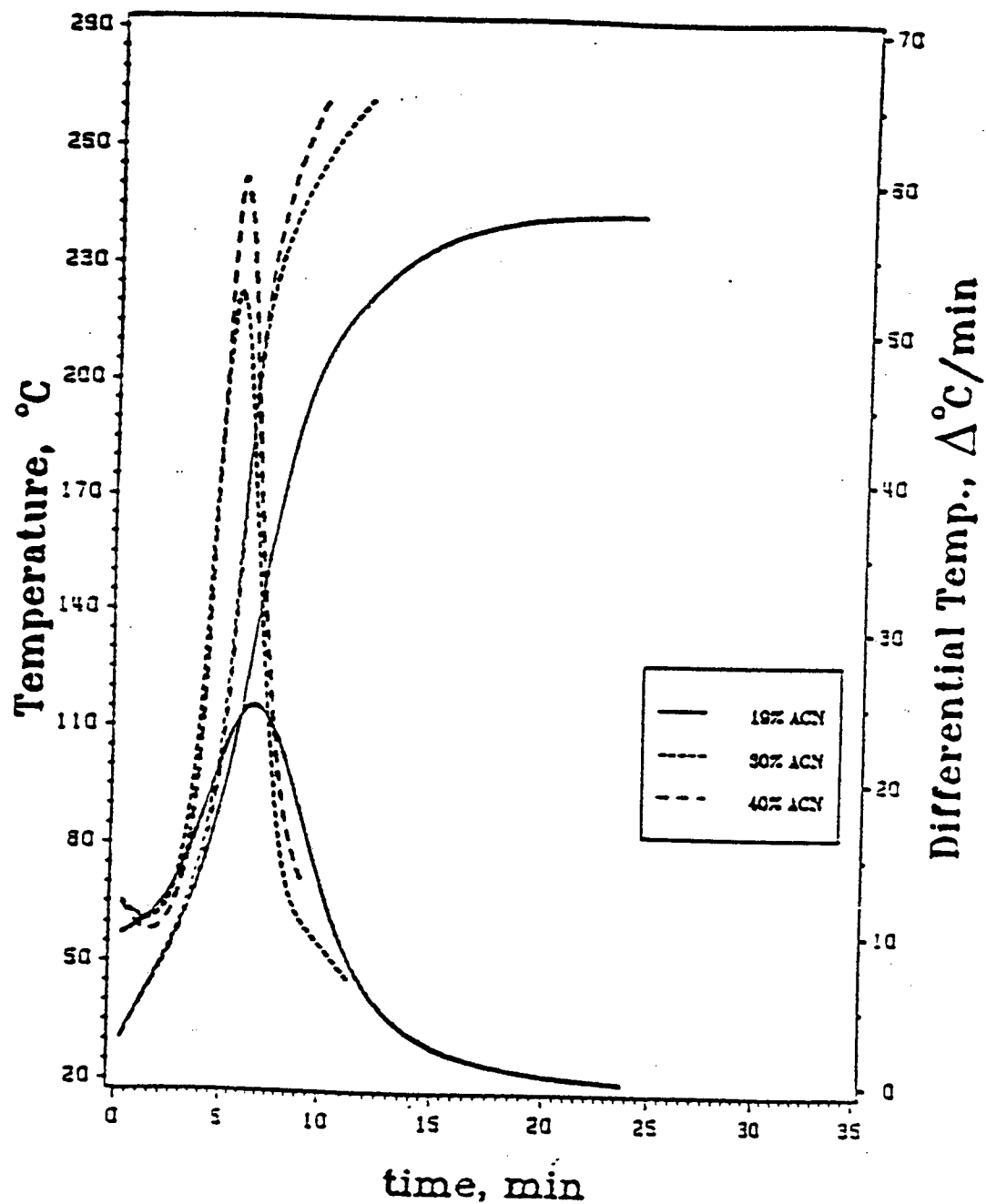
Figure 12.
Variation of the temperatures and heating rates with time for nitrile rubbers (40, 30 &
19% acrylonitrile content) with 2% w/w dicumyl
peroxide in a travelling wave applicator

151
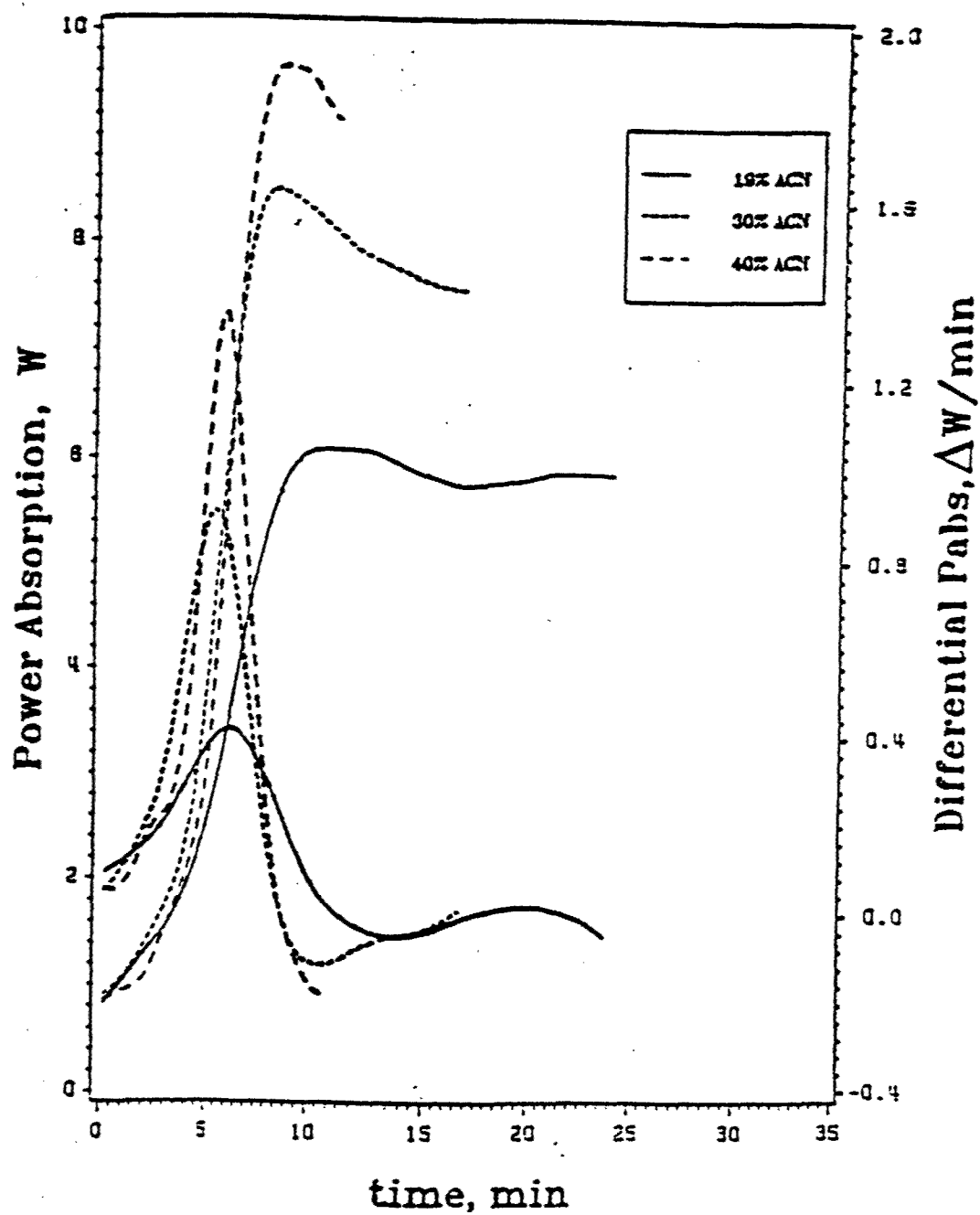
Figure 13.
Variation of the power absorptions and power absorption rates with time for nitrile rubbers (40, 30 & 19% acrylonitrile content) with 2% w/w dicumyl peroxide in a travelling wave applicator
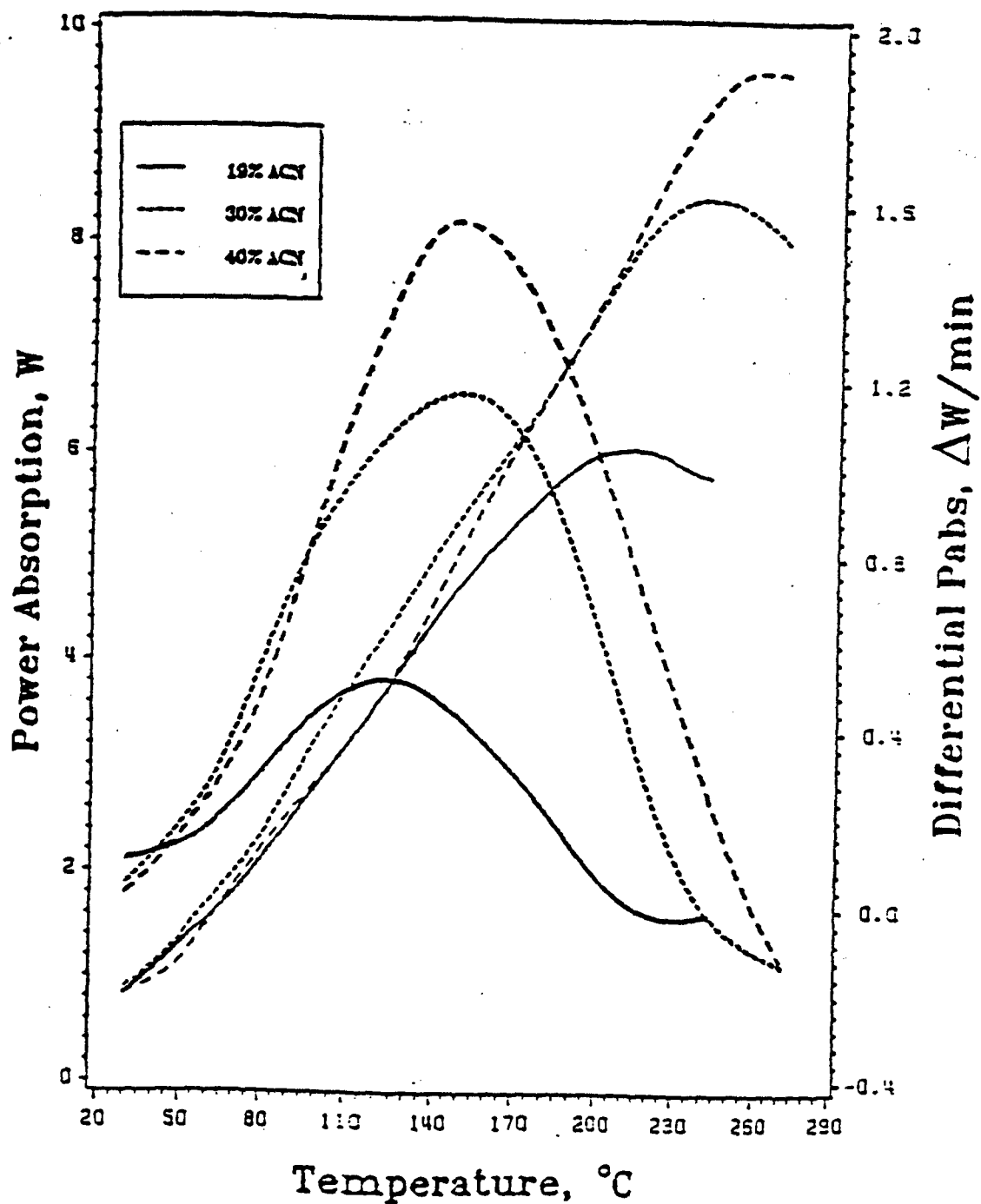
Figure 14.
Variation of the power absorptions and power absorption rates with temperature for
nitrile rubbers (40, 30 & 19% acrylonitrile content) with 2% w/w dicumyl peroxide in a
travelling wave applicator

153
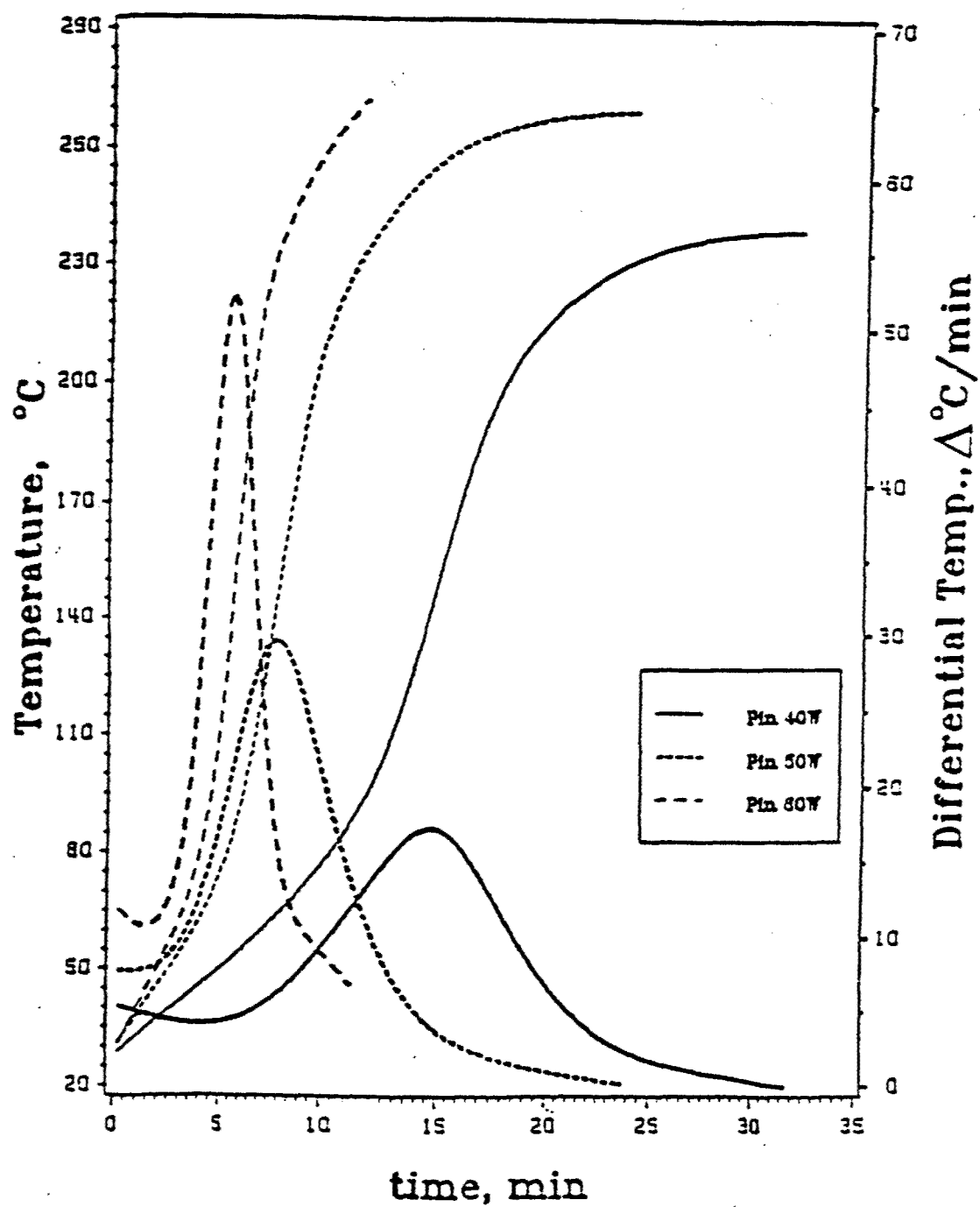
Figure 15.
Variation of the temperature and heating rate with time for 30% acrylonitrile nitrile rubber with 2% w/w dicumyl peroxide in the traveling wave applicator

154
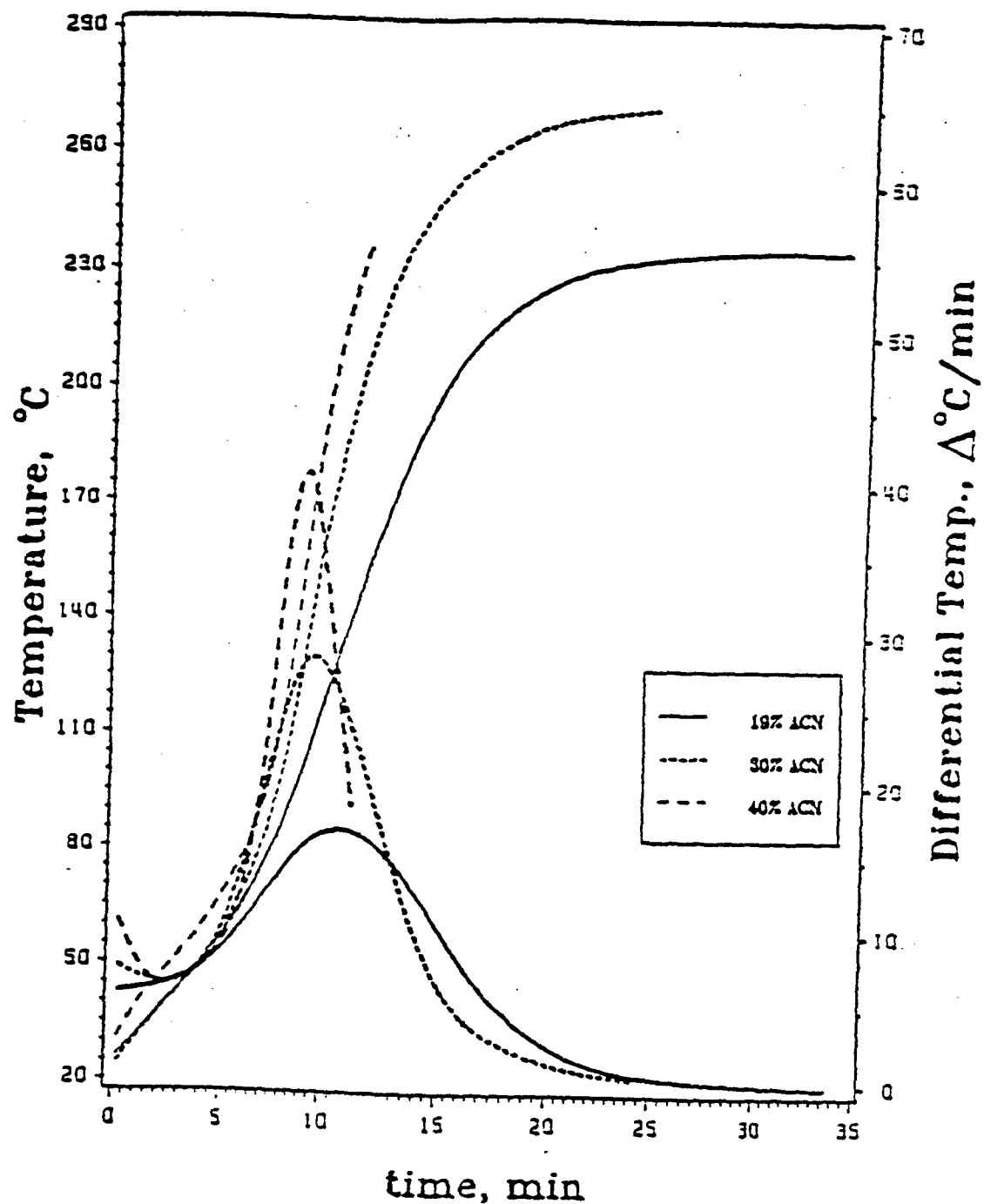
Figure 16.
Variation of the temperature and heating rate with time for nitrile rubbers (40, 30 & 19% acrylonitrile content) with without dicumyl peroxide in the traveling wave applicator; input power was 50 W
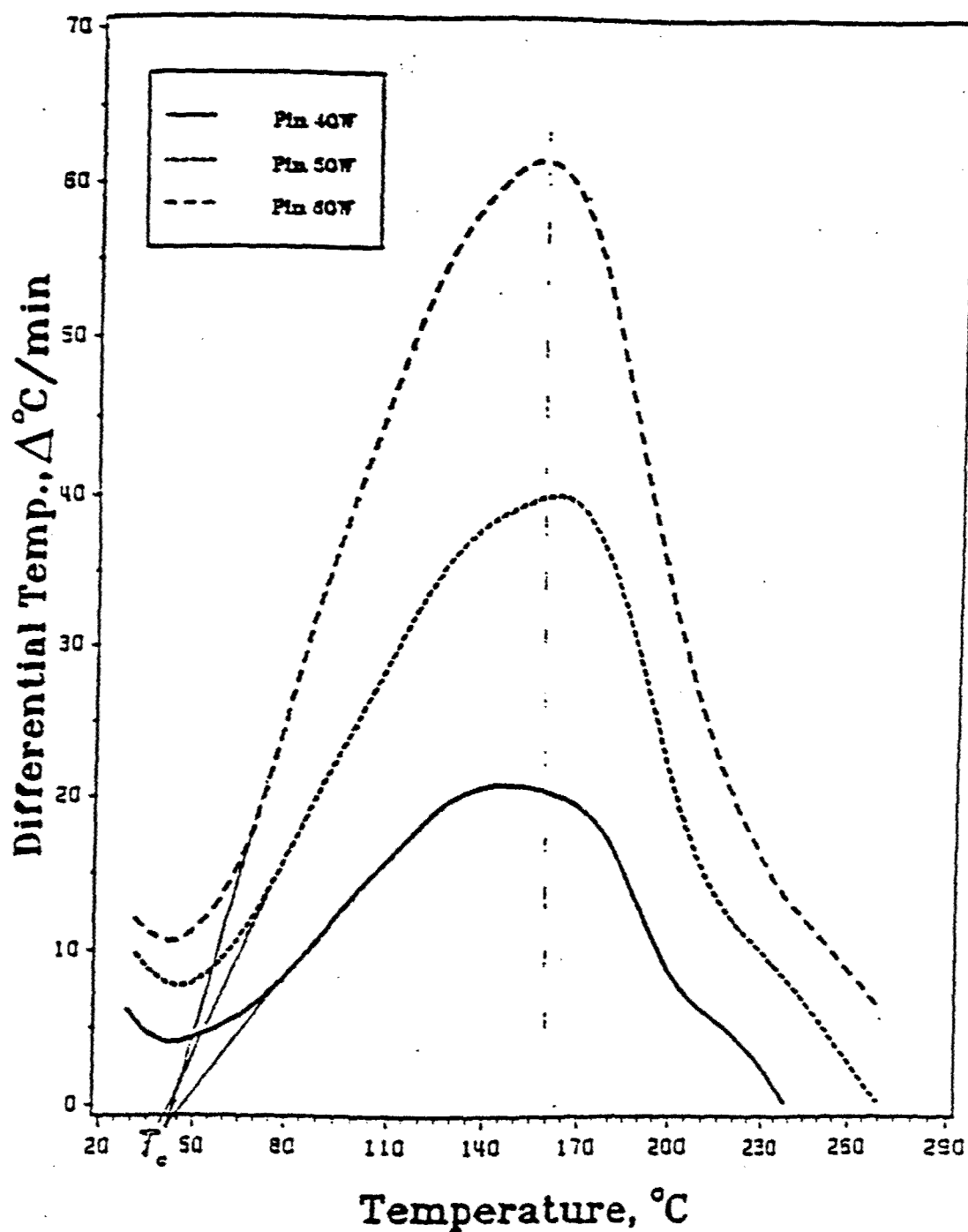
Figure 17.
Variation of theheating rate with temperature for 30% acrylonitrile nitrile rubber with
2% w/w dicumyl peroxide in the traveling wave applicator

156
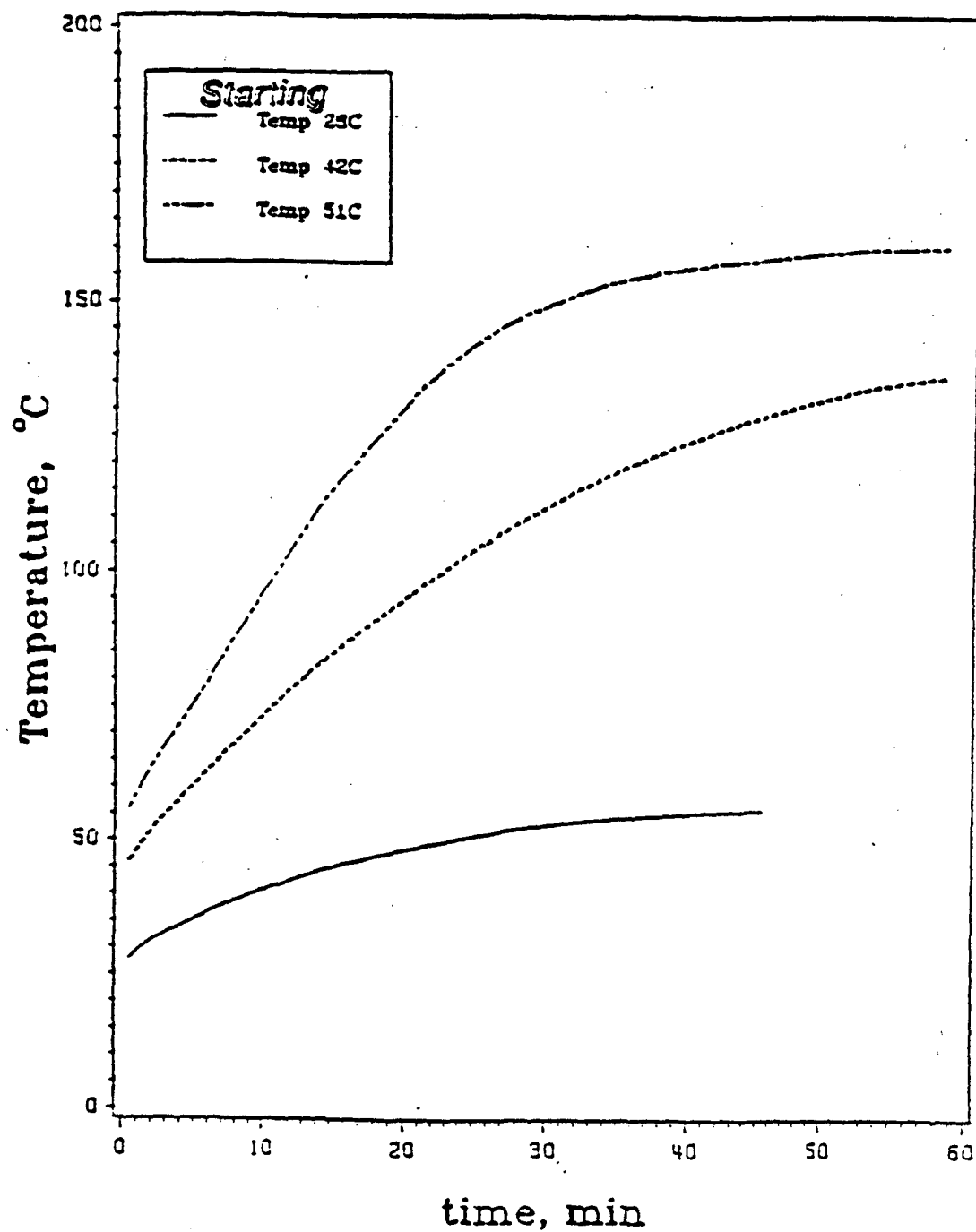
Figure 18.
Variation of the temperature with time for 19% acrylonitrile nitrile rubber with 2% w/w
dicumyl peroxide in the traveling wave applicator; input power was 20.5 W
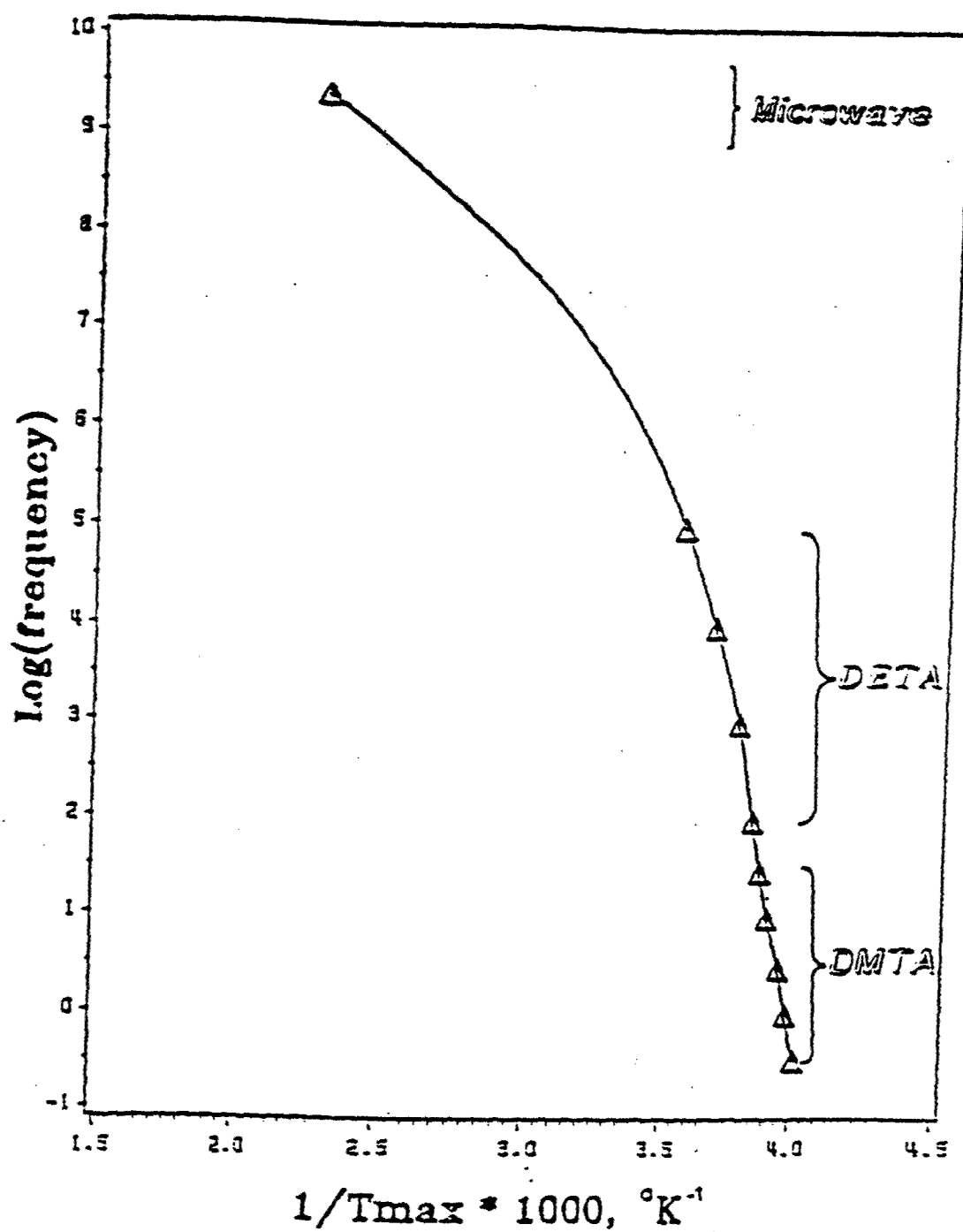
Figure 19.
WLF relationship for 30% acrylonitrile nitrile rubber with
2% w/w dicumyl peroxide in the traveling wave applicator

# THE DIELECTRIC BEHAVIOR OF GLASSY AMORPHOUS POLYMERS AT 2.45 GHz

M. Chen[1], E. J. Sicchi[2], T. C. Ward* and J.E. McGrath

NSF STC: High Performance Polymeric Adhesives and Composites and
Department of Chemistry
Virginia Polytechnic Institute and State University
Blacksburg, VA 24061-0212

## ABSTRACT

The dielectric behavior of glassy thermoplastic polymer in the microwave frequency range was investigated. Specifically, the relationship between energy absorption and temperature for several thermoplastic systems was examined to test the theoretical basis for heating under microwave irradiation. Irradiation under travelling and standing wave conditions were explored. The heating rate versus temperature data at a frequency of 2.45 GHz yielded a microwave calorimetry procedure for examination of the dielectric and relaxation behaviors. Correlations were drawn between a) the apparent activation energy and the critical temperature, and b) the shape of the dielectric spectra at 2.45 GHz and its shape in kHz region. WLF relationships were examined for glassy thermoplastics to show the difference in changing activation energy with temperature.

# INTRODUCTION

This paper focuses on the dielectric behavior of glassy thermoplastics. For thermoplastics at room temperature, the dielectric loss at microwave frequencies consists of background loss as the transitions of dielectric loss at 2.45 GHz are located well above room temperature. Thus, the dielectric behavior of glassy polymers at 2.45 GHz is intrinsically different from that of rubbery polymers. Nitrile rubbers were found to have a critical temperature of dielectric loss, $T_c$, vide infra very close to room temperature (1) and, therefore, could be heated easily from ambient. Other examples of materials which have dielectric loss behavior different from glassy polymers are foodstuffs (2-6) which contain large amounts of water. Since water has a high dielectric loss factor at around room temperature, foodstuffs can be heated rapidly. The goal of this study was to investigate the coupling of microwave energy to glassy thermoplastics and to delineate the fundamental mechanisms involved. The relationship between energy absorption and temperature for thermoplastics requires fundamental clarification. At room temperature, dielectric losses observed for irradiation of thermoplastics at 2.45 GHz have their origins outside the microwave region (7). Numerous dielectric loss spectra in the lower frequency region can be found in the literature (8-17), but few as a function of temperature. The effects of sample temperature must not be neglected because the shape and position of dielectric loss spectra can be displaced into or out the 2.45 GHz region with appropriate changes in temperature.

# THEORY

There are two key equations that describe the heatability of polymers in an applied electric field. The total power absorbed is given by:

$$P = KfE^2\varepsilon'\tan\delta \qquad [1]$$

where P is the power dissipation in W/cm$^3$, K is a constant equal to $55.61 \times 10^{-14}$, f is the applied frequency in Hz, E is the electric field strength in V/cm, $\varepsilon'$ is the dielectric constant and $\tan\delta$ is the dielectric loss tangent. Both $\varepsilon'$ and $\tan\delta$ depend upon both the frequency and the sample temperature. The electromagnetic field energy dissipated as heat per unit volume is proportional to the dielectric loss factor ($\varepsilon'\tan\delta$), the square

160

of the field strength ($E^2$) and the frequency ($f$) of the applied field. The heating rate is given by:

$$\frac{dT}{dt} = \frac{KfE^2 \varepsilon'(T)tan\delta(T)}{\rho C_v} \qquad [2]$$

where $\rho$ is the density of the material, $C_v$ is the specific heat and the other variables are as defined in Equation 1. In this discussion, it is assumed that influences upon the heating rate due to convection, conduction and heats of reaction are negligible.

Both equations are functions of the dielectric properties of the material. The dielectric behavior of polar polymers at various frequencies are depicted schematically in Figure 1 (16). Polymers having high molecular weights cannot be described with a single relaxation time. The $\alpha$ relaxation peak, which is located above the nominal $T_g$ obtained by DSC, is associated with the cooperative motions of the main chain. One or more secondary relaxation effects ($\beta$, $\gamma$ etc.) are associated with the motion of side groups or local groups which may participate in dielectric loss. Ionic conduction, I, is only observed at low frequency and high temperature. The DC conductance, which varies with $\sigma/\omega$ (where $\sigma$ is the conductivity and $\omega$ is the angular frequency), becomes negligible at microwave frequencies. The activation energy of the local chain motion ($\beta$ processes) in amorphous systems is smaller than that of main chain cooperative motions ($\alpha$ processes). In other words, as Figure 1 depicts, when frequency is increased from low to radio frequencies, the $\beta$ process shifts to higher frequencies more rapidly than the $\alpha$ process. Therefore, both loss processes eventually merge at high frequencies.

## EXPERIMENTAL

### MATERIALS

The sources for and $T_g$'s of poly(n-butyl methacrylate) (PBMA), poly(vinyl acetate) (PVAc), poly(ethyl methacrylate) (PEMA), poly(vinyl chloride) (PVC), styrene acrylonitrile copolymer (SAN) and poly(methyl methacrylate) (PMMA) are listed in Table 1. These polymers were used without further purification, but were vacuum dried at just below their respective $T_g$'s for 24 hours immediately before use. Films were prepared by using a platten press (Pasadena Hydraulics, Inc., model number

P210C-X3-5-7-20) in the temperature range of 40-50°C above their respective $T_g$'s. These films were kept in the desiccator until they were used for DETA, DMTA and microwave experiments.

## THERMAL ANALYSIS

The calorimetric responses of samples were measured with a Du Pont Model 912 differential scanning calorimeter (DSC) in order to ascertain the glass transition temperature, $T_g$. For ambient work, nitrogen was used as the purge gas. Indium and lead were used as a calibration standards for temperature and energy. The scanning rate was 10°C/min. Thermogravimetric analyses (TGA) were recorded from 50°C to 750°C at a heating rate 10°C/min by a Du Pont model 951. Air was used as a purge gas at a flow rate of 30 cc/min.

## GEL PERMEATION CHROMATOGRAPHY

Gel permeation chromatography (GPC) was performed on a Waters 150C GPC. To determine absolute molecular weights, detection of eluites was obtained with a refractive index detector and a Viscotek model 100 differential viscometer in parallel. HPLC grade THF was used as the mobile phase at a flow rate of 1.0 ml/min with six UltraStyragel columns (500Å, $10^3$Å, $10^4$Å, $10^5$Å, $10^6$Å and 100Å) in series. Twelve polystyrene standards were used to calibrate the molecular weights via the universal calibration method.

## DISPERSION SPECTROMETER SYSTEMS

Polymer Laboratory's Dielectric Thermal Analyzer (DETA) and Dynamic Mechanical Thermal Analyzer (DMTA) were used to provide relaxation information. Dielectric spectra from -150°C to above $T_g$ were obtained via DETA at fixed frequencies of 0.1, 1, 10 & 100 kHz. Thermal mechanical spectra from -150°C to $T_g$ were studied by using the DMTA at frequencies of 0.3, 1, 3, 10 and/or 30 Hz. All samples were tested in the bending mode. The shifts of the loss tangent peaks with frequency were used to derive the apparent activation energy in each case. Correlations were drawn between a) the apparent activation energy and the critical temperature, and b) the shape of the dielectric spectra at 2.45 GHz and the shape in

162

kHz region. Finally, WLF relationships were examined for glassy thermoplastics to show the difference in changing activation energy with temperature.

## MICROWAVE INSTRUMENTATION

The details of the experimental instrumentation were described previously for the travelling wave applicator (1). A standing wave applicator was also used for processing glassy thermoplastics. The standing wave applicator is shown in Figure 2. The travelling wave applicator may be converted to the standing wave applicator by replacing the adapter, directional coupler and termination load with an adjustable sliding short fastened to the end of the rectangular waveguide. A stub tuner with six probes was mounted between the adapter and the waveguide. Samples in sheet form were packed in the center section of the 1/2 inch inside diameter cylindrical teflon sample holder.

In an ideal travelling wave applicator, the wave only passes through the specimen once. Thus, the electric field strength is relatively low in the travelling mode. Since heating by microwave energy is essentially an interaction between the permanent dipolar molecules of the material to be heated and the electric field component of the microwave energy, travelling wave applicators are not suitable for materials of low loss.

Since only one mode, $TE_{10}$, can propagate freely in the rectangular waveguide, the distribution of electric field strength is related to the peak of the sinusoidal space variation across the width of the waveguide and is located at the center-plane through the broad faces. By placing a sliding short at the end of the waveguide, a standing wave is obtained. Thus, the superposition of the incident and reflected waves which gives rise to a standing wave pattern is created. The voltage maxima of the standing wave would readily couple power to the specimen because the electric field strength is high at the maximum. Indeed, this is sometimes the only way to develop adequate coupling to low loss materials. Conversely, the voltage minima would couple no appreciable power to the material.

For tuning the cavity, the impedance mismatch from the generator to the work load, indicated by the intensity of reflected wave, may be used. The presence of any reflected wave indicates a loss of efficiency in energy transfer. In order to create energy efficiency with the system working as a tuned cavity, the stub tuner was used to adjust the impedance of the work load to a value which the generator could handle. Tuned cavity systems use the microwave energy most efficiently because the radiation

163

from the generator is continuously reflected from the walls of the cavity and pass through the irradiated material many times. The standing wave pattern along the direction of wave propagation is very well defined inside the waveguide and can be monitored via the voltage minima. The precise knowledge of electromagnetic field configurations is necessary to place the dielectric material to be examined in the position of maximum electric field for optimum transfer of the electromagnetic energy. In the case of standing waves, the points of maximum field are also the points of maximum heating throughout the sample volume.

## RESULTS AND DISCUSSION

### THERMAL ANALYSIS AND MOLECULAR WEIGHT DETERMINATIONS

The glass transition temperatures of the polymers studied are shown in Table 1. Additionally, the number average molecular weight, $M_n$, the weight average molecular weight, $M_w$, and the polydispersity as determined by the universal calibration method are given. All of these polymers had a weight average molecular weights on the order of $10^5$ g/mole. The onset temperature for decomposition as measured by thermogravimetric analysis (TGA) is also provided. Microwave heating of these polymers was carried out below the onset of the decomposition temperature in all cases.

### MICROWAVE EXPERIMENTAL RESULTS AND THERMAL SPECTRA FROM DETA

The variations of sample temperature with time for PVAc in the travelling wave applicator is represented in Fgure 3. The various starting temperatures were approximately 0, 15, 30 or 45 °C above $T_g$ (30°C). After the temperature had equilibrated, 50 watts of input power was applied to the system. The temperature rise produced after 20 minutes of processing was minute even at 45°C above the $T_g$ of PVAc. This was due to the fact that the dielectric loss factor, at these temperatures, was still low at the frequency of 2.45 GHz. Similar results were obtained for PBMA processed at 60°C above its $T_g$ (20°C), and for PEMA processed at 30°C above its $T_g$ (66°C). Under these conditions, all three polymers were still in the background dielectric loss region at 2.45 GHz. Hence, little dielectric coupling occurred.

164

The variation of sample temperature vs. time for PVC processed at 50 watts in the travelling mode is presented in Figure 4. The temperature rise at 20 minutes was significant when processed at 28°C above the $T_g$ of PVC (90°C). This particular observation was important. It is known that the dielectric relaxation spectra shift to higher temperature with increasing frequency. Indeed, the "cool side" of the dielectric relaxation spectra of PVC must have shifted into the 2.45 GHz region at 116°C (28°C above $T_g$). How far the $\varepsilon''$ spectra shifts at 2.45 GHz determines the critical temperature for dielectric loss factor, $T_c$, as well as the $T_g$ at 2.45 GHz. $T_c$ gives an approximate indication of the temperature at which the dielectric loss factor, $\varepsilon''$, increases significantly and the onset of rapid heating occurs.

From Equation 1, it is known that power absorption can be increased by increasing the electric field strength. Thus, several experiments were performed where the travelling wave applicator was replaced by the standing wave applicator to increase the electric field strength. The sample was put at the location of maximum electric field in the $TE_{10}$ mode in the waveguide at ambient temperature. The variations of input power, reflected power and sample temperature as a function of time for PVAc in the standing wave applicator are displayed in Figure 5. Input power was kept constant at 16 watts. Reflected power was adjusted to zero at the onset of the experiment by using the stub tuner. The sample temperature rose rapidly for the first 10 minutes. From equation 2, assuming E, $\rho$, $C_v$ are constant, the heating rate is proportional to the dielectric loss, $\varepsilon''$, given the other qualifications. In Figure 6, the heating rate is plotted versus temperature to produce a thermal scan of PVAc at a frequency of 2.45 GHz. This procedure is called microwave calorimetry. The $T_c$ and $T_g$ of PVAc at 2.45 GHz was qualitatively determined to be 65°C and 150°C, respectively, from Figure 6. The thermal conductivity effect was not considered in this short time experiment. For the case of PVAc, shown in Figure 7, the temperature was seen to rise significantly at the starting temperature of 92°C (27°C higher than $T_c$) in the travelling wave applicator indicating that the "cool side" of the dielectric loss spectra of PVAc was in the 2.45 GHz region.

Similar results for PMMA in the standing wave applicator are shown in the Figures 8 and 9. The input power was kept at 21 watts. The rise of temperature was slow in the first 32 minutes; after which time the temperature rose rapidly, as shown in Figure 8. In Figure 9, an induction period below 150°C appears in the plot of heating rate vs. temperature. The $T_c$ of PMMA is about 185°C which is 80°C above its $T_g$. The dielectric behavior at 2.45 GHz for PMMA is different from that of PVAc. Here, examination of the lower frequency loss responses is required to explain these

differences. The dielectric spectra of PMMA obtained via DETA over the temperature range from -80°C to 190°C at frequencies of 0.1, 1, 10 & 100 kHz is depicted in Figure 10. The shape of the spectrum at 100 kHz was similar to that at 2.45 GHz for PMMA. However, in comparing 100 kHz to 0.1 kHz traces, the dielectric spectra gradually separated into two peaks. The peak at the higher temperature was associated with the motion of the main chain $\alpha$ relaxation. The peak at lower temperature was due to the relaxation ($\beta$ relaxation) of the strong electric dipole in the ester (-COOCH$_3$) side group. The $\beta$ peak shifted more rapidly than the $\alpha$ peak as temperature was increased. The merging of the $\alpha$ and $\beta$ relaxations in PMMA at a frequency of about 10 kHz can be clearly seen. In contrast to this behavior, the dielectric spectra of PVAc obtained by the DETA are shown in Figure 10. In PVAc, the side group is linked to the main chain by polar C-O bonds. The polar C-O bonds are expected to induce motion in the main chain to produce a more intense dielectric glass transition than for the case of PMMA where this link is an apolar C-C bond. A closer inspection of the spectra in Figure 10 reveals differences in the dielectric behavior. This difference is clearly evident at 2.45 GHz for PMMA and PVAc, as shown in Figures 7 and 9, since PMMA possess a large $\beta$ dielectric loss relaxation.

To describe the temperature sensitivity of the relaxation process, Arrhenius plots were made from DETA data. The calculation of the apparent activation energy, $\Delta E_a$, was performed in the following way: the maximum temperature for several frequencies was determined from the plot of tan$\delta$ vs. temperature, as shown in Figure 10. A graph of the applied log(frequency) versus the inverse absolute temperature maximum was made. Placement of a straight line through the data over a narrow temperature range, as shown in Figure 11, yielded a slope proportional to the activation energy, $\Delta E_a$:

$$\Delta E_a = -2.303R \times slope \qquad [3]$$

This value, referred to as the "apparent " activation energy, is summarized in the third column of Table 2.

Smaller values of $\Delta E_a$ result in a slower shift of the relaxation with frequency and reduced temperature difference between $T_c$ and $T_g$. For PVAc, the $\Delta E_a$ was 210 kJ/mole and the $T_c$ was 35°C above its $T_g$. For PMMA, the $\Delta E_a$ was 100 kJ/mole and the $T_c$ was 80°C above its $T_g$. PVC, having the highest $\Delta E_a$ of 380 kJ/mole, was easily heated at 28°C above its $T_g$. PBMA, having a $\Delta E_a$ of 130 kJ/mole, was still in the background dielectric loss region at 2.45 GHz even at 60°C above its $T_g$. The low

166

activation energy for PEMA and PSMA was attributed to the merging of the α and β relaxations as shown in Figure 12.

The critical temperature, $T_c$, is an important parameter for microwave processing of polymers. Above $T_c$, a positive slope ($d\varepsilon''/dT$) of the $\varepsilon''$ vs. temperature plot results. This is the region of rapid volumetric heating. In the extreme case, $d\varepsilon''/dT$ can be so large that the sample can char. This phenomenon is termed the "runaway effect". After the material absorbs microwave energy, the temperature rise causes the $\varepsilon''$ to increase which, in turn, results in a further increase of temperature, and so on. Either decreasing the microwave energy or removing the sample is necessary to avoid damage to the sample. Knowledge of the dependence of dielectric behavior on temperature at 2.45 GHz is important in the design of a microwave heating system to take advantage of the rapid heating in the positive side of $d\varepsilon''/dT$ and to avoid the thermal runaway effect.

The Williams-Landel-Ferry (WLF) relationships covering a wide frequency range were investigated. The dielectric behavior of PMMA provided a suitable example. Here, the temperature at the maximum heating rate was chosen as the glass transition temperature at 2.45 GHz. The glass transition temperatures at 10 kHz and 100 kHz were obtained from DETA spectra. Finally, the glass transition temperatures at 0.3, 1, 3, 10 and 30 Hz from the maximum loss moduli E" were obtained from the DMTA spectra. A graph of the dependence of the logarithm of the frequency against the reciprocal of absolute temperature for PMMA is shown in Figure 13. The three points at high temperature obeyed Arrhenius behavior with a constant activation energy. The merging of the α and β relaxation at 10 kHz produced the kink in the WLF curve at approximately 130°C.

The results for SAN in the standing wave applicator are presented in Figures 14 and 15. With input power kept at 32 watts, the temperature rise in the first 6.5 minutes was slow an followed by a rapid temperature increase, as shown in Figure 14. In Figure 15, $T_c$ of SAN was found to be about 145°C and corrresponded to 40°C above its $T_g$. The dielectric spectra of SAN obtained via DETA over the temperature range from 40°C to 190°C at 0.1, 1, 10 & 100 kHz is given in Figure 16. For SAN, $\Delta E_a$ was determined to be 300 kJ/mole. The graph of the dependence of the logarithm of the frequency against the reciprocal of absolute temperature for SAN is shown in Figure 17. The plot exhibits the curvature which is typical for glass-rubber relaxations of amorphous polymers and is consistent with the WLF relationship. Examination of the log(frequency) vs. $1/T_g$ plot reveals either that: a) the dielectric loss at the microwave region was low, or that b) the frequency location plots did not extrapolate dielectric

167

loss dispersions to the microwave frequency range at room temperature for glassy thermoplastics.

A general phenomenon in all these experiments was an initial decrease in heating rate vs. temperature curves. One possible reason for this is related to changes in basic dielectric properties which caused an impedance change as temperature increased. This mismatch may have caused more energy to be dissipated in the source rather than in the load. The second possible reason was that the position of the maximum electric field was shifted toward the microwave source in the first few minutes. In any case, the initial decrease in heating rate was an artifact of the experiment and not a secondary transition.

## CONCLUSIONS

Microwave processing of glassy polymers requires detailed knowledge of how temperature affects the location of the dielectric loss peak within the frequency domain. As a result, several key terms must be defined. For the materials examined, the critical temperatures were obtained from the x-intercept of the 'cool side' tangent curve of the heating rate versus temperature plots at 2.45 GHz. The dispersion curve was centered by using the peak values from Arrhenius extrapolations assuming a constant peak shape at high frequencies. Microwave processing was rapid above the critical temperature because the dielectric loss transition had entered the 2.45 GHz domain for efficient coupling of energy to the polymer. The glass transition temperatures at 2.45 GHz were obtained from heating rate, $(dT/dt)$ or $(d\varepsilon''/dt)$, versus temperature curves. Arrhenius plots of log(frequency) versus the inverse absolute temperature maximum were made from DETA spectra; these experiments showed how sensitive the dielectric loss spectra were to changes in temperature. Finally, WLF plots over a broad range of applied frequencies were made for PMMA and SAN and demonstrated the phenomenon of merging $\alpha$ and $\beta$ relaxations of PMMA at 10 kHz.

Outside the region of dispersion, the dependence of dielectric loss factor on temperature for polar molecules was like that for nonpolar molecules, i.e., $d\varepsilon''/dT$ was small. Within a dispersion region, however, $d\varepsilon''/dT$ was large and positive in the temperature range on the 'cool side' of a dispersion. Also, this region was where rapid, volumetric heating occurred. In other words, the dielectric loss factor depended on the relaxation times as well as the dipole moment. The dipole moment values should be used only in conjunction with the corresponding data for the relaxation times in order to compare the dielectric loss factors. Due to their high molecular

weights, polymer chains possess low mobility and their relaxation times are relatively long. For this reason, increased temperatures were necessary to move the dielectric relaxation spectra of glassy thermoplastics into the microwave region. Plots of dielectric properties as functions of frequency at a single temperature or of temperature at a single frequency, although useful, did not give a complete picture of dielectric behavior. The dielectric spectra of DETA were used to reveal the shift of dielectric relaxation spectra to the microwave region. The plot of heating rate versus temperature via the microwave experiment was used to estimate the $T_c$ and $T_g$ at 2.45 GHz for various glassy thermoplastics. The combination of microwave and conventional thermal heating improved absorption of microwave energy by polymers.

At room temperature, dielectric loss factors of the thermoplastics studied were exceptionally low. Therefore, a high electric field strength was required to ensure a reasonable rate of temperature increase. In general, for the same power applied, the standing wave applicator established much higher electric field strengths than the travelling wave or multimode applicators. From an industrial point of view, low loss thermoplastics at room temperature require standing wave applicators as opposed to travelling wave or multimode applicators for rapid processing.

## ACKNOWLEDGEMENTS

# REFERENCES

1. M. Chen, E. J. Siochi, T. C. Ward and J. E. McGrath, *Poly. Eng. Sci.*, (in press, 1992)

2. D. A. Copson, "Microwave Heating," 2nd ed., The Avi Publishing Co., Connecticut, (1975).

3. E. C. Okress, "Microwave Power Engineering," Vol. 2: Applications, Academic Press, New York, (1968).

4. R. V. Decareau, "Microwaves in the Food Processing Industry," Academic Press, Florida, (1985).

5. P. Fellows, "Food Processing Technology: Principles and Practice," E. Horwood Ltd., New York, (1988).

6. M. Le Maguer and P. Jelen, "Food Engineering and Process Applications, Vol. 1: Transport Phenomena," Elsevier Applied Science Publishers, New York, (1986).

7. A. J. Bur, *Polymer*, 26, 963 (1985).

8. N. G. McCrum, B. E. Read and G. Williams, "Anelastic and Dielectric Effects in Polymeric Solids," John Wiley & Sons, New York, (1967).

9. P. Hedvig, "Dielectric Spectroscopy of Polymers," John Wiley & Sons, New York, (1977).

10. Chen C. Ku and R. Liepins, "Electrical Properties of Polymers: Chemical Principles," Hanser Publishers, New York, (1987).

11. A. Tager, "Physical Chemistry of Polymers," 2nd ed., English translation, Mir Publishers, Moscow, (1978).

12. J. I. Kroschwitz, "Electrical and Electronic Properties of Polymers: A State-of-the-Art Compendium," John Wiley & Sons, New York, (1988).

13. .R. Bartnikas and R. M. Eichhorn, "Engineering Dielectrics Volume IIA Electrical Properties of Solid Insulating Materials: Molecular Structure and Electrical Behavior," ASTM Special Technical Publication 783, Pennsylvania, (1983).

14. A. D. Jenkins, "Polymer Science: A materials science handbook," Vol. 2, North-Holland Publishing Co., London, (1972).

15. J. B. Birks and J. H. Schulman, "Progress in Dielectrics," Vol. 2, John Wiley & Sons, New York, (1960).

16. V. Frosini and E. Butta, *J. Appl. Polym. Sci.*, 11, 527 (1967).

17. P. C. Bandyopadhyay and T. K. Chaki, "Proc. IUPAC, I. U. P. A. C., 28th Macromol. Symp.," 421. Int. Union Pure Appl. Chem., Oxford, UK, (1982).

18. D. K. Cheng, "Field and Wave Electromagnetics," Addison-Wesley Publishing Co., Pennsylvania, (1983).

19. A. C. Metaxas and R. J. Meredith, "Industrial Microwave Heating," Peter Peregrinus, London, (1983).

Table 1

The glass transition temperatures, sources of thermoplastics, molecular weights and the onset of decomposition temperatures of various thermoplastics

| Polymer | Sources | $T_g$, °C | $\overline{M_n} \times 10^{-5}$ | $\overline{M_w} \times 10^{-5}$ | Polydispersity | $T_{decomp}$(°C)* |
|---------|---------|-----------|------------------|------------------|----------------|-------------------|
| PBMA | Aldrich | 20 | 2.37 | 5.41 | 2.28 | 217 |
| PVAc | Aldrich | 30 | 1.72 | 7.26 | 4.21 | 311 |
| PEMA | Inland Leidy | 66 | 0.858 | 1.78 | 2.08 | 225 |
| PVC | Polysciences | 85 | 0.665 | 1.36 | 2.05 | 274 |
| SAN | Union Carbide | 101 | 2.72 | 8.80 | 3.23 | 349 |
| PMMA | Inland Leidy | 105 | 1.39 | 3.21 | 2.30 | 263 |

* The onset of decomposition temperature from TGA in °C.

## Table 2

$T_g$'s and the apparent activation energies in the kHz region for several thermoplastics

| Polymer | $T_g$,°C | $\Delta E_a^*$,(kJ/mole) | Relaxation Phenomena |
|---------|----------|--------------------------|----------------------|
| PMMA | 105 | 100 | α & β partially merge |
| PBMA | 20 | 130 | α & β merge |
| PEMA | 66 | 170 | α & β merge |
| PVAc | 30 | 210 | |
| SAN | 101 | 300 | |
| PVC | 85 | 380 | |

\*  Activation energy, $\Delta E_a$, calculated from the peak temperatures of DETA spectra at 1, 10 & 100 kHz
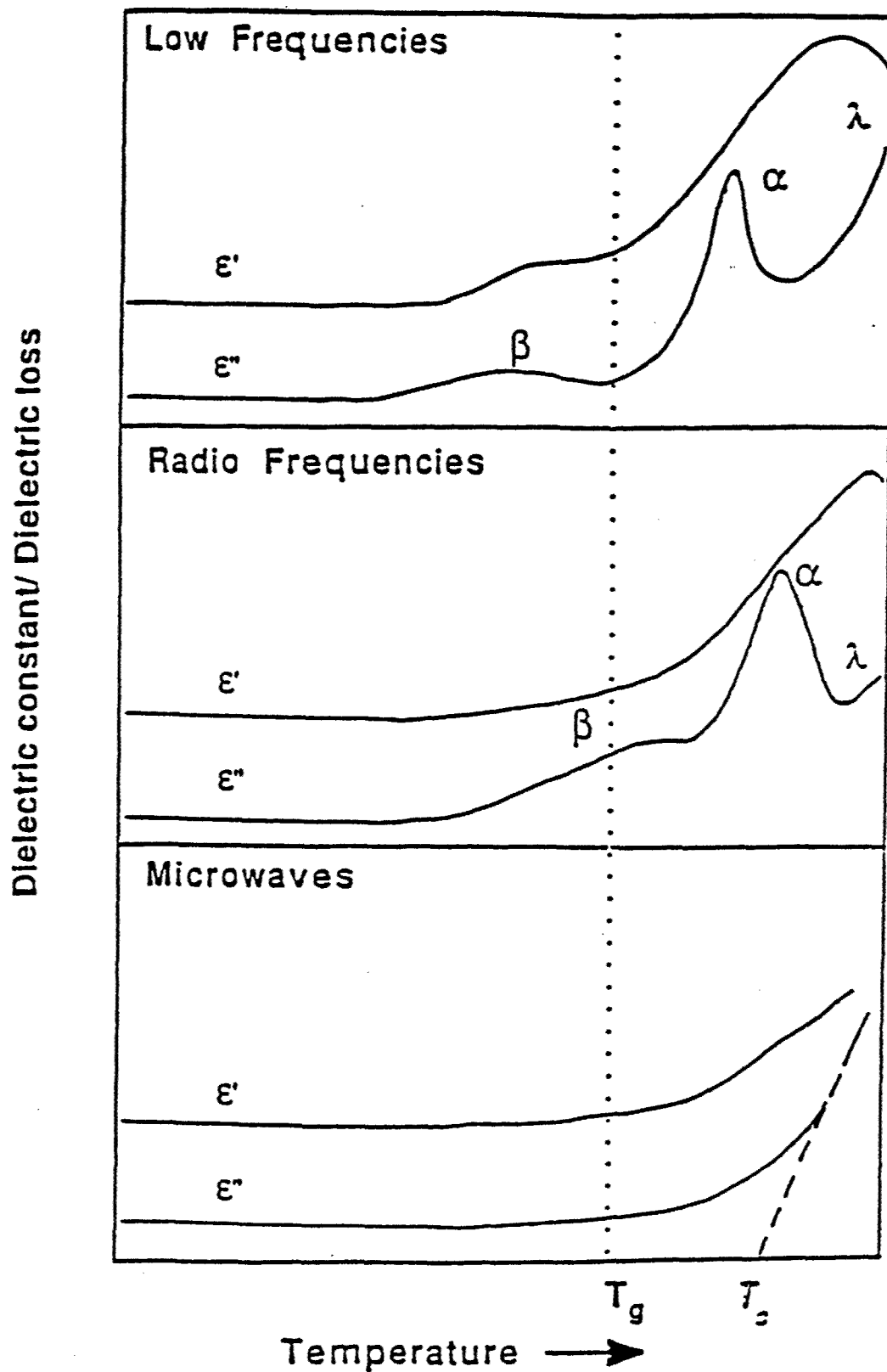
Figure 1.
Schematic representation of the dielectric behavior of polar polymers at various frequencies.
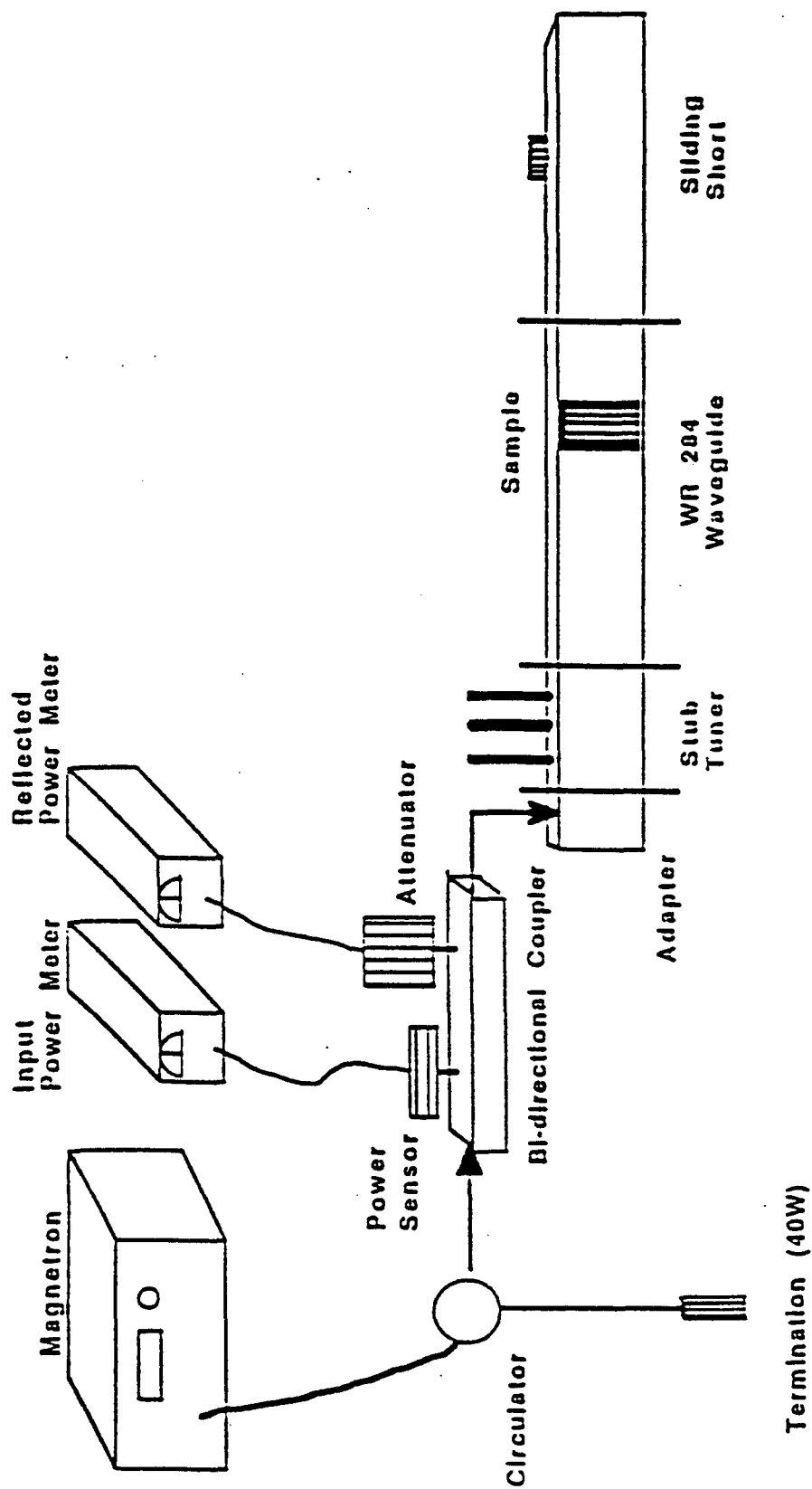
Figure 2.

Schematic of the experimental set-up for the standing wave applicator.
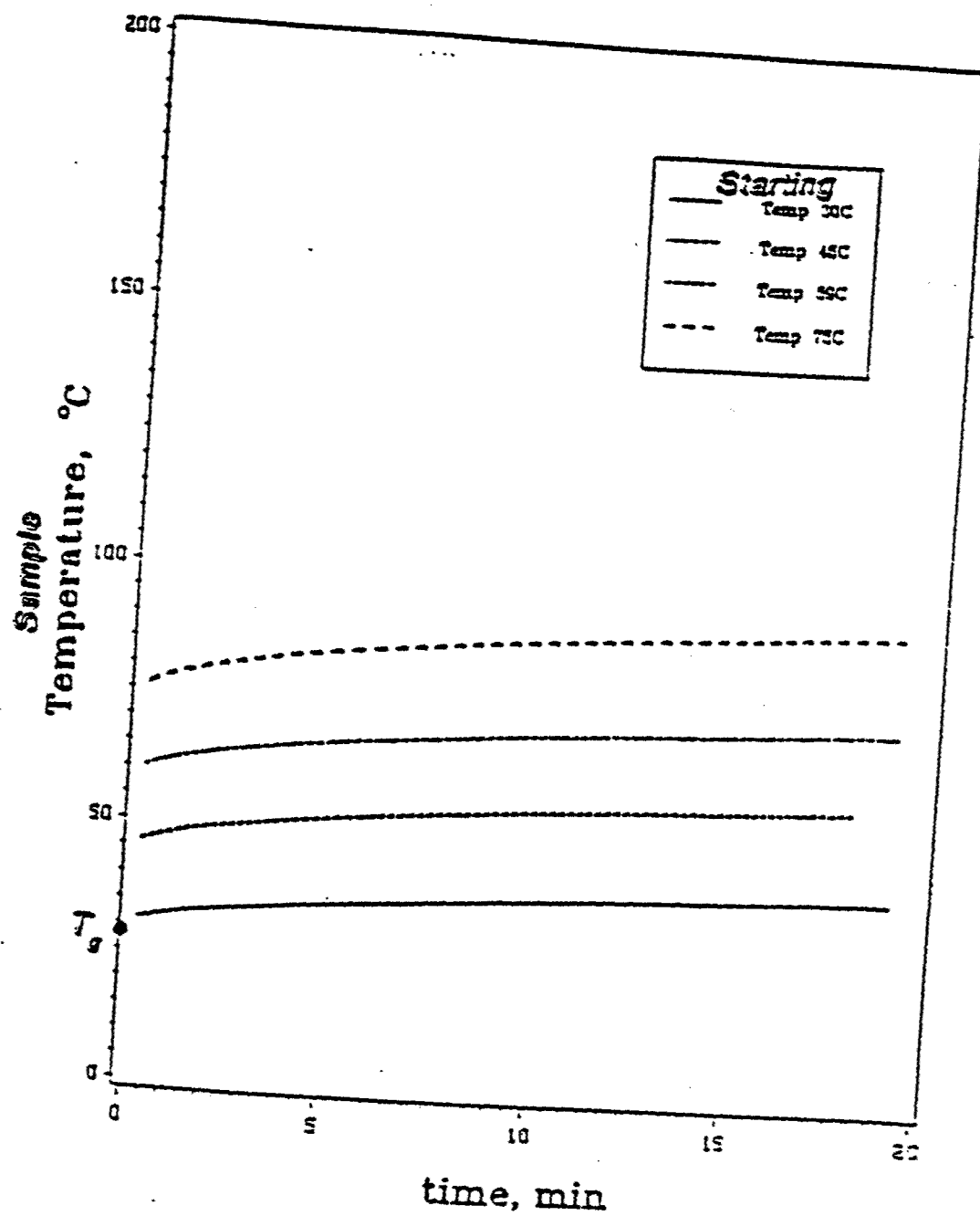
Figure 3.
Variation of the temperature of poly(vinyl acetate) with time in the travelling wave applicator. Input power was 50 watts.

$T_g$ of PVAc = 25°C

176
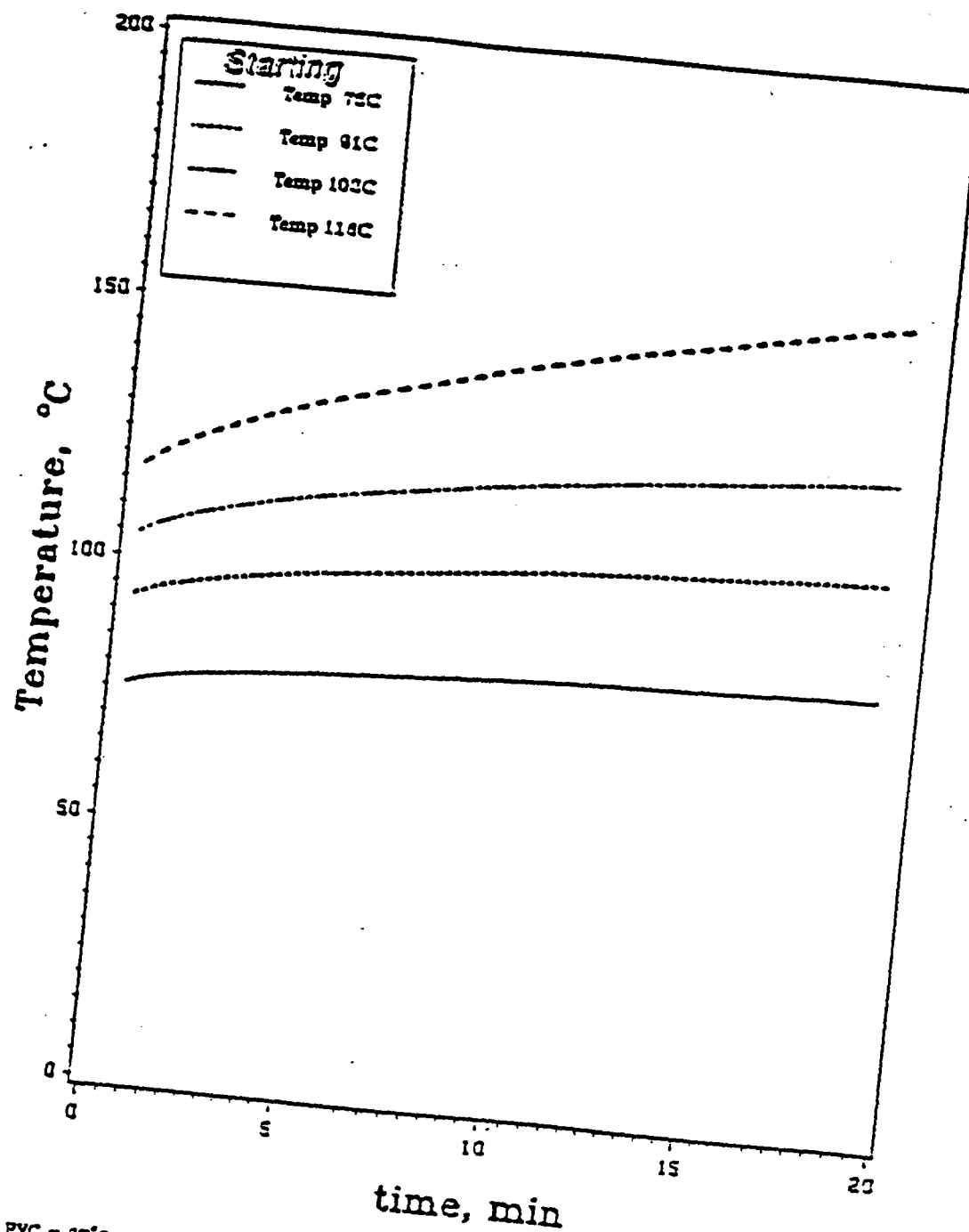
**Figure 4.**
Variation of the temperature of poly(vinyl chloride) with time in the travelling wave applicator. Input power was 50 watts.

$T_g$ of PVC = 87°C

177
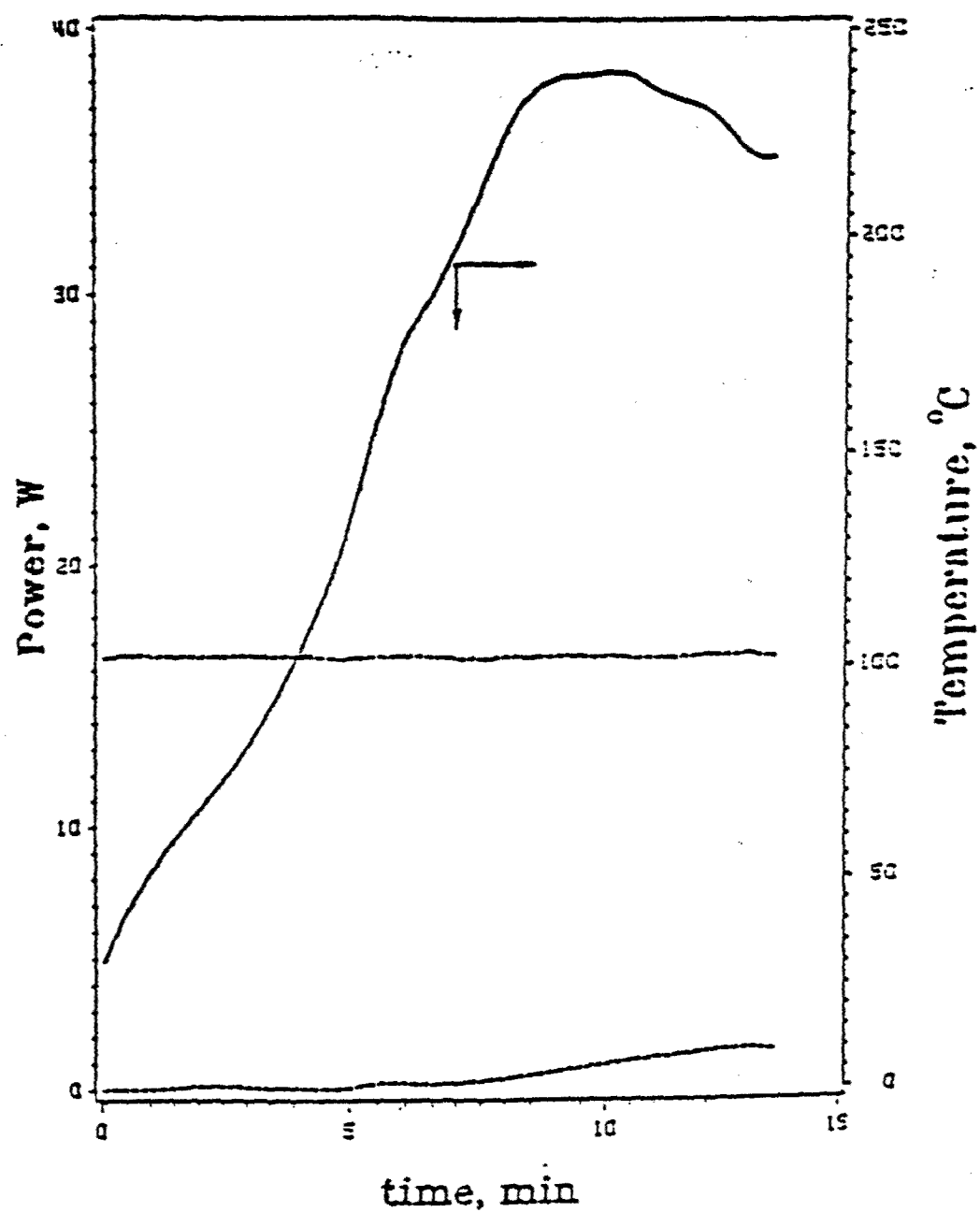
Figure 5.

Variation of the temperature, input power and reflected power with time for poly(vinyl acetate) in the standing wave applicator with a stub tuner.
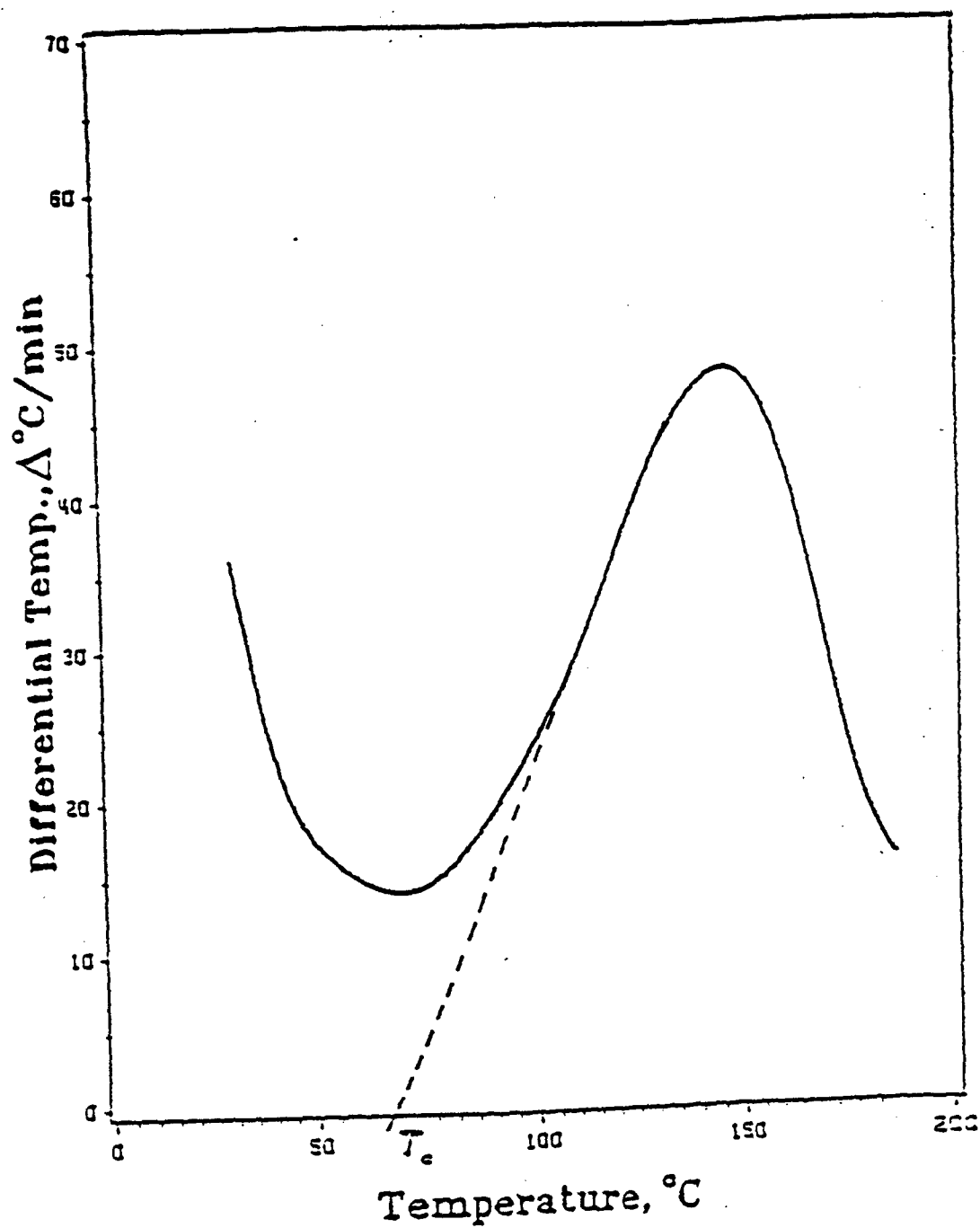
Figure 6.
Heating rate of poly(vinyl acetate) versus temperature in the standing wave applicator
with a stub tuner.

179
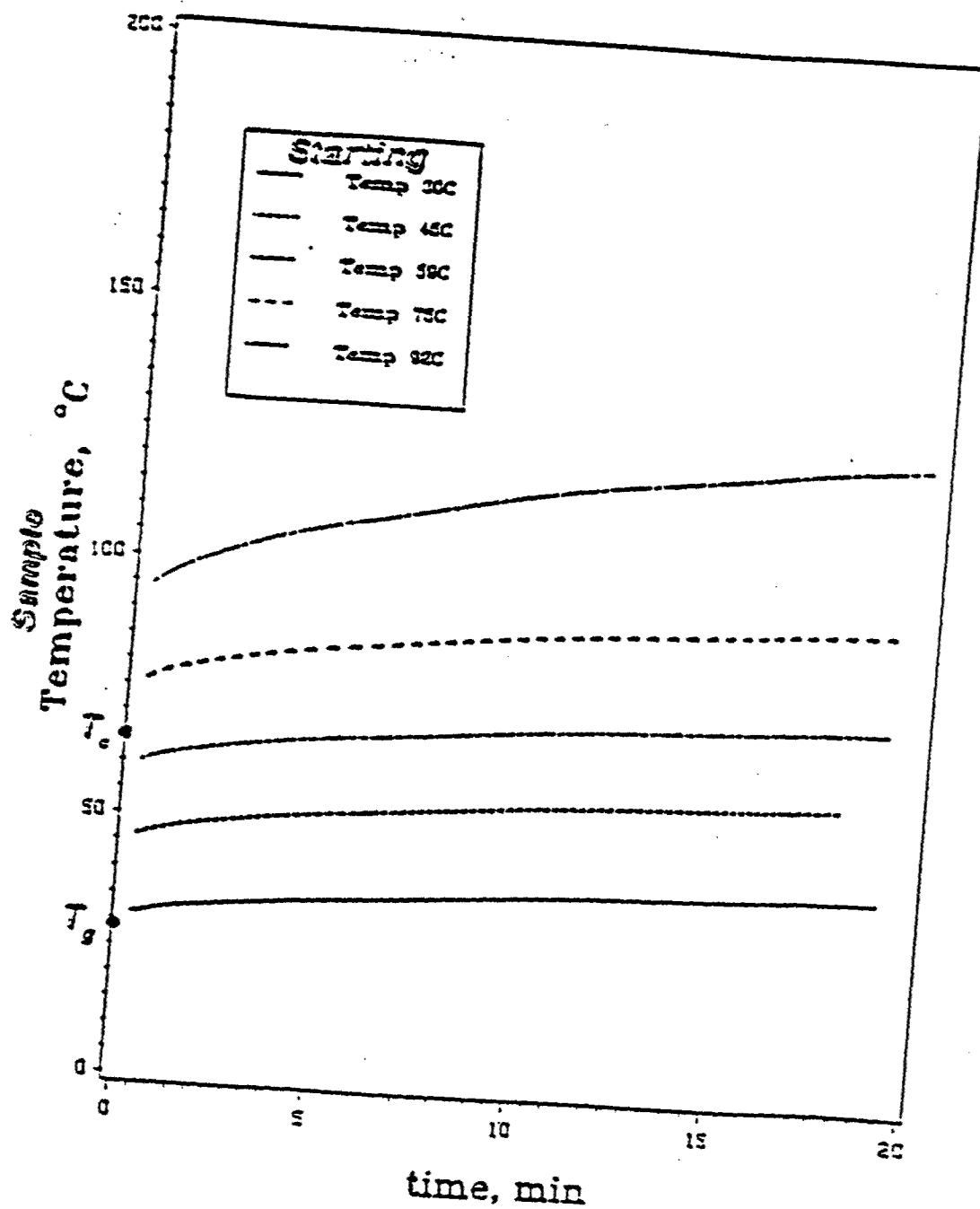
Figure 7.
Variation of the temperature of poly(vinyl acetate) with time in the travelling wave applicator. Input power was 50 watts.

$T_g$ of PVAc = 25°C

180
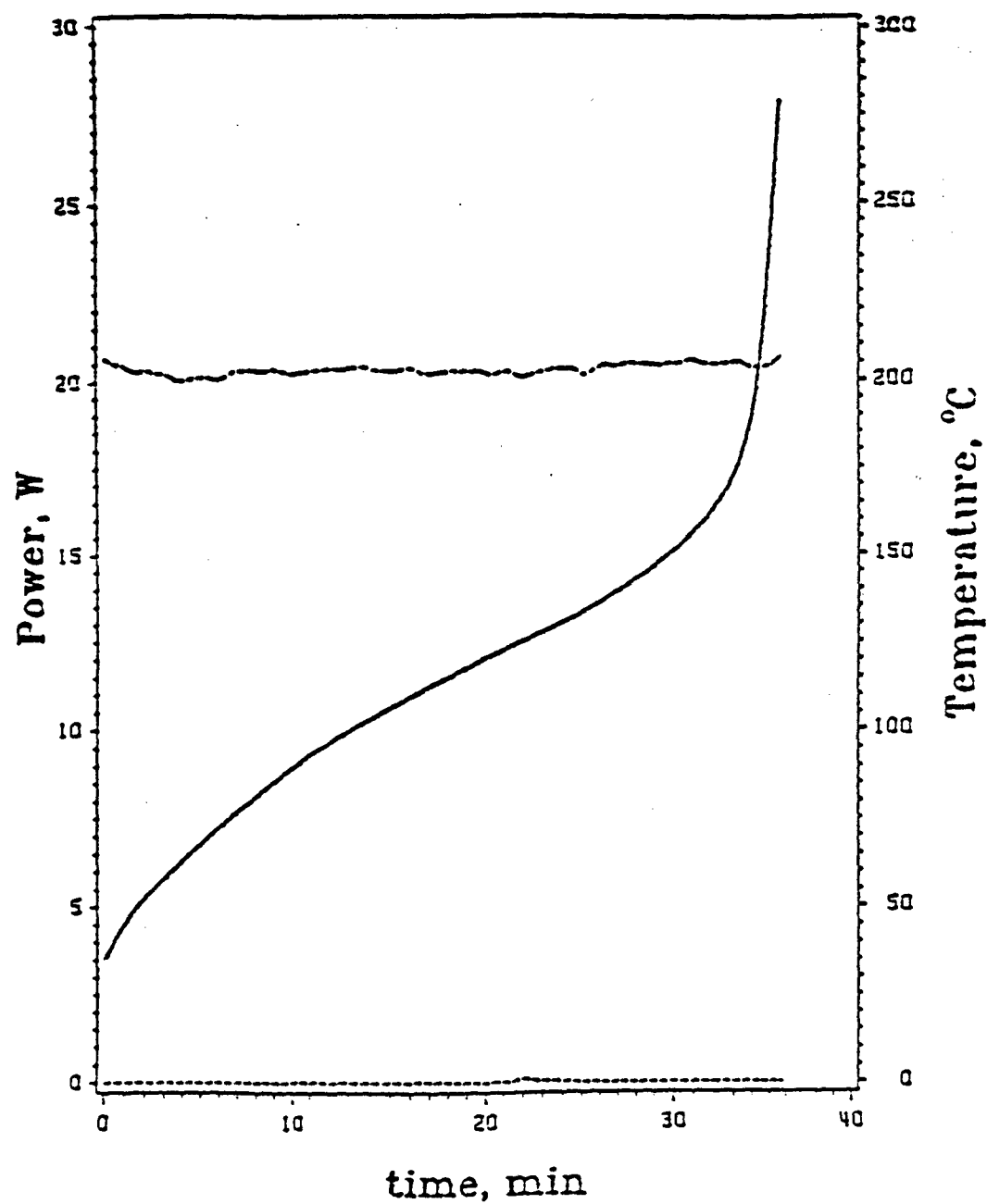
Figure 8.

Variation of the temperature, input power and reflected power with time for poly(methyl
methacrylate) in the standing wave applicator with a stub tuner.
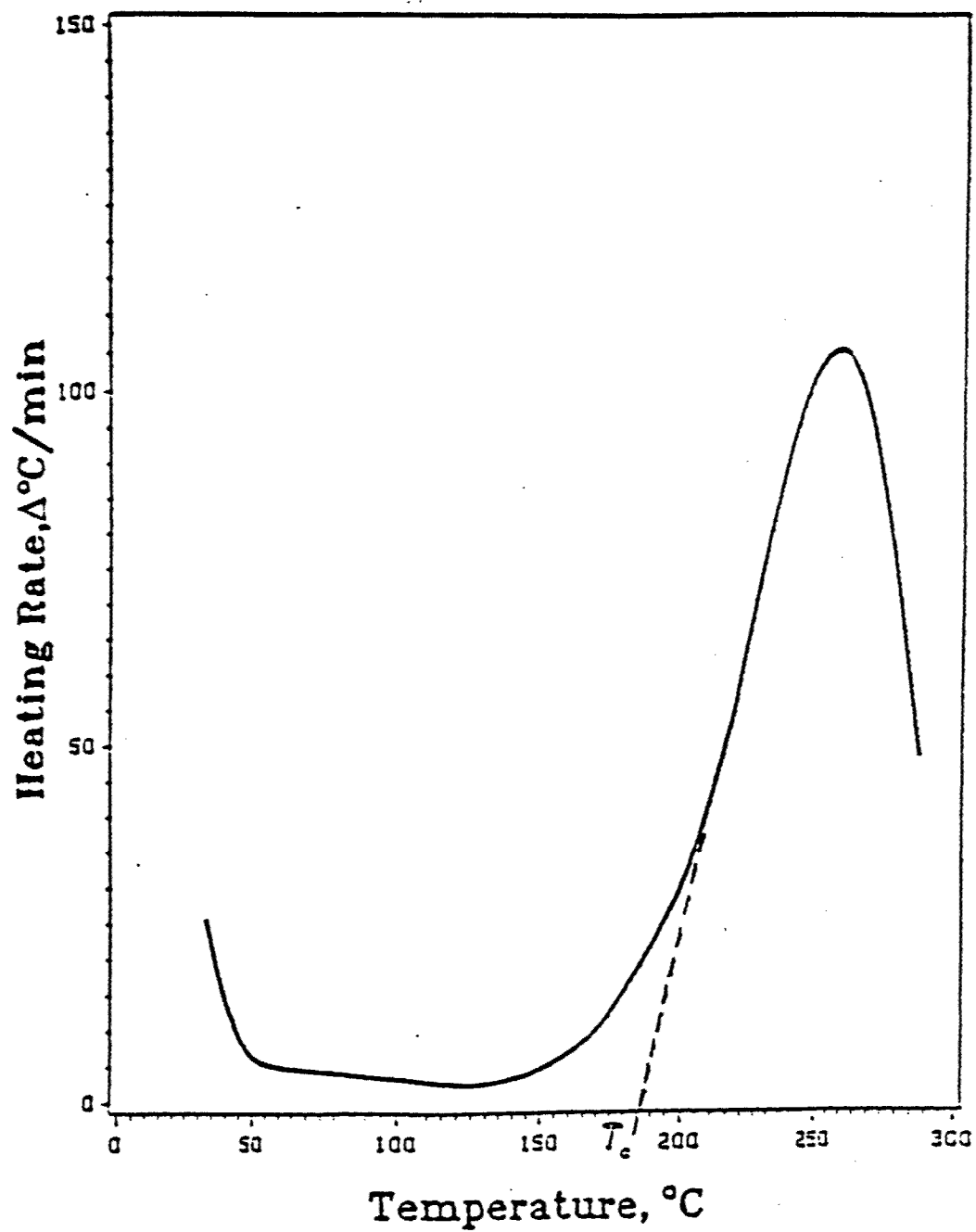
Figure 9.

Heating rate of poly(methyl methacrylate) versus temperature in the standing wave applicator with a stub tuner.
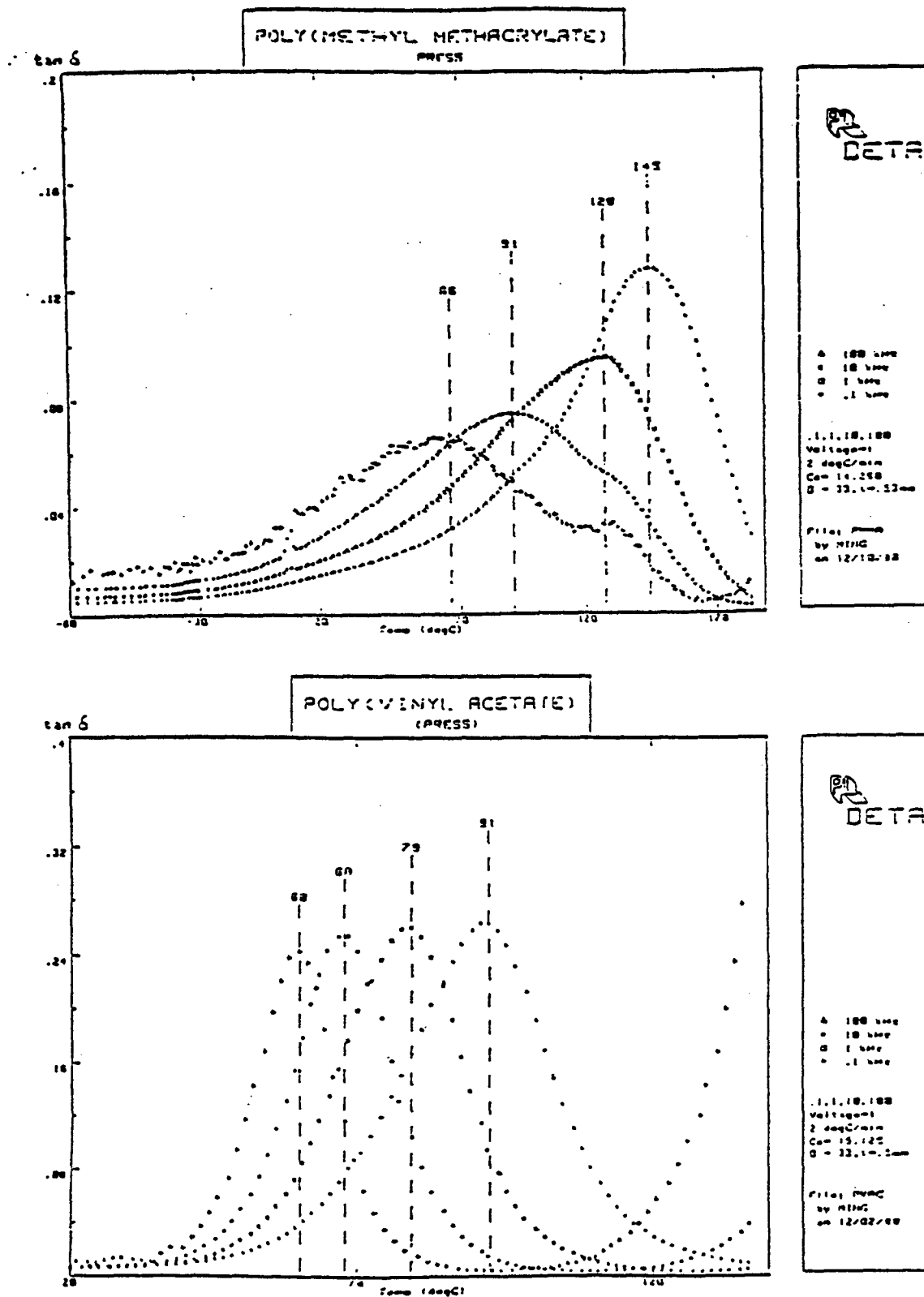
Figure 10.
Temperature dependence of the loss tangent of poly(methyl methacrylate) (top) and
poly(vinyl acetate) (bottom) at various frequencies
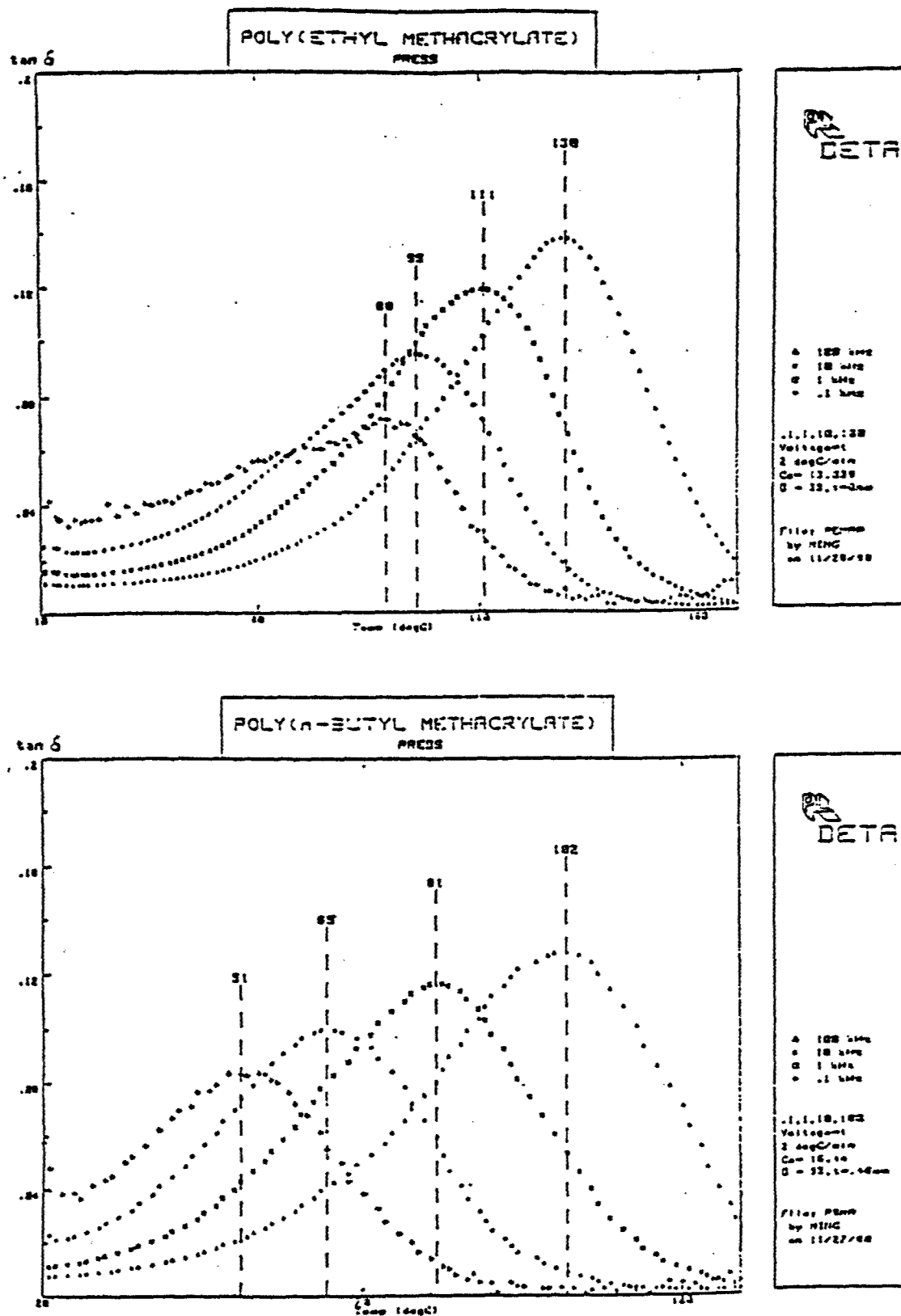
Figure 12.

Temperature dependence of the loss tangent of poly(ethyl methacrylate) (top) and
poly(n-butyl methacrylate) (bottom) at various frequencies

184

Figure 13.
WLF relationship for poly(methyl methacrylate).
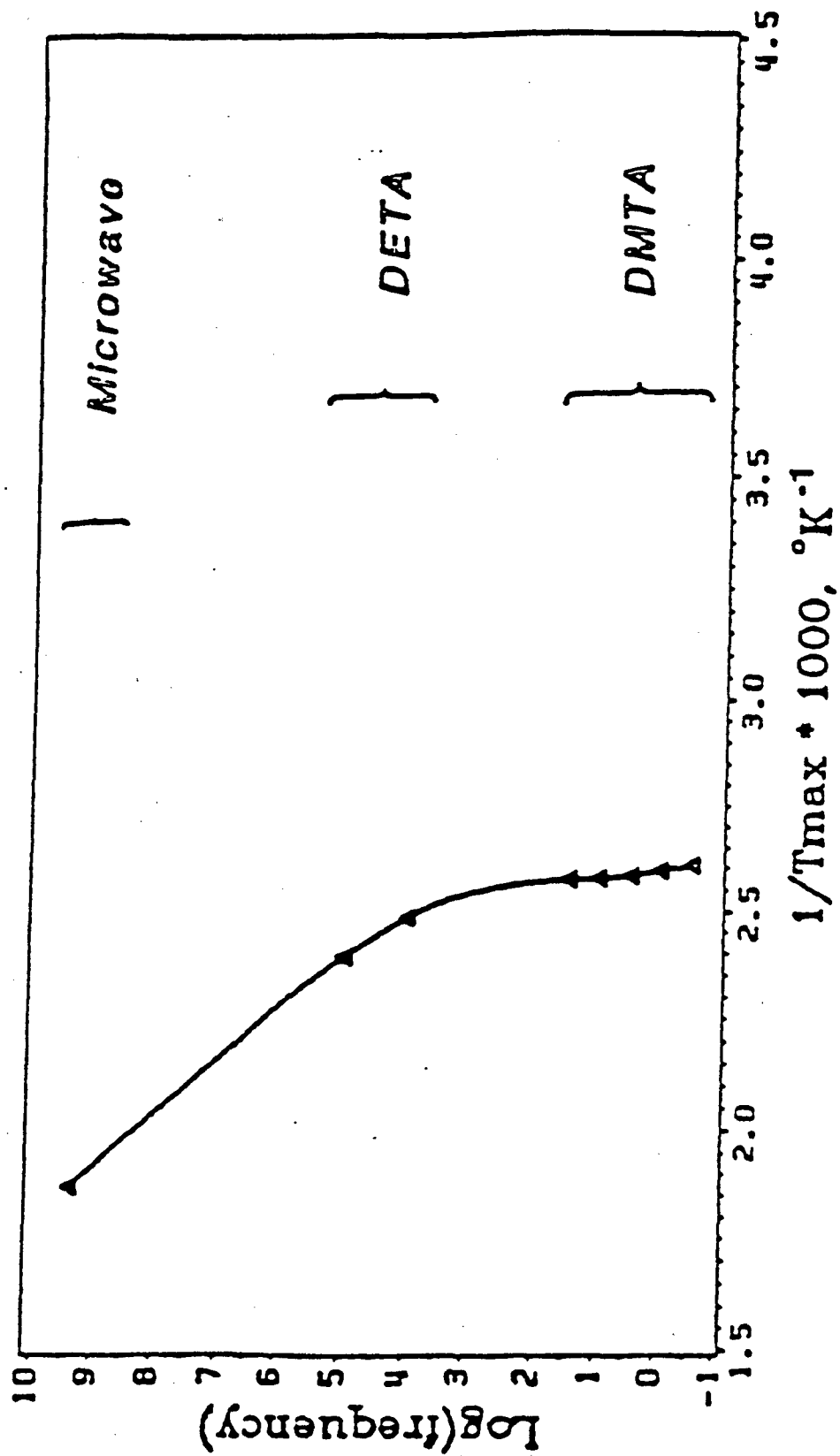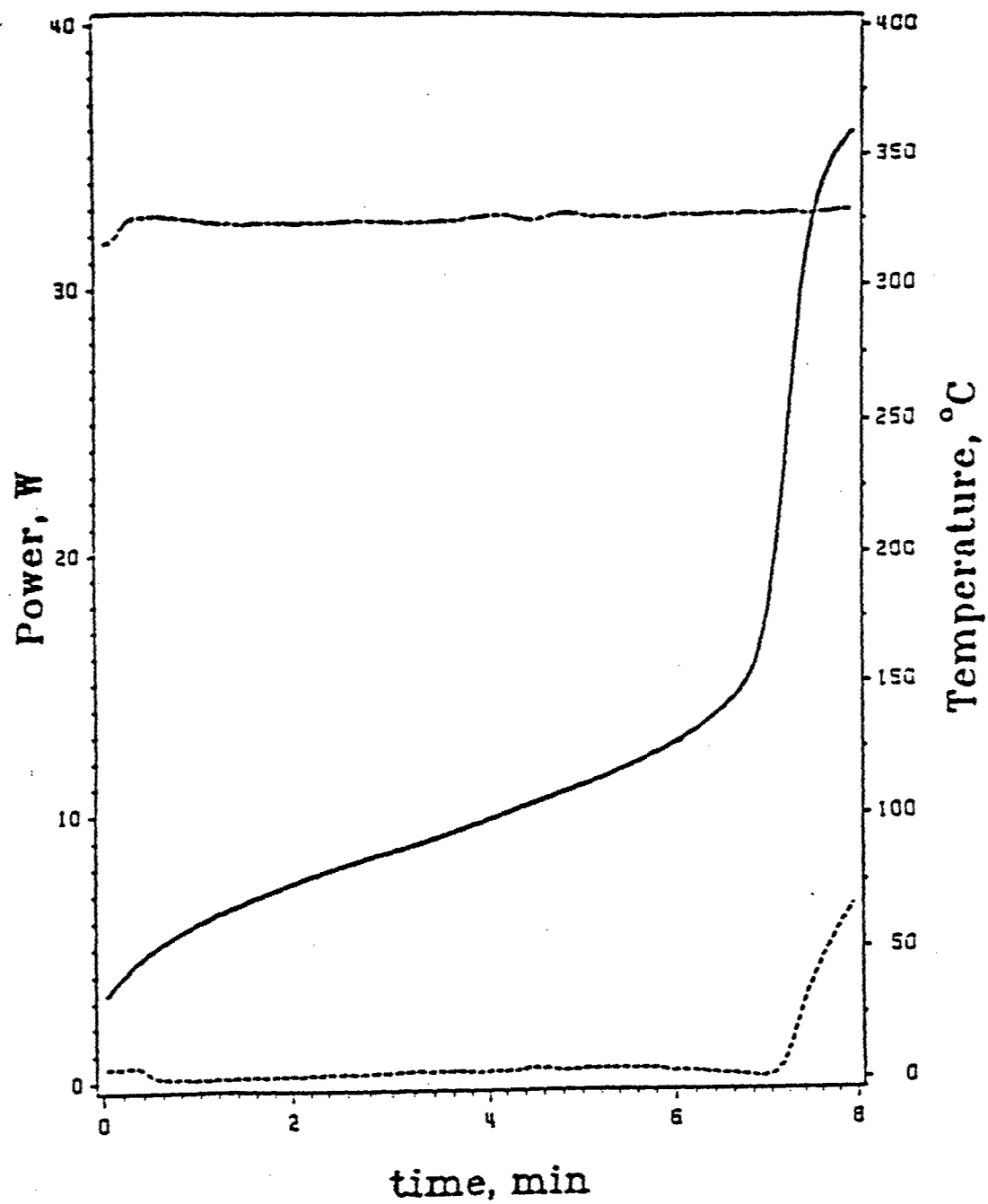
$(d\tau/dt)_{max} = 260°C$ at 2.45 GHz

Figure 14.

Variation of the temperature, input power and reflected power with time for styrene acrylonitrile copolymer in the standing wave applicator with a stub tuner.
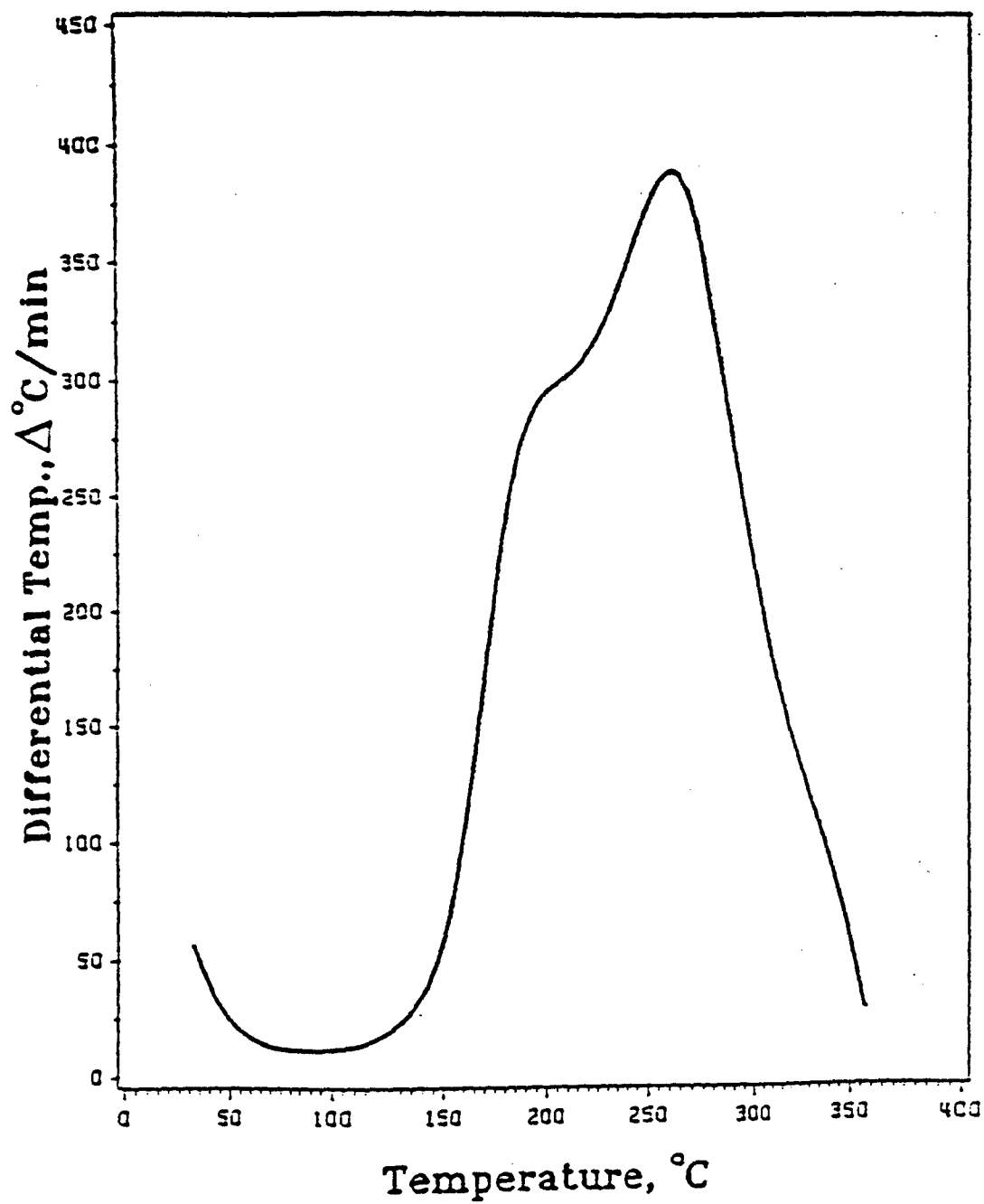
Figure 15.
Heating rate of styrene acrylonitrile copolymer versus temperature in the standing
wave applicator with a stub tuner.
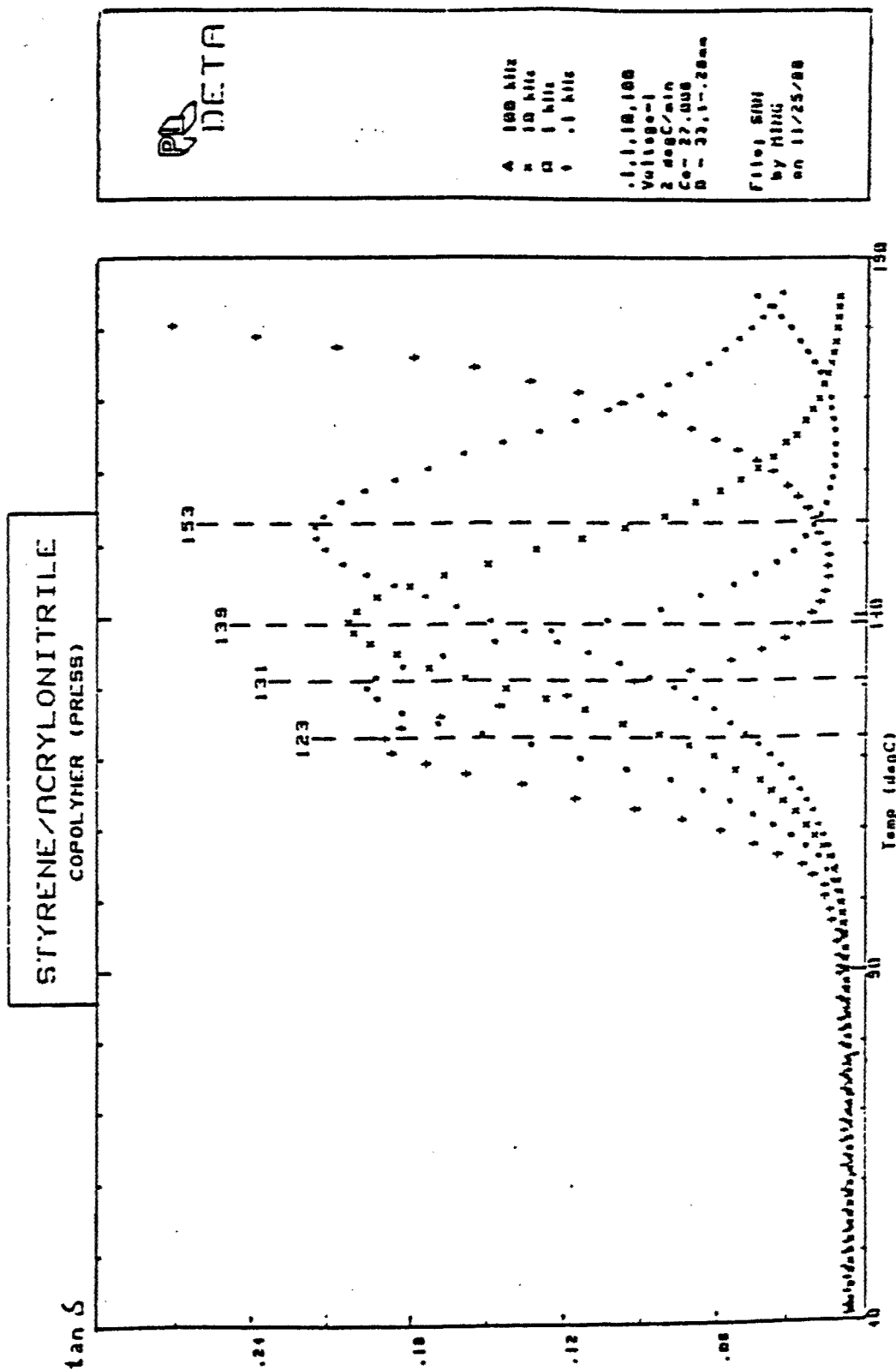
Figure 16.
Temperature dependence of the loss tangent of styrene acrylonitrile copolymer at various frequencies.
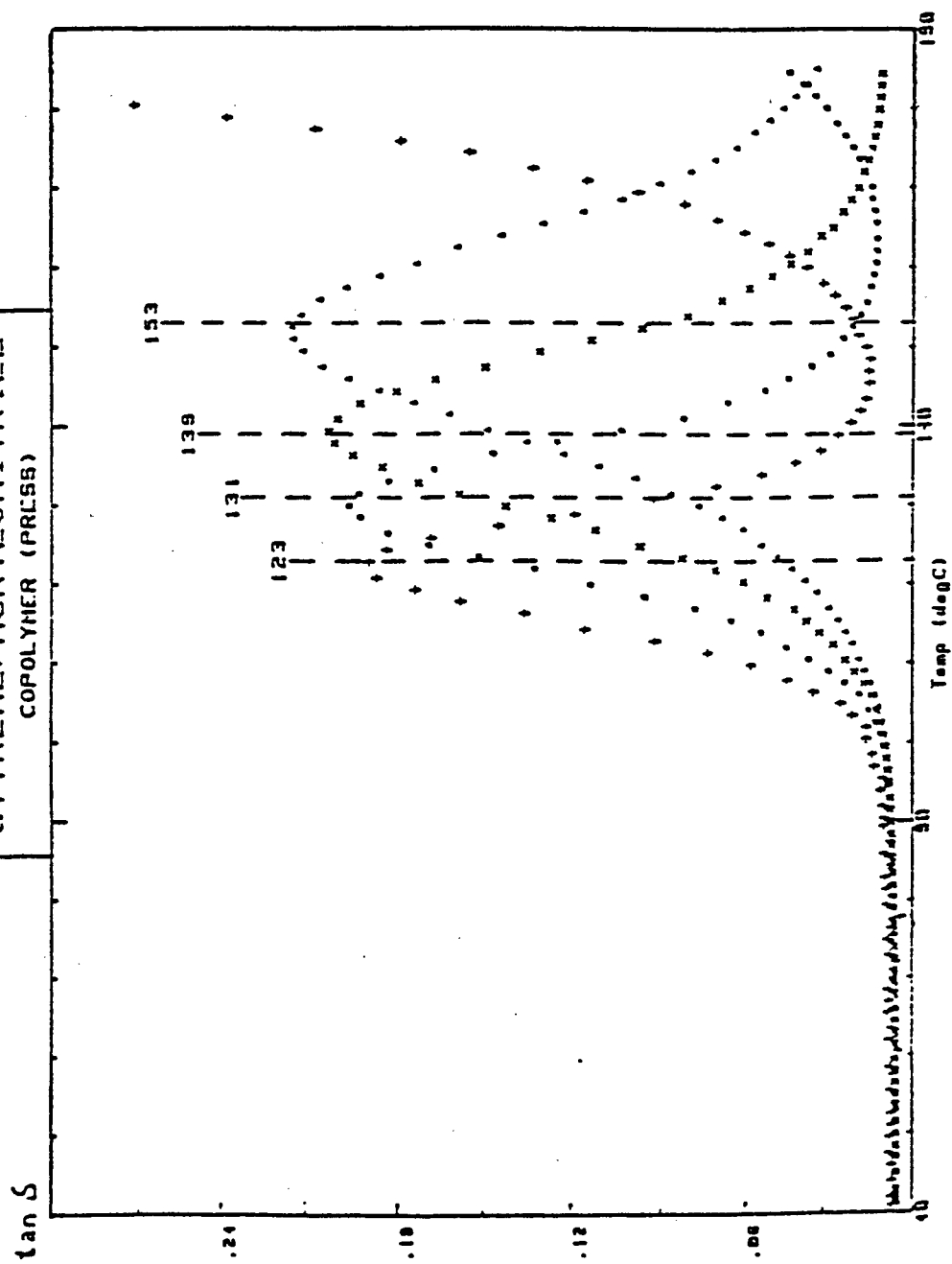
Figure 17.
WLF relationship for styrene acrylonitrile copolymer

189

# THE MICROWAVE PROCESSIBILITY OF SEMICRYSTALLINE POLYMERS

M. Chen[1], J. W. Hellgeth, E. J. Siochi[2], T. C. Ward* and J.E. McGrath

NSF STC: High Performance Polymeric Adhesives and Composites and
Department of Chemistry
Virginia Polytechnic Institute and State University
Blacksburg, VA 24061-0212

## ABSTRACT

The objective of this effort has been to investigate the relationship between polymer structure and microwave absorptivity. In this paper, the microwave processing of semicrystalline polymers such as poly(ether ether ketone) (PEEK), nylons, poly(ethylene terephthalate) (PET) via a cylindrical resonance wave cavity and a rectangular standing wave applicator is described. These polymeric materials were irradiated in a low power ( <50W) electric field at 2.45 GHz. Silicone flexible molds were necessary for improved processing of nylons and PEEK at temperatures below their $T_c$. Rapid heating rates were observed between the glass transition temperature, $T_g$, and the melting temperature, $T_m$, for all these polymers provided that $T_c$ was exceeded. Both Dynamic Mechanical Thermal Analysis (DMTA) and Dielectric Thermal Analysis (DETA) spectra were utilized to predict the heating phenomena between amorphous and semicrystalline materials and to explain the rapid crystallizing rate of PEEK above its glass transition temperature. Correlations were drawn between a) the apparent activation energy and the critical temperature and b) the shape of the dielectric spectra at 2.45 GHz and its shape in kHz region.

# INTRODUCTION

In preceding papers (1,2), microwave energy absorption of nitrile rubbers and the dielectric behavior of amorphous thermoplastics were examined in detail. In contrast to the nitrile rubbers, a combination of microwave and conventional thermal heating was found to improve the absorption of microwave energy by glassy polymers. By externally heating the glassy material above its critical temperature for dielectric loss, $T_c$, the dielectric relaxation peaks observed at low frequency were moved into the microwave region. Within this dispersion region, $d\varepsilon''/dT$ was large and positive on the cool side of the dielectric relaxation versus temperature spectrum and as such, rapid heating occurred.

Since the mechanism of microwave heating is independent of thermal conductivity, microwave heating avoids heat transfer rate problems encountered in conventional thermal heating where the low thermal conductivities of polymers is problematic. Due to the high temperatures needed to process semicrystalline polymers, the avoidance of thermal gradients as a result of microwave processing offers distinct advantages. Microwave energy, with its long wavelength, offers a deeper penetration than ultraviolet (UV) or electron beam irradiation but does not possess sufficient energy to cause bond cleavage. Only accelerated dissipative heating occurs in microwave processing. In this way, energy may be distributed rapidly throughout the volume of the material. Surface overheating or uneven catalyst decomposition is avoided. When two materials are simultaneously subjected to microwave irradiation, the higher loss material will be heated more rapidly than the lower loss material provided that the dispersion as a whole is properly located near $T_c$. In addition, the microwave heating process can be switched at high rates in response to a control signal. Therefore, processing can be controlled more accurately than in conventional methods (3-8).

Several articles have recently appeared in the literature on the microwave processing and diagnosis of epoxy/amine resins as well as nylon 66 (9-15). These same researchers described a field pattern study for a single-mode cylindrical cavity applicator. One particular single mode was found to be especially useful for heating monofilament fibers (16). Other researchers have found that ultradrawing under microwave heating through a circular or rectangular waveguide was most effective for obtaining high modulus materials (17-24).

In this paper, the processing of semicrystalline polymers such as poly(ether ether ketone) (PEEK), nylons, poly(ethylene terephthalate) (PET) via a cylindrical resonance wave cavity and a rectangular standing wave applicator is described.

191

Rapid heating rates were observed between the glass transition temperature, $T_g$, and the melting temperature, $T_m$, for all these polymers provided that $T_c$ was exceeded. By conventional thermal methods, the processing temperature should be greater than the melting temperature of the polymer. As in the previous papers (1,2), both DMTA and DETA spectra were utilized to predict the heating phenomena between amorphous and semicrystalline materials and specifically, to explain the rapid crystallizing rate of PEEK just above its glass transition temperature. Here, the objective was to gain an understanding of the mechanisms involved in absorption of microwave radiation by semicrystalline polymers. Modifications of processing methods were then investigated for improved processing of these materials.

## EXPERIMENTAL

### MATERIALS

The glass transition temperatures, melting temperatures and suppliers of the semicrystalline materials studied and the silicone flexible mold used to support the sample are summarized in Table 1. Films were prepared by using a platten press to heat and mold the polymers just above (0-10°C) their respective $T_m$'s. The amorphous counterparts of the crystalline polymers were prepared by quenching from their melt state into an ice water bath. Samples were then dried in a vacuum oven at just below their respective $T_g$'s for 24 hours. These films were kept in the desiccator until they were used for the DETA, DMTA and microwave experiments. Semicrystalline PEEK was prepared by annealing at 293°C for 50 minutes before dropping into the bath of ice water. Silicone flexible molds were made by mixing the necessary components and vacuum degassing several times. This mixture was cured at room temperature for 24 hours, then further cured under vacuum at 200°C for 24 hours.

### DISPERSION SPECTROMETER SYSTEMS

Polymer Laboratory's Dielectric Thermal Analyzer (DETA) and Dynamic Mechanical Thermal Analyzer (DMTA) were used to provide comprehensive relaxation spectra covering the broad frequency range of 1 Hz to 100 kHz. Dielectric spectra from -150°C to $T_m$ were obtained via DETA at frequencies of 0.1, 1, 10 & 100 kHz. DMTA thermal spectra from -150°C to $T_m$ were obtained by using the DMTA at frequencies of 1, 3 and 10 Hz. The bending mode was used for DMTA testing.

### MICROWAVE APPLICATOR SYSTEM

192

A cylindrical cavity applicator, shown schematically in Figures 1 and 2 (12-13), was used to study the processing of nylon and PEEK. The seven inch cylindrical cavity was designed and constructed by Michigan State University. Several defined modes can exist in this cavity by adjusting the cavity length (25-27) via a sliding short. The $TE_{111}$ mode was chosen to process the polymers described in this paper. The field distributions of the two-dimensional $TE_{11}$ mode and the three-dimensional $TE_{111}$ mode are shown schematically in Figure 3. The lowest mode, $TE_{111}$, exists in this empty cylindrical cavity with a theoretical cavity length of 6.69 cm. Prior to microwave processing, the specimens (1 cm x 1 cm x 0.5 cm) were placed in the trough of a silicone flexible mold. The size of the silicone mold was about 2 cm x 2 cm x 1.2 cm. Two more pieces of silicone mold were stacked to support the specimen and to raise the specimen to the center of the $TE_{111}$ mode. An additional silicone mold was placed on the top of the specimen in order to secure the fiber optic temperature probe (1). The other function of the top mold was to insulate the sample to prevent heat convection losses from the specimen to the air. The cylindrical cavity applicator is quite efficient as the radiation from the source is continuously reflected from the walls of the cavity, passing through the specimen many times until it is absorbed.

Due to the size of the specimen in the form of films, a standing wave applicator, described in detail previously (1,2), was used to process PET. Samples were stacked contiguously and placed into the center section of the 1/2 in. i.d. teflon sample holder.

## RESULTS AND DISCUSSION

### THERMAL DISPERSION SPECTRA FROM DETA AND DMTA

As the molding material may also interact with the applied electromagnetic field and influence the heating of specimens, its heating behavior was examined fully. The temperature dependence of dielectric constant and loss tangent of the silicone flexible mold at 100 kHz is revealed in Figure 4. A transition around -90°C was identified as the glass transition temperature of the silicone rubber. A broad transition between -20°C and 80°C was attributed to the filler. The maximum value of tanδ was 0.016. Thus, the silicone mold was a relatively low dielectric loss material in the microwave field. On this basis, the influence of the molding material upon specimen heating behavior and electromagnetic field interaction near or above a specimen's $T_c$ was considered negligible. However, at temperatures well below $T_c$, the silicone mold interaction with the electric field would yield important heating effects for processing.

The typical dielectric transition spectra (tanδ vs. temperature) of nylon 12 at 0.1, 1, 10 and 100 kHz is displayed in Figure 5. A comparison of nylon 6, 6/12 and 12 DETA spectra demonstrated that the greater number of amide groups in the main chain of nylons forced the transitions to be shifted to slightly higher temperatures. This was expected as the dielectric properties of nylons are mainly determined by inter-molecular and intra-molecular hydrogen bonds of the amide groups. The electrical conductivity is high due to proton transfer along the hydrogen bonding chains. The height of the tanδ peak, however, was difficult to compare. This difficulty was due in part to possible variations in percent crystallinity among the different nylon specimens. The apparent activation energies calculated from the logarithm of frequency versus the reciprocal of absolute temperature in the kHz region are given in Table 2. Nylon 6 had the highest activation energy yet its temperature window between $T_c$ and $T_g$ was smaller than that of nylon 6/12 and nylon 12.

Similarly, the dielectric transition spectra were obtained for amorphous and semicrystalline PEEK specimens. The dielectric loss spectrum of the amorphous material shown in Figure 6 clearly reveals a rapid crystallization phenomenon at 160°C. At the beginning of the transition, the dielectric constant, $\varepsilon'$, and the dielectric loss factor, $\varepsilon''$, increased with rising temperature. This would indicate greater mobility of polar groups along the main chain. The rapid crystallization of PEEK into the crystalline phase resulted in immobilization of the dipoles. As such, the alternating electric field had little effect upon orientation of the dipoles in the polymer. Once beyond the crystallization region, $\varepsilon'$ increased again to a maximum value as the crystallites melted. At higher temperature, the electric field once again could not couple with the sample as the material transformed to the melt state so that $\varepsilon'$ decreased slowly with increasing temperature. Complementary data on this crystallization phenomenon was also obtained via the DMTA experiment of amorphous PEEK at 1 Hz. This is given in Figure 7. Here, the thickness of the specimen was 3 mm and were tested in a dual cantilever mode with a peak displacement amplitude of 20 microns to monitor the viscoelastic properties. The logarithm of storage modulus (in Pascals) drops from 9.6 at 140°C to 6.3 around 155°C indicating the typical 3 decade decay in modulus for the glass to rubber transition. The sudden rise in modulus just above 155°C is due to the rapid crystallization of PEEK. This crystallization phenomena for PEEK can be seen at other frequencies as well. For comparison, the dielectric transition of semicrystalline PEEK is given in the DETA spectra presented in Figure 8. In the glass transition region, $\varepsilon'$ and $\varepsilon''$ increased continuously. The temperature at maximum $\varepsilon''$ for semicrystalline PEEK was almost the same as that for amorphous PEEK. This would indicate amorphous phase involvement. In the DMTA spectra for semicrystalline PEEK, the

logarithm of the storage modulus only drops by 0.6 in the glass transition region. The extremely high activation energy of amorphous PEEK suggested the similarity of heating rates in comparing amorphous PEEK and semicrystalline PEEK.

The DETA spectra of the amorphous PET is illustrated in Figure 9. For PET, the dielectric constant increased in the glass transition region from 70°C to 110°C. Above 110°C, $\varepsilon'$ decreased as crystallinity increased. Between 120°C and 200°C, $\varepsilon'$ decreased slowly. Beyond 200°C, ionic conductivity became significant so that $\tan\delta$ became very large. The logarithm of $\tan\delta$ versus temperature is also given in Figure 10. The crystallization phenomena for PET was detected from the shape of the higher temperature side of the transition region. By increasing the crystallinity, the dielectric $\alpha$ relaxation peak decreased.

All the DETA spectra described above have their $\varepsilon'$ maxima closer to $T_g$ rather than to $T_m$. The activation energies of most of these semicrystalline polymers, as shown in Table 2, were much higher than those of the amorphous polymers mentioned in a preceding paper (2). In general, the more crystalline the polymer, the higher the $T_g$, and the higher the activation energy. Therefore, the shift in the dipolar relaxation spectra caused by frequency rise will be smaller. In other words, the window between $T_c$ and $T_g$ would be smaller for semicrystalline polymers. For a polymer with a wide window between $T_g$ and $T_m$, $T_c$ would be closer to $T_g$ rather than to $T_m$.

MICROWAVE EXPERIMENTAL RESULTS

The temperature variation of nylon 6, nylon 6/12, nylon 12 and the silicone flexible mold with time during irradiation is displayed in Figure 11. Here, the input power was 20 watts at a frequency of 2.45GHz and remained constant throughout the irradiation period. After an initial tuning period (1 minute), the reflected power level fell to less than one watt, but then steadily rose to approximately two watts over the irradiation period. During the first two minutes, the temperature rise was almost the same for all materials. After 2 minutes, the temperature of nylon 6 rose rapidly comparatively. It is suggested that is due either to the higher concentration of polar amide group (or hydrogen bond) or lower percent crystallinity. From a plot of $\varepsilon''$ vs. temperature, the slope, $d\varepsilon''/dT$, was high and positive and, as a consequence, the uncontrolled temperature rise of nylon 6 occurred. This phenomenon is termed the "runaway effect" and may be controlled through modulation of the electric field strength.

In contrast to nylon 6, the heating of nylon 12 and 6/12 started at approximately five minutes with a greater the temperature rise of nylon 6/12 than that of nylon 12.

The reason the final temperature of nylon 6/12 was lower than that of nylon 12 may be due to a difference in sample mass and variation in temperature probe placement. The influence of the silicone mold electromagnetic field interaction upon specimen heating served an important function. It must be noted that the purpose of the silicone mold was to have the mold absorb the microwave energy to heat itself and then transfer that heat to the semicrystalline polymers until their $T_c$'s were encountered. Thus, the function of the silicone mold was similar to the function of the strip heater in the preceding paper (2). For microwave heating of the silicone mold, the intrinsically low loss of the silicone rubber was improved through the introduction of fillers. The high electric field strength in the center of $TE_{111}$ mode developed adequate coupling with the low loss silicone mold to cause heating. The silicone mold had a broad, low dielectric loss spectra as shown in Figure 4. This broad loss transition allowed the mold to be heated easily over a wide temperature range. The silicone mold was heated slowly from room temperature to 95°C in 15 minutes with only 20 watts of input power. At room temperature, below the $T_g$ of nylons, the dielectric loss factors of dried nylons were small and thus, little interaction with the electromagnetic field occurred. Above the $T_c$ of nylons, microwave energy was absorbed by the specimens directly as the dielectric loss factors of nylons were higher than that of the silicone mold.

The microwave energy absorption of nylons was improved by the conductive heating of the specimens from the heat generated by the silicone mold. In Figure 12, a plot of heating rate versus temperature for nylon 6 under these conditions is presented as an example of the heating behavior of semicrystalline polymers. In previous discussions (1,2), the determination of $T_c$ is gained through taking the x-axis intercept of the "cool" side tangent of this peak. However, the critical temperatures for all of the semicrystalline polymers described in this paper could not be evaluated as the silicone mold contributed to the heating rate of the polymers and thus, skewed the mesurement of their intrinsic $T_c$'s. The maximum heating rate was about 360°C/min which is much faster than expected for thermal conductivity in conventional thermal heating.

The heating behavior of amorphous and semicrystalline PEEK was examined. The variation of input and reflected powers and temperature with time for amorphous PEEK is displayed in Figure 13. The input power was 43 watts which was about twice that applied to the nylons. The nominal $T_g$ of PEEK obtained by differential scanning calorimetry (DSC) was greater than 140°C and was dependent on the percentage of crystallinity. In a procedure similar to that used for the nylons, the silicone mold was heated first when starting at room temperature. The heat flowed from silicone mold to the PEEK specimen via thermal conduction at temperatures below the $T_c$ of PEEK. After 7.5 min., the temperature of PEEK was at approximately 170°C and the rate of

temperature rise began increasing. Due to the high activation energy and fast crystallization rate, the $T_c$ of amorphous PEEK was expected to be very close to its $T_g$. The high content of phenyl and ether groups in PEEK lowered the dipolar contribution of the polar ketone group. Thus, the temperature rise was under control for the low loss PEEK. After 11 minutes, the sample temperature tended to level off.

The heating behavior of semicrystalline PEEK was found to be essentially the same as that for the amorphous material. For comparison, the variation of input and reflected powers and temperature with time for semicrystalline PEEK are described in Figure 14. After irradiating the specimens for approximately nine minutes, the temperature rose substantially. The maximum heating rate of the semicrystalline PEEK, determined at the inflection point of this curve, was essentially the same as that for the amorphous material. The similarity of heating rates may be due to two reasons a) rapid crystallization occurs at temperatures just above $T_g$ and b) the heat capacity of the crystalline polymer is lower than the amorphous version. In Figure 14, there was an endothermic peak indicated by the rapid rise in reflected power between 12 and 14 minutes. The temperature dropped at around 350°C which was close to the $T_m$ of PEEK similar to its endothermic behavior found from differential scanning calorimetry.

In contrast to the above experiments, the heating behavior of PET was examined in a recteangular standing wave waveguide. The variation of powers and temperature with time for PET in a rectangular standing wave applicator is depicted in Figure 15. In these experiments, the input power was 20 watts. Here, the temperature increased slowly in the first 2.5 minutes. After 100°C, which may already be in the positive $d\varepsilon''/dT$ region, the temperature rose rapidly. The reflected power increased continuously after 3.5 minutes. PET was heated to its $T_m$ in 5 minutes by microwave processing. Interestingly, this rapid heating rate may cause different kinetic phenomena as compared to conventional thermal heating when the temperature passes through the crystallization zone. In the case of both PET and nylon 6, the heating phenomena showed the thermal runaway effect. Either decreasing the microwave energy or processing by pulsed control is necessary to avoid this runaway.

## CONCLUSION

The silicone flexible mold was necessary for improved energy absorption of nylons and PEEK at temperatures below their $T_c$. This suggests future industrial applications may utilize such multiphase processing. Above $T_c$, nylons and PEEK absorbed the microwave energy internally to rapidly heat above their respective melting points. Nylons, PEEK and PET, with a wide window between $T_g$ and $T_m$, were processed easily by microwave energy because of the rapid heating rates at

197

temperatures just above their $T_g$'s. Thus, their processing times and costs can be reduced. This fast heating rate can overcome the problem of low thermal conductivity of polymers, but computer monitoring of the signal would be needed to control the temperature by on/off power pulsing.

DETA spectra in the kHz region and DMTA spectra in the Hz region were used to explain the similar heating rates of amorphous and semicrystalline PEEK at 2.45 GHz. Amorphous PEEK rapidly decreased in modulus at temperatures just around the $T_g$, but recovered as a result of the fast crystallization which occurred just above $T_g$ in temperature. Therefore, both materials became semicrystalline during low power microwave processing. When a material is heated between its $T_g$ and $T_m$, its rate of crystallization determines the amount of crystallinity which can develop. It may be possible in microwave processing at very high electric field strength, however, to exceed the rate of crystallization so that it wuold be easier to heat the material above its melting point while producing fewer crystallites in the zone above $T_g$.

The heating rate of nylons depended on the percentage of amide group (or hydrogen bonding) in the main chain. The crystallinity not only decreased the values of $\varepsilon''$, but also moved the maximum of the $\alpha$ and $\beta$ relaxations to higher temperatures (or lower frequencies). The change in crystallinity affected the $\alpha$ relaxation processes more than the $\beta$ relaxation processes. In terms of microwave processing, it is important to consider the effect of crystallinity on the position of the dielectric loss peaks as well as their loss peak amplitudes.

## ACKNOWLEDGEMENTS

198

# REFERENCES

1. M. Chen, E. J. Siochi, T. C. Ward and J. E. McGrath, *Poly. Eng. Sci.*, in press (1992)

2. M. Chen, E. J. Siochi, T. C. Ward and J. E. McGrath, *Poly. Eng. Sci.*, in press (1992)

3. A. C. Metaxas and R. J. Meredith, "Industrial Microwave Heating," Peter Peregrinus, London (1983).

4. D. A. Copson, "Microwave Heating," 2nd ed., The Avi Publishing Co., Connecticut (1975).

5. E. C. Okress, "Microwave Power Engineering Vol. 2: Applications," Academic Press, New York (1968).

6. P. Fellows, "Food Processing Technology: Principles and Practice," E. Horwood Ltd., New York (1988).

7. M. Le Maguer and P. Jelen, "Food Engineering and Process Applications Vol. 1: Transport Phenomena," Elsevier Applied Science Publishers, New York (1986).

8. H. F. Mark, N. M. Bikales, C. G. Overberger and G. Menges, "Encyclopedia of Polymer Science and Engineering, Vol. 5: Dielectric Heating to Embedding," 2nd ed., John Wiley & Sons, New York (1986).

9. J. Jow, M. C. Hawley, M. C. Finzel and J. Asmussen, *J. Microwave Power EE*, 24, (1989).

10. J. Jow, J. D. Delong and M. C. Hawley, *SAMPE Quarterly*, 20, 46 (1989).

11. J. Jow, M. C. Hawley and M. Finzel, *Rev. Sci. Instrum.*, 60, 96 (1989).

12. J. Jow, M. C. Hawley, M. Finzel and T. Kern, *Polym. Eng. Sci.*, 28, 1450 (1988).

13. J. Jow, M. C. Hawley, M. Finzel, J. Asmussen, Jr., H. H. Lin and B. Manring, *IEEE Trans. Microwave Theory Tech.*, MTT-35, 1435 (1987).

14. J. Asmussen, H. H. Lin, B. Manring and R. Fritz, *Rev. Sci. Instrum.*, 58, 1477 (1987).

15. B. Manring, Master Thesis, Michigan State University, East Lansing, MI (1988).

16. H. F. Huang, *J. Microwave Power*, 11, 305 (1976).

17. M. Amano and K. Nakagawa, *Polym. Commun.*, 28, 119 (1987).

18. M. Amano and K. Nakagawa, *Polymer*, 28, 263 (1987).

19. K. Nakagawa and T. Konaka, *Polymer*, 27, 1553 (1986).

20. Y. Takeuchi, K. Nakagawa and F. Yamamoto, *Polymer*, 26, 1929 (1985).

21. K. Nakagawa, T. Konaka and S. Yamakawa, *Polymer*, 26, 84 (1985).

22. Y. Takeuchi, F. Yamamoto, K. Nakagawa and S. Yamakawa, *J. Polym. Sci. Polym. Phys. Ed.*, 23, 1193 (1985).

23. K. Nakagawa, O. Maeda and S. Yamakawa, *J. Polym. Sci. Polym. Lett. Ed.*, 21, 933 (1983).

24. A. E. Zachariades and R. S. Porter, "High Modulus Polymers: Approaches to Design and Development," Marcel Dekker, Inc., New York (1988).

25. V. K. Varadan, V. V. Varadan, Y. Ma and W. F. Hall, *IEEE Trans. Microwave Theory Tech.*, MTT-34, 251 (1986).

26. T. K. Ishii, "Microwave Engineering," The Ronald Press Co., New York (1966).

27. Y. F. Chen and Charles Y. C. Lee, *Polym. Mater. Sci. Eng.*, 60, 680 (1989).

Table 1

Thermal properties and sources of semicrystalline polymer

| Polymer | $T_g$, °C | $T_m$, °C | Source |
|---|---|---|---|
| PEEK | 150 | 334 | ICI |
| Nylon 6 | 63 | 229 | Polysciences |
| Nylon 612 | 46 | | SP$^2$ |
| Nylon 12 | 37 | 178 | SP$^2$ |
| Silicone mold | | | GE |
| PET | 81 | ~260 | SP$^2$ |

SP$^2$   (Scientific Polymer Products)

Table 2

$T_g$, $T_m$ and the activation energies in the kHz region of polymers

| Polymer | $T_g$ (°C) | $T_m$ (°C) | $\Delta E_a{}^*$ (kJ/mole) | $\Delta E_a\#$ (kJ/mole) | Remark |
|---------|-----------|-----------|---------|---------|--------|
| PEEK | 150 | 334 | 790 | 810 | Q in ice water |
| | | | 550 | | Cooled in DETA |
| Nylon6 | 63 | 229 | 370 | 410 | Q in ice water |
| | | | 350 | 380 | Q in press |
| Nylon612 | 46 | | 270 | 320 | Q in ice water |
| Nylon12 | 37 | 178 | 230 | 270 | Q in ice water |
| PET | 81 | 260 | 420 | 420 | Q in ice water |
| | | | 350 | 340 | Q in press |

* Activation energy calculated from the peak temp. of 1,10 & 100 kHz

# Activation energy calculated from the peak temp. of 0.1,1,10 & 100 kHz

Q: quenched
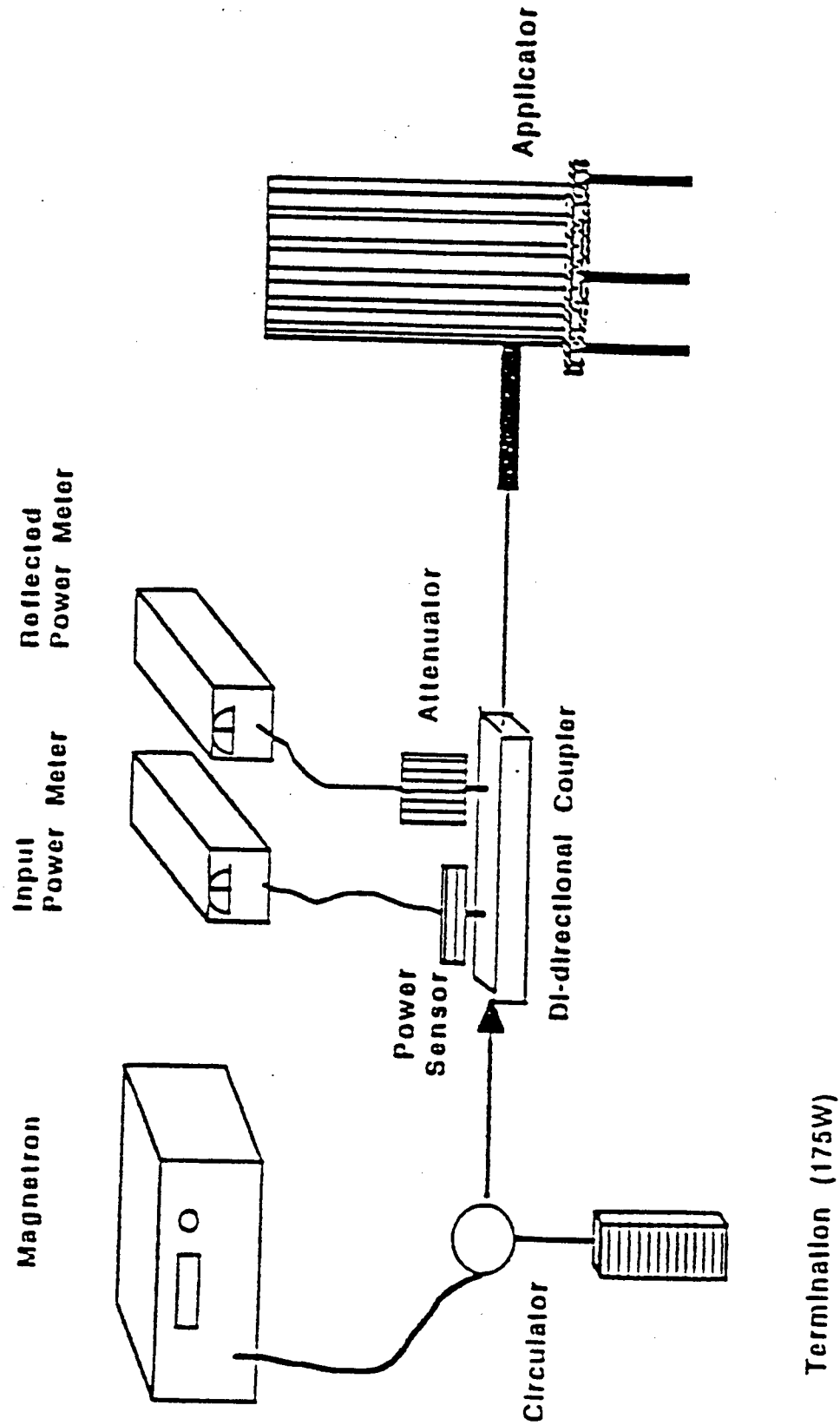
Figure 1.

Schematic of the experimental set-up for the cylindrical cavity applicator.
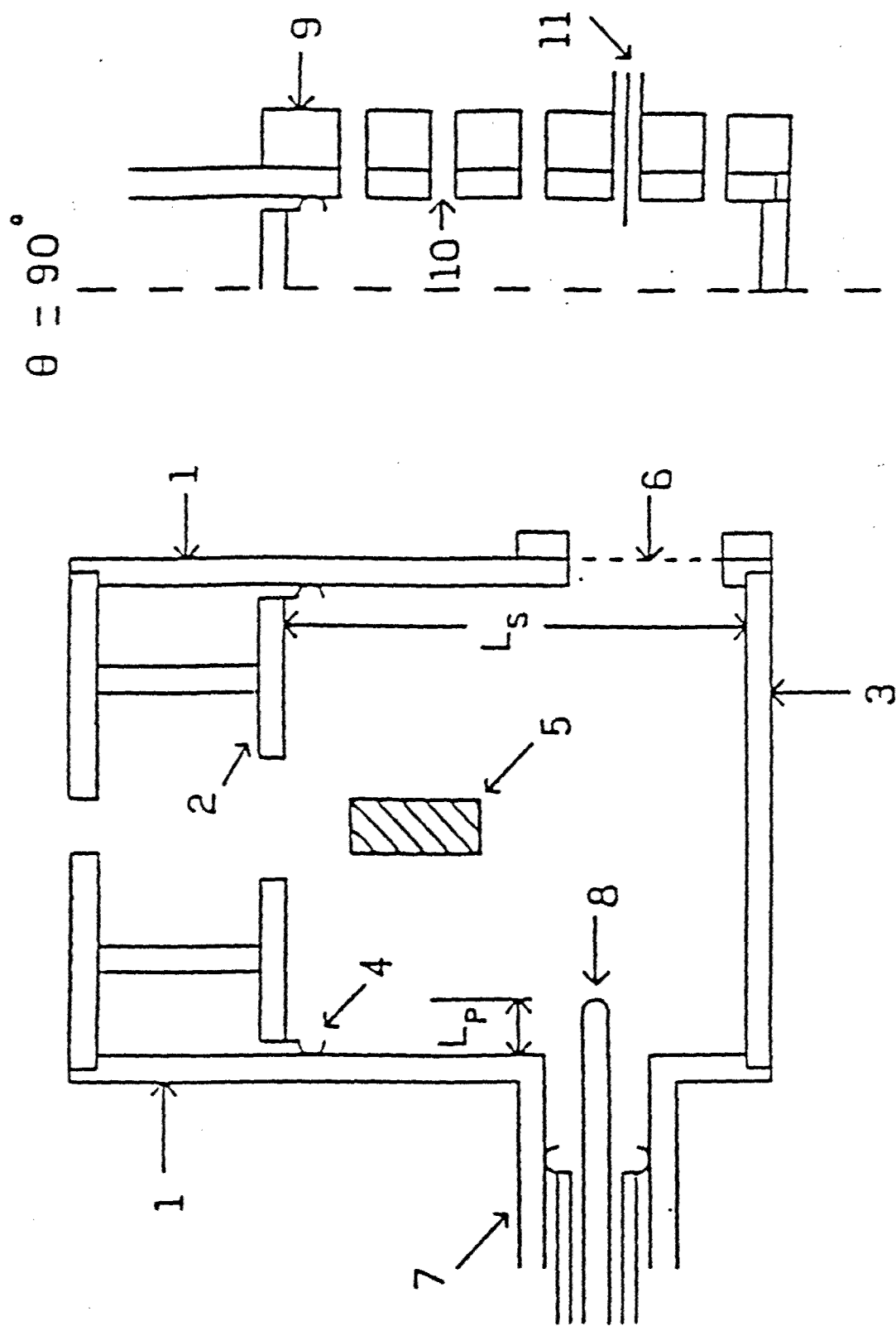
Figure 2.

Cross sectional view of the cylinderical cavity applicator. Full cross section is the θ = 0° plane passing through the input probe. Partial cross section θ = 90° displays the coaxial input. The numbered items are (1) conducting cylindrical shell, (2) sliiding short, (3) end plate, (4) silver finger stock, (5) process material, (6) screened viewing port, (7) coaxial input port, (8) adjustable coupling probe, (9) brass microcoax probe holder, (10) diagnostic holes and (11) micrococax electric field probe. [ref. 14]
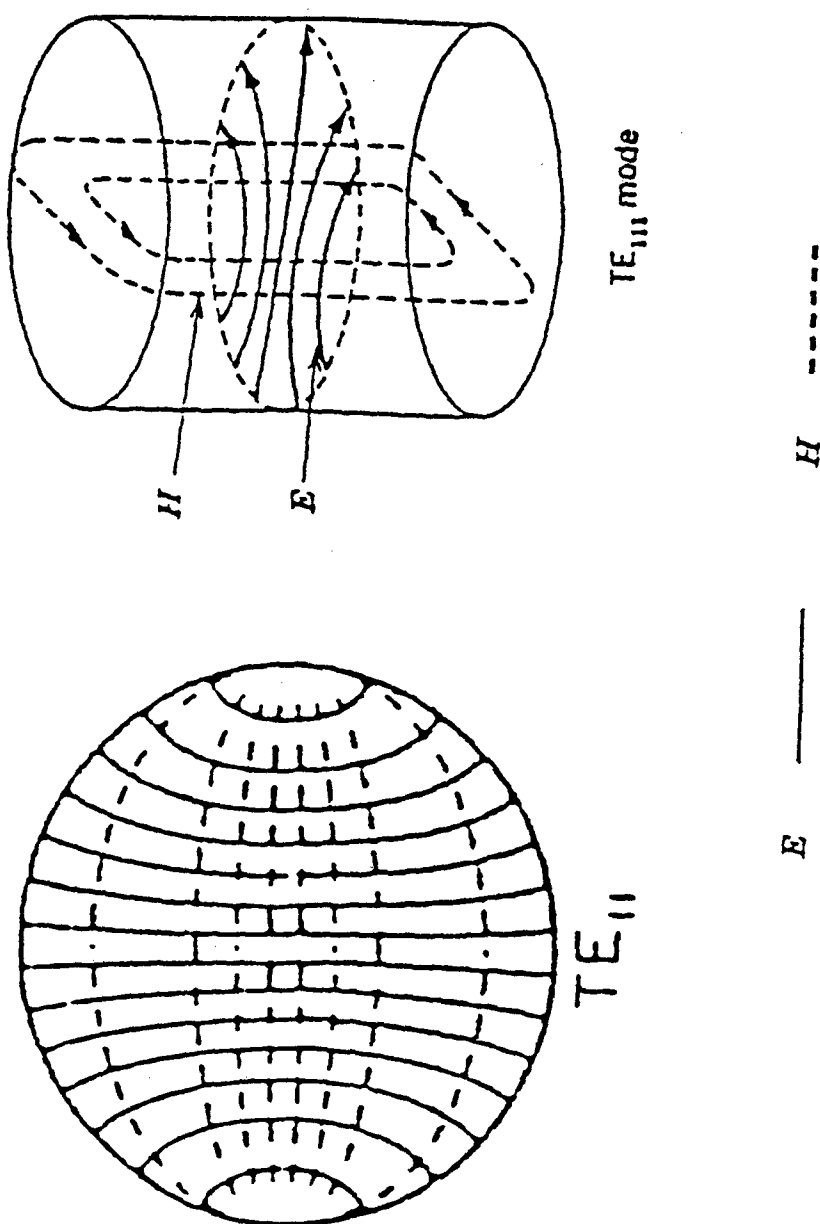
$TE_{11}$   field distribution for a circular waveguide.

$TE_{111}$   field distribution for a cylindrical cavity.

Figure 3.

Field lines for two-dimensional $TE_{11}$ mode and three-dimensional $TE_{111}$ mode.
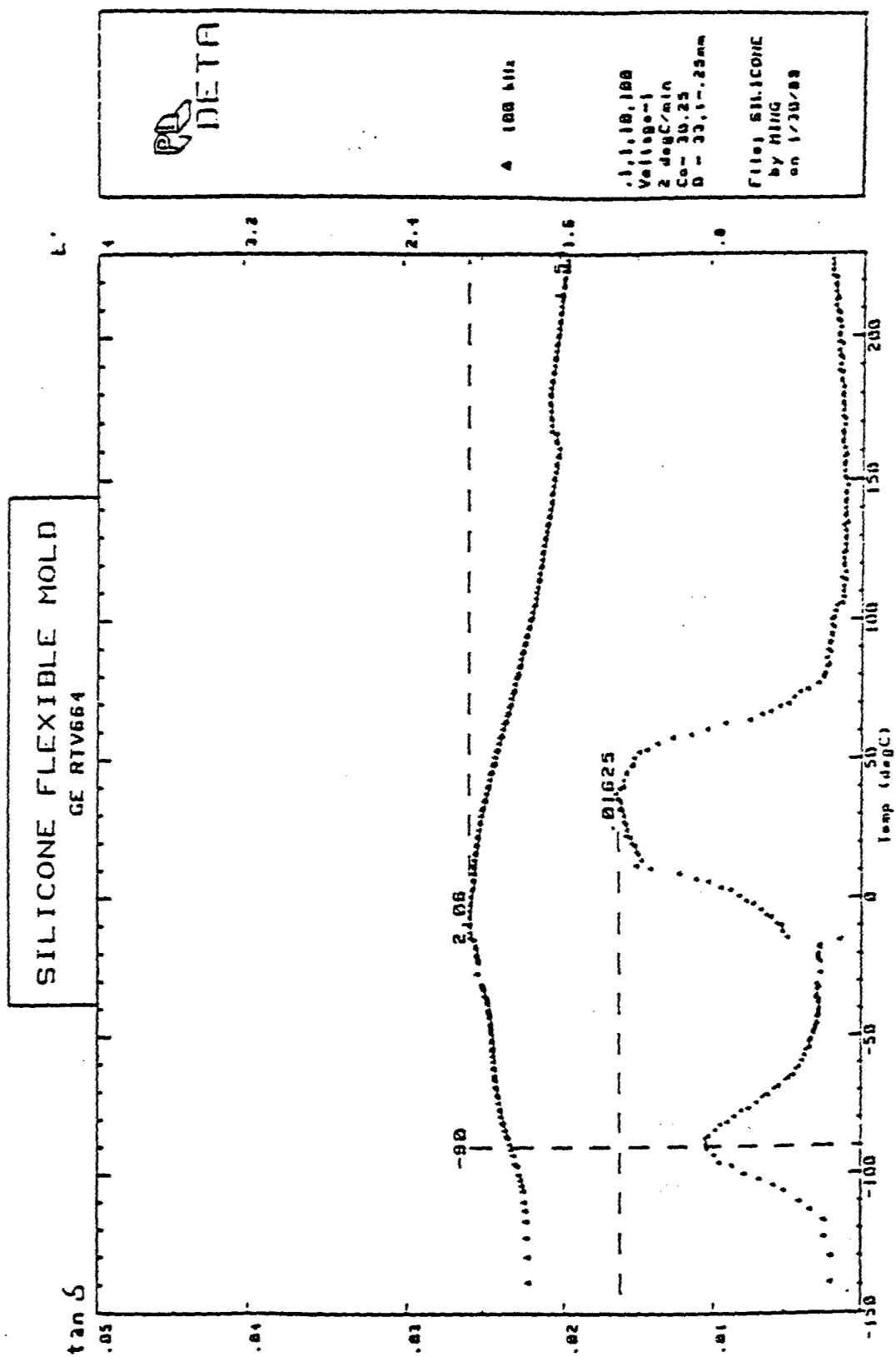
Figure 4.

Temperature dependence of the dielectric constant and the loss tangent of silicone flexible mold at 100 kHz.
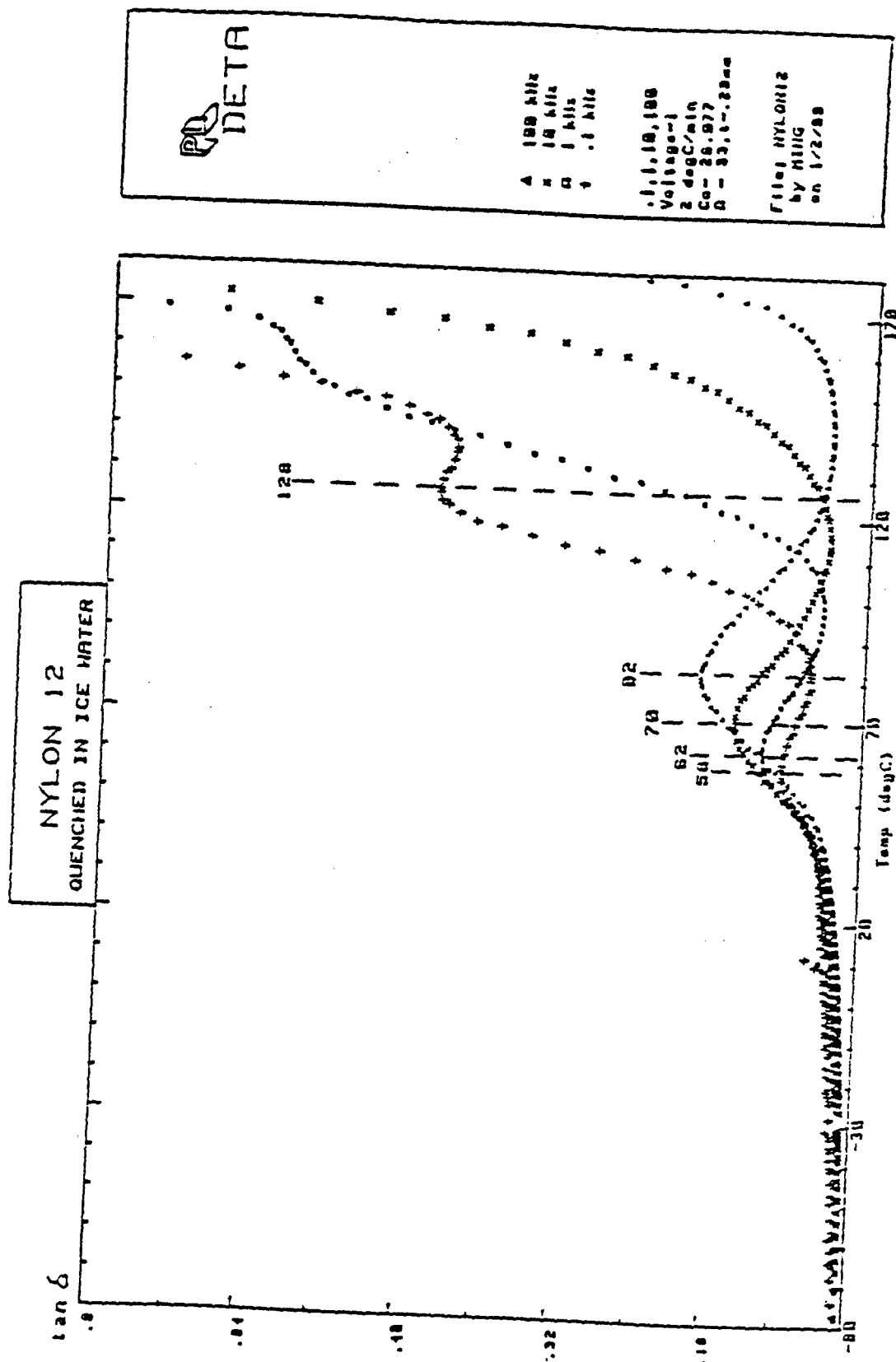
Figure 5.

Temperature dependence of the loss tangent of nylon 12 at various frequencies.
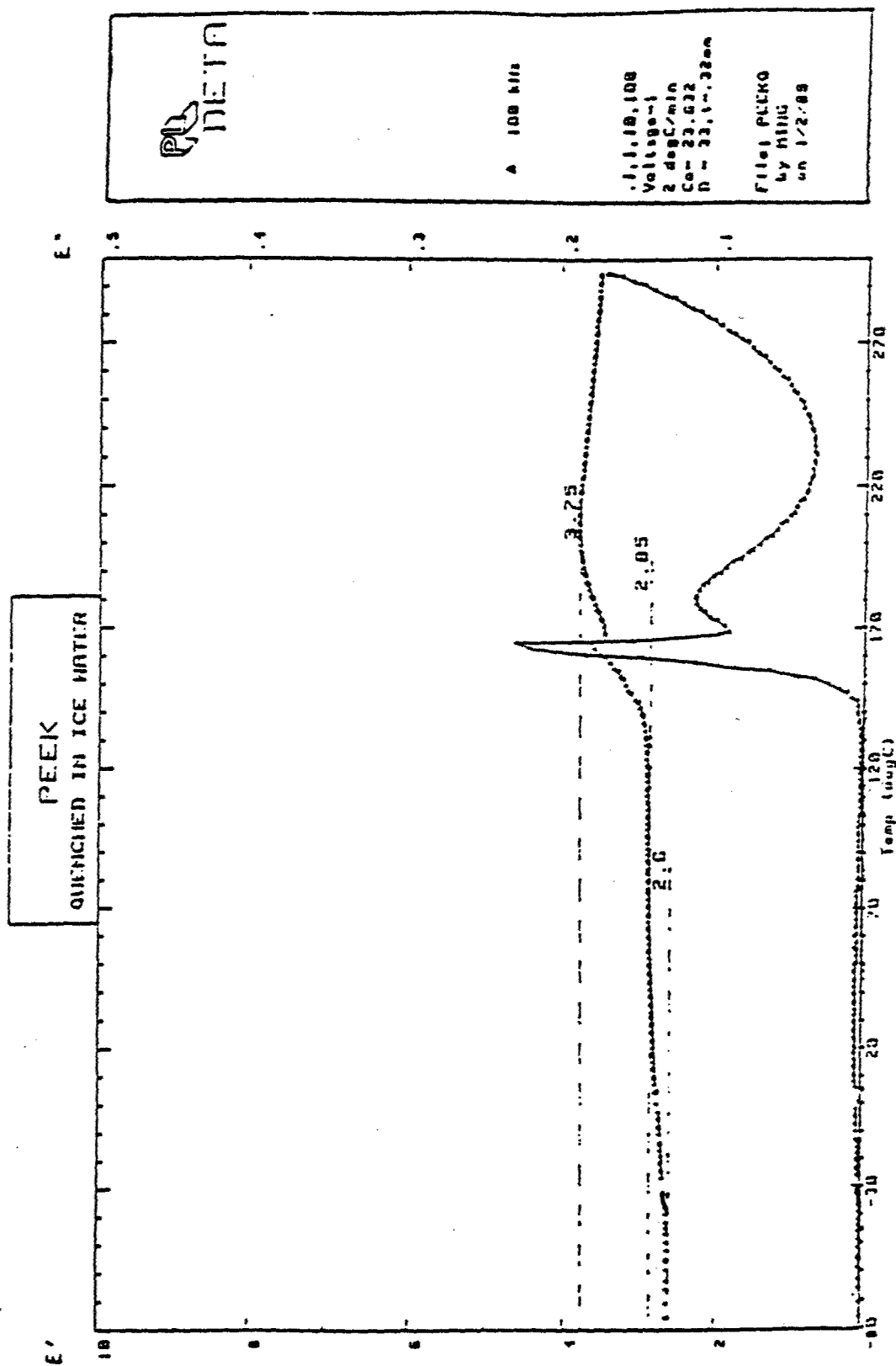
Figure 6.
Temperature dependence of the dielectric constant and the dielectric loss factor of amorphous PEEK at 100 kHz.

Figure 7.

Temperature dependence of the storage modulus of amorphous PEEK at various frequencies.

Figure 8.

Temperature dependence of the dielectric constant and the dielectric loss factor of semicrystalline PEEK at 100 kHz.
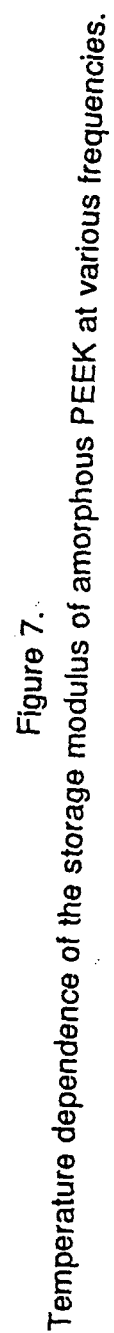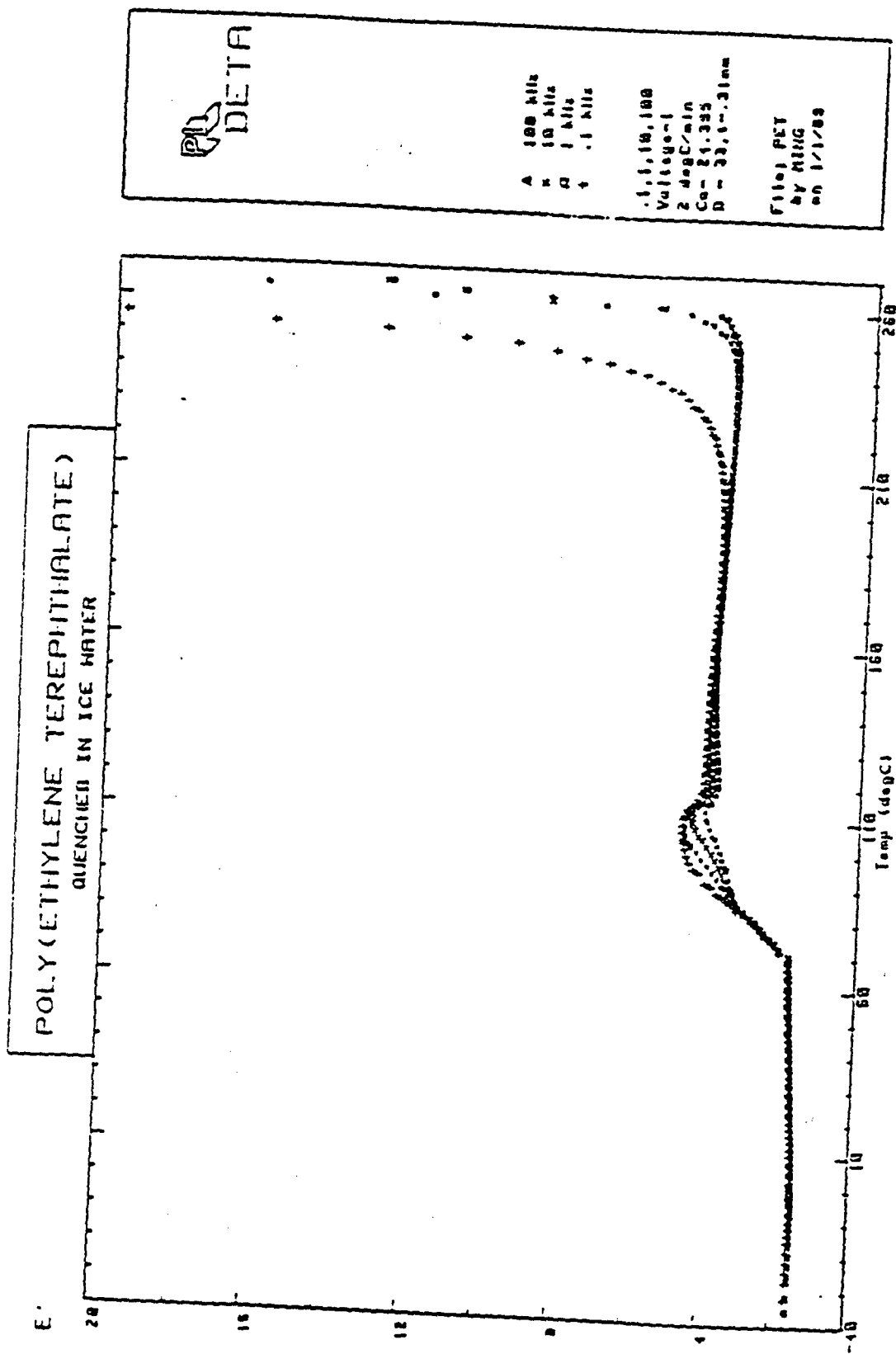
Figure 9.
Temperature dependence of the dielectric constant of PET at various frequencies.
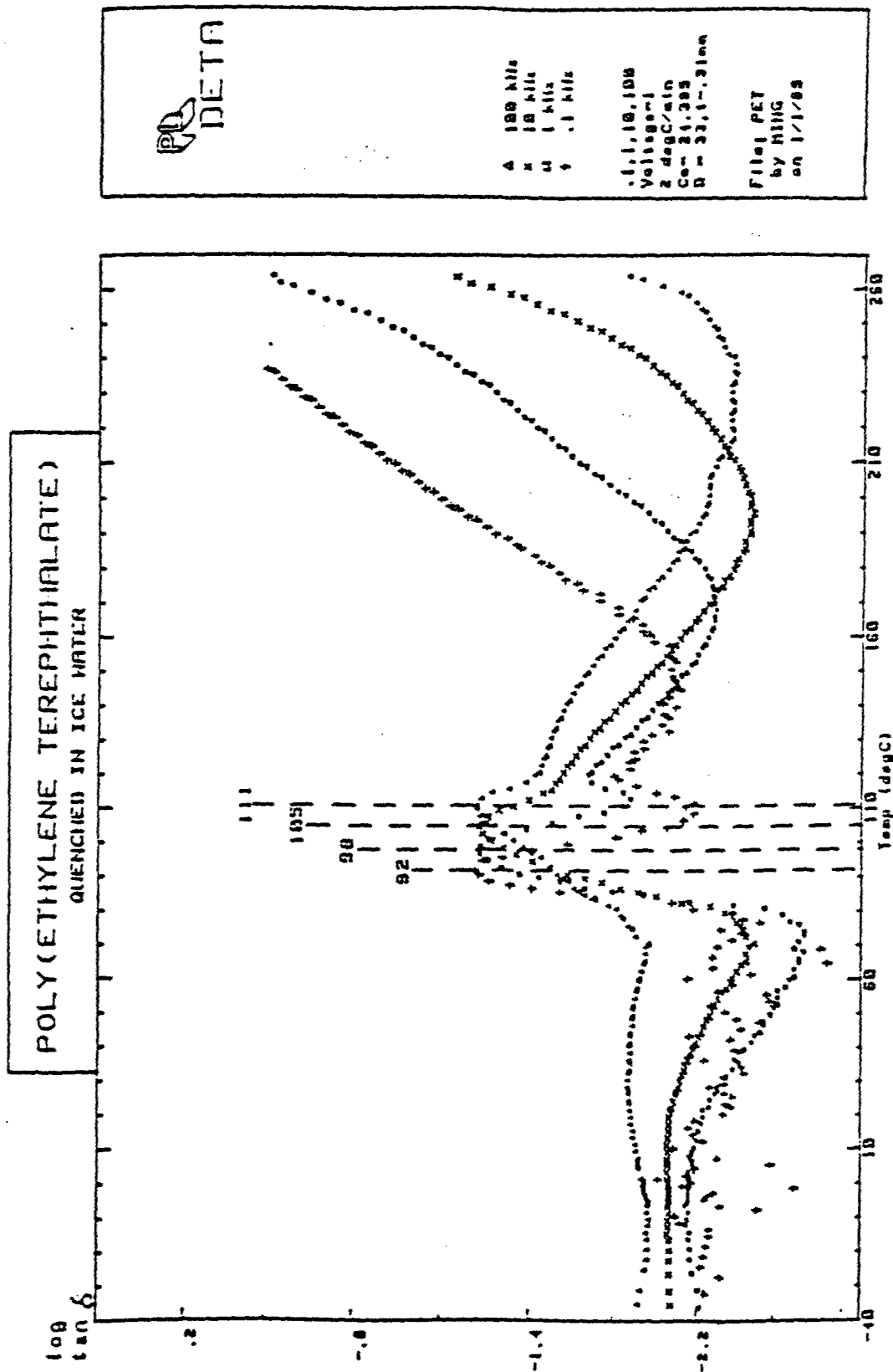
Figure 10.

Temperature dependence of the logarithm loss tangent of PET at various frequencies.
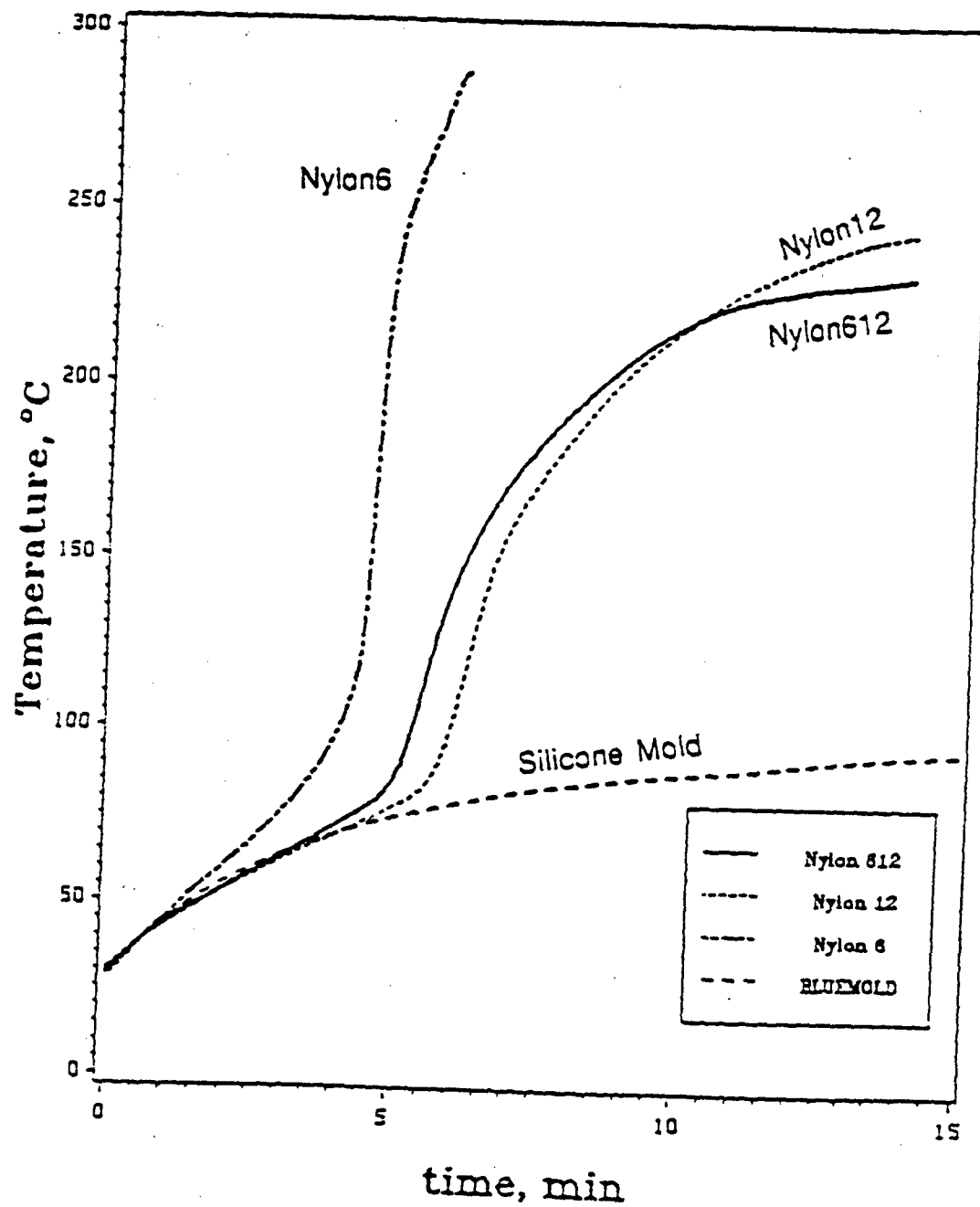
Figure 11.
Variation of the temperature of nylons and silicone mold with time in the center of $TE_{111}$ mode of a cylindrical cavity applicator. Input power was 20 watts.

213
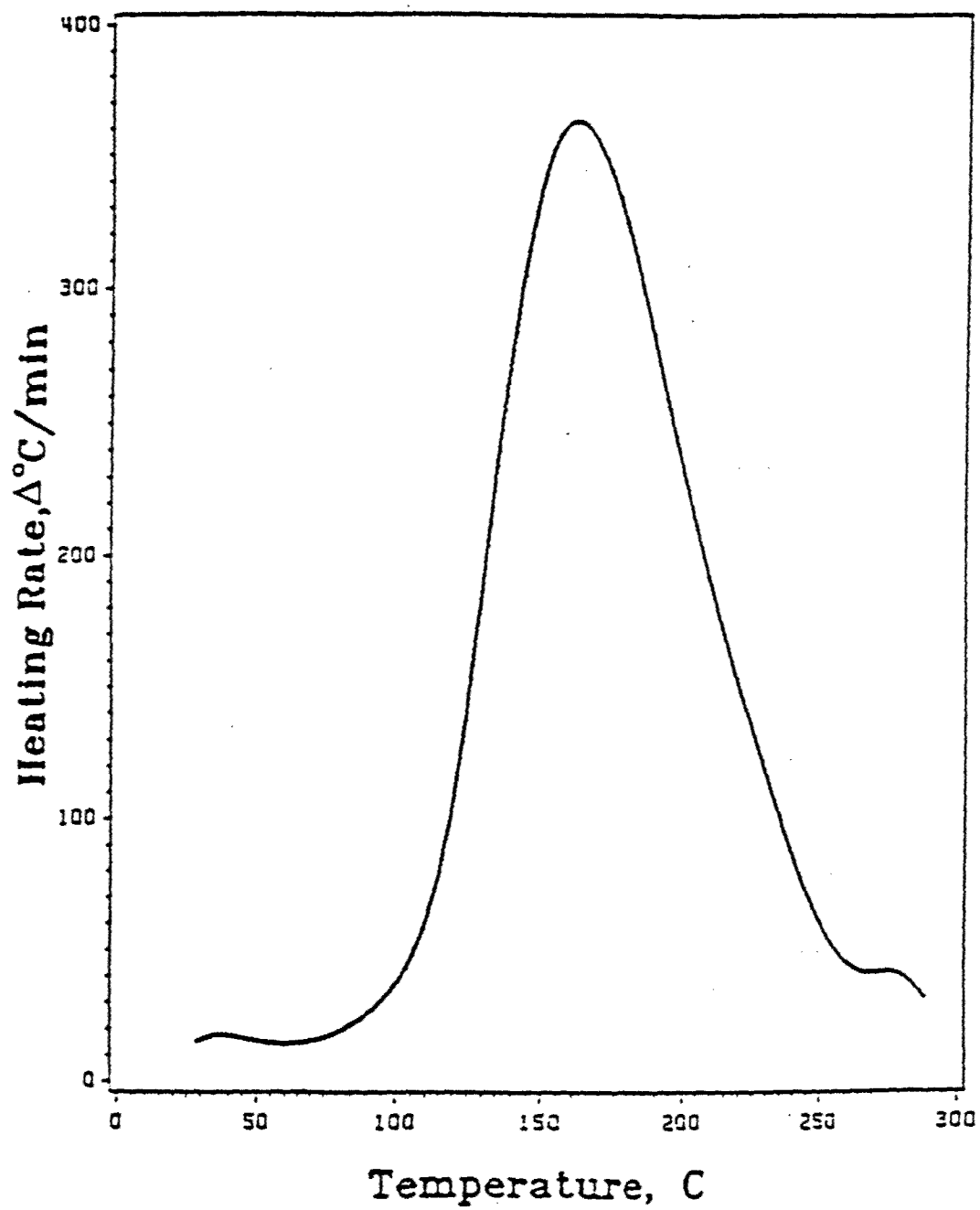
Figure 12.
Heating rate of nylon 6 versus temperature in the
center of $TE_{111}$ mode of a cylindrical cavity applicator.

Figure 13.

Variation of the temperature, input power and reflected power with time for amorphous
PEEK in the center of $TE_{111}$ mode of a cylindrical cavity applicator.

215

Figure 14.

Variation of the temperature, input power and reflected power with time for
semicrystalline PEEK in the center of TE₊₂₁₆mode of a cylindrical cavity applicator.

216

Figure 15.

Variation of the temperature, input power and reflected power with time for PET in the standing wave applicator with a stub tuner.
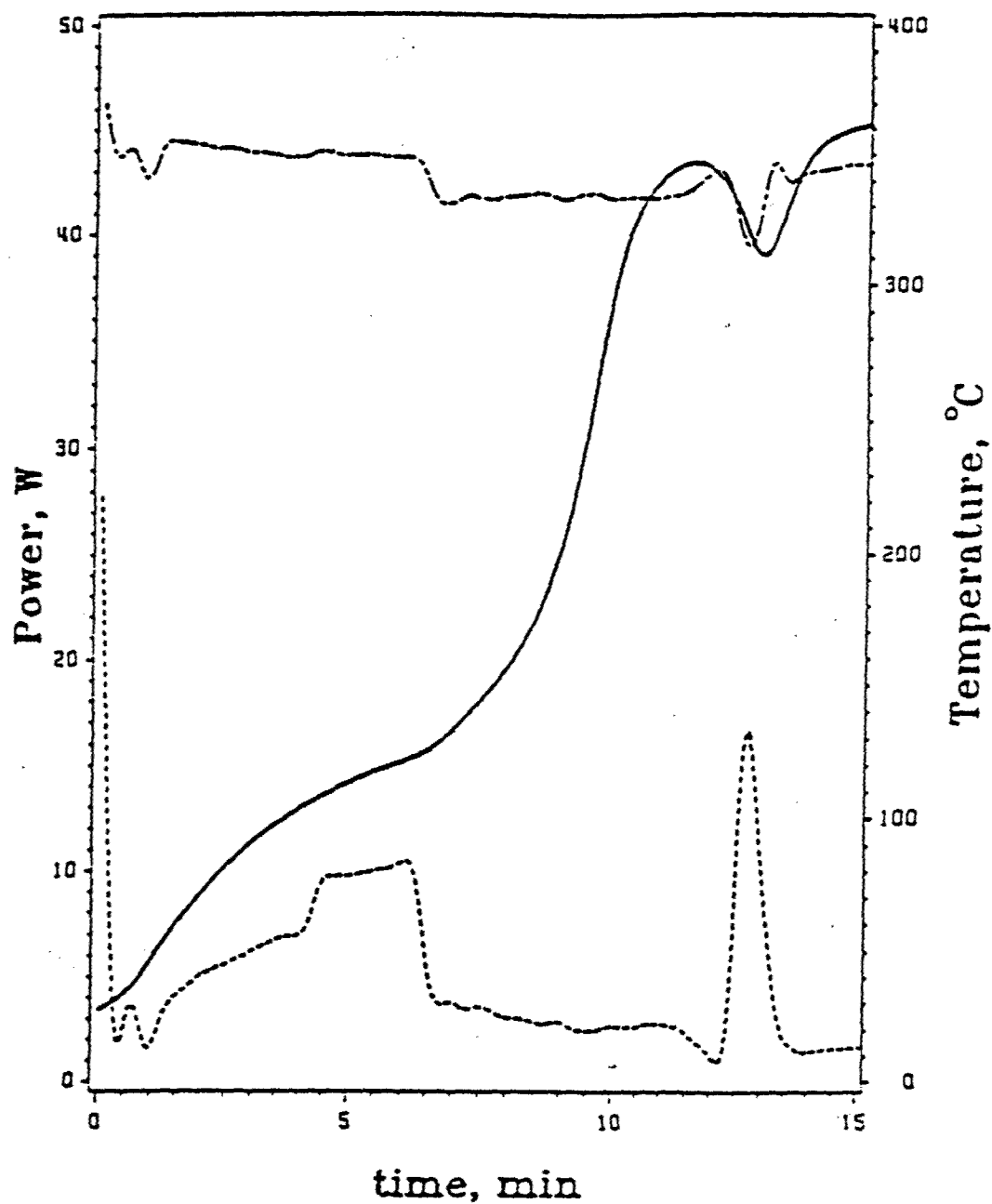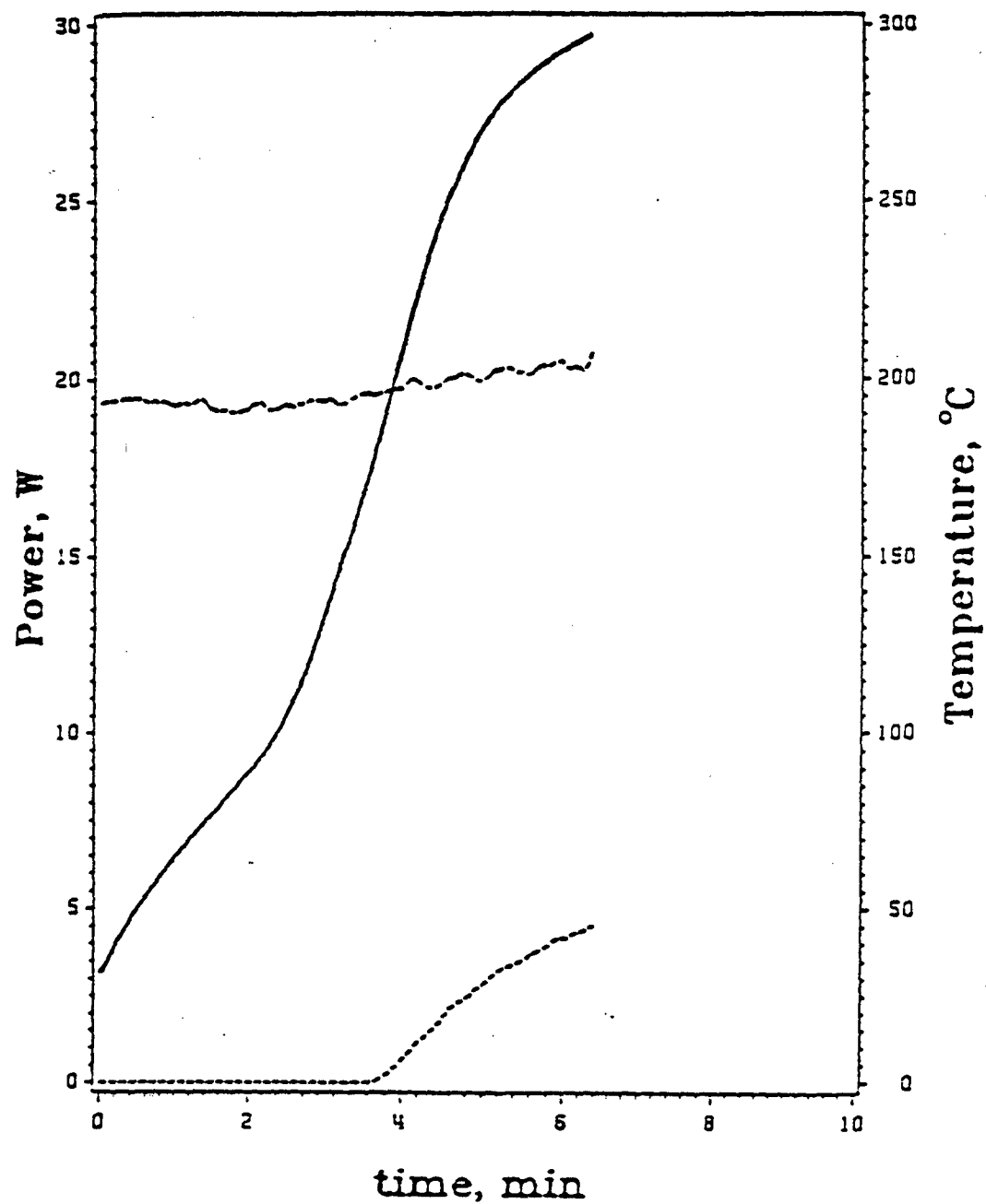
TOP     :INPUT POWER
BOTTOM :REFLECTED POWER
SOLID LINE :TEMPERATURE

# MICROWAVE PROCESSING OF POLYMERS AND POLYMERIC COMPOSITES

DR. CHARLES Y-C LEE
Air Force Materials Laboratory, WRDC/MLBP, Wright-Patterson Air Force Base,
OH 45433-6533

Microwave energy is commonly considered as a fast and efficient source of energy for heating materials. This perception can be easily verified by the proliferation of microwave ovens in household kitchens and the emerging usage of the technology in the food industry. From the standpoint of material science, coupling of microwave energy into materials during processing can be more than just shortening the heat-up time in conventional thermal treatment; this energy source can provide an additional degree of control over the properties developed during processing.

Under a multidisciplinary research program sponsored by Defense Advanced Research Projects Agency (DARPA) and managed by the US Air Force and Army, many fundamental issues of applying this technology to polymer and composite processing were addressed. The following seven papers are based on work supported by this program.

Researchers at Michigan State University (J. Asmussen and M. Hawley) designed an applicator with closed loop control so that the coupling of microwave energy into polymeric and composite materials could be studied in a controlled manner. The cavity enabled the setting of a well defined resonance mode prior to sample loading and the close loop control was used to change the power input level to accommodate material properties changes during processing by maintaining a well controlled heating profile.

Researchers at Virginia Polytechnic Institute (J. McGrath and T. Ward) have used this applicator and discovered many interesting phenomena in microwave processing of polymeric materials. Among the findings was the selectivity of chemistry in microwave coupling where one type of chemistry (imidization) was favored over another type (acetylenic reaction), thus potentially providing a new dimension of control over polymer synthesis and processing. The apparent activation energy of the kinetics appeared to be affected also, indicating that the effect was more than just a more efficient transfer of energy into the material bulk. In processing a two-component system, the phase separation morphology of the resultant samples can be controlled by the microwave energy coupling conditions. Other researchers at VPI (G. Wilkes et al) extended this technology to other materials including ceramers and found that the properties development can be accomplished in minutes instead of days.

While heating of dielectric materials and polymeric/glass fiber composites can be accomplished readily, application of microwave energy to carbon fiber composites has always been hampered by the conductive nature of the carbon fibers. Research conducted in the Materials Laboratory showed that the heating profile of composite laminates could be influenced by the mode setting of the cavity, location of the sample in the cavity, orientation of the sample relative to the power probe and stacking sequence of the laminates. Researchers at Michigan State University (M. Hawley) showed that under appropriate conditions, energy could be coupled into carbon fiber composite laminates with controlled heating and an even temperature distribution profile.

Other than the heating profile of a heterogeneous material like composites, another issue that needs to be addressed is the properties of the interfaces between the materials that may respond differently to the microwave energy. It was shown (L. Drzal) that microwave energy coupling could alter the interphase properties between the fiber and the matrix. Comparing thermally cured specimens with these cured by microwave, Drzal found that not only the interfacial shear strength was different, but the failure mode at the interface was also altered.

For successful processing of composites, pressure application is just as important as thermal control. To address this aspect of composite processing, Foster-Miller designed and constructed a pressure applicator that can be used in a microwave environment. This applicator was integrated into the cavity applicator designed by Michigan State University. With the intent of studying the feasibility of applying this technology in composite manufacturing, McDonnell Douglas Research Laboratory explored other energy coupling mechanisms that can be more compatible with aerospace composite parts.

As a whole, the project attempts to address many issues fundamental to the application of microwave energy in processing polymers and polymeric composites. The integrated effort necessitates technology and information transfer between workers from many different disciplines. Continuing activities in this area will allow the development of microwave processing technology to proceed on a sound and scientific foundation.

Acknowledgment

Processing of Polymers and Polymer Composites in a Microwave Applicator

Martin C. Hawley and Jianghua Wei
Department of Chemical Engineering, Michigan State University, E. Lansing,
MI 48824

## ABSTRACT

Polymers and polymer composites have been processed in a cylindrical
resonant microwave applicator at a frequency of 2.45GHz. Stoichiometric
mixtures of two epoxy/amine systems, DGEBA (Diglycidyl Ether of Bisphenol
A)/DDS (4,4'-Diaminodiphenyl Sulfone) and DGEBA/mPDA(m-Phenylene Diamine),
were microwave and thermally cured isothermally using a thin film technique.
FTIR was used to determine the extent of cure. Increased reaction rates
were observed in microwave cure when compared to those of thermal cure. The
rate increase due to microwave effects was much greater for the DGEBA/DDS
system than for DGEBA/mPDA. Also, crossply and unidirectional 24-ply and
72-ply graphite/epoxy laminates(AS4/3501-6 prepreg, Hercules Corp.), were
processed using microwave radiation. The flexural properties of the
microwave processed composites were strongly dependent on the resonant
heating mode. Comparable flexural properties were obtained for the
unpressurized microwave processed composites and the pressurized autoclave
processed composites. Proper controlled-hybrid modes are required to
process composites of high mechanical properties. The procedures for
obtaining these controlled-hybrid modes are described.

## Introduction

The control of heating rate and temperature is essential in the
processing of polymers and polymer composites in order to obtain high
quality products. Microwave heating offers several advantages when compared
to conventional thermal heating [1,2]. These advantages include: high
efficiency of energy conversion, rapid heating rate, high heating
selectivity, relatively uniform heating through the cross-section, and good
process controllability. Because of these advantages, microwave heating can
be used in many applications, such as food processing [3], chemical
processing, and medical therapy [4]. The control of heating rate during
microwave processing of thermosetting polymers and polymer composites can be
used to eliminate the temperature excursion during the process.

Several types of microwave applicators have been used to investigate
the processing of polymers and polymer composites at a frequency of 2.45
GHz. These include: commercial multimode microwave ovens[9,12],
waveguides[8,12], and single mode resonant cavities [1,5,6,7,10,13,14,15].
Generally speaking, all of these applicators can be used to process polymers
and non-conducting fiber reinforced polymer composites. Only the tunable
resonant cavity, however, has been used successfully to process crossply and
thick-section graphite fiber/epoxy composites[1]. The inability to process
crossply and thick-section graphite fiber/epoxy composites in waveguides was
attributed to a strong skin depth effect [8,9]. Graphite fiber/epoxy
composites processed in a commercial microwave oven resulted in fixed field
strength distributions, and the input power could not be transferred to the
composite efficiently due to impedance mismatch. Also, the composites could
not be uniformly cured due to the non-uniform field. The tunable resonant
cavity is unique in the following features:
1) The ability to obtain a resonant standing electromagnetic field
to transfer input energy efficiently into the composite.
2) The ability to select an appropriate resonant heating mode to heat
the composite uniformly.

220

3) The ability to maintain the selected resonant heating mode to prevent the loss of resonance.

This paper summarizes the results of microwave processing of epoxy resins and continuous graphite fiber/epoxy composites in a cylindrical tunable resonant microwave applicator .

Experiment.

Detailed experimental procedures and the associated microwave system for the processing of polymers and polymer composites at 2.45 GHz have been described elsewhere [1,6,13,15,16]. Figure 1 shows the cylindrical tunable resonant microwave cavity used in the processing. The cavity length Lc and coupling probe length Lp can be adjusted for tuning purposes, i.e. to generate a desired electromagnetic field pattern inside the cavity.
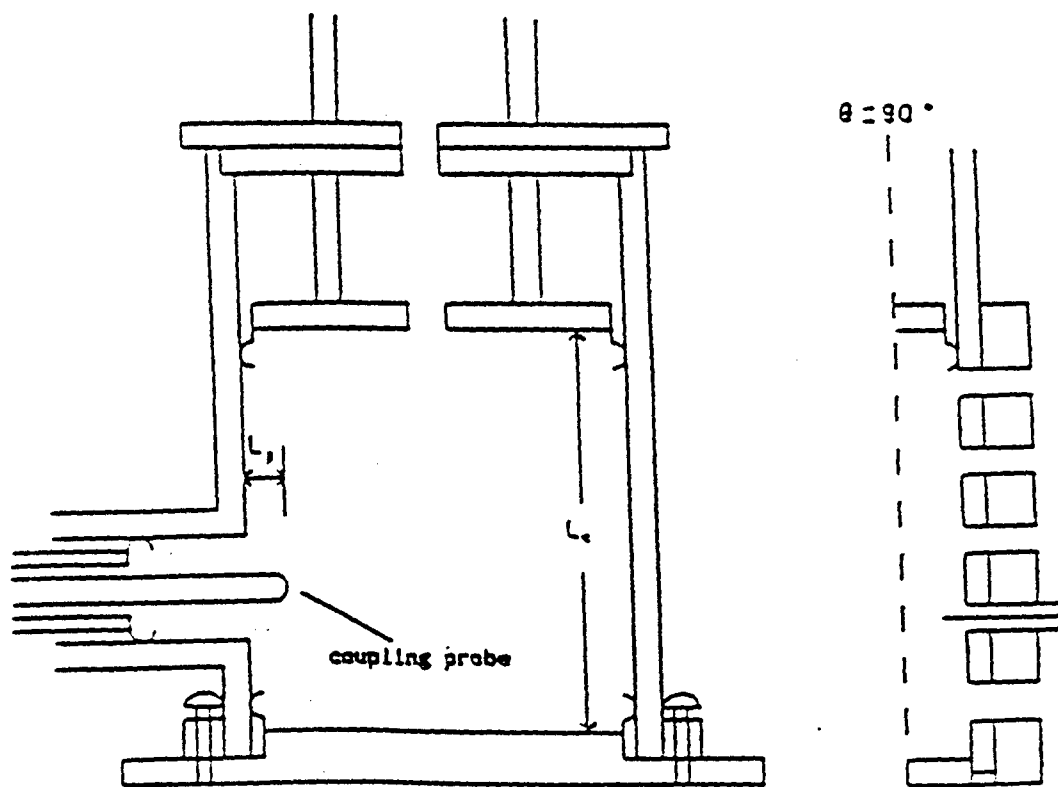


Fig. 1 Diagram of the cylindrical tunable microwave resonant cavity

In the microwave curing of polymers, a thin film technique was developed and a $TE_{111}$ resonant heating mode was used. Two epoxy resins, stoichiometric mixtures of DGEBA (Diglycidyl Ether of Bisphenol A)/DDS (4,4'- Diaminodiphenyl Sulfone) and DGEBA/mPDA(m-Phenylene Diamine), have been isothermally cured for various lengths of time at different temperatures in the microwave applicator. Fourier transform Infrared(FTIR) spectroscopy(Perkin-Elmer 1850) was used to determine the extent of cure. Details of this novel thin film technique have been reported elsewhere [6,15]. A parallel thermal cure study of the same epoxy resins was carried out for comparison of the reaction rates.

221

In the microwave processing of composites, the top ply fiber direction of the composite was oriented perpendicular to the coupling probe. The composites were 7.6 cm square laminates made from Hercules AS4 (graphite fiber)/3501-6(epoxy) prepreg. The samples were placed about 3.5 cm above the bottom plate of the cavity. Resonant heating modes were used to process the laminates. A low power, swept-frequency microwave source (range of 1.7 to 4.3 GHz) was used to locate the resonant heating mode. For a certain cavity length and coupling probe length, corresponding electromagnetic fields over a wide frequency range were generated inside the cavity. For a given input power, the reflected power varied depending on the electromagnetic field patterns. The reflected power at each frequency was displayed on an oscilloscope in a continuous power absorption curve. The zero power reflection point was used to identify resonance. Two types of resonant heating modes, pseudo-single (PS) and controlled-hybrid (CH) modes, were observed on the oscilloscope, as shown in Figure 2.



(a) controlled-hybrid mode                    (b) pseudo-single mode
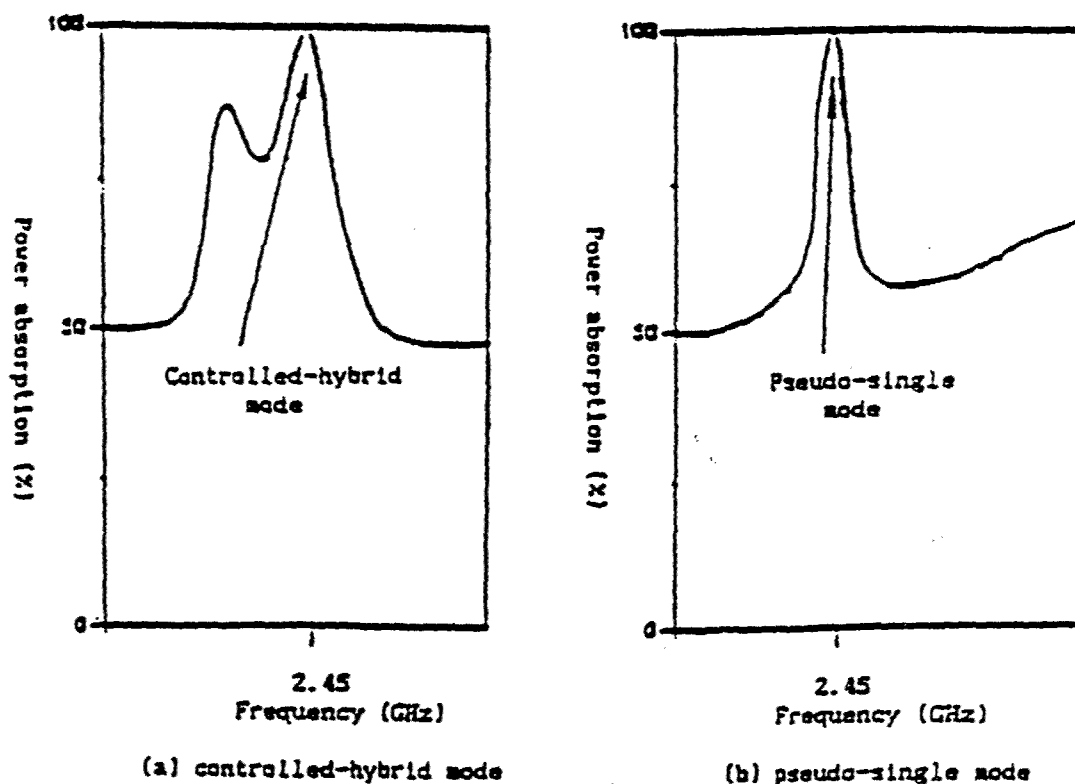
Fig. 2 Typical resonant power absorption curve

Several resonant modes (PS and CH) at 2.45 GHz were used to process composites using the single frequency source. No pressure was applied to the laminate during microwave processing. The input power used to process 24 ply unidirectional and crossply composites was 45 Watts and 60 Watts, respectively. An on/off microwave coaxial switch was used to limit the process temperature to 160°C. The total process time was 90 minutes. To maintain the same resonant heating mode during the processing, continuous fine tuning of the cavity length and coupling probe length were required. This was accomplished by keeping the reflected power below one percent of total input power. The fine tuning was used to compensate for the change of the complex dielectric constant resulting from the change of sample temperature, extent of cure, and fiber volume fraction. The radial electric field strength along the axial direction 90° from the coupling probe was

222

measured during the processing.  Four temperatures on the surface of the laminate were measured using fluoroptic probes (Luxtron 750).  Thermal processing of both 24-ply unidirectional and crossply composites using similar heating rate and processing time was done for comparison.  Also, unidirectional and crossply 24-ply composite laminates were thermally processed in the autoclave using the manufacturer's suggested cure cycle for comparison.  A pressure of 100 psig was applied during the autoclave processing.  The flexural strength and modulus of microwave and autoclave processed composites were determined using the ASTM D790 3-point flexural test method.

The concept of microwave processing (MP)modes was developed based on experiments of 24-ply laminate[1].  Microwave processing modes are defined as the resonant modes which give a uniform spatial temperature profile during processing and result in composites with high flexural properties. This concept was applied to the processing of 72 ply unidirectional and crossply composites.  The extent of cure distribution in the microwave processed 72 ply unidirectional composite was determined by Differential Scanning Calorimetry(DSC).

Results and Discussion

In the microwave curing of polymers, microwave radiation absorption occurs primarily at the location of epoxide and amine groups.  Enhanced reaction rates using the thin film technique were observed in microwave curing when compared to those of thermal curing as shown in Figure 3.  A significant increase in reaction rate has been observed in the DGEBA/DDS system while only a slight increase has been observed for DGEBA/mPDA. Microwave effects are higher for DGEBA/DDS system than in DGEBA/mPDA because DDS has a higher dipole moment than mPDA.  The details of microwave effects on the curing of epoxy resins have been reported elsewhere[6].



Time (min.)

223
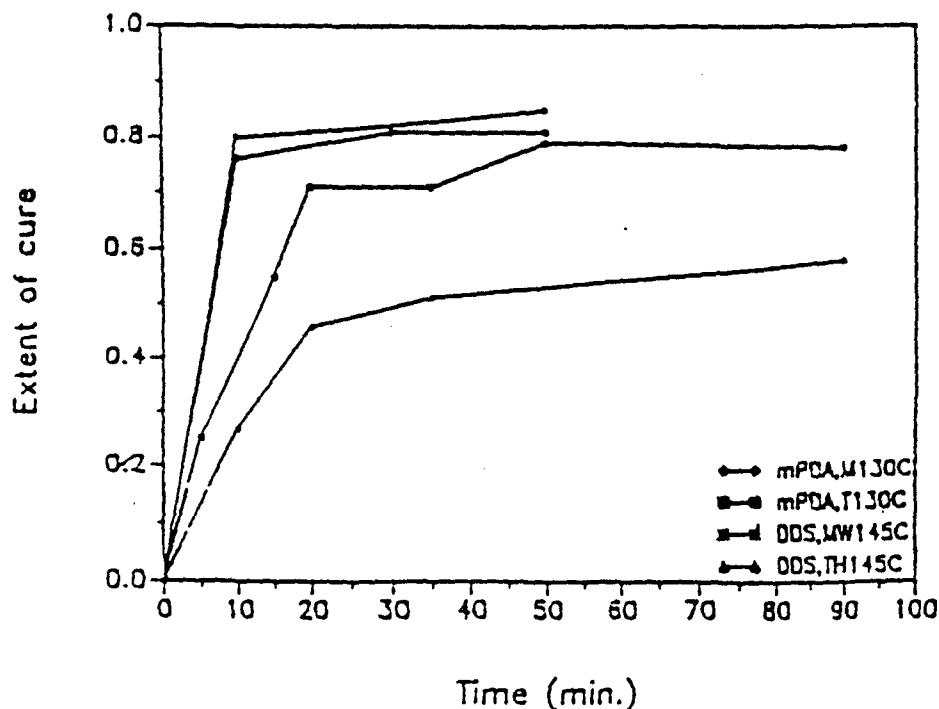
Figure 4 shows the measured flexural properties of microwave and thermally processed 24-crossply AS4/3501-6 composites. The flexural properties of 24-ply unidirectional composites have been reported elsewhere[10]. These results show that both crossply and unidirectional AS4/3501-6 composites can be successfully processed in the tunable resonant cavity. The flexural properties of microwave cured composites were found, however, to be strongly dependent on the processing mode used.
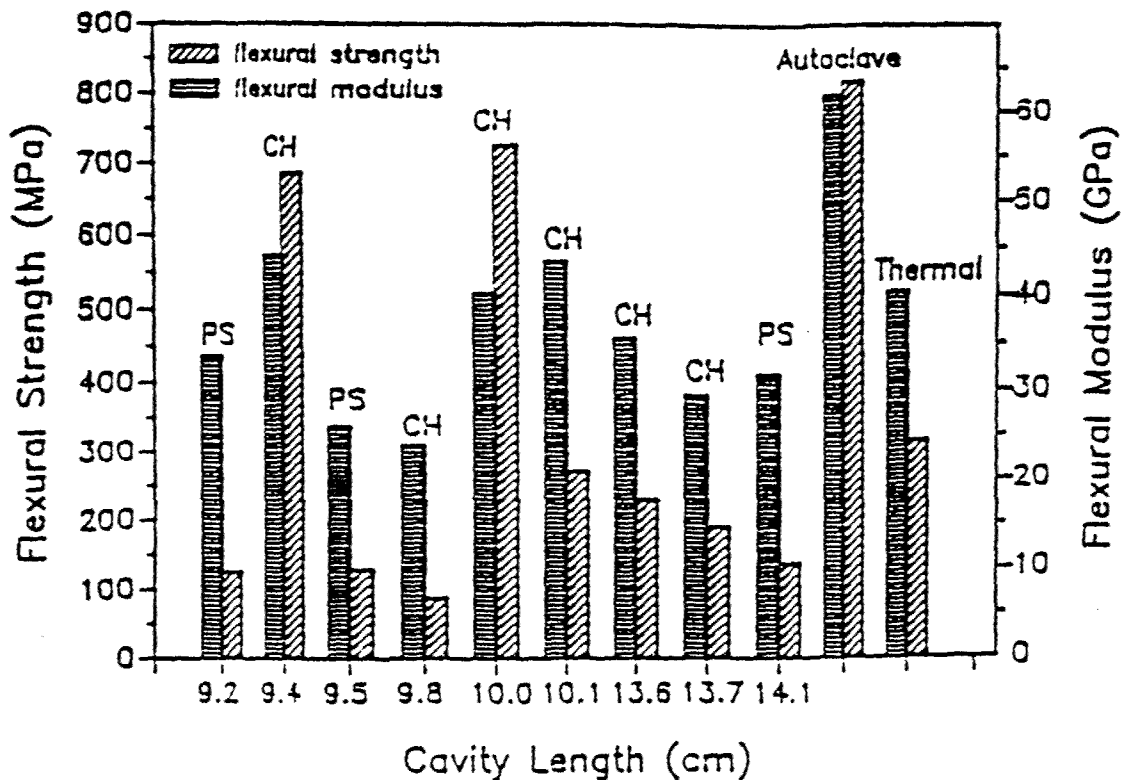


Fig. 4 Flexural properties of microwave and thermally processed 24-crossply AS4/3501-6 composites

Figure 4 shows that microwave processing is a promising technique. The highest flexural strength of unpressurized microwave processed composite(724 MPa) is more than two times of the strength for the unpressurized thermally processed composite(314 MPa). The unpressurized microwave processed composites show comparable flexural strength to those of pressurized autoclave processed samples(317 MPa). Figure 4 also shows that the crossply composites processed in a PS resonant heating mode (such as at Lc =9.19cm and 14.13cm) have relatively lower flexural properties. Only those crossply composites processed in certain CH modes (such as Lc=9.95 cm and 9.40 cm) have high flexural properties. High flexural properties were directly related to a uniform temperature profile during microwave processing[1]. Temperature profiles were controlled by the electric and magnetic field patterns of the resonant heating mode which corresponded to the cavity length and coupling probe length. Previous results also showed that only certain CH modes have the proper electric field patterns to result in a uniform temperature profile during microwave processing[1]. Microwave processing (MP) modes are defined as the resonant heating modes which give a uniform spatial temperature profile during processing and result in

224

composites with high mechanical properties(flexural properties). By relating the processing conditions, e.g. types of resonant heating mode and the radial electric field strength, to the flexural properties of processed composites, the microwave processing (MP) modes were found to be CH modes with the maximum radial electric field strength at the axial position of the composite. The experimental procedures for locating the MP modes are summarized as follows:

1) Adjust cavity and coupling probe length to obtain controlled-hybrid resonant mode using low-power, swept-frequency microwave source.

2) Replace the low-power, swept-frequency microwave source with a high-power, single frequency(2.45 GHz) source.

3). Measure the radial electric filled strength along axial direction to check whether the maximum strength is at the sample location.

4) If so, the selected mode is a process mode and the system is ready to process. If not, repeat above procedure until the cavity meets both criteria.

The above procedures were applied to find MP modes for 72-ply crossply and unidirectional AS4/3501-6 composites. The MP modes for 72-ply crossply and unidirectional samples were found to be at cavity lengths of 13.7 cm and 10.1 cm, respectively. Both unidirectional and crossply 72-ply composites were successfully processed under these conditions. Uniform surface temperatures were obtained in both cases. It is interesting to note that the interior temperature of the sample was always higher than the surface temperatures as shown in Figure 5. This shows that a significant electromagnetic field exists at the interior of the composite.
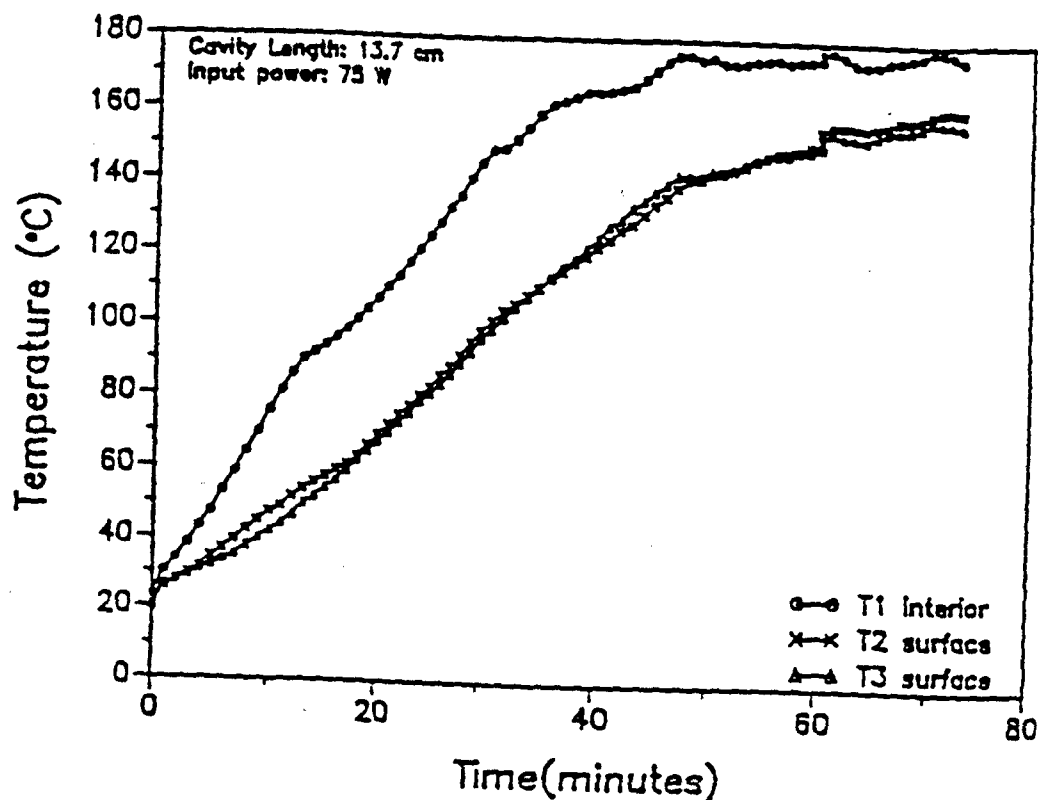


Fig. 5  Temperature/time profile of 72-ply unidirectional AS4/3501-6 composite during microwave processing

225

Figure 5 strongly suggests a uniform power absorption rate on surface. The higher initial and final interior temperature may be due to higher interior power absorption rate or the combination of surface heat loss and a higher interior power absorption rate of the composite. Figure 5 also demonstrates that the strong exothermic excursion can be controlled during the microwave processing of thick-section graphite fiber/epoxy composites. Figure 6 shows the cross-sectional extent of cure distribution, as determined by DSC. In the microwave processed 72-ply unidirectional composite. A uniform distribution of the extent of cure is observed through the cross section.
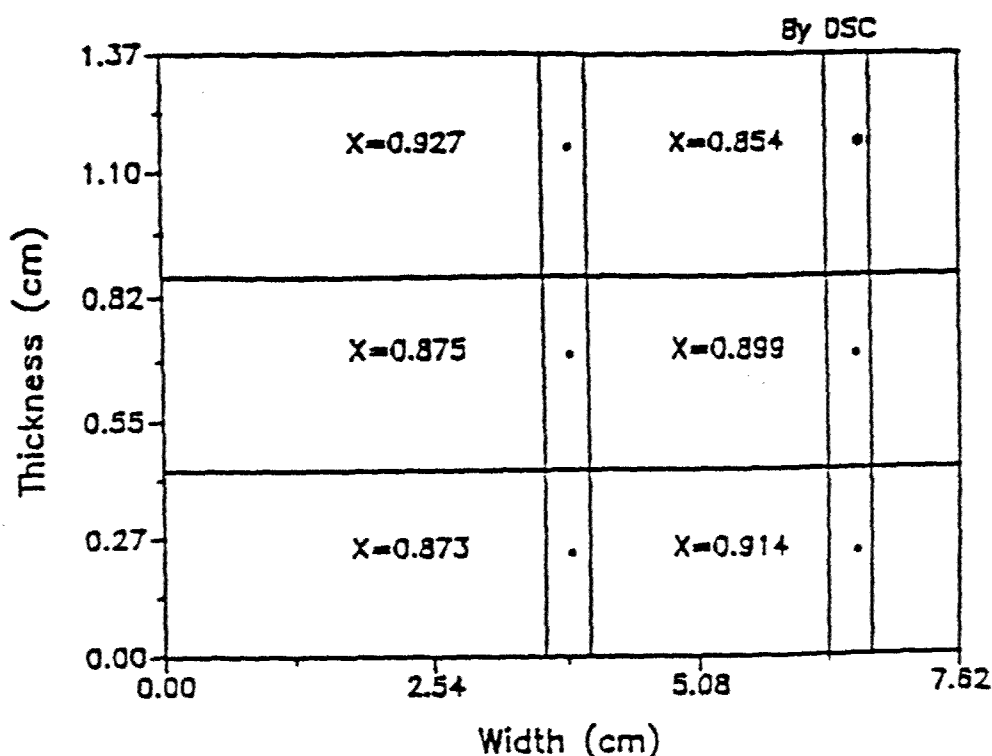


Fig. 6  Extent of cure distribution in the cross-section of microwave processed 72-ply unidirectional composite

Conclusion

Two epoxy resins, stoichiometric mixtures of DGEBA/mPDA and DGEBA/DDS, have been cured in the tunable cavity at 2.45 GHz using a $TE_{111}$ mode and a thin film technique. Increased reaction rates and higher extents of cure were observed in microwave cured samples as compared to those of thermal cured samples. The effects of microwave radiation on the curing of thermosetting polymers were found to be a function of the dipole moments of the monomer and the curing agent.

Graphite/epoxy composites, 24-ply crossply and 72-ply unidirectional and crossply, were successfully processed in the tunable resonant cavity. The flexural properties of processed composites were strongly dependent on the electromagnetic field pattern. Comparable flexural properties were observed between unpressurized microwave processed composites and pressurized autoclave processed samples. The concept of microwave processing (MP) modes was described and the procedure for the selection of such modes was described.

226

# REFERENCES

1 . J. Wei, J. Jow, J. D. DeLong, and M. C. Hawley, 2nd Topical Conf. on Emerging Tech. in Mat., AIChE annual meeting, SF, CA, Nov. (1989).

2 . I. J. Chabinsky, Materials Research Society Symposium Proceedings, 24, 17, (1988).

3 . R.D. Smith, EPRI, Report EM-3645, (1984).

4 . R. Paglione, F. Stetzer, J. Mendecki, E. Friedenthal, and C. Botstein, Mic. J., 24 (2), 71, (1981).

5 . J. Wei, J. Jow, J.D. DeLong, and M.C. Hawley, 7th ICCM, Beijing, P.R. China, June, (1989)

6 . J. Wei, J.D. DeLong, and M.C. Hawley, Proceedings of the American Society for Composite, 5th Tech. Conf., June, Michigan, p239, (1990).

7 . Agrawal, R. and L. T. Drazel, J. Adhesion, 29, 63-79, (1989).

8 . W.I. Lee and G.S. Springer, J. Composite Materials, 18, 357 (1984).

9 . W.I. Lee and G.S. Springer, J. Composite Materials, 18, 387 (1984).

10. G.L. Vogel, J. Jow, J.D. DeLong, and M.C. Hawley, Proc. Am. Soc. Comp. 4th Tech. Conf. Comp. Mat., Oct., (1989).

11. Normans Strand, Mordern Plastics, 54, 64, (1980).

12. A. Gourdenne and Le Q. Van, POlymer Preprints, 22, 125, (1981).

13. J. Jow, M. C. Hawley, M. Finzel and T. Kern, Polym. Eng. Sci., 28, 1450, (1988).

14. J. Jow, J.D. DeLong, and H.C. Hawley, SAMPE, Quarterly, 20, p 46,(1989).

15. J. D. DeLong, J. Jow, and M. C. Hawley, 2nd Topical Conf. on Emerging Tech. in Mat., AIChE annual meeting, SF, CA, Nov. (1989).

16. J. Wei, Fabrication of experimental setup and procedure for microwave curing of AS4/3501-6 composite laminate, Research Complex, MSU, 1989.

# ELECTROMAGNETIC PROCESSING OF POLYMERS:
## I. BASIC CONCEPTS AND MOLECULAR DESIGN OF THE MACROMOLECULES

J. C. HEDRICK, D. A. LEWIS*, T. C. WARD AND J. E. MCGRATH**
Department of Chemistry, NSF Science and Technology Center: High
Performance Polymeric Adhesives and Composites, Virginia Polytechnic
Institute and State University, Blacksburg, Virginia 24061-0212

*Current address: IBM Research, T. J. Watson Research Center; P. O. Box
218, Yorktown Heights, NY 10598

**To whom correspondence should be addressed.

ABSTRACT

Microwave processing has been utilized to process thermosetting
polymeric materials. Specifically, fundamental studies relating epoxy
network generation to processing conditions have been investigated in a
tunable cylindrical cavity operating at a frequency of 2.45 GHz. These
studies demonstrate that fully cured networks can be generated in ten
minutes with the retention of good mechanical properties. Furthermore,
toughened epoxy systems which utilize carefully designed amine terminated
poly(arylene ether sulfone) thermoplastics as reactive oligomers have
resulted in novel phase separated morphologies. In fact, it has been
demonstrated that the morphology in these multiphase systems can actually
be controlled by utilizing microwave processing. Bismaleimide toughened
systems, devised by similar strategies, have demonstrated a 10-20 fold
reduction in the time required to achieve full cure.

## INTRODUCTION

The utilization of microwave radiation to process polymeric materials
has been demonstrated in our laboratory [1-8] and elsewhere [9-18].
Accelerated reaction rates have been reported in many systems such as epoxy
resins [1,5,9-11], imidization reactions [4], crosslinking reactions of
terminally functionalized thermoplastics [1,2], and urethane
polymerizations [16]. The mechanism of the accelerated reaction rates is
uncertain. Microwave radiation (MR) unlike higher energy forms of
radiation is not energetic enough to cause ionization or chain scission in
polymeric materials; thus, the chemistry which occurs may be identical to
that observed during conventional thermal processing. Two proposals have
been put forth to explain the enhanced reaction rates. The first
attributes the acceleration to the novel mechanism of energy transfer with
electromagnetic processing. Typically, polymers are processed in a thermal
environment where heat is slowly conducted from the sample boundary to the
sample interior. Microwave radiation, alternatively, results in uniform
and rapid volumetric heating due to the interaction of the electromagnetic
radiation with the permanent dipole moments in the polymer. Thus, polymers
can be heated significantly faster while maintaining good thermal
uniformity. The second proposal, put forward by Lewis et al. [4],
attributes the accelerated reaction rates to localized heating on the
atomic level. This postulate was based on kinetic studies of a model
solution imidization reaction and predicts a temperature enhancement around
the dipole moments which couple with the radiation. The localized
temperature enhancement corresponds to approximately 50°C.

Microwave processing offers a number of potential advantages over conventional thermal processing. Polymeric materials can be cured/heated more uniformly through thick cross-sections due to the large penetration depth of electromagnetic radiation. Uniform heating of this type may result in a reduction of residual stress associated with thermal gradients during processing. Other advantages include significantly reduced cure times in thermosets, increased throughput, and the possibility of substantially reduced capital and operating costs. Despite these advantages, there has been limited commercialization of this technique, since there remains, as yet, no systematic examination of the critical parameters required for good process control.

In this investigation, the effect of MR on several high performance polymeric systems has been studied. Specifically, the crosslinking reaction kinetics of poly(arylene ether ketone) based thermosetting bismaleimides were investigated. Using conventional processing technology, the cure time in this system is very long, restricting many applications. However, with MR processing the long, complex curing cycle required for optimization of mechanical properties may be substantially reduced.

The effect of microwave radiation on thermoplastic toughened epoxy resin systems has also been investigated. This system has demonstrated significant enhancements in fracture toughness over the neat epoxy resins, while still retaining the modulus and high temperature performance, which is in contrast to rubber toughened epoxy resins. In this paper, MR processing has been utilized to control morphology by accelerating the epoxide reaction and quenching morphological development at gelation prior to complete phase separation. Control of this type may be very important in toughened epoxy resin networks since material properties, especially fracture toughness, are strongly dependent on morphology.


EXPERIMENTAL

The equipment utilized for microwave processing is shown schematically in Figure 1. It consists of a Raytheon magnetron that generates continuous microwave energy at a frequency of 2.45 GHz. A tunable, cylindrical (17 cm diameter) brass applicator [19] resonating in the $TE_{111}$ mode was utilized for the processing experiments. The incident and reflected radiation was monitored via power meters so the impedance mismatch in the applicator could be corrected and the critical coupling maintained as the dielectric properties of the polymer changed during processing. Temperature was monitored continuously by fiber optic fluorescence sensors at several positions within the samples.

Thermosetting bismaleimides based on bismaleimidodiphenylmethane (BMI), maleimide terminated poly(arylene ether ketone)s oligomers (MI-PEK) (<Mn>=5,400) and blends of BMI and MI-PEK (Figure 2) were processed from thin ("1 mm) cold pressed powder samples isothermally at 220°C. High processing powers ("40 to 60 watts) were needed to heat these materials due to their low dielectric loss. After irradiation, samples were extracted in a soxhlet apparatus using chloroform as a solvent to determine the percent gelation. For comparative purposes "thermal" cures were conducted in a forced air convection oven and extracted in a similar manner.

Thermoplastic modified epoxy resins were prepared by reacting recrystallized DGEBA (diglycidyl ether of bisphenol A) epoxy resin (DER 332) with an amino functional poly(arylene ether sulfone) (PSF) oligomer possessing a number average molecular weight of 16,000 gm/mole. The crosslinked network was prepared by reacting DGEBA in a 2:1 molar ratio
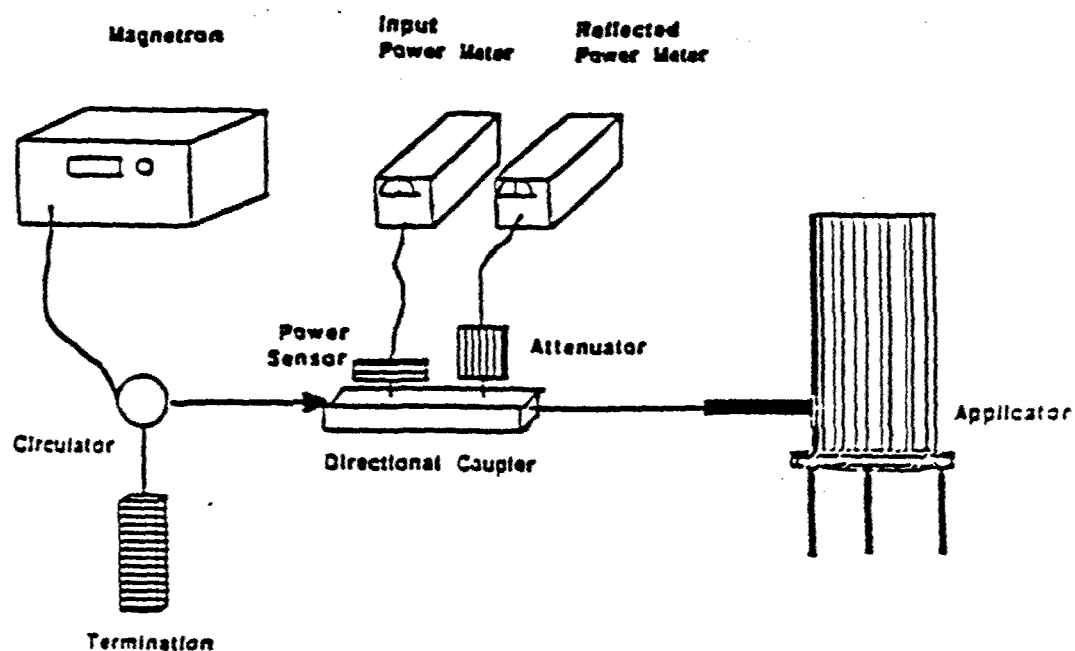
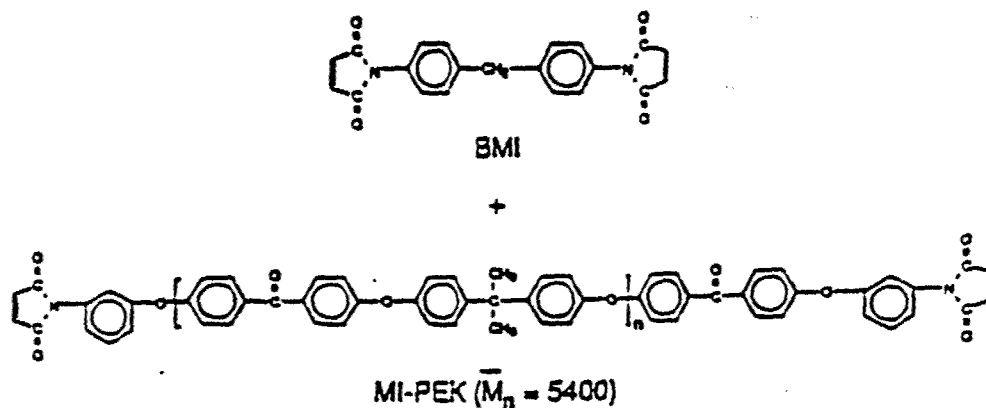Figure 1. Schematic representation of the equipment utilized for microwave processing.



BMI

+

MI-PEK ($\overline{M}_n$ = 5400)

Figure 2. Preparation of bismaleimide/maleimide terminated poly(arylene ether ketone) blends.

230

with respect to the PSP oligomer and a curing agent, 4,4'-diaminodiphenylsulfone (DDS) as shown in Figure 3. The modified epoxy resins were processed at variable microwave powers ranging from 7.5 to 35 watts for various time intervals. The maximum temperature achieved for all the cured systems was ~250°C. Percent conversion was determined utilizing a DuPont differential scanning calorimeter (Model 912) at a heating rate of 10°C/min. For comparative purposes networks were also cured thermally at 190°C for two hours and postcured at 240°C for 1 hour in a forced air convection oven. The morphology of the resulting microphase separated thermosets was investigated using scanning electron microscopy (SEM). SEM micrographs were taken using an International Scientific Instrument Model SX-40 with an electron beam voltage of 15,000 volts.


## RESULTS AND DISCUSSION

It has been proposed [20] that bismaleimides undergo an addition polymerization at elevated temperatures via a free radical mechanism to generate a crosslinked network as shown in Figure 4. The isothermal (220°C) microwave curing behavior of BMI, MI-PEX, and their respective 50/50 weight percent blend is shown in Figure 5. Insoluble networks were generated as exemplified in this plot in as little 10-30 minutes employing MR processing. In fact, the curing rate was further accelerated by increasing the amount of the lower molecular weight BMI component. This is probably due to a combination of two factors: (i) as molecular weight decreases the weight percent of the reactive functional endgroups increased; and (ii) as molecular weight decreases, the melt viscosity decreases, thus there is an increase in mobility. Both of these factors would be expected to be important in a diffusion controlled thermosetting reaction. However, they are especially significant in MR processed systems since microwave absorptivity increases with both a higher content of polar groups (i.e. maleimide endgroups) and enhanced mobility.

The thermally processed bismaleimides exhibited a similar trend to the microwave cured specimens as shown in Figure 6. An acceleration in reactivity was observed as the molar mass between the reactive endgroups decreased. Comparison of Figures 5 and 6, however, demonstrates the enormous capabilities of MR processing. With MR curing complete gelation was reached in only 10-30 minutes as opposed to 1-10 hours for thermally processed bismaleimides. This represents up to a 10 to 20 fold reduction in the curing time.

Microwave processing has also been employed to process thermoplastic toughened epoxy resin networks. Typically brittle epoxy resin networks when employed in structural applications are toughened by the incorporation of a second component which microphase separates during curing. Toughness enhancement is strongly related to the morphological structure of the resulting network. The actual mechanism(s) for the increased toughness is still greatly debated [20-24]. However, it is generally believed that the enhancement is either due to the high tear energy of the discrete phase (i.e. rubber or thermoplastic) [21] or possibly due to plastic shear yielding in the vicinity of the crack tip which increases the size of the plastic zone and blunts the sharp crack [22-24]. The toughening effect is most likely a combination of all the mechanisms listed above; the most prevalent of which, however, is unique to the particular system.

It has been demonstrated in our laboratory [5] that an 8-10 fold enhancement in the curing rates of epoxy resin networks can be achieved with MR processing. In the current investigation, an epoxy resin based on DGEBA and DDS was modified with 15 weight percent of an amino

231

DGEBA (large excess)

+

BISPHENOL-A POLYSULFONE

EPOXY CAPPED BIS-A POLYSULFONE

+

EXCESS DGEBA

+

DDS

THERMAL
OR
MICROWAVE

CROSSLINKED NETWORK
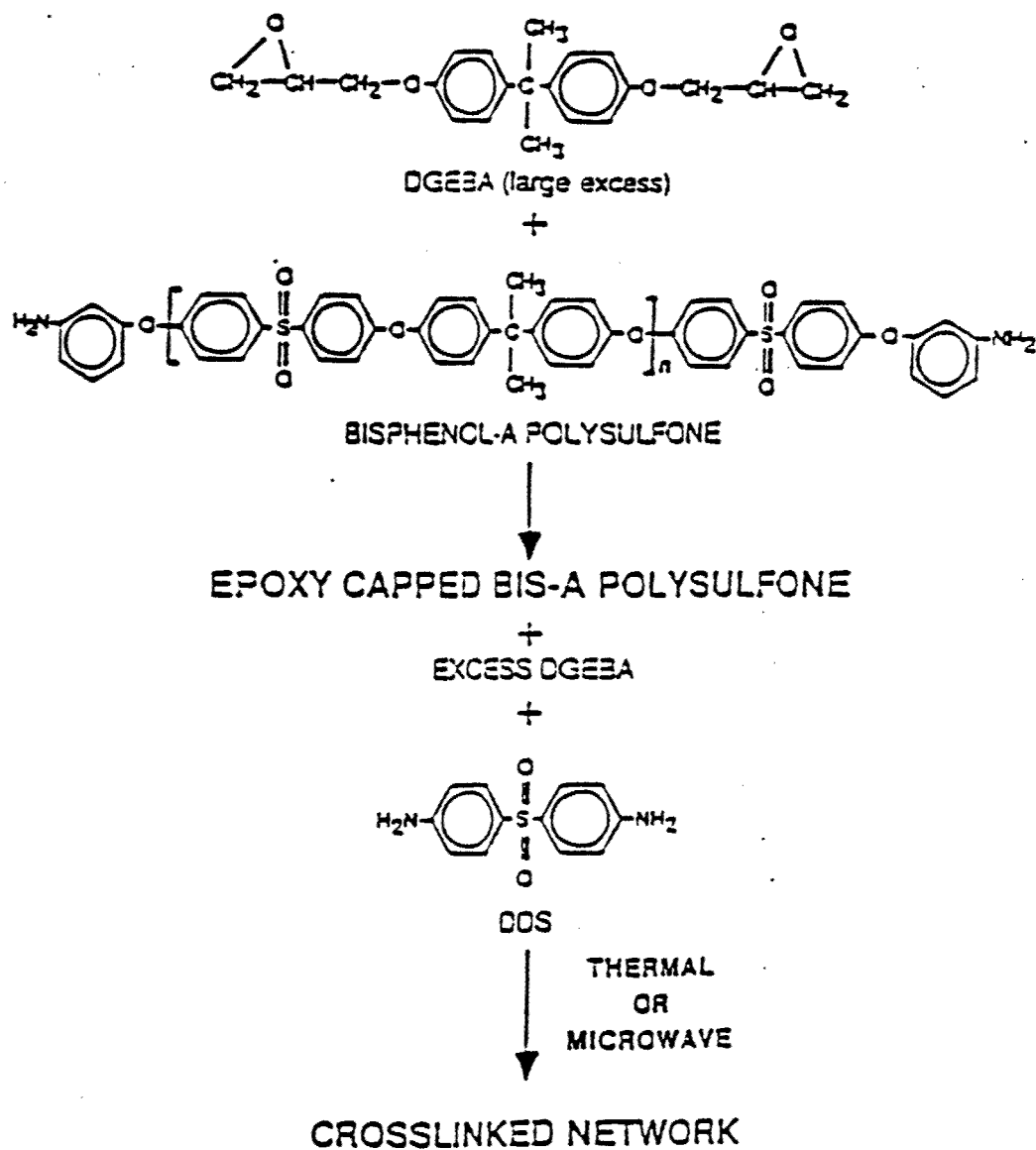
Figure 3. Synthesis of thermoplastic modified epoxy resin networks.
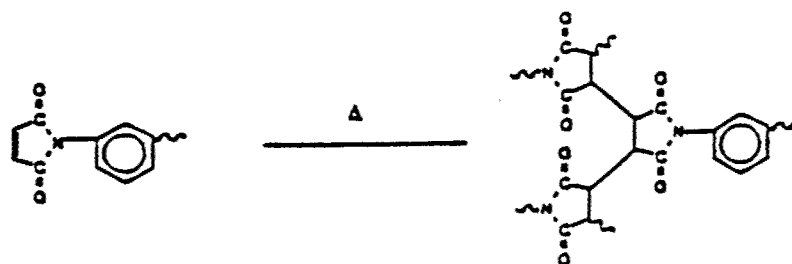


Figure 4. Schematic representation of the bismaleimide thermally induced
free radical crosslinking reaction.

232
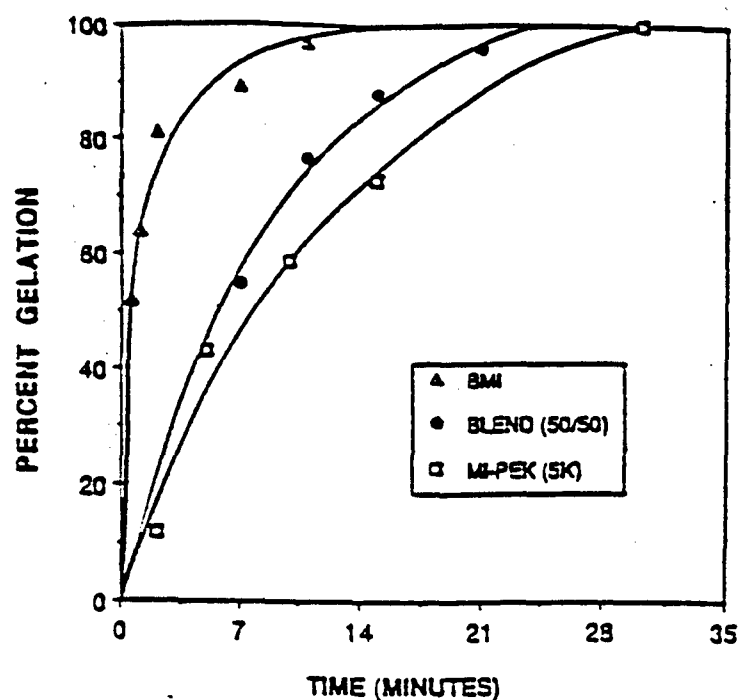
Figure 5. Isothermal (220°C) microwave curing behavior of bismaleimidodiphenylmethane, maleimide terminated poly(arylene ether ketone) and their 50/50 weight percent blend.
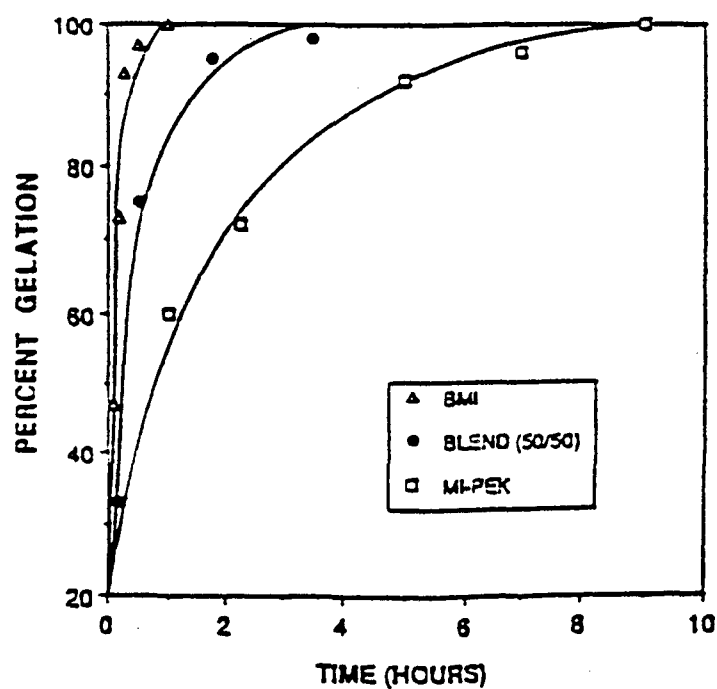


Figure 6. Thermal curing behavior of bismaleimidodiphenylmethane, maleimide terminated poly(arylene ether ketone) and their 50/50 weight percent blend.

233

Thermally Cured
(2 hrs. @ 190°C, 1 hr @ 240°C)

Microwave Cured
(1 hr. @ 7.5 watts)

Microwave Cured
(12 min. @ 15 watts)

Microwave Cured
(4 min. @ 25 watts)

Microwave Cured
(2 min. @ 35 watts)

Figure 7. SEM micrographs (50,000x) demonstrating control of morphology in thermoplastic modified epoxy resin networks with microwave processing (bar = 0.5 μm).

functionalized poly(arylene ether sulfone) (PSF) oligomer (Figure 3). In this system the PSF oligomer initially forms a homogeneous mixture with monomeric epoxy reagent before undergoing an in situ phase separation process during curing. Phase separation is thermodynamically promoted; however, it is controlled by the competing effects of incompatibility, rate of nucleation and growth, and the quenching of morphological development by gelation [25].

Accelerated MR processing has been employed in this investigation to control the morphological structure by controlling the rate at which gelation is reached, since phase separation is halted at the gel point. Scanning electron microscopy (SEM) results shown in Figure 7 clearly demonstrate that morphological control with variable power processing is feasible. Indeed, low power (7.5 watts) EM processing yielded networks exhibiting morphologies that were analogous to thermally cured systems with approximately 0.5 um spheres of PSF evenly dispersed in the epoxy resin matrix. This suggested that an equivalent degree of phase separation was achieved with the two processing techniques. However, as power was increased, for example to 15, 25 or 35 watts, the morphology became less-defined. In fact, the networks cured at 35 watts for two minutes shared little to no phase separation, while the networks cured at powers of 15 and 25 watts demonstrated intermediate degrees of phase separation.

Essentially, phase separation is thermodynamically favored but controlled by kinetics. With high power processing the kinetics of phase separation cannot compete with the increased reactivity and the 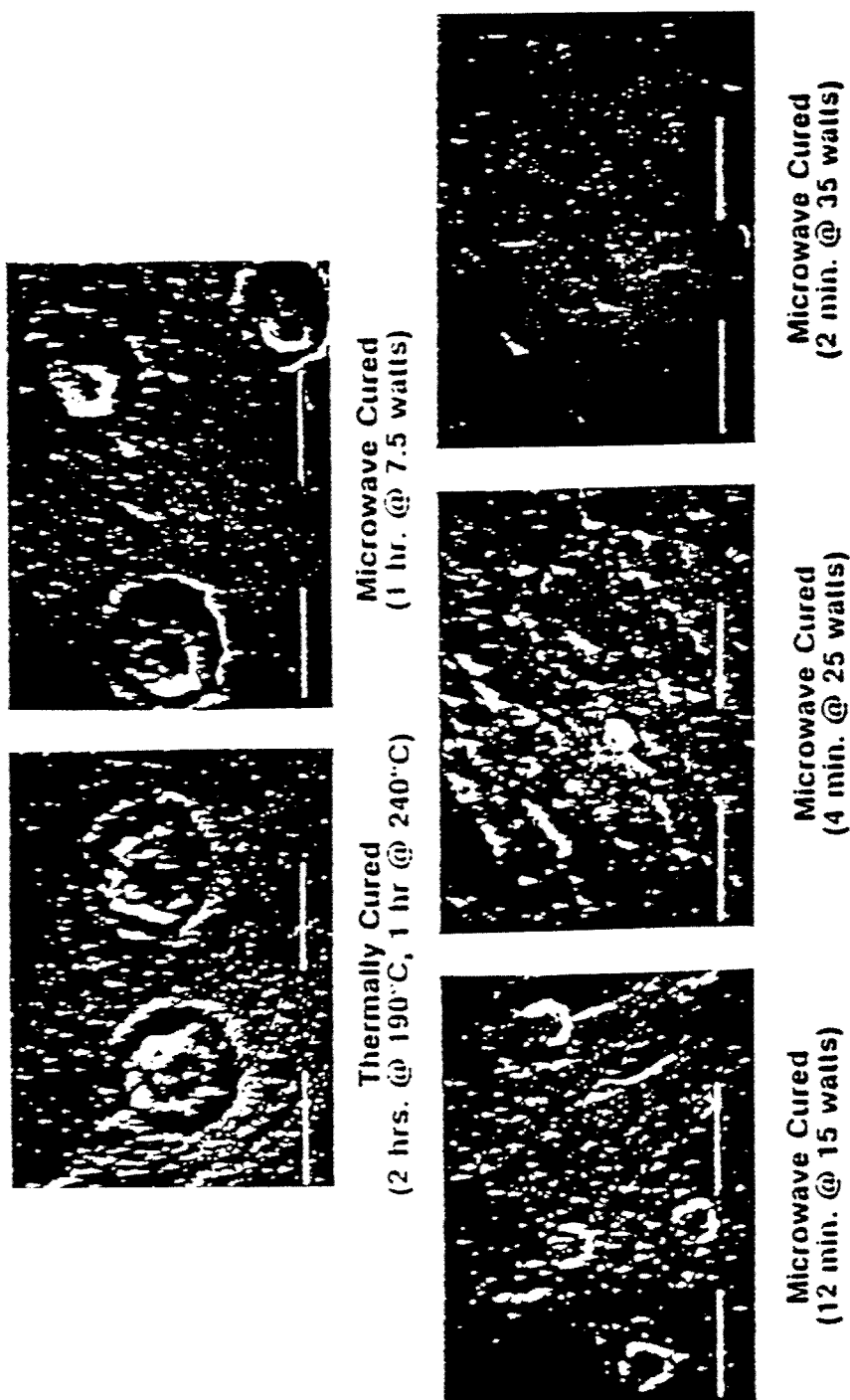morphology development is quenched due to gelation. Thus, the resulting morphologies were incompletely phase separated (or phase mixed) as has been demonstrated previously in our laboratory with dynamic mechanical thermal analysis [3]. Morphological control of this type may be critical to the optimization of mechanical property performance in toughened epoxy resin networks.


## CONCLUSIONS

Microwave processing has been effectively utilized to process polymeric materials. Accelerated reaction rates have been observed in man reactive thermosetting systems such as bismaleimides and epoxy resin networks. The 10-20 fold reduction in the time required to achieve full cure may be advantageous in reducing the long, complex cure cycles of high performance thermosets. Furthermore, morphological control in thermoplastic modified epoxy resin networks has been achieved with accelerated MR processing, since morphological development is quenched at gelation.

## REFERENCES

1. J. C. Hedrick, D. A. Lewis, G. D. Lyle, T. C. Ward, and J. E. McGrath Proceedings of the American Society for Composites, Fourth Technical Conference (Technomic Publishing Co., 1989) pp. 167-176.

2. J. C. Hedrick, D. A. Lewis, G. D. Lyle, T. C. Ward and J. E. McGrath, Poly. Mat. Eng. Sci., 60, 439 (1989).

3. D. A. Lewis, J. C. Hedrick, J. E. McGrath and T. C. Ward, in *Microwave Processing of Materials*, eds. W. H. Sutton, M. H. Brooks and I. J. Chabinsky (MRS Publications, 1988) pp. 181-188.

4. D. A. Lewis, T. C. Ward, J. D. Summers and J. E. McGrath, Polym. Preprints, <u>29</u> (1), 174 (1988).

5. J. C. Hedrick, D. A. Lewis, T. C. Ward and J. E. McGrath, Polym. Preprints, <u>29</u> (1), 363 (1988); <u>28</u> (2), 303 (1987).

6. G. D. Lyle, J. C. Hedrick, D. A. Lewis, J. S. Senger, D. H. Chen, S. D. Wu and J. E. McGrath, in *Polyimides: Materials, Chemistry and Characterization*, eds. C. Feger, M. M. Khojasteh and J. E. McGrath (Elsevier Sci. Publishers, Amsterdam, 1989) pp. 213-227.

7. M. Chen, J. E. McGrath and T. C. Ward, Polm. Mat. Eng. Sci., <u>60</u>, 443 (1989).

8. Y. P. Chen, J. P. Pollard, J. D. Graybeal and T. C. Ward, Polym. Preprints, <u>29</u> (1), 207 (1988).

9. Q. Le Van and A. Gourdenne, Eur. Polym. J., <u>23</u> (10), 177 (1987).

10. N. Beldjoudi, A. Bouazizi, D. Douibi and A. Gourdenne, Enr. Polym. J., <u>24</u> (1) (1988).

11. E. Karmazsin and P. Satre, Thermochimica Acta, 93, 305 (1985).

12. S. M. Senger, J. Jow, J. D. Delong and M. Hawley, SAMPE Quarterly, <u>20</u> (2), 14 (1989).

13. J. Jow, J. D. Delong and M. C. Hawley, SAMPE Quarterly, <u>20</u> (2) (1989).

14. J. Jow, M. C. Hawley, M. Finzel and T. Kern, Polym. Eng. Sci., 28 (22), 1450 (1988).

15. J. Jow, M. C. Hawley, M. C. Finzel and J. A. Amussen, Rev., Sci., Instrum., <u>60</u> (1) (1989).

16. E. Jullien and R. Valot, Polymer, <u>24</u>, 810 (1983); <u>26</u>, 506 (1985).

17. K. Nakagawa and T. Konaka, Polymers, <u>27</u>, 1030 (1986); <u>27</u>, 1553 (1986).

18. T. Konaku, K. Nakagawa and S. Yamakawa, Polymer, <u>26</u>, 462 (1985); <u>26</u>, 1929 (1985).

19. J. Asmussen, H. Lin, B. Manring and R. Fritz, Rev. Sci. Instrum., <u>58</u> (8), 1477 (1987).

20. H. Stenzenberger, Brit. Polym. J., <u>20</u>, 383 (1988).

21. S. Kunz-Douglass, P. W. R. Beaumont and M. F. Ashby, J. Mat. Sci., <u>15</u>, 1109 (1980).

22. A. J. Kinloch, S. J. Shaw, D. A. Tod and D. L. Hunston, Polymer, <u>24</u>, 1341 (1983); <u>24</u>, 1355 (1983).

23. A. F. Yee and R. A. Pearson, J. of Mat. Sci., <u>21</u>, 2462 (1986); <u>21</u>, 2475 (1986).

236

24. S. C. Kim and H. R. Brown, J. Mat. Sci., 22, 2589 (1987).

25. L. T. Manzione, J. K. Gillham and C. A. McPherson, J. Appl. Polym. Sci., 26, 889 (1981); 26, 906 (1981).

ELECTROMAGNETIC PROCESSING OF POLYMERS:
II. QUANTITATIVE INVESTIGATIONS OF MICROWAVE PROCESSED THERMOPLASTICS
(MICROWAVE CALORIMETRY)

M. CHEN*, M. A. ZUMBRUM, J. C. HEDRICK, J. E. MCGRATH AND T. C. WARD**
Department of Chemistry, NSF Science and Technology Center: High
Performance Polymeric Adhesives and Composites, Virginia Polytechnic
Institute and State University, Blacksburg, Virginia 24061-0212

*Current Address: Institute of Materials Science and Engineering, National
Sun Yat-Sen University, Kaohsiung, Taiwan, People's Republic of China

**To whom correspondence should be addressed.

ABSTRACT

The microwave heatability of various thermoplastic polymers was
investigated. The concept of microwave calorimetry was proposed to
quantitatively illustrate how viscoelastic behavior controlled microwave
heatability. Specifically, heating rate as a function of sample
temperature revealed a distinct maximum which was identified as the Tg at
2.45 GHz. The critical temperature, $T_c$, necessary for rapid microwave
heating was identified by drawing a tangent to the heating rate curve and
extrapolating to a critical value at zero heating rate. In separate
experiments, low frequency (100 kHz) dielectric measurements were made
which show the frequency dependence of Tg by means of Arrhenius activation
energy plots. In general, the larger the activation energy, the closer the
critical heating temperature, $T_c$, was to the Tg determined by DSC. The
smaller the activation energy, the further dielectric loss shifted with
increased frequency so that $T_c$ was very far from Tg determined by DSC.

INTRODUCTION

Microwave radiation in tuned waveguides has been successfully used to
process numerous reactive [1-17] and non-reactive [17-22] polymers. In
this paper, a better understanding of microwave processing of non-reactive
systems was achieved by using the proposed concept of microwave calorimetry
in conjunction with low frequency dielectric measurements. This technique
was conceived based on Equation 1 for capacitive heating of non-reactive
polymers [23]:

$$dT/dt = K \, \omega \, E^2 c' \, (T) \tan \delta_e \, (T) \, / \, \rho \, C_v \qquad (1)$$

where $dT/dt$ = heating rate, K = constant, $\omega$ = applied frequency, $\rho$ =
polymer density, $C_v$ = heat capacity, E = electric field strength and (c'
tan $\delta_e$ ) = dielectric loss, assuming absence of convection losses or
conductive heating. Since the sample heating rate was directly
proportional to the dielectric loss, low frequency dielectric analyses were
conducted to predict the shift of the dielectric loss into the microwave
region. The presence of this relaxation is necessary for the conversion of
electrical into thermal energy.

The dipolar dielectric loss of polymeric materials depends very strongly
on temperature and frequency [24-26]. Schematically, Figure 1 depicts the
temperature and frequency dependence of the $T_g$ ($\alpha$ transition) and a lower
temperature secondary transition ($\beta$ transition). As frequency is

increased, the β transition shifts to higher temperature much more rapidly than the α transition does due to the lower activation energy processes of the β transition; however, each polymer possesses its own activation energy depending upon the magnitude of the intermolecular and intramolecular forces. By measuring the dielectric loss tangent (tan $\delta_e$) as a function of temperature at various frequencies, one can construct Arrhenius plots. The slope of such plots is proportional to the energy of activation ($\Delta E = -2.303 R \cdot$ slope) for a particular relaxation phenomenon. As sample temperature increases, therefore, the dipolar dispersion peak shifts further into the microwave region thereby providing a mechanism for increasing the heating rate. The rate at which the dispersion peak shifts toward the microwave region indicates the potential microwave processability and how far the critical temperature for microwave heating, $T_c$, is from the $T_g$ as measured by DSC. In this study, the Arrhenius activation energy of the glass transition was obtained from the dependence of dipolar dielectric loss on frequency and temperature as measured by experimentally convenient dielectric thermal analysis.

In separate microwave calorimetry experiments, the heating rates of various polymers upon exposure to microwave radiation were measured. A plot of heating rate versus sample temperature yields a curve having a maximum at the temperature which corresponds to the polymer's $T_g$ at 2.45 GHz. Drawing a tangent to the side of the curve before $T_g$ and extrapolating to zero heating rate supplies the critical temperature, $T_c$, which identifies when the dielectric loss peak enters the GHz region and provides a mechanism for rapid microwave heating. These microwave calorimetry results ($T_c$ and $T_g$ at 2.45 GHz) were combined with the low frequency dielectric measurements of the Arrhenius activation energy to predict microwave heatability of various thermoplastic polymers.


EXPERIMENTAL

The microwave processing equipment was assembled in three basic configurations. The first two configurations utilized a rectangular (WR 284) waveguide coupled to a Raytheon® (model PGM-10X1) 85 watt source operating at 2.45 GHz. Only one mode, the $TE_{10}$, propagates freely in the rectangular WR 284 waveguide. The $TE_{10}$ mode has an electric field vector (E) which has only one component, linearly polarized parallel to the narrow faces of the waveguide, producing a maximum midway through the cavity. By connecting a terminator (Narda® model 369BNF) to the end of the waveguide, as shown in Figure 2, a low electric field strength traveling wave was generated. A sliding short (Microlab® model S630C) affixed to the end of the waveguide, illustrated in Figure 3, reflected the wave back and forth through the sample resulting in a standing mode wave which produced an electric field strength considerably higher than in the traveling wave mode. In the case of the rectangular waveguide configurations, a strip heater was fastened to the exterior of the waveguide to heat the sample to the desired initial temperature to shift the dielectric loss closer to the microwave region. The third waveguide configuration, shown in Figure 4, utilized a cylindrical cavity 18 cm in diameter operating in the $TE_{111}$ mode and was designed and constructed at Michigan State University [27]. In all cases, sample temperature was monitored via a fluoroptic temperature probe connected to a Luxtron (model 750) Fluoroptic Thermometry System®. Input, reflected, and in the case of the traveling mode, transmitted powers were recorded via Hewlett Packard® (model 435B) power meters.

Table 1 summarizes the glass transition temperatures, platten pressing temperatures, and suppliers of the thermoplastic polymers used in this

239
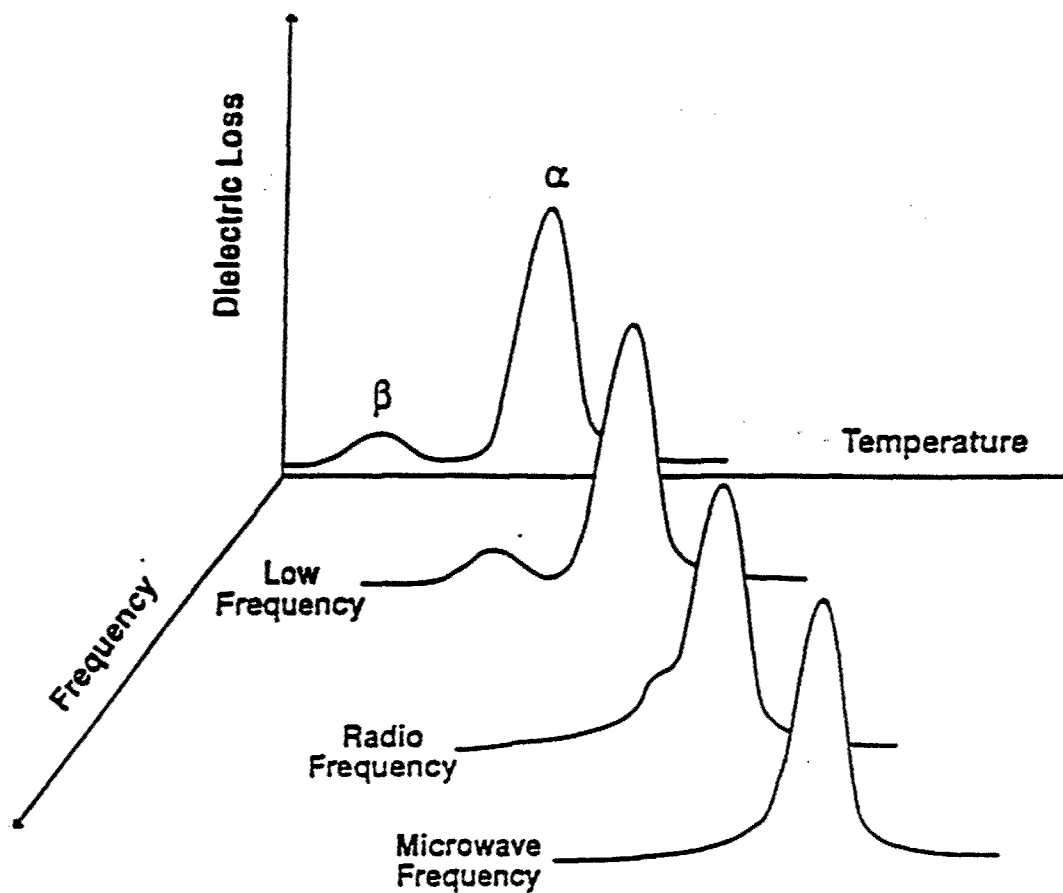
Figure 1. Schematic depiction of the frequency and temperature dependence of dielectric loss for polymeric materials. The low activation energy β transition shifts to higher temperatures faster than the α transition as frequency increases.
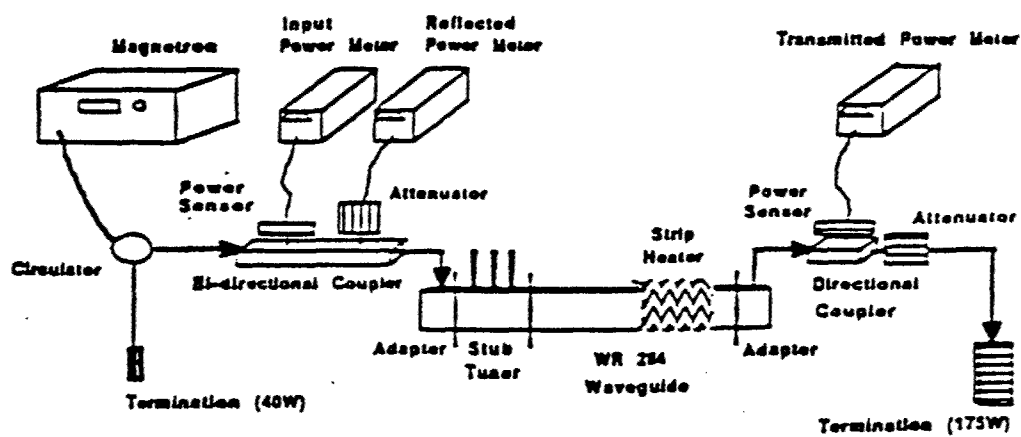


Figure 2. Microwave configuration for processing via a travelling wave mode.

240
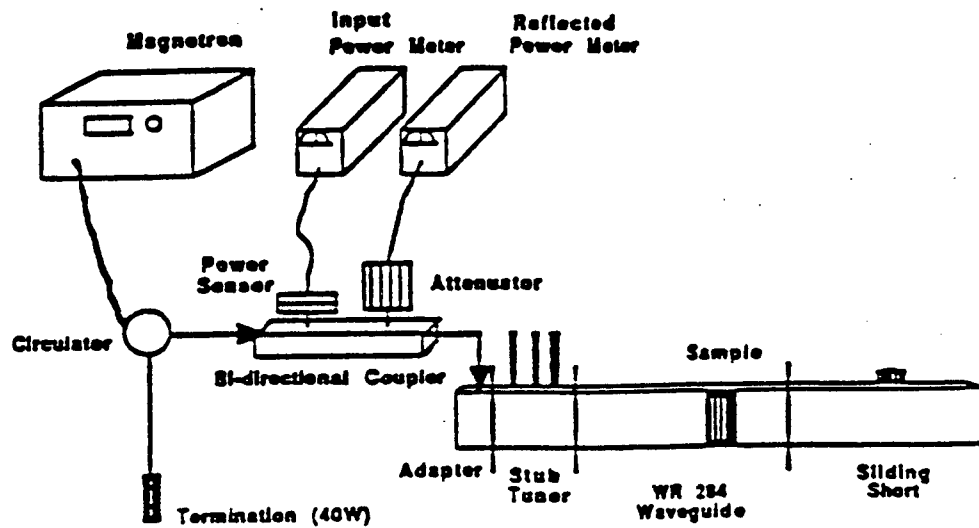
Figure 3. Microwave configuration for processing with the high electric field strength standing wave mode.
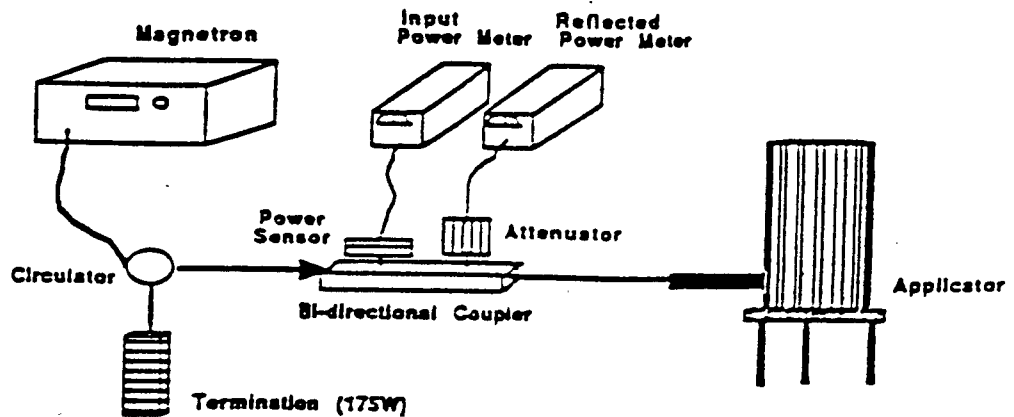


Figure 4. Cylindrical applicator for microwave processing in the $TE_{111}$ standing mode.

241

study. All polymers were dried for 24 hrs. under vacuum just below their respective $T_g$'s prior to use. The samples consisted of pressed films (0.3 to 0.3 mm in thickness) stacked together to produce 0.4 cm thick blocks which were placed into teflon cylinders (1.25 cm ID, 1.6 cm OD, and 2.95 cm height) for microwave processing.

Dielectric thermal analyses (DETA) were performed using a Polymer Laboratories® DETA over the frequency range of 0.1 to 100 kHz. Thermal scans were obtained from -150 to 300°C at a heating rate of 2°C/min. using 33 mm diameter stainless steel electrodes covered with aluminum foil. Maxima in the loss tangent traces were used to identify the $T_g$ as a function of frequency.


## RESULTS AND DISCUSSION

The basic heating rate equation for thermoplastic polymers (Equation 1) requires that both the electric field strength and the dielectric loss properties be sufficiently large to obtain rapid volumetric heating. The processing of PVAc in both the traveling and standing mode applicators was conducted to illustrate how microwave heatability depends upon the electric field strength. The temperature of PVAc, shown in Figure 5, increased very little for the first 20 minutes of irradiation at 50 Watts input power in the traveling waveguide (see Figure 2), even at elevated starting temperatures induced by a strip heater to enhance microwave absorptivity. Increasing the electric field strength by utilizing the standing mode applicator (see Figure 3) resulted in a rapid increase in sample temperature from 30 to 200°C within 7 minutes, as seen in Figure 6. The rate of rise in sample temperature (dT/dt) for PVAc in the standing wave applicator was recorded as a function of temperature, as shown in Figure 7. Above a threshold temperature, designated as the critical temperature for microwave processing, $T_c$, the sample heating rate increased very rapidly. The critical temperature corresponds to the temperature at which the dielectric loss peak just enters the microwave region where loss mechanisms transform the electrical energy into thermal energy (see Figure 1). The heating rate reached a maxima, however, and decreased once above 150°C. Since the heating rate is directly proportional to the dielectric loss, the maxima corresponds to the $T_g$ of PVAc at 2.45 GHz. Above the $T_g$, the heating rate decreased due to the inefficiency of coupling in the electromagnetic radiation as the fluid state was approached. For this reason, we have identified this technique as microwave calorimetry for identifying $T_c$ and $T_g$ at 2.45 GHz.

Low frequency DETA measurements of tan $\delta_e$ at 0.1, 1, 10 and 100 kHz for PVAc are shown as a function of temperature in Figure 8. The activation energy for PVAc (210 kJ/mol) was obtained from the slope of the Arrhenius plot shown in Figure 9. Activation energies for PVC (380 kJ/mol), SAN (300 kJ/mol), PEMA (170 kJ/mol), PBMA (130 kJ/mol) and PMMA (100 kJ/mol) were obtained using the same method and are shown in Figure 9.

The combination of microwave calorimetry measurements ($T_g$ and $T_c$ at 2.45 GHz) with activation energy measurements to predict microwave heatability for thermoplastic materials was also addressed. The temperature difference between the critical heating temperature and the $T_g$ (determined by DSC at 10°C/min.) was found to depend upon the magnitude of the activation energy, as summarized in Table 2. In particular, the higher the activation energy, the closer the $T_c$ was to the $T_g$, since the dielectric loss peak was relatively insensitive to frequency changes, as in the case of PVC. The $T_c$ was found to be very far from the $T_g$ for PMMA due
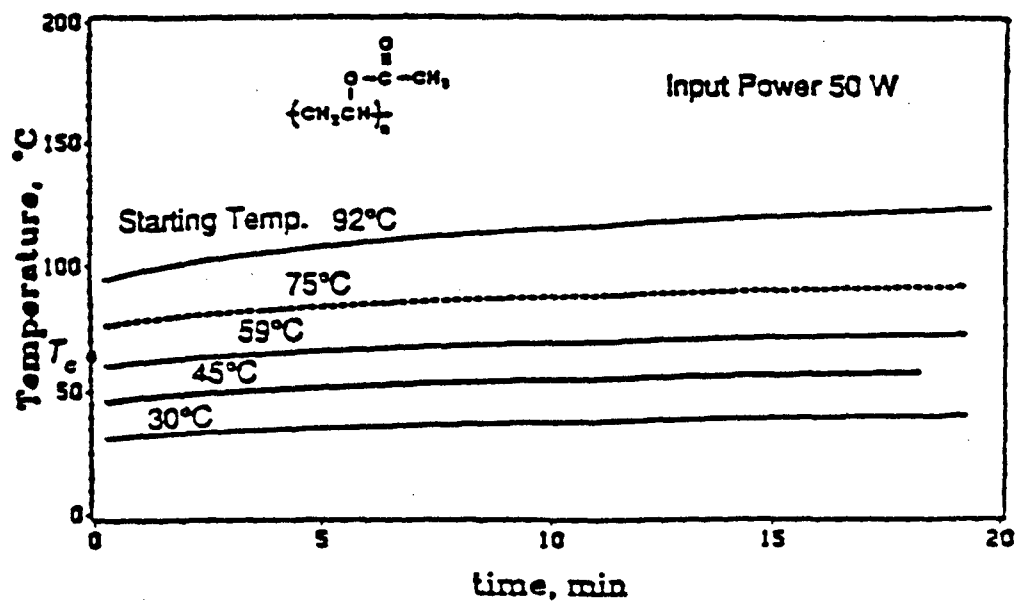
Figure 5. Time-temperature profile for PVAc in the travelling mode. Starting sample temperatures were established by a strip heater fastened to the exterior of the cavity.

$T_g$ of PVAc = 25°C
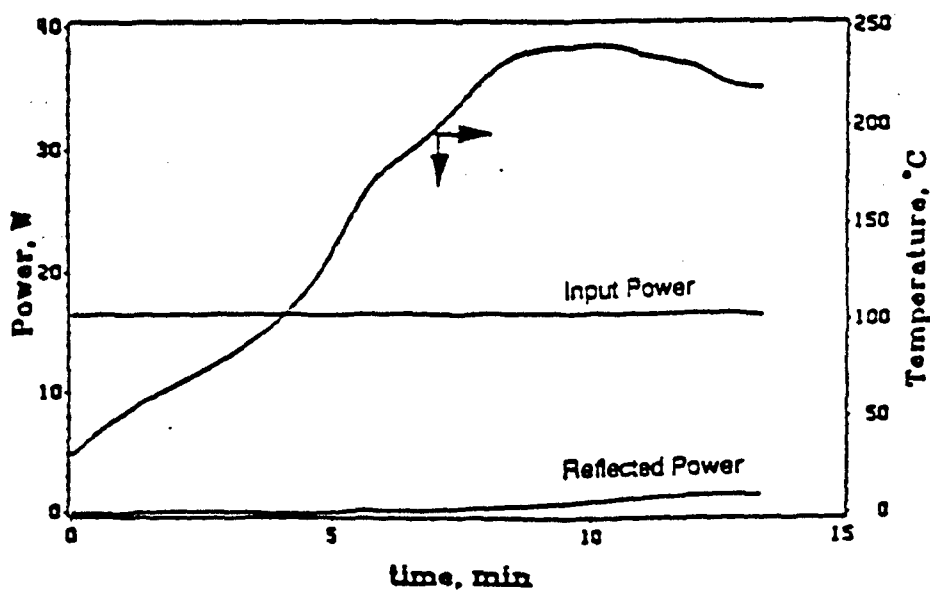


Figure 6. Time-temperature profile for PVAc in the standing mode at 17 Watts input power.

243
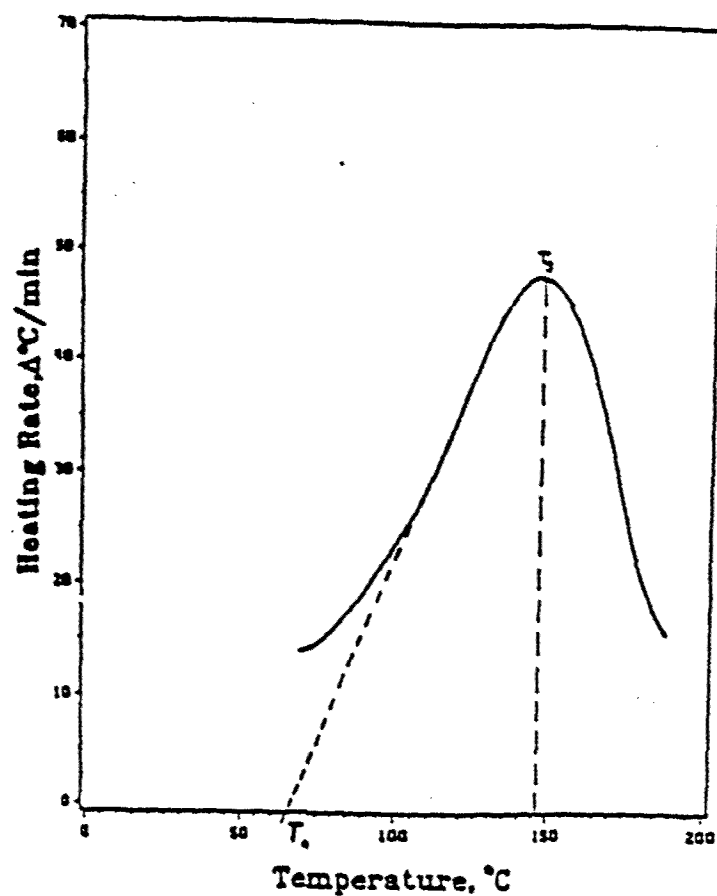
Figure 7. Heating rate (dT/dt) as a function of sample temperature provides the critical temperature, $T_c$, and the $T_g$ at 2.45 GHz.
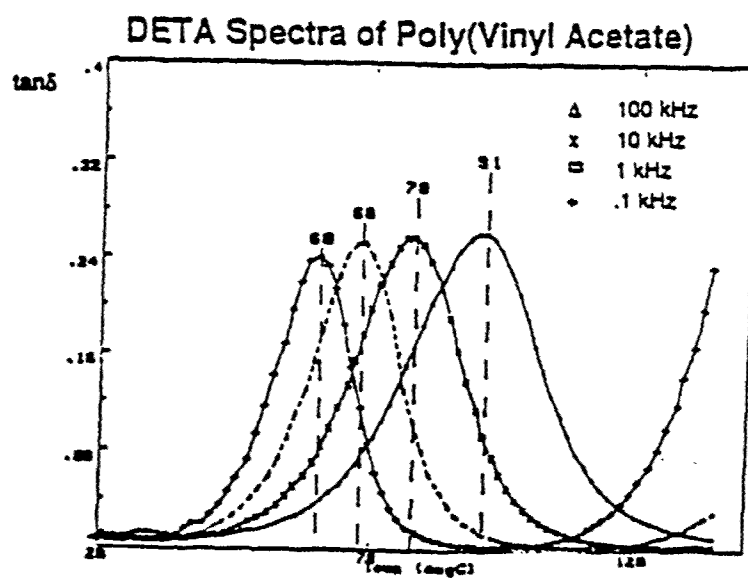


Figure 8. Dielectric thermal scan of PVAc to measure $T_g$ as a function of frequency for the construction of Arrhenius activation energy plots.

244
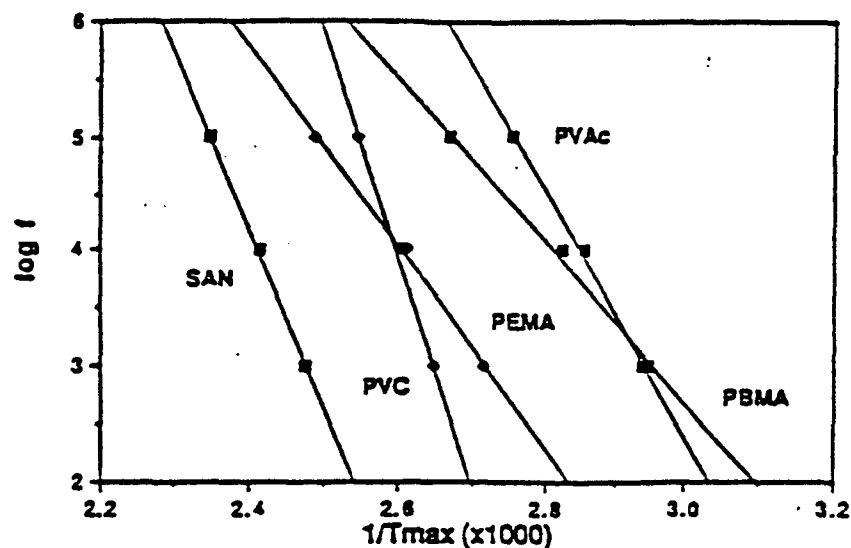
Comparison of the slopes: PVC>SAN>PVAc>PEMA>PBMA

$$\Delta E_a = -2.303R \times \text{slope}$$

Figure 9. Arrhenius plot for various thermoplastic polymers. Activation energies were calculated from the slopes with PVC having the largest slope.

Table I. Various thermoplastics used in this study.

| Polymer | $T_g$ (°C) | Press Temp. (°C) | Supplier |
|---------|--------|------------------|----------|
| PMMA | 105 | 180 | Inland Leidy |
| PMMA | 20 | 85 | Aldrich |
| PEMA | 66 | 115 | Inland Leidy |
| PVAc | 30 | 71 | Aldrich |
| SAN | 101 | 155 | Union Carbide |
| PVC | 85 | 145 | Polysciences |

Table II. Effect of activation energy on the distance between $T_c$ and $T_g$.

| Polymer | $\Delta E_a$ (kJ/mole) | $T_c - T_g$ (°C) |
|---------|--------------|-------------------|
| PMMA | 100 | 80 |
| PVAc | 210 | 35 |
| PVC | 380 | 28 |

245

to the small activation energy which was attributed to the frequency sensitivity of the dielectric loss peak.


## CONCLUSIONS

The processing of thermoplastic polymers via microwave radiation in tuned waveguides can be greatly enhance by understanding the dielectric response as a function of temperature and frequency. In particular, low frequency dielectric analyses were used to conveniently measure the frequency sensitivity of various thermoplastics by determining their Arrhenius activation energies. In addition, microwave calorimetry has led to the identification of a critical temperature, $T_c$, necessary for effective microwave heating. By combining the results of Arrhenius analyses with microwave calorimetry, one can understand how far the dielectric loss was shifted with frequency toward the critical temperature necessary for microwave heating.

## REFERENCES

1. M. Chen, J. E. McGrath and T. C. Ward, Polym. Mater. Sci. Eng., 60, 443 (1989).

2. Y. F. Chen, Y. C. Lee, Polym. Mater. Sci. Eng., 60, 680 (1989).

3. J. C. Hedrick, D. A. Lewis, G. D. Lyle, S. D. Wu, T. C. Ward and J. E. McGrath, Polym. Mater. Sci. Eng., 60, 438 (1989).

4. J. C. Hedrick, D. A. Lewis, T. C. Ward and J. E. McGrath, Polym. Prepr., 29 (1), 363 (1988).

5. J. C. Hedrick, D. A. Lewis, G. D. Lyle, T. C. Ward and J. E. McGrath, Proceedings of the American Society of Composites, Fourth Technical Conference (Technomic Publishing Co., 1989) pp. 167-176.

6. D. A. Lewis, J. C. Hedrick, J. E. McGrath and T. C. Ward, in Microwave Processing of Materials, eds. W. H. Sutton, M. H. Brooks and I J. Chabinsky (MRS Publications, 1988) pp. 181-188.

7. D. A. Lewis, T. C. Ward, J. D. Summers and J. E. McGrath, Polym. Prepr., 29 (1), 174 (1988).

8. J. C. Hedrick, D. A. Lewis, T. C. Ward and J. E. McGrath, Polym. Prepr., 28 (2), 303 (1987).

9. J. Jow, J. D. Delong and M. C. Hawley, SAMPE Quarterly, 20 (2), 46 (1989).

10. J. Jow, Ph.D. Dissertation, Michigan State University, East Lansing, MI, 1988.

11. J. Jow, M. C. Hawley, M. Finzel and T. Kern, Polym. Eng. Sci., 28, 1450 (1988).

12. A. Bouazizi and A. Gourdenne, Eur. Polym. J., 24, 889 (1988).

13. Y. Baziard and A. Gourdenne, Eur. Polym. J., 24, 881 (1988).

14. Y. Baziard and A. Gourdenne, Eur. Polym. J., 24, 873 (1988).

15. Y. Baziard, S. Breton, S. Toutain and A. Gourdenne, Eur. Polym. J., 24, 633 (1988).

16. Y. Baziard, S. Breton, S. Toutain and A. Gourdenne, Cur. Polym. J., 24, 521 (1988).

17. M. Chen, Ph.D. Dissertation, Virginia Tech, Blacksburg, VA, 1989.

18. B. Manring, Master Thesis, Michigan State University, East Lansing, MI, 1988.

19. A. E. Zachariades and R. S. Porter, High Modulus Polymers: Approaches to Design and Development, Marcel Dekker, Inc., New York, 1988.

20. M. Amano and K. Nakagawa, Polym. Commun., 28, 119 (1987).

21. M. Amano and K. Nakagawa, Polymer, 28, 263 (1987).

22. M. Amano and T. Konaka, Polymer, 27, 1553 (1986).

23. A. C. Metaxas and R. J. Meredith, Industrial Microwave Heating, Peter Peregrinus, London, 1983.

24. N. G. McCrum, B. E. Read and G. Williams, Anelastic and Dielectric Effects in Polymeric Solids, John Wiley & Sons, New York, 1967.

25. P. Hedvig, Dielectric Spectroscopy of Polymers, John Wiley & Sons, New York, 1977.

26. A. R. Von Hippel, Dielectric Materials and Applications, The Technology Press of M.I.T. and John Wiley & Sons, New York, 1988.

27. J. Asmussen, H. H. Lin, B. Manring and R. Fritz, Rev. Sci. Instrum., 58, 1477 (1977).

# FEATURES OF MICROWAVE PROCESSING OF INORGANIC/ORGANIC HYBRID NETWORKS (CERAMIC) MATERIALS.

D. E. RODRIGUES and G. L. WILKES
Polymer Materials and Interface Laboratories
Department of Chemical Engineering
Virginia Polytechnic Institute & State University
Blacksburg, Va 24061.

## INTRODUCTION

Over the last two decades the sol gel technique has become very popular because of its ability to yield a multicomponent inorganic glass at low temperatures[1,2]. More recently, techniques to incorporate organic species into a sol gel network of metal alkoxides has been developed and studied[3-7]. One technique developed in our laboratory is to incorporate oligomers endcapped with metal alkoxide functionalities into a reaction mixture of TEOS, water and acid catalyst. The resulting materials, often cured at ambient temperatures, can be tough and transparent monoliths. This technique is important in that it helps to overcome some of the defects of pure sol gel silicate structures such as cracks, voids and brittleness. The high temperature structural properties of these materials, however, are limited because of the organic component. This approach provides the ability to make a wide range of materials with vastly different properties depending upon the polymer and metal alkoxide chosen. Novel properties displayed by these materials make them attractive for certain technological applications such as coatings, films and fibers. One of the main drawbacks of the ambient temperature curing process is the relatively long reaction time which hinders immediate utilisation of the product. As would be expected, the extent of reaction has been found to be dependent on the $T_g$ of the oligomer under consideration. In the case of high $T_g$ oligomers (e. g. polysulfones) the reaction has to be completed at elevated temperatures (above the $T_g$) in order to acheive a high extent of reaction. In the case of ceramers containing functionalized poly(tetramethyleneoxide) (PTMO) oligomer, curing time can vary between 48 to 100 hours before the final gel can be successfully handled and tested. In order to enhance the rates of reaction and determine the effect of such an acceleration on the physical properties, samples were reacted at elevated temperatures using microwave heating and conventional oven curing. When microwaves were used the curing time has been found in some cases to be reduced dramatically from 60 hours to twenty minutes. In this paper structure-property relationships of these "microwaved" materials will be compared and contrasted with similar materials cured in a conventional oven at equivalent elevated temperatures as well as room temperature cured materials. Time-temperature studies of the reactants were also conducted in a travelling wave guide. These studies were done primarily to gain some insight as to the effect of microwaves on specific reactants. analyzer.

## EXPERIMENTAL

Sample formulation for the experiment consisted of 60wt% of TEOS with the remainder constituted by triethoxysilane endcapped PTMO of a number average molecular weight of 2000 g/mol. Water was added in an amount equivalent of 100wt% since this is the stoichiometric amount required to hydrolyse all alkoxy functionalities present in the reaction mixture. Hydrochloric acid (10N) was added to catalyse the reaction. The initial reaction mixture when expressed in terms of the notation developed by Huang(3) is TEOS(60)-PTMO(2000)-100-0.048 as defined in Fig. 1. N, N dimethylformamide (DMF) and isopropanol (IPA) were used as solvents to promote miscibility between the polymer, water and TEOS. The nature of the reaction has been discussed in detail elsewhere (3). The elevated temperature chosen for the curing study was 70°C for both, the conventionally cured as well as the microwaved samples. Samples were mixed for twenty minutes according to the procedure shown in Fig. 2. In the case of the oven cured samples, the reaction mixture was then poured into Teflon coated Pyrex petri dishes and immediately placed into convection ovens stabilized at the aforementioned temperature. They were left in the oven for a period of two hours after which they were removed and subjected to physical testing. These samples will be denoted by "O. C. 70C" to represent those samples cured in the conventional oven.

Microwaved samples were prepared in a manner identical with that of their oven cured counterparts; the chief exception being that they were placed in a custom made cylindrical microwave cavity and heated due to the coupling between the reaction mixture and the microwaves. A frequency of 2.45GHz was used with a maximum power of 10W The cylindrical cavity is tunable which provides the ability to significantly improve the Q-factor of the cavity significantly. The cavity was operated in the $TE_{111}$ mode. Samples were heated to 70°C in the cavity. These materials are denoted by "M. W. 70C". The temperature was raised to the maximum desired value in approximately 400 seconds and held at that temperature for an additional 800 seconds making the total time in the cavity equal to 20 minutes. The microwave heating profile is displayed in Fig. 3. Temperatures were monitored by a fiber optic probe. Tuning of the cavity was used to maintain the sample at the 70°C temperature. Finally, as stated above, samples were also cured at room temperature. The same reactants were cast into petri dishes and allowed to remain at ambient conditions for six days before physical testing, the longer time being necessary for gelation and curing.

| ITEM | DESCRIPTION |
|------|-------------|
| TEOS | Tetraethylorthosilicate |
| (60) | Wt% Of TEOS To Oligomer |
| PTMO(2K) | Functionalized Oligomer (MW) |
| 100 | Ratio Water To Alkoxide (Mol%) |
| 0.048 | Ratio Acid To Alkoxide (Mol%) |
| (THF/IPA) (DMF/IPA) | Solvents For Compatibility |

**Figure 1. Nomenclature for the sol gel hybrid:TEOS(60)-PTMO(2K)-100-0.048**

## IPA. DMF. PTMO. TEOS

MIX FOR 20 MINUTES AT RT

## ADD WATER. HCl

MIX FOR 2 MINUTES AT RT

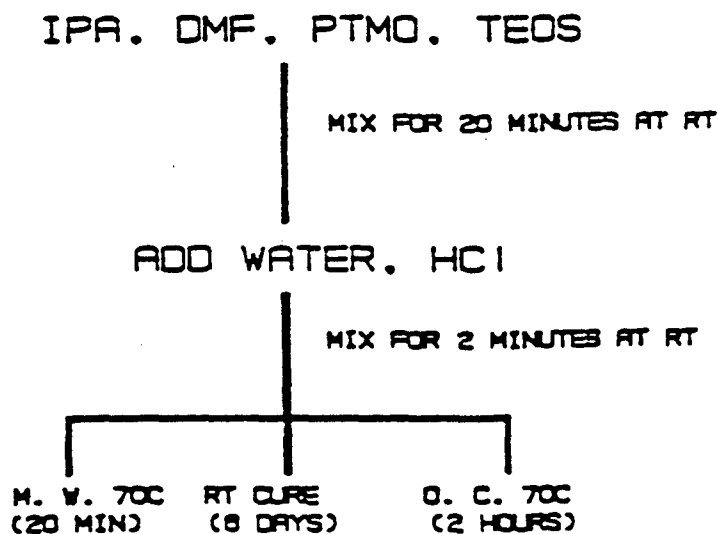| M. W. 70C | RT CURE | O. C. 70C |
|-----------|---------|-----------|
| (20 MIN) | (6 DAYS) | (2 HOURS) |

**Figure 2. Schematic for the preparation of ceramer sol gels**
IPA = 2-Propanol, TEOS = Tetraethylorthosilicate
DMF = n, n dimethylformamide, PTMO = triethoxysilane
endcapped polytetramethyleneoxide,

Stress strain tests were performed on an Instron model no. 1122. These tests were carried out at room temperature immediately after removal from the microwave cavity, the convection oven or the six day casting. Dogbone samples having a 10 mm gaugelength were tested at a crosshead speed of 2mm/min. Sample thickness varied from 5 mils to 15 mils. A minimum of five tests were run on each material type. Dynamic mechanical analysis was carried out on a Rheovibron DDV-IIC. These tests were run at a frequency of 11Hz in the temperature range of -100°C to 170°C. Structural features of the materials were investigated using a small angle Xray scattering (SAXS) facility with a Siemens Kratky camera system using $CuK_\alpha$ ($\lambda$ = 1.54Å) radiation. A position sensitive dectector was used in conjunction with the Kratky camera.

Time temperature microwave heating studies were conducted in a rectangular waveguide WR284 with a travelling wave. The technique used here is shown in Fig. 4 and consists of placing 5 ml of the sample to be tested in a Teflon sample holder. The sample holder has a small hole at the top for inserting the fiber optic probe. The power input to the cavity is fixed at 5W. The sample is then positioned in the cavity at a point of minimum reflected power as measured on the power meter. The temperature is then measured as soon as the power is turned on. The heating rate is indicative of the dielectric loss factor of the material at the frequency of 2.45GHz.
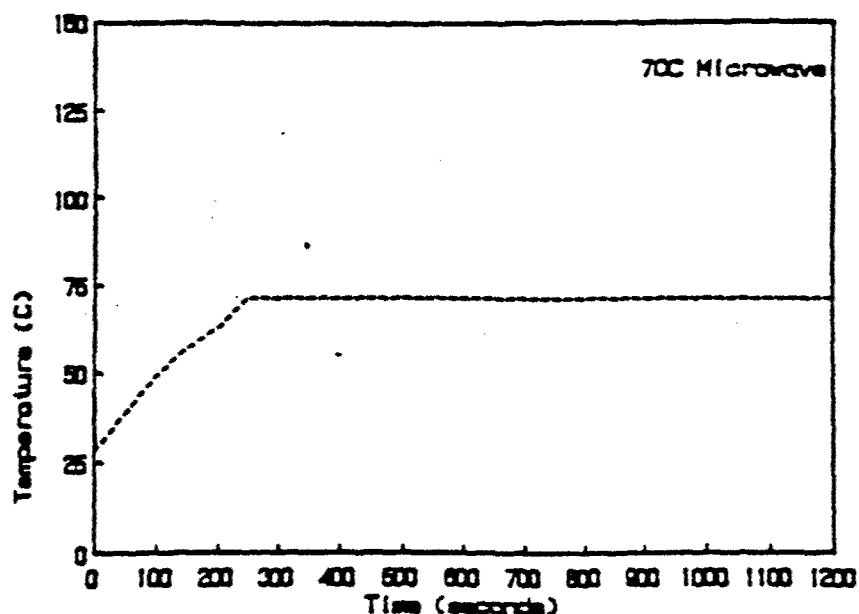
249

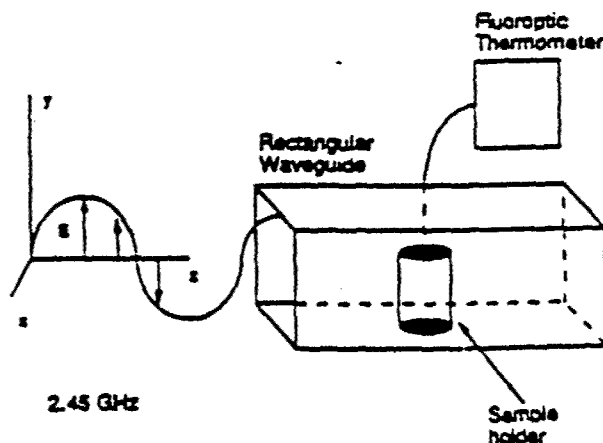Figure 3. Microwave heating profile for the material heated to 70°C.



Figure 4. Schematic of applied electric field, waveguide and sample
holder for the time-temperature study.

RESULTS AND DISCUSSION

Samples were subjected to ambient temperature stress strain analysis almost immediately after thermal processing (within two hours). The results for the stress-strain analysis are summarized in Table I. Samples cured at 70°C using microwaves show a high modulus of 250MPa. which is approaching the value of a polymeric glass. The stress at break is approximately 40MPa and the elongation at break is 21%. The materials cured in a conventional oven at 70°C show a modulus of only 4MPa and have an elongation at break of 50%. This indicates that the oven cured material was reacted to a much lower extent than the microwave cured material. This can be explained in terms of the coupling that occurs between microwaves and the polar reactants which is strongly dipole dependent. There is evidence from other studies to indicate that this coupling can enhance reaction kinetics if reactive sites are dipolar[9]. Principle reactive sites for network development in this reaction are the hydroxyl moities on the silanol molecule formed after hydrolysis. The coupling between the microwaves and the silanol group seem to promote a higher extent of reaction as can be seen from the time temperature studies. In addition this higher level of reaction causes considerably higher densification of the inorganic phase relative to the O.C.70C. as can be indirectly confirmed from the SAXS scattering results to be discussed later. In Fig. 5 a plot of temperature vs time for the reaction mixture without acid catalyst and with acid catalyst reveals some significant differences. Both samples show an almost instantaneous rise in temperature. The difference in the

250

| FRESH | MODULUS(MPA) | σ (MPa) | ELONG(%) |
|---|---|---|---|
| M. W. 70C (20 MIN) | 250 | 40 | 21 |
| RT cure (8 DAYS) | 153 | 29 | 20 |
| O. C. 70C (2 HRS) | 4 | 1 | 50 |
| AGED (1 MONTH) | | | |
| M. W. 70C | 380 | 38 | 21 |
| R. T. cure | 380 | 40 | 21 |
| O. C. 70C | 150 | 7 | 7 |

**Table I. Results of the stress-strain study conducted at ambient conditions immediately after curing and after aging the materials for one month.**
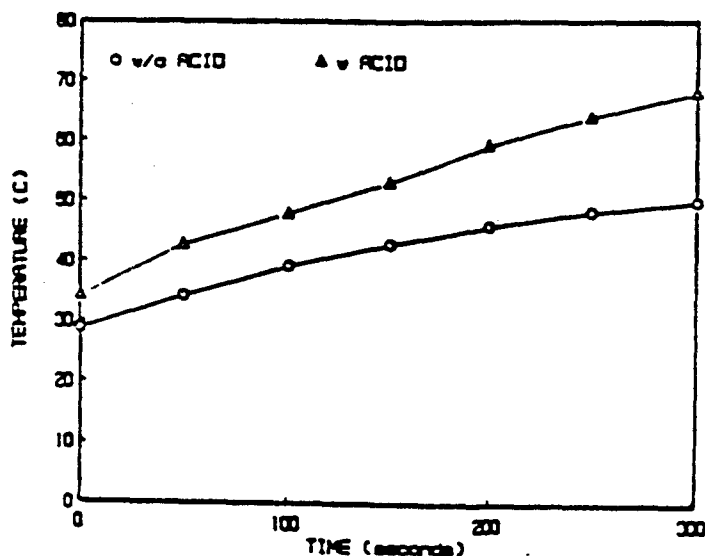


**Figure 5. Time temperature profile for the reactive solution before and after the addition of acid catalyst.**

Initial temperatures at t = 0 is because of the heat of reaction. However, with time it can be seen that sample containing catalyst heats much faster and this can be attributed to the absorption of the silanol which are produced as a result of the hydrolysis. This lends credence to the idea that silanol is an efficient absorber of microwave energy. Another observation worth mentioning here is that when the reaction was carried out with different metal alkoxides such as titanium isopropoxide and zirconium isopropoxide, which are much faster reacting and hence require extremely little water for hydrolysis, there is not much difference between microwave curing and oven curing. Hence the presence of water for hydrolysis is an important factor in increasing the rate of reaction when microwaves are utilized for the TEOS containing systems. Room temperature cured samples take almost six days to cure completely and display modulus, stress at break and elongation at break values intermediate between those of the microwaved and the oven cured samples. These samples display dynamical mechanical behavior similar to those cured in the microwave field and are also microphase separated in a manner similar to those cured with microwaves. In the case of the oven cured samples, heating of the material at 70°C for two hours clearly does not produce an equivalent extent of reaction. This also seems to affect the long term properties of the sample as can be seen from the mechanical properties obtained on samples that have been aged at ambient conditions for one month as shown in Table 1. The slow reaction rate in the convection oven as well as evaporation of some solvents (i. e. isopropanol-b. p. 82°C) may cause some amount of diffusion limitation in the reaction mixture which

251

would help explain the rather weak and tacky gel obtained.

The dynamic mechanical analysis storage modulus (shown in Fig 6.) of the various samples follow a trend similar to that displayed by the static modulus tests. The values match quite closely with the Instron tests conducted at the same temperature. It can also be seen that there is a small increase in the stiffness of the microwaved and six day RT cured samples as the temperature is raised above 50°C. This indicates that the samples were not fully reacted and therefore undergo some additional reaction at the slow heating rate (2°/min) in the DMA instrument. It is at this stage, worthwhile to point out that curing with microwaves at 70°C even for extended periods of time, will not bring the material to its final properties because of the presence of DMF. The DMF being highly polar evaporates at 153°C and currently experiments are being conducted to determine whether this aging process can be accelerated significantly by going to a higher temperature or curing for longer period of time in the cavity. The increase in stiffness is considerable in the case of the O.C.70C material which substantiates our earlier postulation of a much lower extent of condensation. There could also be an evaporation of water, solvent and by products of the reaction which, with their loss would, contibute to an enhancement of the storage modulus. The fact that the storage modulus values at the upper limiting temperature of 170°C is identical for all three samples shows that reactants are not lost due to evaporation in the oven cured sample. This fact is also substantiated by thermogravimetric analysis where the remaining material at 600°C is around 32 wt% of the initial amount analysed. The Tan $\delta$ (Fig. 7) behavior as seen at 11Hz provides some useful information about the morphology of these systems. The glass transition displayed by these systems is due to the PTMO oligomer. In general the Tan $\delta$ response displays some bimodal character with cooperative PTMO segmental motion beginning at -90°C. The onset of cooperative segmental motion at this temperature indicates the presence of some pure or rich PTMO phase in all three systems. The lower temperature peak which typically appears between -90°C and 10°C can be attributed to a mixture of endlinked PTMO and incompletely condensed TEOS. This mixture causes a broadening of the peak when compared with the loss dispersion of pure crosslinked PTMO. The higher temperature peak is believed to be due to more oligomer entrapped/encapsulated by the highly densified glassy domains. The relative extents of these two types of PTMO (pure PTMO vs PTMO trapped in a more glassy surrounding) determines the position and breadth of the peak as well as the extent of bimodal behavior. In the case of the O.C.70C, sample the lower temperature peak displays a Tan $\delta$ value of almost 0.45 and occurs at ca. -40°C. This suggests a relatively small amount of endlinking, especially when compared with the room temperature and M. W. 70C cured materials which peak at -10°C and 0°C respectively. The higher temperature peak for the O. C. 70C material snows very little loss behavior in the range of 30 -100°C thereby indicating very little polymer encapsulation and constriction by the densified SiO$_2$. This conclusion is supported by the SAXS behavior as will be discussed later. The room temperature and M.W.70C materials on the other hand display a Tan $\delta$ behavior indicative of a higher degree of phase separation of PTMO from the silicate phase as well as a higher extent of encapsulation as can be seen from the higher value of the Tan $\delta$ peak at around 100°C. The microwave cured material displays the lowest loss response of the three cured materials and the lower temperature peak has a maxima of 0.1 at 0°C indicating a higher extent of crosslinking of the oligomer.
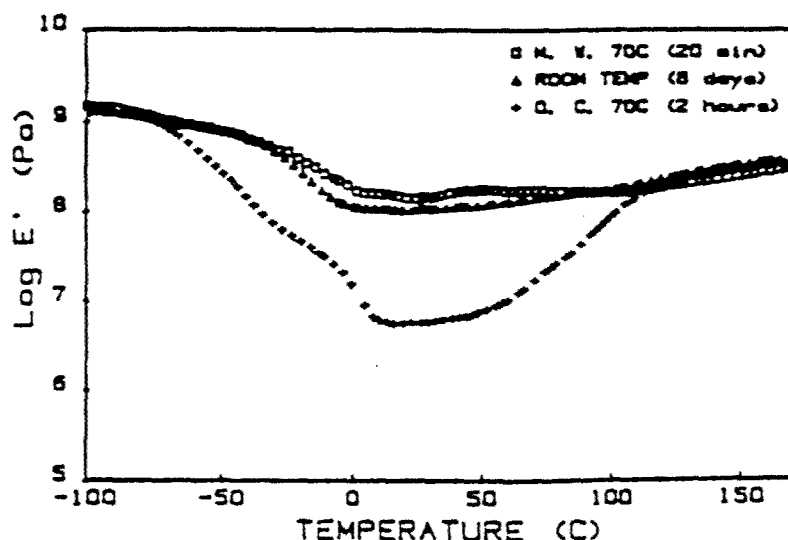


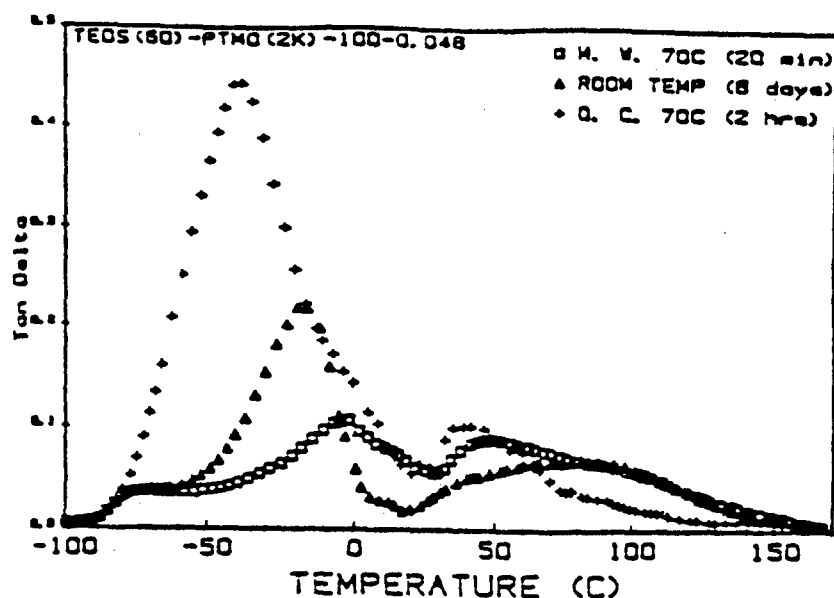Figure 6. Dynamic Storage modulus at a frequency of 11 Hz.

252

**Figure 7. Dynamic loss modulus at a frequency of 11 Hz.**

The SAXS profiles (shown in Fig. 8) for the microwave cured and room temperature cured materials are much sharper.(peaking at around 0.08nm⁻¹) when compared with the oven cured materials. The intensity of the scattering peak is dependent not only upon the degree of phase separation between the two phases but also upon the extent of reaction within the silicate phase. The higher the densification within the inorganic rich phase the higher will be the scattering intensity. Based on this, the scattering curve for the oven cured material suggests that there is a larger amount of mixing as indirectly observed from the greater peak breadth which shows a spacing around $0.1nm^{-1}$ The low scattering intensity for the O. C. 70C material also indicates a low degree of reaction within the inorganic phase too. Since the high purity inorganic phase has a higher electron density than the polymer or the mixture of polymer and incompletely condensed TEOS, consequently a higher scattering intensity would indicate a higher degree of reaction and densification. The SAXS peak for the microwaved material shows a higher scattering intensity thereby indicating a higher degree of reaction and hence greater densification than the room temperature cured material. With regard to the partial microphase morphologies they appear to be nearly identical since both provide an average interdomain spacing of ca. 140Å. Further details regarding analysis of the higher tail region will be presented in a future publication.
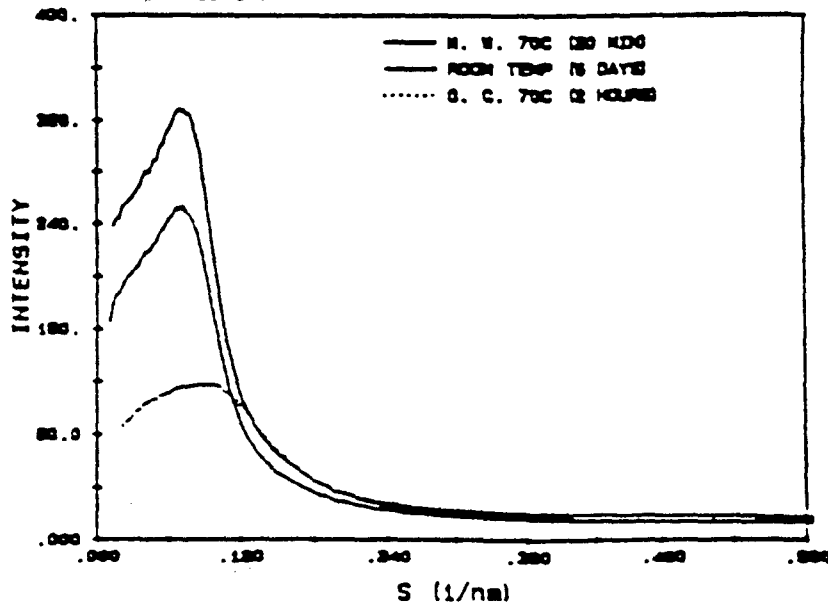


**Figure 8. Small angle scattering profiles of the three differently cured**
**materials show intensity vs S, where S is defined as** $\frac{2}{\lambda}\sin(\frac{\theta}{2})$ .
$\theta$ **is the radial scattering angle.**

## CONCLUSIONS

The use of microwave processing is a quick and efficient method of curing ceramers. Not can curing time be shortened but a much lower power is used for microwave processing conventional processing. The nature of the reactive groups play an important role in the curing these materials because of the ability of the microwaves to couple with these dipole containing species. Conventionally cured materials require considerably longer time periods for curing.

## ACKNOWLEDGEMENTS

## REFERENCES

1) Dislich, H. Agnew. Chem. Int. Ed. Engl. 1971, 10(5)363.
2) Yoldas, B. E. J. Mate. Sci. 1977, 12, 1203.
3) Hao-Hsin Huang, Thesis, VPI&SU, 1987.
4) Wilkes, G. L.; Orler, B.; Huang, H.; Polym. Prep. 1985, 26(2), 300.
5) Huang, H.; Orler, B.; Wilkes, G. L.; Macromolecules 1987, 20(6) 1322.
6) Phillipp, G.; Schmidt, H.; J. Non-Cryst. Solids 1984, 63, 283.
7) Schmidt, H.; Seiferling, B. Mate. Res. Soc. Symp. Proc. 1986, 73, 739.
8) Glaser, R. H.; Wilkes. G. L.; Bronimann, C. E. J. Non-cryst. Solids, In press.
9) Ginzton E. L. Microwave Measurements, McGraw Hill Book Co. 1957.
10) Lewis, D. A.; Ward, T. C.; Summers, J. D.; McGrath, J. E. Polym. Prep. 1988, 29(1), 174.

254

# ENHANCED CHEMICAL BONDING AT THE FIBER-MATRIX INTERPHASE
## IN MICROWAVE PROCESSED COMPOSITES

L. T. DRZAL, K. J. HOOK, AND R. K. AGRAWAL
 Composite Materials and Structures Center, Department of Chemical
Engineering, Michigan State University, East Lansing, Michigan 48824-1326

ABSTRACT

The effect of microwave processing on the chemical interactions occurring
between the carbon fiber surface and the epoxy matrix constituents was
investigated using X-ray Photoelectron Spectroscopy (XPS). Monofunctional
model compounds of the matrix constituents were exposed to the carbon fibers
at temperatures similar to those encountered during composite processing.
The microwave treatment resulted in a substantial increase in the amount of
chemical interaction between the fiber surface and the epoxy resin but
little difference for the amine component of the matrix when compared to
thermal processing. An epoxy resin/amine hardener adduct compound used to
determine the hydroxyl group interaction with the carbon fiber surface
indicated a low level of chemical interaction of the hydroxyl with the
carbon fiber surface under the conditions used in this study.

INTRODUCTION

    Electromagnetic processing involving the use of microwave frequency
energy offers a new approach to composite processing in which energy is
coupled directly into the material without reliance on conduction and
convection. An earlier published result [1] reported that in carbon
reinforced epoxy composites, significant changes in fiber to matrix adhesion
were measured when microwave processing was used in place of thermal
processing. Under identical conditions, no change in adhesion to aramid or
glass fibers was detected with the epoxy. The conductive nature of the
carbon fiber has been shown to result in a preferential absorption of
electromagnetic energy causing the fibers to attain a higher temperature
than the surrounding epoxy matrix. This study was undertaken to determine
if the increased temperature of the fiber resulted in a change in the
chemical bonding between fiber and matrix which was a reason for the
increase in adhesion.
    Since it is not possible to determine the chemical bonding between a
carbon fiber and epoxy matrix in the solid state with current analytical
techniques, a model monofunctional system consisting of a single carbon
fiber embedded in a large tensile dogbone shaped cavity was selected as the
experimental configuration. It provided conditions identical to those used
in the earlier microwave processing studies. In this manner, the samples
could be processed with either thermal or microwave energy under identical
conditions without polymerization taking place. Specific chemical
interactions between the functional groups on the model compounds and the
carbon fiber surface could take place in the same manner as in the solid
state. The unreacted species could then be removed with low temperature
solvent extraction and the carbon fiber surface could be analyzed with X-ray
Photoelectron Spectroscopy to quantitate chemical interaction between the
amine or epoxy functionality and the carbon fiber surface.

## EXPERIMENTAL

PAN based AS-4 fibers with a proprietary oxidative surface treatment obtained from Hercules Inc. have been used in this study. The epoxy resin used in this investigation is a diglycidal ether of bisphenol-A (Epon 828, Shell Chemical Co.) and the curing agent used is a meta-phenylene diamine (m-PDA, Aldrich Chemical Co.). Comparisons were made using these materials, between the effects of equivalent thermal cure and microwave cure cycles on the chemical reactions resulting in each of the respective procedures.

All of the thermal cure and microwave experiments were conducted to attain the same system temperatures between 80 and 130 C. Microwave power was coupled into the specially designed cavity through an adjustable excitation probe at a frequency of 2.45 GHz. Table I summarizes the various thermal and microwave treatments applied to the AS4 fibers.

Subsequent to the various surface treatments, samples of the treated carbon fibers were analyzed with the use of a Perkin-Elmer PHI 5400 x-ray photoelectron spectrometer. Pass energies were set at 178.95 eV for the survey scans (0-1000 eV) and at 8.95 eV for the high resolution narrow scans of the elemental regions. The curve fitting was carried out using a modified Gauss-Newton non-linear least squares optimization procedure that is part of the instrumental software. with the "graphitic" C 1s peaks set at 284.6 eV [2][3][5].

Complete experimental details can be found in [6].

## RESULTS AND DISCUSSION

High resolution, narrow energy window scans were collected for the carbon and oxygen regions of each of the respective treatments. Examples of these curve resolved scans are shown in Figures 1 and 2. Figure 1 contains the same region of the different XPS spectra binding energies from 281.0 to 295.0 eV which is the carbon 1s region. Figure 2 contains the binding energy region from 529.5 to 537.5 eV which is the oxygen 1s region.

Thermal and Microwave Epoxy Resin Treatments. As a result of the thermal epoxy treatments, there is a significant increase in the C 1s peak II intensity (at 286.2 eV) of both treatment "b" (12.5% of area - Figure 1b) and treatment "c" (15.7% of area - Figure 1c) over the as-received AS4 fiber (Figure 1a). Peak II corresponds to the C-O type chemical bond. There is also a small decrease in peak III ( at 287.6 eV), C=O type bond, for both of the treatments. Figure 1d shows the effects of a microwave curing procedure on the chemical bonding that occurs between the epoxy resin and the fiber surface. The C 1s signal shows a strong shoulder at 286.2 eV which indicates a large increase in the surface C-O concentration (19.0 % of area). The increase in this peak intensity is significantly greater than in the case of either of the thermal treatments. This is marked by a large increase in the C-O type of functional group which would correspond to a greater concentration of epoxy resin molecules being chemically bound to the surface than in the case of the thermal treatments.

The O 1s curve fits for the thermal and microwave epoxy resin treatments reflect an increase in peak II(at 533.9 eV) which corresponds well with the results from the C 1s region. Compared to the as-received AS4 fiber (Figure 2a) there is a general increase in the C-O bonds at the surface from the lowest temperature thermal treatment (Figure 2b) to the highest thermal
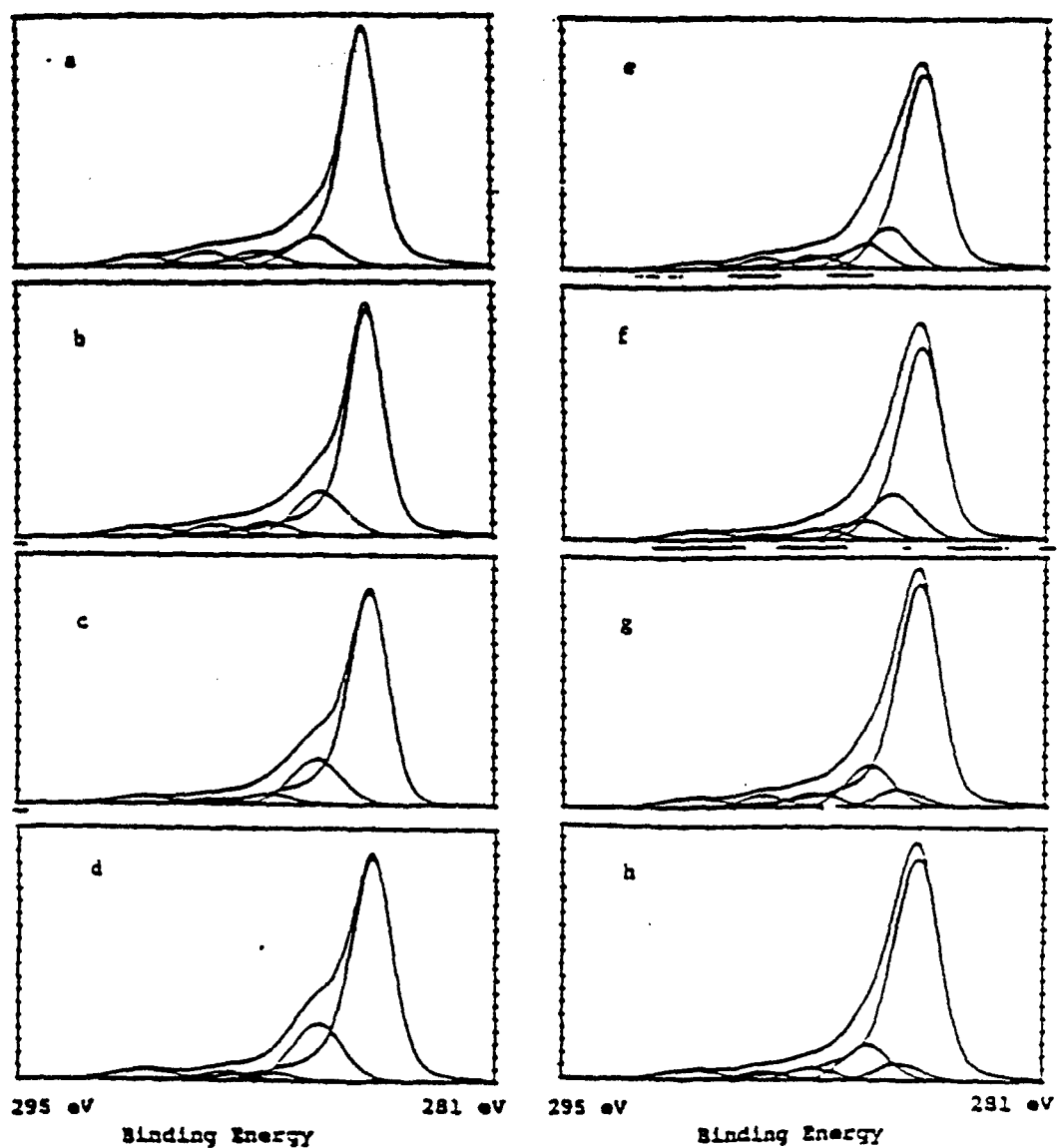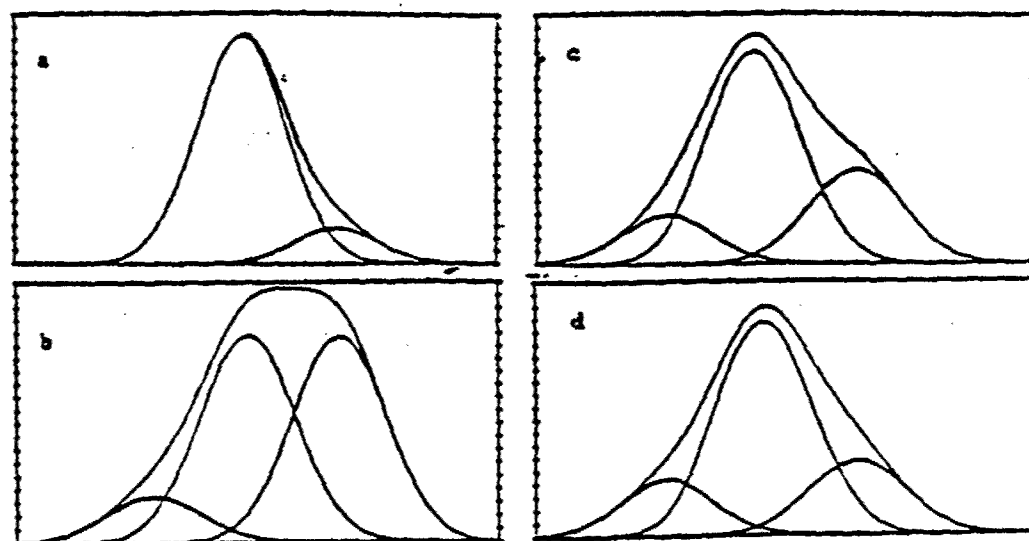
Figure 1. Curve fit Carbon 1s XPS Spectra from 281.0 to 295.0 eV binding energy. a) AS4 fiber 'as-received; b) Epoxy Treatment at 80C-thermal; c) Epoxy Treatment at 150C-thermal; d) Epoxy Treatment-Microwave; e) mPDA Treatment at 130C-thermal; f) mPDA Treatment-Microwave; g) Hydroxyl Adduct Treatment at 130C-thermal; h) Hydroxyl Adduct Treatment-Microwave.

257

Figure 2. Curve fit Oxygen 1s Spectra from 529.5 to 537.5 eV bindi:
energy.  a) AS4 fiber "as-received; b) Epoxy Treatment at 80C-thermal;
Epoxy Treatment at 150C-thermal; d) Epoxy Treatment-Microwave.

Table I.  Chemicals and thermal or microwave exposure treatment conditio:
for AS4 fibers used in this study.

| Fiber | Treatment |
|---|---|
| a | As-received AS4 |
| b | Epoxy at 80C-thermal |
| c | Epoxy at 150C-thermal |
| d | Epoxy-microwave |
| e | mPDA at 130C-thermal |
| f | mPDA-microwave |
| g | hydroxyl adduct at 130C-thermal |
| h | hydroxyl adduct-microwave |

Table II.  Oxygen 1s to Carbon 1s and Nitrogen 1s to Carbon 1s percents
each AS4 fiber treatment calculated from XPS spectra.

| Fiber | O 1s/C 1s (%) | N 1s/C 1s (%) |
|---|---|---|
| a | 10.4% | 4.0% |
| b | 11.8% | 4.5% |
| c | 13.8% | 3.5% |
| d | 16.5% | 4.1% |
| e | 9.9% | 7.6% |
| f | 7.3% | 8.2% |
| g | 9.9% | 4.9% |
| h | 10.1% | 5.6% |

258

treatment (Figure 2c). The microwave treatment (Figure 2d) produces the highest level of increase however.

Thermal and Microwave m-PDA Hardener Treatments. The most noticeable change in these treatments is the appearance of C-N intensity in the C 1s peak shape (at 285.4 eV in Figure 1e and 1f). This suggests the occurrence of a chemical reaction between the fiber surface and the amine hardener molecule. Both of the m-PDA treatments i.e. thermal and microwave, indicate an increase in the nitrogen concentration at the surface of the fiber to about the same level.

Thermal and Microwave Hydroxyl Adduct Treatments. There is no significant difference between the oxide intensities of the adduct treatments and the "as received" fiber as shown by the spectra in Figure 1g and 1h. This would seem to indicate that the reactivity of the hydroxyl group on the adduct molecule with the fiber surface is very low.

Table II summarizes the major changes in the oxygen and nitrogen to carbon ratios resulting from the exposure of these model compounds to the carbon fiber surface. These changes can be taken as an indication of the amount of chemical bonding to the carbon fiber surface after exposure to the reactants under either thermal or microwave environments. The fiber treated with the epoxy shows an increasing oxygen to carbon ratio over the baseline fiber with increasing thermal treatment (a-b-c) but the largest increase is with the microwave treatment (d). The nitrogen to carbon ratio for fibers treated with the amine shows little difference between thermal or microwave treatment (e-f). Within experimental error, no chemisorption of the hydroxyl functionality is detected in either environment.

## CONCLUSIONS

The use of a microwave heating environment can result in a substantial increase in the amount of chemical interaction between the fiber surface and the epoxy resin and amine components of the matrix. Overall the amount of chemical interaction occurring at the fiber surface is small. However, the use of the microwave curing procedure effectively doubled the degree of chemical interaction occurring between the fiber and the epoxy resin in comparison with the most effective thermal treatment (i.e. 150 degree C).

Chemical interaction of primary amine with the carbon fiber surface was the same in either the thermal or microwave environment when the amine was not competing with the epoxy group for the carbon fiber surface.

The use of an adduct compound to study possible interaction between the fiber surface and the adduct hydroxyl group indicates a low to insignificant interaction under these conditions.

Overall the extent of chemical bonding of an epoxy-amine polymer with the AS-4 carbon fiber surface is less than 5% when processed thermally. Microwave processing appears to substantially increase the probability of chemical bonding in the solid state. The combined results suggest that the change in composite performance resulting from the use of a microwave curing procedure, instead of the more typical thermally cured process, may be partly due to an increase in the chemical interactions between the fiber surface and the matrix material.

259

## References

1.  R. K. Agrawal and L. T. Drzal, J. Adhesion, 29, 63-79 (1989)
2.  P. M. A. Sherwood and Y. Xie Appl. Spec., 43(7), 1153, (1989)
3.  D. T. Clark and H. R. Thomas, J. Polym. Sci., Polm. Chem. Ed., 16, 791, (1978)
4.  L.T. Drzal, M.J. Rich, and P. F. Lloyd, J. Adhesion, 16, 1-30, (1983).
5.  A. Proctor and P. M. A. Sherwood, J. Electron Spec., 27, 39, (1982)
6.  K. J. Hook, R. K. Agrawal and L. T. Drzal, J. Adhesion, (in press)

260

# THE CONSOLIDATION AND PROCESSING OF GRAPHITE FIBER/POLYMER COMPOSITES BY CONTROLLED MODE MICROWAVES

D.J. TREACY*, D.A. EVANS*, J.S. BOYCE*, J.F. McCOY* AND B.H. TREADWAY*
*Foster-Miller, Inc., 350 Second Avenue, Waltham, MA 02154-1196

## ABSTRACT

Composite laminates have been cured under pressure in a tunable microwave cavity. A 7-in. diam cavity with a sliding short was tuned to produce single mode or controlled hybrid mode standing waves at 2.45 GHz. Graphite/epoxy laminates were processed with power inputs as low as 2 W/g.

A low loss press was designed and built to operate inside the cavity. The press can apply 100 psi pressure on a 9-in. square laminate. An empirical approach has been used to develop processing conditions for high quality laminates. Graphite/epoxy composites were cured in 90 min or less. A simple on-off temperature control loop modulated power input to the cavity with a coaxial switch.

Mechanical testing and differential scanning calorimetry have been used to evaluate the composites. The material properties have been related to processing conditions.

## INTRODUCTION AND BACKGROUND

Foster-Miller is currently involved in a program to develop technology to cure polymeric composites using microwave energy. Because the energy is directly coupled into the material (as opposed to convective heating), the potential exists to shorten cure times. Since microwave radiation is penetrating, potential may exist for improved curing of thick structures, which is often problematic with conventional convective cures.

Early work on cavity curing was performed at Michigan State University (MSU) by Profs. Assmussen and Hawley. Owing to problems with conventional microwave approaches, MSU focused on understanding and modelling the cure process in a 2.45 GHz single mode cavity of circular cross section. While MSU experiments and analysis furthered understanding of basic mechanisms and phenomena, a number of practical questions remained.

The Air Force and DARPA enlisted Foster-Miller, Inc. to work in concert with MSU to help address some of these issues. In general, the interactions of microwaves with realistic part geometries and laminate constructions are thought to be too complex to be predicted analytically, especially when tooling is added to a cavity. As a result, an empirical approach is required to find conditions for optimum cure. For continuity, Foster-Miller began investigations in 2.45 GHz cavity similar to that used by MSU. Additionally, Foster-Miller was tasked to incorporate a mold tool to apply controlled pressure during cure and instrumentation to monitor temperature and control heating. This paper is a report of progress in this effort.

## INVESTIGATION APPROACH

As considerable effort by others had gone into composite curing of unconsolidated samples in a single mode cavity, we concentrated our effort on development of techniques for consolidating test specimens which are then cured in a single mode or hybrid mode cavity: in particular, in a 7-in. diam cavity at 2.45 GHz. After consideration of several alternatives, we selected a platen press approach. This is a straightforward consolidation technique but does require design considerations particularly since the microwave absorption of the press

should be minimized, while at the same time the press must have the required mechanical strength to consolidate the samples. The following section describes the press which was designed and built.

As samples are produced, mechanical properties of subsections are tested. These include differential scanning calorimetry (DSC) and three-point flexural testing. This is to allow assessment of the level of curing and uniformity of curing. Also, these results will permit comparison with autoclave processed laminates.


EQUIPMENT PROCESSING


Mold Tool

The primary consideration in the development of a pressure applicator to be used within the resonant cavity was to ensure that the tool would cause minimal distortion or interference with the field(s). Ideally, the tool would be a microwave transparent, such that all energy coupled into the cavity would be absorbed in the laminate and not the tool. However, an equally strong consideration was the structural properties of the material as it had to be capable of applying up to 100 psi pressure on a 3 x 3 in. laminate, equivalent to 900 lb to force. Size is constrained by the relatively small size of the cavity (7-in. diam), and holes through the cavity must be held small in size and number to minimize effect on resonant modes of the cavity.

With these considerations, a simple platen press concept was developed into a design and then fabricated. Figure 1 depicts the tool which is made of a silicone filled glass cloth material, classified a NEMA G-7. Dielectric constant and loss dissipation factors are 3.9 and 0.003, respectively.

The mold tool/cavity setup is shown in Figure 2. (Note: only one plate is shown in Figure 2.) The entire mold tool and cavity baseplate assembly drops down below the cavity for loading the laminate and placing the sensors. Once the laminate is in place, the top plate is pulled down against the laminate and bottom plate. Then the entire mold tool/baseplate
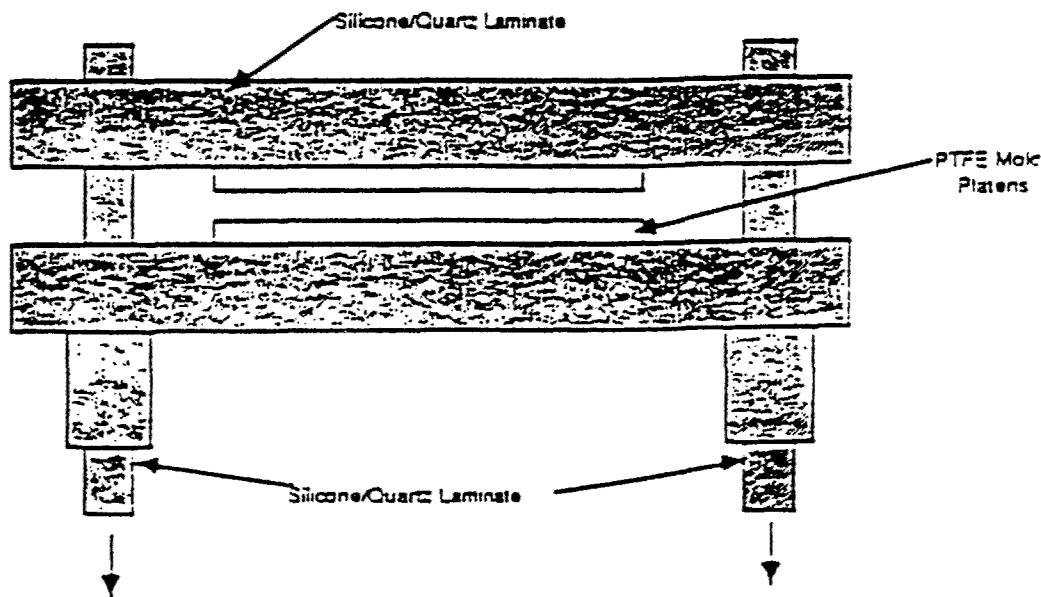


Figure 1. Platen Press Mold Tool Design for Use in a 7-in. Diam
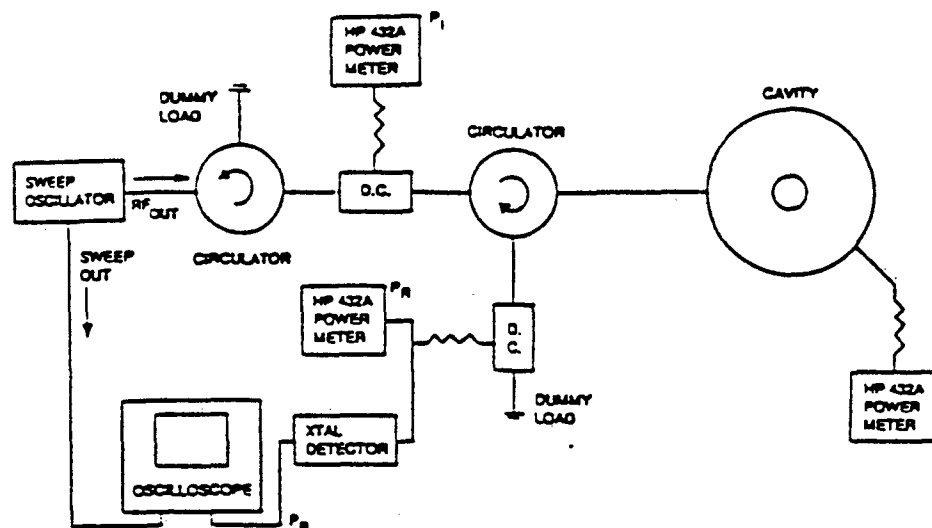Resonant Microwave Cavity

262

Figure 3. Microwave Equipment Setup for Low Power Cavity Tuning

then joined to form one 24-ply sample. For processing in the cavity, these samples were wrapped in nonporous teflon and glass bleeder cloth, one layer each, then envelope-bagged in teflon film and placed in a square silicone rubber dam.

Heating patterns within the cavity were investigated by placing cross-ply laminates within the mold tool perpendicular to the coupling probe, with a circle of thermographic paper between the sample and the platen. The sample was then heated with 120W of power for 10 min. This was sufficient to allow the hottest parts of the laminate to heat to over 100°C, at which temperature the paper changed from white to black, thus leaving a permanent record of the sample's history. Trials were made at mold heights of 0, 25, 57, and 95 mm; each mode that could be tuned to at each height was investigated. It was found that the sample-tool structure rendered the heating pattern's position insensitive; each pattern heated the sample at the edge, leaving a cold spot in the center. This behavior continued for unidirectional laminates, circular laminates, and laminates oriented 45 deg to the coupling probe.

Further investigation using a clear pyrex disk in place of the top platen (allowing direct visual observation of the sample during cure) and a series of temperature-sensitive color indicators revealed that the samples reached approximately 170°C in 30 min at 120W of heating power; this was further verified by thermocouple thermometer readings taken immediately after the sample was removed from the cavity.

Samples were processed under 100 psi mold tool pressure according to the schedule shown in Table I. Each set of conditions shown was used to cure both a unidirectional and a quasi-isotropic laminate. Schedules 1, 3, and 4 produced laminates which appeared consolidated to the eye and ear; schedule 2 samples were noticeably overcured. Each of the unidirectional laminates showed some evidence of spot-overheating, from the least case of the schedule 4 laminate being discolored to the extreme case of the schedule 2 laminate having areas where the resin was obviously burned away.

Cured samples were tested for flexural strength using a United Floor Model Electromechanical Testing Machine. Four, one-half inch wide samples were cut from each laminate. These specimens were then used for a three-point bending test using a 2-in. support span. After failure, a representative of each tested laminate was cut for testing in a Perkin-Elmer PC-Series DSC 7 differential scanning calorimeter.
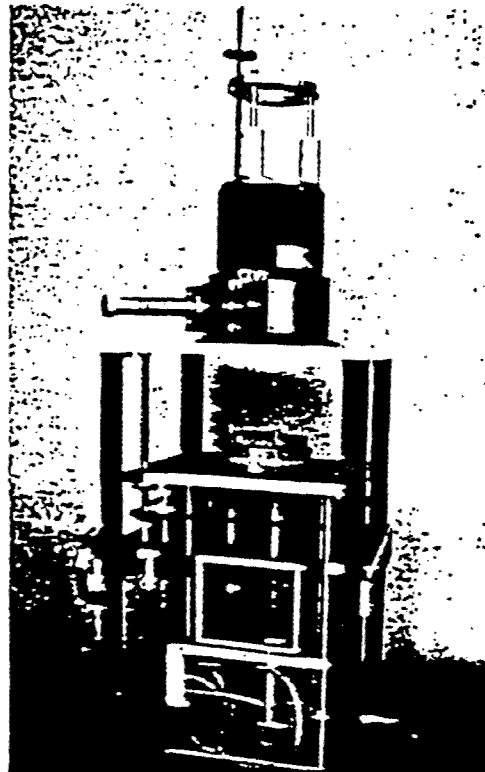
264

Figure 2. Mold Tool/Resonant Cavity Setup

assembly is slowly raised into place by means of a hand crank and gearing system. The mold tool assembly itself can then be further adjusted in height within the cavity by means of a second handcrank/gearing mechanism.

## Microwave Equipment

The cavity in which the sample is cured is a standard 7-in. diam single mode 2.45 GHz cavity made by Havemat. Two power sources were used. A lower power ($\leq$200 mV) sweep oscillator, usually 100 MHz bandwidth centered at 2.45 GHz, was used for tuning; that is, to allow the operator to locate all the resonant modes. This is shown in the block diagram of Figure 3. Axial field strength in the cavity was sampled through small ports located on the cavity sidewall using a probe connected to a power meter. With this equipment, resonant modes can be identified.

The equipment used for actual curing of composites is essentially the same as the low power setup, except that a thermal feedback control has been introduced and the oscilloscope has been removed from the loop because the frequency is no longer swept around a center frequency. The RF power source is an Opthos MPG-4M which operates at a continuous frequency of 2.45 GHz and at a power level from 0 to 120W.

## Sample Processing and Testing

Several samples of AS4-3501-6 graphite/epoxy laminated composites were processed. One series of samples was laid up using 12 unidirectional plies. Another series was laid up as quasi-isotropic 0/45/90/-45 deg cross-ply laminates 12 plies thick. These laminates were laid up as 12-in. squares, then cut to 3-in. square samples. Two such 12-ply samples were
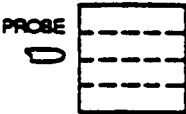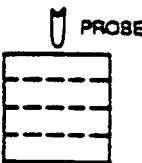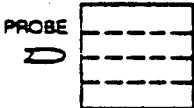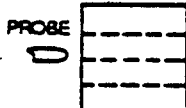
263

Table I. Curing Schedule

| Sample No. Series | Cavity Height (mm) | Mold Tool Height (mm) | Power Application | Total Cure Time |
|---|---|---|---|---|
| 1 | 120 | 57 | Pulsed | 40 min |
| 2 | 120 | 57 | Continuous | 75 min |
| 3 | 60 | 00 | Pulsed | 70 min |
| 4 | 120 | 57 | Pulsed | 90 min |

## RESULTS

Results of sample processing and testing are presented in Table II. Sample layout presents the orientation of the sample cut sections (dashed lines) relative to the cavity feed probe. As expected, the percentage cure increases generally as the energy (time) applied to the sample. Furthermore, the strength, as represented by the flexural strength, tracks with the measured percentage cure.

Flexural strength, which tests both shear and compressive strengths, are approximately uniform over the samples for both 4/X-ply and 1/UNIDIX. Differences in strength magnitude between these samples are due to

Table II. Cure and Strength Results

| Sample No./ Description | Time Power Applied at 3 W/g | Sample Layout | Cure by DSC (%) | Flexural Strength (Ksi) |
|---|---|---|---|---|
| 4/X-ply | 90 min | PROBE | 97.2 | 75.4 |
| | | | - | 73.7 |
| | | | - | - |
| | | | - | 76.2 |
| 4/UNIDIX | 90 min | PROBE | 98.6 | 97.3 |
| | | | - | 74.3 |
| | | | - | 16.2 |
| | | | - | 16.4 |
| 2/X-ply | 75 min | PROBE | - | 18.4 |
| | | | - | 25.6 |
| | | | 81.4 | 43.0 |
| | | | - | 15.0 |
| 1/UNIDIX | 40 min | PROBE | - | 25.3 |
| | | | - | 35.8 |
| | | | 66.8 | 27.4 |
| | | | - | 33.8 |

differences in percentage of curing resulting from the differences in curing energy (time).

The large variation in strength of the 4/UNIDIX sample may be due to the combination of probe location and fiber orientation. With the unidirectional orientation of fibers, heat diffusion is expected to strongly favor the fiber direction, and thus, not be as effective at spreading out hot spots as on cross-ply laminates. Also, field coupling may be different between unidirectional and cross-ply laminates which could lead to stratified curing effects.

Flexural strength values for the well-cured specimens are respectable. Product data (Hercules No. 844-3) list a maximum room temperature flexural strength of 260,000 psi for a unidirectional laminate. This represents ideal layup and curing conditions. The samples in the program were not laid up in an ideal manner. There is no assurance of removal of interlaminar air. Also, vacuum bagging was not used. Taking a maximum expected strength of a cross-ply to be one half of a unidirectional laminate, then something like 130 Ksi is close to the ideal strength expected. Sample 4/X-ply measured at about 74 Ksi is a good value considering all the processing conditions.

## CONCLUSIONS AND FUTURE INVESTIGATIONS

Consolidated graphite/epoxy laminate samples can be cured in a resonant microwave cavity with respectable flexural strength. Further investigation is required to determine optimum processing conditions and limitations of the technique. Further empirical exploration of this cavity for uniform heating of unidirectional laminates is necessary in particular. Also, it is likely that mode stirring and multimode cavities will be explored for more complex shapes than the 3-in. square test samples used to date.

## ACKNOWLEDGEMENTS

266

# MICROWAVE HEATING FOR MANUFACTURING CARBON-FIBER THERMOPLASTICS

A.C. LIND*,  L.N. MEDGYESI-MITSCHANG*,  J.E. KURZ**,  H.F. MCKINNEY**,  A F.C. WEAR**

*McDonnell Douglas Research Laboratories, P.O. Box 516, St. Louis, MO 631
**McDonnell Aircraft Company, P.O. Box 516, St. Louis, MO 63166

## ABSTRACT

Traditionally, polymeric composite parts are heated and consolidated an autoclave. For large parts, such as transport aircraft fuselages submarine hulls, size becomes a limiting factor. To overcome this limit tion and to reduce labor costs we are developing an automated tape placemer process. In this process we build composite parts one layer at a time wit tape containing carbon fibers impregnated with a thermoplastic. As the tap comes into contact with the part, we apply heat to melt the thermoplasti and apply pressure to consolidate the tape to the part. To support thi effort we have developed a proprietary microwave applicator that is suitabl for rapidly heating carbon-fiber composites in an automated tape placemen process. Small carbon-fiber/poly(aryl-ether-ether-ketone) parts made usin the microwave applicator have interlaminar shear strengths of 100 MP (14.5 ksi), which is almost equal to the 103 MPa (15.0 ksi) obtained usin an autoclave.

## INTRODUCTION

Traditionally, composite parts have been formed using autoclave techniques. For large parts such as transport aircraft fuselages, size becomes a limiting factor. Tape placement employing microwave heating has been proposed as an alternative to autoclave consolidation. In this process we will build composite parts one layer at a time with tape containing carbon fibers impregnated with a thermoplastic. As the tape comes into contact with the part, we will apply microwaves to heat and melt the thermoplastic and apply pressure to consolidate the tape to the part, as shown in Figure 1. One or more infrared temperature sensors will be used to control the microwave power to the applicator.

The use of electromagnetic energy in the microwave frequency range has been explored as an energy source for the consolidation and cure of composite materials in numerous studies over the past decade. Perceived ad-
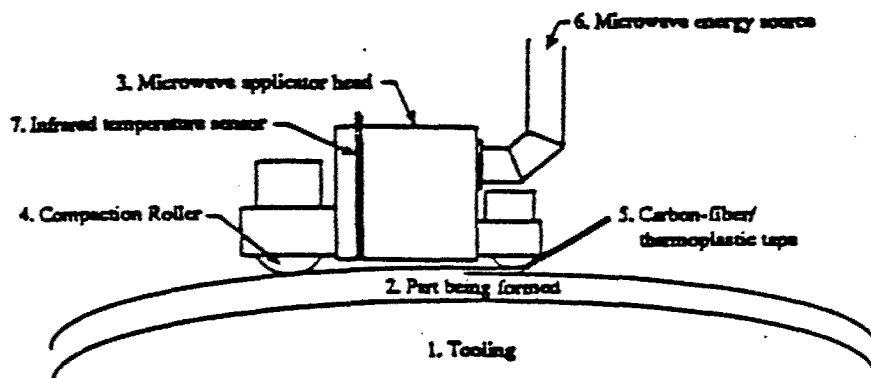
Figure 1. Concept drawing; showing use of a microwave
applicator in a tape-placement part forming device.

vantages are more efficient energy use [1,2], shorter processing cycles [3]
and adaptability to artificial intelligence control of the processing cycle.
A variety of waveguide and cavity microwave applicators have been tried
unsuccessfully to heat continuous carbon fiber reinforced composite materi-
als [4]. The principal impediment is that when the incident electric field
is polarized parallel to the fibers, nearly total reflection occurs. For
cross aligned fibers, nearly total transmission results. In either case,
there is insufficient energy coupling and heating of the material to achieve
consolidation or cure.

The objective of this program was to show that microwave energy can be
efficiently coupled into continuous fiber reinforced composites. The effort
focused on the coupling problem with conductive fibers since that was the
major barrier preventing the wide spread use of this technology for struc-
tural composite processing.

MICROWAVE HEATING OF CARBON-FIBER COMPOSITES

Microwave heating of a carbon-fiber composite is caused by resistive
losses encountered by the induced conduction currents. This is signifi-
cantly different from the heating of foodstuffs in a conventional microwave
oven where dielectric losses occur. In the carbon-fiber composites the
conduction currents are large and the voltages are small; i.e., the carbon
fiber composite has a very low microwave impedance of the order of 0.5 ohms.
In most foodstuffs the voltage is large and the dielectric displacement
currents are small; i.e., foodstuffs have a moderately large microwave
impedance of the order of 100 ohms. Fortunately, the microwave impedance of

268

air is about 377 ohms; thus, microwaves in a microwave oven couple well with most foodstuffs. The very low impedance of carbon-fiber composites causes the microwaves in a microwave oven to be reflected from their surface and very little heating occurs. Thus, our objective was to design a microwave applicator that would couple microwaves into low impedance carbon-fiber composites to adequately heat them for fiber placement and filament winding processes.

The conductivity of carbon-fiber composites at microwave frequencies is large enough to satisfy the condition [5-6]

$$\sigma \gg 2\pi f \epsilon , \qquad (1)$$

where $\sigma$ is the conductivity (S/m), $f$ is the rf frequency (Hz), and $\epsilon$ is the dielectric permittivity, which is of the order of the free-space permittivity, $\epsilon_0 = 8.854 \times 10^{-12}$ F/m. When this condition is satisfied and the dimensions of the composite are much larger than the skin depth

$$\delta = (1/\pi f \mu \sigma)^{1/2}, \qquad (2)$$

where $\mu$ is the magnetic permeability, usually equal to that of free space $\mu_0 = 4\pi \times 10^{-7}$ H/m, then two simplifying approximations can be made which facilitate the calculation of the rf field in the composite [7]

i) treat the object as a superconductor which is impenetrable by the rf magnetic field; i.e., the rf magnetic field at the surface is parallel to the surface, and

ii) break the surface of the object into small regions that are considered to be planar into which plane electromagnetic waves propagate normal to the surfaces.

The magnetic intensity H (ampere turns/m) of the plane electromagnetic wave propagating into a conducting object decays exponentially with increasing distance into the object as

$$H(d) = H_s \exp(-d/\delta), \qquad (3)$$

where $H_s$ is the magnetic intensity at the surface and d is the distance from the surface along the propagation path. The conductivity of carbon-fiber composites is anisotropic. For fiber placement and filament winding processes the conductivity of the composite in a direction lying in the plane of the plies and at right angles to the rf magnetic field direction (i.e., in a direction parallel to the rf electric field) is the appropriate

269

electrical conductivity to use in the expression for the skin depth. This conductivity was determined to be 25,000 S/m for typical carbon-fiber cross-ply composite materials [5,6,8]. If the attenuation experienced by a plane wave propagating into the surface a distance d is required in dB, it can be calculated from

$$\text{Attenuation} = 8.68 \; d/\delta \quad (dB). \qquad (4)$$

The rf power crossing a unit area ($W/m^2$) at the location d is given by [9]

$$P(d) = [H(d)]^2 \; (\pi f \mu_0 / \sigma)^{1/2} . \qquad (5)$$

The quantity $(\pi f \mu_0 / \sigma)^{1/2}$ is the electrical impedance of a conducting material, which is 0.62 ohms at 2.45 GHz for composites having a conductivity of 25,000 S/m.

In our previous work we determined that a power density of about 1000 $W/cm^2$ would be required to heat carbon-fiber composites in a filament winding manufacturing process. Using this power density at d=0 in equation (5), with a conductivity of 25,000 S/m and a frequency of 2.45 GHz, yields a magnetic intensity at the surface of 4020 ampere-turns/m. Generating this magnetic field at the surface presents a problem. For example, if this magnetic intensity were to be generated by causing a current to flow from a 1 cm wide electrode to the composite surface, across a 1 cm length of composite to another 1 cm wide electrode, the current would have to be 40.2 amperes and the voltage across the electrodes would then be 24.9 volts (40.2 amperes/cm times 24.9 volts/cm equals 1000 $W/cm^2$). It is obvious that this amount of current passing between the 1 cm-wide electrodes and the thermoplastic-coated carbon-fibers would result in considerable arcing especially when the electrodes are required to slide across the composite during the filament winding process. Thus, such an applicator is not appropriate.

As a result we designed a proprietary microwave applicator that does not require currents to flow between the applicator and the surface of the composite material. We are in the process of patenting this microwave applicator, so it can not be described in detail. Its efficiency was estimated to be 87% and it was measured to be greater than 67%.

The microwave heating as a function of depth in the composite governed by Equations (2)-(5). Equation (2) predicts the skin depth 2.45 GHz to be 0.064 mm for a conductivity of 25,000 S/m. This skin depth is about one half the thickness of a typical carbon-fiber/thermoplastic

270

tape, which is advantageous for a thermoplastic tape placement process where heating of only a single tape and a thin layer on the surface of the part is required. Heating to much greater depths would waste energy and might adversely deform the part.


## TESTS USING THE MICROWAVE APPLICATOR

A pre-formed carbon-fiber poly(aryl-ether-ether-ketone) (PEEK) plate, 0.64 cm thick and weighing 0.52 kg was installed on the end of the applicator. The microwave power supply was turned on and operated at power levels from 1,000 watts to 2,400 watts for a period of three minutes. The total energy transferred into the cavity was 5160 Watt-minutes. The temperature of the specimen rose to about 278°C. From the temperature-rise information and the known specific heat the estimated efficiency of coupling of the energy into the specimen was 67%.

A piece of carbon-fiber/PEEK unidirectional single-ply tape 0.15 mm thick, 15 cm wide, and 25 cm long was taped down to the back of a pre-consolidated, cross-ply, carbon-fiber/PEEK panel. A Kapton film was placed over this tape and sealed to the plate using a high-temperature Press-Tite sealing compound. The bag was then evacuated to provide a clamping pressure of about 0.1 MPa between the surface of the plate and the tape. A thermocouple was attached to the outside center surface of the plate and the power/time/temperature measurements were recorded during a microwave heating experiment, as shown in Table I.

Table I. Results of microwave heating experiment

| Forward power (watts) | Reflected power (watts) | Incremental time (sec) | Indicated temperature (°C) |
|---|---|---|---|
| 1,000 | 175 | 120 | 93 |
| 2,000 | 375 | 30 | 143 |
| 2,000 | 500 | 30 | 154 |
| 2,000 | 500 | 30 | 190 |
| 2,000 | 600 | 30 | 225 |
| 0 | 0 | 60 | 227 |

90-221-15a

The sample was removed from the test chamber and examined. The specimen had become so hot in the center of the plate that the Kapton bag was charred. When the Kapton bag was removed we observed that the tape was bonded to the original pre-consolidated plate. About half of this bonded region showed a shiny surface having essentially the identical characteristics of the pre-consolidated plate.

271

The fusion bonding of the tape to the pre-consolidated material, while admittedly crude, is considered to be a major step in the development of the use of microwaves for forming useful structures from conductive fiber materials. With this development it becomes conceptually feasible to develop a continuous tape-placement process in which carbon-fiber/thermoplastic tapes are wound onto a mandrel to produce useful structures.

The microwave applicator was also used to make multi-layer carbon-fiber/PEEK composites samples suitable for measuring their interlaminar shear strength. These samples were made by hand stacking a multi-layer structure, vacuum bagging it, and heating it with the microwave applicator. Because the microwaves heated only the top layer, about two minutes were required for the heat to penetrate all the layers. The measured interlaminar shear strength of these samples ranged from 98 to 101 MPa (14.2 to 14.7 ksi). This compares favorably with autoclave processed carbon-fiber/PEEK samples whose interlaminar shear strength is about 103 MPa (15.0 ksi).

## CONCLUSIONS

We have demonstrated that it is feasible to efficiently couple microwave power into a carbon-fiber composite part using our proprietary microwave applicator. The design of this applicator is suitable for use in automated tape placement manufacturing processes.

## ACKNOWLEDGMENT

REFERENCES

1. J. Jow, M.C. Hawley, M. Finzel, J. Asmussen Jr., H.-H. Lin, an B. Manring, IEEE Trans. Microwave Theory Tech. **35**, 1435 (1987).

2. Y.-F. Chen and C.Y.-C. Lee, Polym. Mater. Sci. Eng. **60**, 680 (1989).

3. J.C. Hedrick, D.A. Lewis, G.B. Lyle, S.D. Wu, T.C. Ward, an J.E. McGrath, Polym. Mater. Sci. Eng. **60**, 438 (1989).

4. W.I. Lee and G.S. Springer, J. Comp. Macl. **18**, 357 (1984), ibid, **18**, 387 (1984).

5. A.C. Lind and C.G. Fry, Nuclear Magnetic Resonance Nondestructive Evaluation of Composite Materials, Report MDC QA035, WRDC/MLLP Contract F33615-87-C-5247, 25 June 1989.

6. A.C. Lind, C.G. Fry, and C.H. Sotak, J. Appl. Phys. (accepted).

7. L.D. Landau and E.M. Lifshitz, _Electrodynamics of Continuous Media_ (Addison and Wesley, 1960) p. 190.

8. A.C. Lind and T.R. Wenger, Measurements of the Complex Dielectric Constant of Lossy Fibers and Rods at Microwave Frequencies, Rev. Sci. Instrum. **58**, 844, (1987).

9. R.F. Harrington, _Time-Harmonic Electromagnetic Fields_ (McGraw-Hill, New York 1961) p. 50.